

PDF hosted at the Radboud Repository of the Radboud University Nijmegen

The following full text is a publisher's version.

For additional information about this publication click this link.

<http://hdl.handle.net/2066/197556>

Please be advised that this information was generated on 2023-04-13 and may be subject to change.



Stargardt disease

Toward clinical trials

Stanley Lambertus

Stargardt disease

Toward clinical trials

Stanley Lambertus

The work presented in this thesis was carried out within the Radboud Institute for Health Sciences.

Research described in this thesis was financially supported by Stichting A.F. Deutman Researchfonds Oogheelkunde; Nederlandse Oogonderzoek Stichting; Gelderse Blindenstichting; Deutsche Forschungsgemeinschaft; BONFOR GEROK Program, Faculty of Medicine, University of Bonn; the National Institute for Health Research Biomedical Research Centre at Moorfields Eye Hospital National Health Service Foundation Trust and UCL Institute of Ophthalmology; Fight For Sight; The Macular Society; Moorfields Eye Hospital Special Trustees; Moorfields Eye Charity; the Foundation Fighting Blindness; Retina UK; and by the following foundations that contributed through Uitzicht: Stichting MD fonds, Landelijke Stichting voor Blinden en Slechtzienden, and Oogfonds.

Financial support for the publication of this thesis was kindly provided by Radboud University Nijmegen; Landelijke Stichting voor Blinden en Slechtzienden; Rotterdamse Stichting Blindenbelangen; Stichting A.F. Deutman Researchfonds Oogheelkunde; Stichting Blindenhulp; Stichting voor Ooglijders; ChipSoft B.V.; Medical Workshop B.V.; and Synga Medical B.V.

All funding organizations had no role in the design or conduct of this research. They provided unrestricted grants.

©2018, Stanley Lambertus, Nijmegen, the Netherlands

Selected images in Chapter 1 are licensed under the Creative Commons Attribution-ShareAlike 4.0 International (CC BY-SA 4.0). No others parts of this publication may be reproduced or transmitted in any form without prior written permission by the copyright holder. Supplemental material is available online.

Cover design and lay-out	Stanley Lambertus <i>Inspired by Shutterstock</i>
Photograph of the author	DUTZU Photography
Printed by	Ipskamp Printing B.V.
Publisher	Radboud University
ISBN	978-94-92896-95-7
NUR	876

Stargardt disease

Toward clinical trials

PROEFSCHRIFT

ter verkrijging van de graad van doctor
aan de Radboud Universiteit Nijmegen
op gezag van de rector magnificus prof. dr. J.H.J.M. van Krieken,
volgens besluit van het college van decanen
in het openbaar te verdedigen op vrijdag 21 december 2018

om 12:30 uur precies

door

Stanley Lambertus
geboren op 18 november 1987
te Gendringen

Promotoren

Prof. dr. C.B. Hoyng

Prof. dr. G.J. van der Wilt

Prof. dr. B.J. Klevering

Manuscriptcommissie

Prof. dr. H.G. Brunner

Dr. R.J.E. Pennings

Prof. dr. A.J. Lotery (University Hospital Southampton, Verenigd Koninkrijk)

“Research on rare diseases illuminates key aspects of human physiology. Common diseases are beginning to be dissected into collections of “rare” molecularly defined subgroups. These advances in our understanding of human pathophysiology have the potential to relieve human suffering through precision medicine. But to improve clinical medicine, new treatments for rare diseases and disease subtypes must be evaluated using special clinical trial designs and analyses that address the statistical challenges associated with small sample sizes.”

— Edward L. Korn, Lisa M. McShane and Boris Freidlin —

Table of contents

Abbreviations	VIII
Visual acuity conversion chart	IX
CHAPTER 1 Introduction	
1.1 Stargardt disease	3
1.2 A history of treatment evaluation	11
1.3 Toward clinical trials for Stargardt disease	14
1.4 Aims of this thesis	15
CHAPTER 2 Natural history of Stargardt disease	
2.1 Early-onset Stargardt disease: phenotypic and genotypic characteristics <i>Ophthalmology. 2015 Feb;122(2):335-44</i>	23
2.2 Progression of late-onset Stargardt disease <i>Invest Ophthalmol Vis Sci. 2016 Oct 1;57(13):5186-5191</i>	43
CHAPTER 3 Diagnosing Stargardt disease	
3.1 The absence of fundus abnormalities in Stargardt disease <i>Submitted</i>	59
3.2 Differential disease progression in atrophic age-related macular degeneration and late-onset Stargardt disease <i>Invest Ophthalmol Vis Sci. 2017 Feb 1;58(2):1001-1007</i>	75
CHAPTER 4 Measuring progression in Stargardt disease	
4.1 Asymmetric inter-eye progression in Stargardt disease <i>Invest Ophthalmol Vis Sci. 2016 Dec 1;57(15):6824-6830</i>	93
4.2 Highly sensitive measurements of disease progression in rare disorders: developing and validating a multimodal model of retinal degeneration in Stargardt disease <i>PLoS One. 2017 Mar 29;12(3):e0174020</i>	109
4.3 Lipofuscin-associated photo-oxidative stress during fundus autofluorescence imaging <i>PLoS One. 2017 Feb 24;12(2):e0172635</i>	127

CHAPTER 5	Discussion	
5.1	Relevance of disease classification	152
5.2	Identification and selection of patients	155
5.3	Endpoints in clinical trials	156
5.4	Meaningful outcome measures	161
5.5	When present becomes history	162
CHAPTER 6	Summary	
6.1	Summary	171
6.2	Samenvatting	173
6.3	Ringkasan	175
	Dankwoord	179
	Curriculum vitae	183
	Publications	183
	Portfolio	187

Abbreviations

A2E	N-retinylidene-N-retinylethanolamine
ABCA4	adenosine triphosphate (ATP)-binding cassette, sub-family A, member 4 transporter The ABCA4 protein was previously denoted as ABCR (Chapter 2.1). For consistency, this abbreviation has been changed to ABCA4 throughout this thesis.
AF	autofluorescence allele frequency <ul style="list-style-type: none">• qAF quantitative autofluorescence• DDAF definitely decreased autofluorescence• QDAF questionably decreased autofluorescence• SW-AF short-wavelength autofluorescence
AMD	age-related macular degeneration
ANSI	American National Standards Institute
ASTM	American Society of Testing and Materials
CACD	central areolar choroidal dystrophy
CI	confidence interval
CNV	choroidal neovascularization
CF	counting fingers
CT	computed tomography
ELM	external limiting membrane
EMA	European Medicines Agency
ERG	electroretinography <ul style="list-style-type: none">• ffERG full-field electroretinography• mfERG multifocal electroretinography• PERG pattern electroretinography
ETDRS	Early Treatment Diabetic Retinopathy Study
ExAC	Exome Aggregation Consortium
EZ	ellipsoid zone
FA	fluorescein angiography
FAF	fundus autofluorescence
FAM	Fundus Autofluorescence Imaging in Age-related Macular Degeneration
FDA	U.S. Food and Drug Administration
GA	geographic atrophy
GPS[+]	fine granular pattern with peripheral punctate spots
HM	hand movements
ISCEV	International Society for Clinical Electrophysiology of Vision
IQR	interquartile range
logMAR	logarithm of the minimum angle of resolution
LOVD	Leiden Open (source) Variation Database
MC	Monte Carlo
MRI	magnetic resonance imaging
NI	not identified
NIH	National Institute of Health
NIR	near-infrared reflectance
NA	not available
NP	not performed
OCT	optical coherence tomography <ul style="list-style-type: none">• SD-OCT spectral-domain optical coherence tomography
OD	optical density

OR	odds ratio
PE	phosphatidylethanolamine
PhyloP	phylogenetic <i>P</i> values
PolyPhen-2	polymorphism phenotyping version 2
PRPH2	Peripherin-2
RPE	retinal pigment epithelium
Q ₁	first interquartile
Q ₃	third interquartile
RMSE	root-mean-square error
RPE	retinal pigment epithelium
SD	standard deviation
	<ul style="list-style-type: none"> MSDR mean-to-standard-deviation ratio
SE	standard error
SIFT	sorting intolerant from tolerant
STGD1	Stargardt disease
	<ul style="list-style-type: none"> EO-STGD1 early-onset Stargardt disease IO-STGD1 intermediate-onset Stargardt disease LO-STGD1 late-onset Stargardt disease
VA	visual acuity
	<ul style="list-style-type: none"> BCVA best-corrected visual acuity

Visual acuity conversion chart

	Decimal notation	U.S. notation	logMAR
Normal vision	1.6	20/12.5	-0.2
	1.25	20/16	-0.1
	1.0	20/20	0
	0.8	20/25	0.1
Mild visual impairment	0.63	20/32	0.2
	0.5	20/40	0.3
	0.4	20/50	0.4
	0.32	20/63	0.5
Moderate visual impairment	0.25	20/80	0.6
	0.2	20/100	0.7
	0.16	20/125	0.8
	0.125	20/160	0.9
Severe visual impairment	0.1	20/200	1.0
	0.08	20/250	1.1
	0.063	20/320	1.2
	0.05	20/400	1.3
Profound visual impairment	0.04	20/500	1.4
	0.032	20/630	1.5
	0.025	20/800	1.6
	0.02	20/1000	1.7
(Near-)blindness	less than 0.02 20/1000		1.8
			1.9
			2.0
			2.1



1.1 Stargardt disease

The first cases of what is now known as Stargardt disease were described in the late 19th century. Back then, Stargardt disease, as well as most other retinal dystrophies, was commonly regarded as an infectious or inflammatory disease: central choroiditis. Patients were often suspected for tuberculosis or lues. They were treated accordingly, but these patients eventually could no longer read, perceive colors, or recognize faces. In 1885, Lang described a 30-year old woman with progressive vision loss and retinal features most reminiscent of Stargardt disease:¹

“The patient noticed that her sight was failing six years ago, and it has gradually got worse since then, but without causing any discomfort [...]. In the [foveal] region, there is considerable disturbance of the retinal pigment with increased pigmentation in one or two places. [...]

In the posterior part of fundus, there are numerous small round, or oval yellowish-white patches scattered in every direction; they do not assume any regular distribution, but the oval ones generally have their long axis at right angles to the retinal vessels. They are apparently situated in the superficial part of the choroid.”

It was not until 1909 when these retinal features were recognized as a familial progressive macular dystrophy by Karl Stargardt, whose name now has been solidly linked to the disease.² A central macular atrophy with irregular or pisciform yellow-white fundus flecks (Figure 1) characterizes Stargardt disease (prevalence, 1:8000–1:10000).^{3, 4, 5} These flecks are predominantly located in the macula and represent lipofuscin granules containing toxic bisretinoids. These toxic compounds accumulate over time in the retinal pigment epithelium, which results in atrophy of the retinal pigment epithelium and photoreceptor cells.^{6,7} Both flecks and atrophic lesions can extend beyond the vascular arcades,⁸

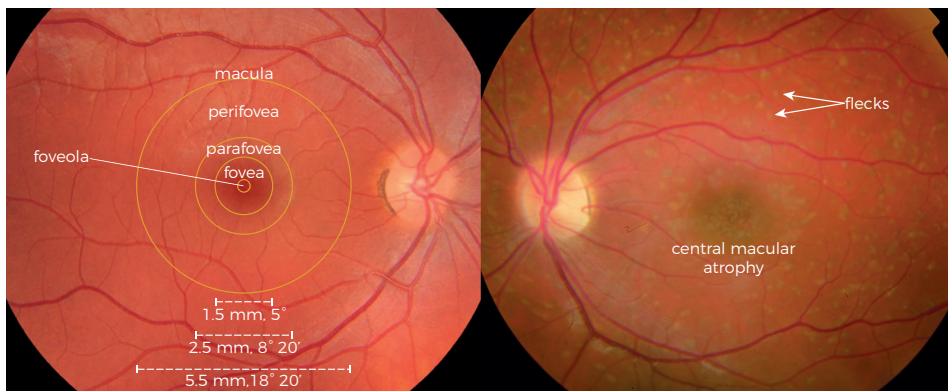


Figure 1. (Left) Overall topography of the human retina on fundus photography. (Right) Stargardt disease.

Gross anatomy of the eye

Light rays diverge in all directions from their source and must be refracted to eventually come to a sharp focus on the retina. The strongest refraction occurs through the cornea, which is the front surface of the eye. It then goes through the circular opening in the iris: the pupil. The pupil will constrict as the light becomes brighter, and so will it dilate as the light becomes dimmer. The pupil contributes to the sharp focus by narrowing its size, reducing spherical and chromatic aberrations, which tend to blur the image. Moreover, a narrow pupil increases the depth of field: the distance within which objects are seen sharply. Passing through the pupil, the light goes through the crystalline lens, which has adjustable refractive power. This allows objects at various distances to be brought into sharp focus. It is then in the retina where photons are transformed into electrical signals. These signals are sent through the optic nerve, along the visual pathway, and finally processed in the occipital cortex at the posterior of the brain that eventually create our vision (Figure 2).

as centrifugal expansion continues to progress into eventual retina-wide degeneration.⁹⁻¹²

Although Stargardt disease was originally considered a juvenile macular degeneration,² patients may experience the first visual complaints between their first until the seventh decade of

life.¹³⁻¹⁶ The heterogeneity in the age at onset reflects heterogeneity in the natural disease course. The extremes can be described as early-onset or childhood-onset Stargardt disease and late-onset Stargardt disease. These subtypes have distinct progressions: early-onset Stargardt disease is characterized by minor initial abnormalities, but with a rapid progression toward chorioretinal degeneration.¹⁴ Late-onset Stargardt disease contains features of a relatively intact fovea that is often surrounded by atrophic retinal pigment epithelium lesions.^{13, 15} The patients with an intermediate disease onset are expected to be in between these extremes.

Retinal imaging

On fluorescein angiography, the choroidal background fluorescence is characteristically blocked in Stargardt disease due to the excess lipofuscin accumulation in the retinal pigment epithelium, which has been described as a dark choroid.¹⁷ The yellow-white flecks appear hypofluorescent at first, but eventually become hyperfluorescent as atrophy develops. Although these diffuse hyperfluorescent flecks may obscure a dark choroid, it can still be visible in the peripapillary area or in the peripheral retina.¹⁸

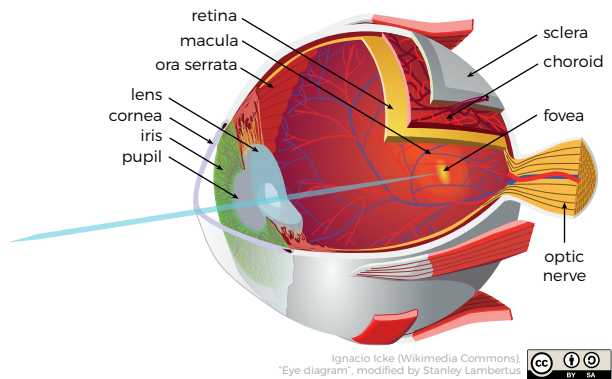


Figure 2. Anatomy of the human eye.

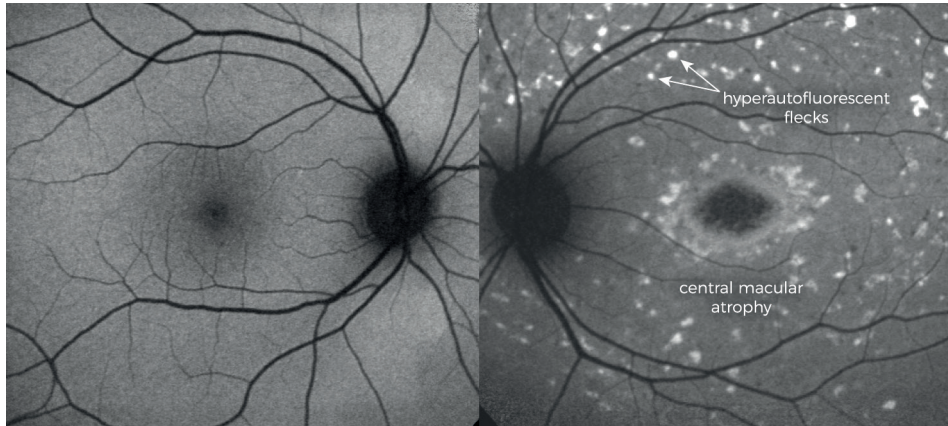


Figure 3. (Left) Fundus autofluorescence image of a normal retina. (Right) The yellow-white fundus flecks in Stargardt disease are hyperautofluorescent. This indicates increased accumulation of lipofuscin fluorophores. Areas of decreased autofluorescence indicate reduced lipofuscin demand due to photoreceptor loss.

In the aid of diagnosing and monitoring Stargardt disease, fluorescein angiography has now been replaced by fundus autofluorescence imaging. Fundus autofluorescence imaging visualizes the distribution of lipofuscin in the retinal pigment epithelium. The

Retinal architecture

The retina is a highly specialized transparent neural layer for capturing and processing light. However, its unique sophisticated architecture of ten layers makes it also vulnerable to dysfunction. The outer retina comprises the [1] retinal pigment epithelium and the photoreceptor layer. The retinal pigment epithelium has vital functions for the maintenance of photoreceptors, phagocytosis of photoreceptor outer segments being one of the most relevant one in this thesis. Photoreceptors are continuously being exposed to light and oxygen, which facilitates the formation of free radicals. These radicals damage the photoreceptor membranes over time, which therefore need to be continuously renewed. Old outer segments are continuously being shed by the retinal pigment epithelium and replaced by new discs at a 10% per 24 hour rate.¹⁹ Undigested outer segment parts eventually form lipofuscin granules, which accumulate as we age.⁷ Rods and cones, forming the [2] photoreceptor layer, contain an inner and an outer segment. The cell organelles are located in the inner segment. The inner segment ellipsoid zone reflects photoreceptor integrity and health. The conversion of light to electric signals, i.e., phototransduction, occurs in the outer segment. In cones, the outer segments contain many invaginations of the surface membrane; in rods, they are entirely discontinuous of the surface membrane and form individual disk membranes. The structural supportive junctions between photoreceptors and Müller glia compose the [3] external limiting membrane. The cell bodies of photoreceptors compose the [4] outer nuclear layer. Photoreceptors interconnect through synapses with bipolar and horizontal cells in the [5] outer plexiform layer. The inner retina contains the [6] inner nuclear layer, composed of amacrine, bipolar, horizontal, and Müller cells. These cells interconnect with ganglion cells in the [7] inner plexiform layer. The cell bodies of the ganglion cells are situated in the [8] ganglion cell layer, from which the axons form the [9] nerve fiber layer. The inner retina is finally separated from the posterior vitreous by the [10] internal limiting membrane (Figure 4).

yellow-white fundus flecks are hyperautofluorescent, indicating increased accumulation of lipofuscin fluorophores.^{20, 21} These hyperfluorescent changes may be visible prior to changes on ophthalmoscopy. Areas of decreased autofluorescence indicate reduced lipofuscin demand due to photoreceptor loss. Autofluorescence is absent in case of complete retinal pigment epithelium loss, which represents a late manifestation in Stargardt disease (Figure 3).²²⁻²⁵ However, there are concerns that patients with Stargardt disease are at risk for light toxicity during fundus autofluorescence imaging.¹⁵ The accumulation of bisretinoids is accelerated in Stargardt disease, and particularly these bisretinoids are identified as potent photosensitizers in animal studies. Whether the mechanism of photochemical damage involves changes in either lipofuscin or molecules within the visual cycle such as all-trans-retinal, patients with Stargardt disease are likely to be more susceptible to photic injury than healthy individuals.^{14, 16}

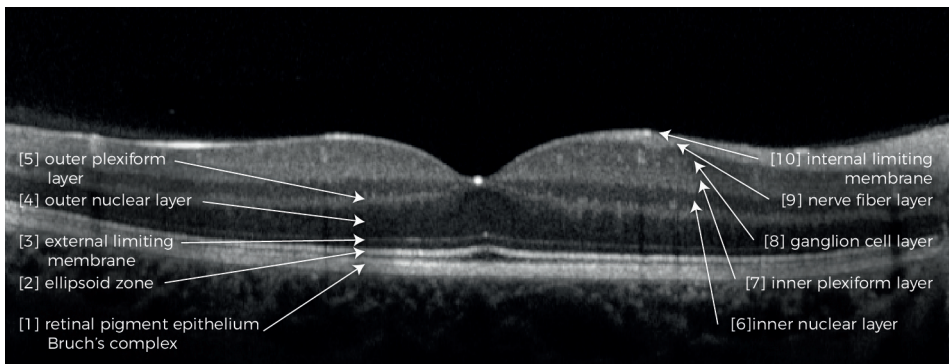


Figure 4. Spectral-domain optical coherence tomography of the human retina. A horizontal scan through the fovea reveals several hyperreflective (white) bands, which correlate with the anatomical layers of the retina. [1] retinal pigment epithelium / Bruch's complex [2] ellipsoid zone [3] external limiting membrane [4] outer nuclear layer [5] outer plexiform layer [6] inner nuclear layer [7] inner plexiform layer [8] ganglion cell layer [9] nerve fiber layer [10] internal limiting membrane.

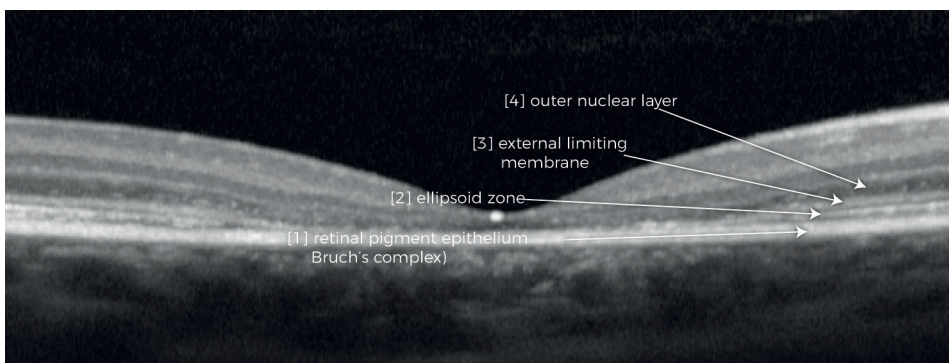


Figure 5. Spectral-domain optical coherence tomography in Stargardt disease. The outer retinal layers are thinned and recede centrifugally from the fovea. The hyperreflective band of the external limiting membrane is thicker than in a normal retina.

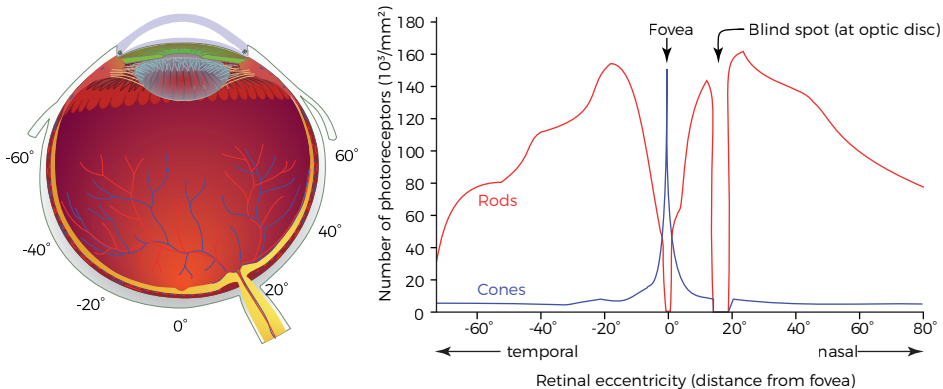
Photoreceptor topography

Approximately 100 million rods dominate the peripheral retina, which extends from the vascular arcades to the ora serrata. Cone photoreceptors (± 5 million) dominate the central retina: the macula lutea (Figure 6). The border of the macula (5.5 mm), overlaps with the path of the vascular arcades. The macula can be subdivided in a perifoveal area, parafoveal area, fovea, foveola, and umbo. The umbo (0.15–0.20 mm) lies at the very center of the macula and has the highest visual acuity with the highest cone density. The diameter of its cones is narrowed and elongated due to crowding. At the foveola (0.35 mm), the metabolic demands of these densely packed cones are extremely high, which are met by direct contact with the retinal pigment epithelium, and through the processes of Müller glia cells.^{26, 27} The foveola, a 22° clivus, and a thick margin comprises the fovea (1.5 mm). The margin is surrounded by the parafoveal belt (0.5 mm width), which has a regular ten-layer retinal architecture. The perifoveal belt finally (1.5 mm) surrounds the parafovea (Figure 1).

The retinal layers can be visualized with high resolution on a cross-sectional retinal scan: spectral-domain optical coherence tomography (Figure 4). Thickening of the external limiting membrane has been suggested as the earliest sign prior to any other structural or functional abnormalities. It may reflect a gliotic response to cellular stress at the photoreceptor level).^{28, 29} The photoreceptor inner segment ellipsoid zone may recede earlier than the retinal pigment epithelium, indicating that spectral-domain optical coherence tomography can be more informative than fundus autofluorescence imaging in early stages (Figure 5).^{30, 31}

The ABCA4 gene

Stargardt disease is an autosomal recessive retinal dystrophy associated with disease-causing sequence variants in the adenosine triphosphate-binding



Left: Ignacio Icke (Wikimedia Commons). "Schematic diagram of the human eye", modified by Stanley Lambertus
Right: Cmglee (Wikimedia Commons). "Human photoreceptor distribution", modified by Stanley Lambertus



Figure 6. The distribution of rods and cones. The density of the receptors is shown in degrees of visual angle relative to the position of the fovea for the left eye. The cone receptors are concentrated in the fovea. The rod photoreceptors are absent from the fovea and reach their highest density 10 to 20° peripheral to the fovea. No photoreceptors are present in the blind spot.

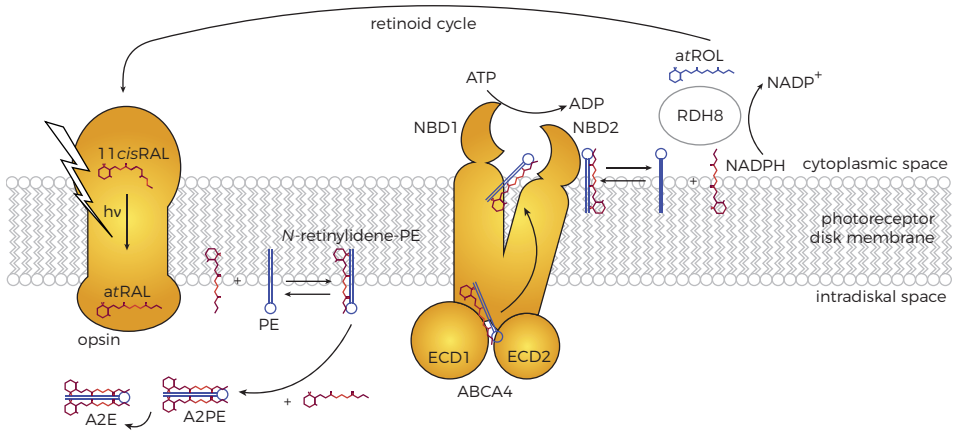


Figure 7. The formation of bisretinoids in absence of ABCA4 protein function.

cassette, subfamily A, member 4 (ABCA4) gene.^{32, 33} The carrier frequency of ABCA4 sequence variants is up to 1 in 20,³⁴ and a nearly ever increasing number of more than 1000 variants has been reported.³⁵⁻³⁸ The ABCA4 protein, localized in the disk membranes of both cones and rods,^{39, 40} plays an essential role in the retinoid cycle. Via the retinoid cycle, 11-cis-retinal must be continuously regenerated from all-trans-retinal to maintain vision. All-trans-retinal is released into the lumen of the disk membranes and condensates with phosphatidylethanolamine (PE) to form N-retinylidene-PE.^{20, 41} Likewise, 11-cis-retinal and phosphatidylethanolamine form N-11-cis-retinylidene-PE.^{42, 43} These adducts are transported by the ABCA4 protein from the lumen into the cytoplasmic space. Dysfunction or absence of ABCA4 leads to excessive accumulation of N-11-cis-retinylidene-PE and N-retinylidene-PE adducts. They can form potentially toxic compounds, such as N-retinylidene-N-retinylethanolamine (Figure 7).⁴⁴ These bisretinoids undergo photo-oxidation and produce reactive oxygen and nitrogen species,^{45, 46} and eventually leads to the aforementioned irreversible damage to the retina.^{5, 6, 32}

Phototransduction and the retinoid cycle

Photons are absorbed by visual pigments at the outer segment disk membranes of photoreceptors. Visual pigment consists of an α -helical integral membrane protein, opsin, and a chromophore: 11-cis-retinal, a vitamin A isomer. The interaction between the opsin and 11-cis-retinal determines the spectral sensitivity, which is tuned to a particular wavelength of maximal absorption. In cones, three types of visual pigment give a continuous range of colors to our sight in photopic, i.e., bright conditions. Rods have one type of visual pigment for scotopic, i.e., dim conditions.⁴⁷ When a photon is absorbed, 11-cis-retinal isomerizes to all-trans-retinal. This triggers a chain of enzymatic reactions, eventually leading to membrane hyperpolarization and neurotransmitter release at the photoreceptor terminal synapse.^{48, 49} Recovery starts after phototransduction, where all-trans-retinal dissociates from the opsin. After being transported from the lumen into the cytoplasmic space by ABCA4, all-trans-retinal is reduced to all-trans-retinol and then transported to the retinal pigment epithelium. In several steps, all-trans-retinol is then finally converted to 11-cis-retinal.

Classifications of Stargardt disease

Several classifications and staging methods have been described for Stargardt disease. These classifications are based on the extent of retinal abnormalities, electrophysiologic findings and genotype-phenotype correlations (Table 1).

Phenotype according to Fishman.			
Stage I	Stage II	Stage III	Stage IV
Atrophic macular lesion with localized flecks	Retinal flecks throughout posterior pole	Resorbed flecks	Extensive atrophic-appearing changes of retinal pigment and choroid
Electroretinography according to Lois.			
Group 1	Group 2	Group 3	
Severe pattern ERG abnormality	Additional generalized cone dysfunction	Additional generalized rod dysfunction	
Genotype according to Van Driel.			
Mild	Moderate	Moderate/severe	Severe
(Risk for) age-related macular degeneration	Stargardt disease	Cone-rod dystrophy	Retinitis pigmentosa

Table 1. Classifications and staging of Stargardt disease. ERG = electroretinography.

Fishman et al. differentiated four distinct retinal features that reflect the phenotypes of Stargardt disease: [I] an atrophic-appearing macular lesion with localized perifoveal flecks, [II] retinal flecks throughout the posterior pole, [III] resorbed flecks, and [IV] extensive atrophic-appearing changes of the retinal pigment epithelium and choroid.^{50,51}

Lois et al. suggested phenotypic subtypes of Stargardt disease based on electroretinography. Electroretinography measures the total electrical activity response from cones and rods to a light stimulus. The International Society for Clinical Electrophysiology of Vision (ISCEV) provides the minimum standard of measurements for electroretinography.⁵² Full-field electroretinography is used to study the total degree of retinal dysfunction, in which the rod system is measured in dark-adapted conditions (dim flash, 0.01 cd-s/m² and bright flash, 11.0 cd-s/m²). The cone system is measured in light-adapted conditions (3.0 cd-s/m² at 2 Hz and 30 Hz). Pattern electroretinography provides information about macular and retinal ganglion cell function (using a temporally modulated patterned stimulus). In Stargardt disease, three patterns of retinal potentials were identified based on measurements of these ISCEV standards. The first pattern comprises severe pattern electroretinography abnormality with normal full-field electroretinography. It reflects dysfunction confined to the macula. The second pattern includes a generalized cone system dysfunction, consistent with a clinical diagnosis of cone dystrophy. The third includes both cone and rod system dysfunction, i.e., cone-rod dystrophy (Figure 8).⁵³⁻⁵⁵

Van Driel et al. proposed a classification based on the expected residual function of the ABCA4 protein by the severity of mutations (Figure 9).⁵⁶ Missense variants are generally

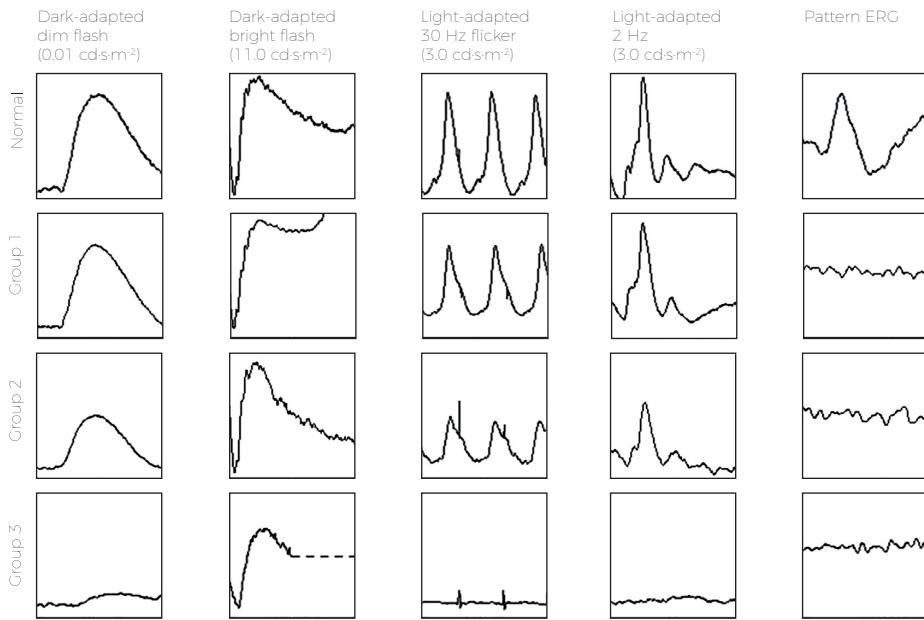


Figure 8. Electoretinographic findings in Stargardt disease. Group 1, severe pattern electoretinographic abnormality; group 2, additional generalized cone dysfunction; group 3, additional generalized rod dysfunction. ERG = electroretinography.

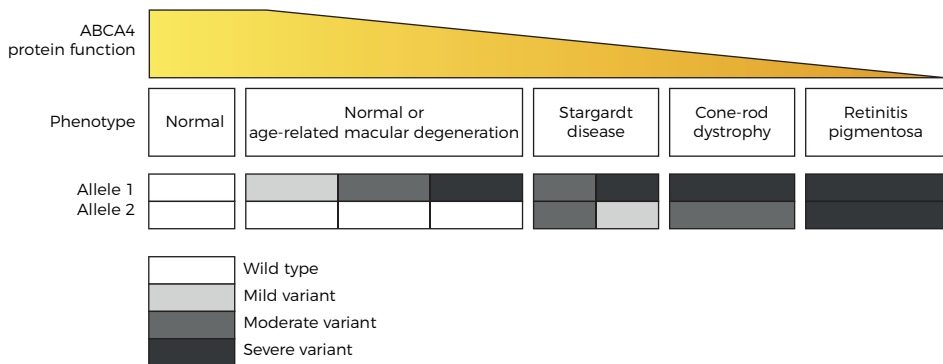


Figure 9. Genotype-phenotype correlation model adapted from Van Driel et al.

associated with mild, late-onset disease, while severe “null” variants, which result in zero protein function, are associated with severe, early-onset disease.⁵⁶⁻⁵⁹ The classification extends the putative associations of ABCA4 variants from the presumed mildest phenotype of age-related macular degeneration (one mild ABCA4 variant) to the most severe phenotype of retinitis pigmentosa (two severe ABCA4 variants). Arguably, variants in the ABCA4 gene are also associated with cone dystrophy, cone-rod dystrophy and atypical retinitis pigmentosa.^{56, 60-65}

Management and treatment

Currently, patients are advised to avoid excessive light exposure, e.g., by wearing ultraviolet-protective sun glasses. Bright ultraviolet light has been demonstrated to accelerate retinal degeneration in animal models^{66, 67} and there are some indications that total blockage of light slows down disease progression.⁶⁸ Patients are also advised not to take vitamin A supplementation, which is supported by animal studies showing accelerated accumulation of lipofuscin with vitamin A supplementation.^{20, 69} Despite the lack of sound evidence, these measures will probably prevent an accelerated disease progression.

However, no treatment is readily available to slow or stop disease progression. Gene therapies, cell-based therapies, as well as pharmacological therapies trials are now in progress. Gene therapy aims to slow down or prevent retinal regeneration by targeting intact photoreceptors and is therefore preferable in the earliest disease stages. A Phase I/II clinical trial is now ongoing where a functional ABCA4 gene will be injected subretinally using a lentiviral vector SAR422459. A proof of concept has already been demonstrated in animal studies,⁷⁰⁻⁷² and there have been no safety concerns in humans, although there has not been any evidence of efficacy until now.⁷³ Stem cell therapy aims to replace lost retinal pigment epithelium cells, which can be useful in late disease stages. A Phase I/II trial using human embryonic stem cell derived retinal pigment epithelium cells also showed no safety concerns,^{74, 75} but as the defective ABCA4 protein function is not corrected, it may be insufficient to slow down disease progression. Finally, pharmacological strategies are being developed to target several aspects of the retinoid cycle, and include phloroglucinol, fenretinide and C20-D₃-vitamin A.⁷⁶⁻⁷⁸

1.2 A history of treatment evaluation

These new treatments need to be carefully evaluated to understand their potential effects. Support of the highest level of empirical evidence is required to eventually come toward an effective treatment. Nowadays, this process is known as a clinical trial: the bedrock of evidence-based medicine. “*Evidence-based medicine is the conscientious, explicit, judicious and reasonable use of modern, best evidence in making decisions about the care of individual patients.*”⁷⁹ It integrates the best available empirical evidence, thus not solely based on theories and intuition. Both clinical expertise as well as external evidence are to be combined to achieve the best practice for the individual patient. Without clinical trials, we may conclude that useless treatments are helpful, or that helpful treatments are useless. Although the standards in science have evolved significantly, their basic concepts still hold—and continue to be refined.

In the 1990s, David Sackett brought the ‘art of medicine’ forward from expert opinion-based practice on to a new paradigm for health care which stresses on evidence from clinical research.⁸⁰ Although Sackett is considered the pioneer of evidence-based medicine, its origins are ancient.

Fair comparisons

During the Siege of Jerusalem (597 BC), Daniel proposed King Nebuchadnezzar II of the Neo-Babylonian Empire a trial to prove he could be fit for service having only vegetables and water instead of wine and meat; after ten days, Daniel’s group appeared to be healthier and stronger than the royal children who dined at the King’s table.⁸¹ Arguably, this was the first reported clinical trial.⁸² Indeed, he followed two of its basic: [1] two groups with different treatments, and [2] a finite length for outcome evaluation.

However, it was not until the Islamic Golden Age (9th century) that the need for comparison with a similar untreated control group was recognized by some of the greatest luminaries in medicine that time. The Persian Al-Razi, a pioneer in neurology and ophthalmology, detested theoretical conclusions that did not correlate with clinical findings. Therefore, he refined his treatments by testing the validity of ther-



Figure 10. James Lind on board the H.M.S. Salisbury treating sailors for scurvy. His experiment is considered to be the first prospective controlled clinical trial.

apies and theories in practice, one of which included bloodletting for early symptoms of meningitis. Although bloodletting would not be recommended today, his approach reflects the essential feature of a fair comparison by treating one group and intentionally withholding treatment from the other group.^{83, 84}

Ibn Sīnā wrote the *Al-Qanun fi al-Tibb* (Canon of Medicine) in 1012. This book contained rules for assessing the effects of drugs. He argued that not only theories “dealing with the principles of medicine” are important, but empirical observations “how to put those principles into practice” as well.⁸⁵ European and Middle Eastern countries had relied on his work for over six centuries, and is still very relevant today.

Several centuries later, James Lind, a Scottish naval surgeon conducted a now famous prospective controlled trial. Back then, many sailors suffered from scurvy in a few months at sea. Lind hypothesized that citrus fruits could cure scurvy. In 1747, he divided twelve scurvy patients on board the *Salisbury* into six pairs. Everyone had the same diet, but, in addition, the first pair was given a cider, the second elixir vitriol, the third vinegar, the fourth seawater, the fifth oranges and lemon, and the sixth a spicy paste with barley water (Figure 10, previous page). The sailors who received the oranges and lemon clearly recovered from scurvy within a week. Nowadays, James Lind is commonly regarded as the father of clinical trials.⁸⁶

Double-blind randomized controlled trials

From 1800 onwards, study design became increasingly important for clinical trials. In 1894, the ophthalmologist Webster Fox performed an immediate capsulotomy following the removal of cataract with alternating cases to allocate his patients, and concluded there was less danger of inflammation than when this capsulotomy was performed in a separate intervention later.⁸⁷ Treatment allocation by alternating cases is a randomization method to prevent foreknowledge of treatment assignments.

The first randomized trial in ophthalmology was performed by Arnall Patz, comparing a high or low oxygen routine for 'retrolental fibroplasia' (retinopathy of prematurity) on a random basis, enabling unbiased analysis of the results. At the end of the first year, seven of twenty-eight infants in the high-oxygen group had advanced retrolental fibroplasia, but none of the thirty-seven cases on low oxygen.⁸⁸

After World War II, the randomized clinical trial methodology developed rapidly, which also occurred in the field of ophthalmology with the foundation of the National Eye Institute, prioritizing careful trial design, of which the Diabetic Retinopathy Study is one of the best-known studies.⁸⁹

Clinical endpoints

An important issue on trial design that still holds through time is choosing the right endpoint: an endpoint which is able to evaluate the safety and effectiveness of new treatments. An endpoint needs to distinguish a potential treatment effect from the effect of time. To identify such endpoints, natural history studies are needed. In 1364, Francesco Petrarca already stressed the effect of nature's time, proposing trials whether people would be better off relying on nature rather than seeking medical treatment.⁹⁰

The quality-adjusted life years won are the eventual outcomes that matter to patients. However, this clinical endpoint would require long follow-up when it is used as the

primary outcome of interventional trials. Besides clinical meaningfulness, an endpoint should also be feasible, reliable and sensitive. Such an endpoint may be found in other measurements which are expected to reflect changes in a clinically meaningful endpoint. They can enable the design of clinical trials with short observation times and small group sizes, and consequently allow a larger number of candidate drugs to be tested in a less costly and time-consuming way. Outcomes, intended to substitute for a clinical endpoint, are so-called surrogate outcomes. It is a 'biomarker', i.e., a laboratory measurement or physical sign which is used in therapeutic trials as a substitute for the eventual clinical endpoint.⁹¹

1.3 Toward clinical trials for Stargardt disease

The past few decades have seen considerable advances in our understanding of clinical phenotypes, natural history, and molecular genetics of rare inherited retinal diseases, including Stargardt disease.⁹² These advances have led to the first steps to a cure with gene therapy,^{70, 71} cell-based therapy,^{74, 75} and pharmacological therapy.^{77, 78} To come toward an effective treatment for Stargardt disease, we need to achieve the best possible level of empirical evidence. Several clinical safety trials have passed and have now proceeded to the next phase, in which the efficacy of therapy is being studied.

Clinical trials for Stargardt disease face unique, but evident challenges because of inherent small populations amenable to treatment and vast heterogeneity within that group. Stargardt disease has a remarkable wide range of severity both at clinical presentation and natural progression. These features are still incompletely described, and consequently difficult to be recognized. Such difficulties lead to failure in detecting significant efficacy changes at follow-up. Moreover, obtaining an accurate description of the full spectra of Stargardt disease also has important implications for selecting patients to participate in clinical trials. The aforementioned classifications based on electrophysiological findings, genotypic and phenotypic characteristics are helpful in describing general characteristics, but still do not suffice; evidence on any therapeutic effects in ongoing trials is still lacking.

Despite the challenges, access to a treatment can only be provided by regulatory approval similar to common diseases, and thus requires establishment of its effectiveness by evidence.⁹³ A randomized-controlled design is still considered the gold standard to adjudicate therapeutic efficacy, and includes an appropriate sample size, statistical power, and methods to minimize bias⁹⁴; all of which has been learnt since the Iron Age. However, this is unfeasible with conventional methods in diseases with a low prevalence, and potentially individually tailored therapies with specific trial populations.^{95, 96} Clinical trials need to be adapted to small populations.

1.4 Aims of this thesis

This thesis provides a strategy for future studies which aim to identify an effect of novel treatments in Stargardt disease. Herein, not only do the challenges of treatment evaluation which have been present since ancient history still apply, but its rare nature and vast heterogeneity also pose additional challenges. These challenges can be overcome by three universal steps:

- Evaluate the effect of nature's time (**Chapter 2**)
- Select the right patients (**Chapter 3**)
- Choose the appropriate method for outcome evaluation (**Chapter 4**)

Natural history of Stargardt disease

Chapter 2 describes unique phenotypic and genotypic characteristics of subgroups within the vast heterogeneity of Stargardt disease, established in the context of previously emerged classifications and staging.^{50, 53, 56} Deep phenotyping will help identify which patients can benefit most from new treatments, and which features are most important to measure in clinical trials. The results are supported by genetic characteristics. Understanding of the natural history provides the basis to create models to describe disease progression.

Diagnosing Stargardt disease

Chapter 3 reveals challenges in the clinical diagnosis of Stargardt disease from the very limited retinal abnormalities in young patients in early diagnosis to the abnormalities mimicking age-related disease in older patients. Early and correct diagnosis is of paramount importance in patient selection at the right time for the right trials.

Measuring progression in Stargardt disease

Chapter 4 creates models of disease progression in Stargardt disease. It reveals the differences in inter-eye concordance between the subtypes of Stargardt disease and gives insight into its consequences in clinical trial design. We simulated potential treatment effects in the youngest and the oldest patients and identified the benefits of a composite outcome measure to assess efficacy in clinical trials for Stargardt disease. Fundus autofluorescence imaging is an important tool to measure disease progression. Its potential phototoxic effect will also be discussed here.

General discussion

Chapter 5 discusses the studies described in this thesis with broad and future perspectives.

References

1. Lang W. Central choroiditis, with disseminated patches in remainder of fundus. *Trans Ophthal Soc UK* 1885;5:140-1.
2. Stargardt K. Über familiäre, progressive degeneration in der makulagegend des auges. *Graefes Arch Clin Exp Ophthalmol* 1909;71:534-50.
3. Blacharski PA. Fundus flavimaculatus. In: Newsome DA, ed. *Retinal dystrophies and degenerations*. New York: Raven Press, 1988.
4. Cideciyan AV, Aleman TS, Swider M, et al. Mutations in ABCA4 result in accumulation of lipofuscin before slowing of the retinoid cycle: a reappraisal of the human disease sequence. *Hum Mol Genet* 2004;13(5):525-34.
5. Sparrow JR, Wu Y, Kim CY, Zhou J. Phospholipid meets all-trans-retinal: the making of RPE bisretinoids. *J Lipid Res* 2010;51(2):247-61.
6. Sun H, Smallwood PM, Nathans J. Biochemical defects in ABCR protein variants associated with human retinopathies. *Nat Genet* 2000;26(2):242-6.
7. Sparrow JR, Boulton M. RPE lipofuscin and its role in retinal pathobiology. *Exp Eye Res* 2005;80(5):595-606.
8. Franceschetti A. A special form of tapetoretinal degeneration: fundus flavimaculatus. *Trans Am Acad Ophthalmol Otolaryngol* 1965;69(6):1048-53.
9. Cideciyan AV, Swider M, Schwartz SB, et al. Predicting Progression of ABCA4-Associated Retinal Degenerations Based on Longitudinal Measurements of the Leading Disease Front. *Invest Ophthalmol Vis Sci* 2015;56(10):5946-55.
10. Armstrong JD, Meyer D, Xu S, Elfervig JL. Long-term follow-up of Stargardt's disease and fundus flavimaculatus. *Ophthalmology* 1998;105(3):448-57; discussion 57-8.
11. Cukras CA, Wong WT, Caruso R, et al. Centrifugal expansion of fundus autofluorescence patterns in Stargardt disease over time. *Arch Ophthalmol* 2012;130(2):171-9.
12. Cideciyan AV, Swider M, Aleman TS, et al. ABCA4 disease progression and a proposed strategy for gene therapy. *Hum Mol Genet* 2009;18(5):931-41.
13. Fujinami K, Sergouniotis PI, Davidson AE, et al. Clinical and molecular analysis of Stargardt disease with preserved foveal structure and function. *Am J Ophthalmol* 2013;156(3):487-501.e1.
14. Fujinami K, Zernant J, Chana RK, et al. Clinical and molecular characteristics of childhood-onset Stargardt disease. *Ophthalmology* 2015;122(2):326-34.
15. Westeneng-van Haften SC, Boon CJ, Cremers FP, et al. Clinical and genetic characteristics of late-onset Stargardt's disease. *Ophthalmology* 2012;119(6):1199-210.
16. Rotenstreich Y, Fishman GA, Anderson RJ. Visual acuity loss and clinical observations in a large series of patients with Stargardt disease. *Ophthalmology* 2003;110(6):1151-8.
17. Fish G, Grey R, Sehmi KS, Bird AC. The dark choroid in posterior retinal dystrophies. *Br J Ophthalmol* 1981;65(5):359-63.
18. Jayasundera T, Rhoades W, Branham K, et al. Peripapillary dark choroid ring as a helpful diagnostic sign in advanced stargardt disease. *Am J Ophthalmol* 2010;149(4):656-60.e2.
19. Anderson DH, Fisher SK, Steinberg RH. Mammalian cones: disc shedding, phagocytosis, and renewal. *Invest Ophthalmol Vis Sci* 1978;17(2):117-33.
20. Sparrow JR, Gregory-Roberts E, Yamamoto K, et al. The bisretinoids of retinal pigment epithelium. *Prog Retin Eye Res* 2012;31(2):121-35.
21. Charbel Issa P, Barnard AR, Singh MS, et al. Fundus autofluorescence in the *Abca4(-/-)* mouse model of Stargardt disease--correlation with accumulation of A2E, retinal function, and histology. *Invest Ophthalmol Vis Sci* 2013;54(8):5602-12.
22. Lois N, Halfyard AS, Bird AC, et al. Fundus autofluorescence in Stargardt macular dystrophy-fundus flavimaculatus. *Am J Ophthalmol* 2004;138(1):55-63.
23. von Ruckmann A, Fitzke FW, Bird AC. In vivo fundus autofluorescence in macular dystrophies. *Arch Ophthalmol* 1997;115(5):609-15.

24. Smith RT, Gomes NL, Barile G, et al. Lipofuscin and autofluorescence metrics in progressive STGD. *Invest Ophthalmol Vis Sci* 2009;50(8):3907-14.
25. Saksens NT, Fleckenstein M, Schmitz-Valckenberg S, et al. Macular dystrophies mimicking age-related macular degeneration. *Prog Retin Eye Res* 2014;39:23-57.
26. Østerberg GA. Topography of the Layer of Rods and Cones in the Human Retina. *Acta Ophthalmol [Suppl]* 1935;6:1-102.
27. Curcio CA, Sloan KR, Kalina RE, Hendrickson AE. Human photoreceptor topography. *J Comp Neurol* 1990;292(4):497-523.
28. Lee W, Noupou K, Oll M, et al. The External Limiting Membrane in Early-Onset Stargardt Disease. *Invest Ophthalmol Vis Sci* 2014.
29. Burke TR, Yzer S, Zernant J, et al. Abnormality in the external limiting membrane in early Stargardt disease. *Ophthalmic Genet* 2013;34(1-2):75-7.
30. Burke TR, Rhee DW, Smith RT, et al. Quantification of peripapillary sparing and macular involvement in Stargardt disease (STGD1). *Invest Ophthalmol Vis Sci* 2011;52(11):8006-15.
31. Ergun E, Hermann B, Wirtitsch M, et al. Assessment of central visual function in Stargardt's disease/fundus flavimaculatus with ultrahigh-resolution optical coherence tomography. *Invest Ophthalmol Vis Sci* 2005;46(1):310-6.
32. Allikmets R, Singh N, Sun H, et al. A photoreceptor cell-specific ATP-binding transporter gene (ABCR) is mutated in recessive Stargardt macular dystrophy. *Nat Genet* 1997;15(3):236-46.
33. Hoyng CB, Poppelaars F, van de Pol TJ, et al. Genetic fine mapping of the gene for recessive Stargardt disease. *Hum Genet* 1996;98(4):500-4.
34. Jaakson K, Zernant J, Kulm M, et al. Genotyping microarray (gene chip) for the ABCR (ABCA4) gene. *Hum Mutat* 2003;22(5):395-403.
35. Zernant J, Xie YA, Ayuso C, et al. Analysis of the ABCA4 genomic locus in Stargardt disease. *Hum Mol Genet* 2014;23(25):6797-806.
36. Fujinami K, Zernant J, Chana RK, et al. ABCA4 gene screening by next-generation sequencing in a British cohort. *Invest Ophthalmol Vis Sci* 2013;54(10):6662-74.
37. Zernant J, Schubert C, Im KM, et al. Analysis of the ABCA4 gene by next-generation sequencing. *Invest Ophthalmol Vis Sci* 2011;52(11):8479-87.
38. Lin B, Cai XB, Zheng ZL, et al. Clinical and genetic analyses reveal novel pathogenic ABCA4 mutations in Stargardt disease families. *Sci Rep* 2016;6:35414.
39. Sun H, Nathans J. Stargardt's ABCR is localized to the disc membrane of retinal rod outer segments. *Nat Genet* 1997;17(1):15-6.
40. Molday LL, Rabin AR, Molday RS. ABCR expression in foveal cone photoreceptors and its role in Stargardt macular dystrophy. *Nat Genet* 2000;25(3):257-8.
41. Liu J, Itagaki Y, Ben-Shabat S, et al. The biosynthesis of A2E, a fluorophore of aging retina, involves the formation of the precursor, A2-PE, in the photoreceptor outer segment membrane. *J Biol Chem* 2000;275(38):29354-60.
42. Quazi F, Molday RS. ATP-binding cassette transporter ABCA4 and chemical isomerization protect photoreceptor cells from the toxic accumulation of excess 11-cis-retinal. *Proc Natl Acad Sci U S A* 2014;111(13):5024-9.
43. Quazi F, Lenevich S, Molday RS. ABCA4 is an N-retinylidene-phosphatidylethanolamine and phosphatidylethanolamine importer. *Nat Commun* 2012;3:925.
44. Weng J, Mata NL, Azarian SM, et al. Insights into the function of Rim protein in photoreceptors and etiology of Stargardt's disease from the phenotype in *abcr* knockout mice. *Cell* 1999;98(1):13-23.
45. Sparrow JR, Parish CA, Hashimoto M, Nakanishi K. A2E, a lipofuscin fluorophore, in human retinal pigmented epithelial cells in culture. *Invest Ophthalmol Vis Sci* 1999;40(12):2988-95.
46. Wu Y, Fishkin NE, Pande A, et al. Novel lipofuscin bisretinoids prominent in human retina and in a model of recessive Stargardt disease. *J Biol Chem* 2009;284(30):20155-66.
47. Solomon SG, Lennie P. The machinery of colour vision. *Nat Rev Neurosci* 2007;8(4):276-86.
48. Ebrey T, Koutalos Y. Vertebrate photoreceptors. *Prog Retin Eye Res* 2001;20(1):49-94.
49. Wald G. Molecular basis of visual excitation. *Science* 1968;162(3850):230-9.


50. Fishman GA. Fundus flavimaculatus. A clinical classification. *Arch Ophthalmol* 1976;94(12):2061-7.
51. Fishman GA, Stone EM, Grover S, et al. Variation of clinical expression in patients with Stargardt dystrophy and sequence variations in the ABCR gene. *Arch Ophthalmol* 1999;117(4):504-10.
52. McCulloch DL, Marmor MF, Brigell MG, et al. ISCEV Standard for full-field clinical electroretinography (2015 update). *Doc Ophthalmol* 2015;130(1):1-12.
53. Lois N, Holder GE, Bunce C, et al. Phenotypic subtypes of Stargardt macular dystrophy-fundus flavimaculatus. *Arch Ophthalmol* 2001;119(3):359-69.
54. Fujinami K, Lois N, Davidson AE, et al. A longitudinal study of stargardt disease: clinical and electrophysiologic assessment, progression, and genotype correlations. *Am J Ophthalmol* 2013;155(6):1075-88.e13.
55. Zahid S, Jayasundera T, Rhoades W, et al. Clinical phenotypes and prognostic full-field electroretinographic findings in Stargardt disease. *Am J Ophthalmol* 2013;155(3):465-73.e3.
56. van Driel MA, Maugeri A, Klevering BJ, et al. ABCR unites what ophthalmologists divide(s). *Ophthalmic Genet* 1998;19(3):117-22.
57. Maugeri A, van Driel MA, van de Pol DJ, et al. The 2588G-->C mutation in the ABCR gene is a mild frequent founder mutation in the Western European population and allows the classification of ABCR mutations in patients with Stargardt disease. *Am J Hum Genet* 1999;64(4):1024-35.
58. Maugeri A, Klevering BJ, Rohrschneider K, et al. Mutations in the ABCA4 (ABCR) gene are the major cause of autosomal recessive cone-rod dystrophy. *Am J Hum Genet* 2000;67(4):960-6.
59. Fakin A, Robson AG, Fujinami K, et al. Phenotype and Progression of Retinal Degeneration Associated With Nullizigosity of ABCA4. *Invest Ophthalmol Vis Sci* 2016;57(11):4668-78.
60. Lewis RA, Shroyer NF, Singh N, et al. Genotype/Phenotype analysis of a photoreceptor-specific ATP-binding cassette transporter gene, ABCR, in Stargardt disease. *Am J Hum Genet* 1999;64(2):422-34.
61. Riveiro-Alvarez R, Lopez-Martinez MA, Zernant J, et al. Outcome of ABCA4 disease-associated alleles in autosomal recessive retinal dystrophies: retrospective analysis in 420 Spanish families. *Ophthalmology* 2013;120(11):2332-7.
62. Klevering BJ, Deutman AF, Maugeri A, et al. The spectrum of retinal phenotypes caused by mutations in the ABCA4 gene. *Graefes Arch Clin Exp Ophthalmol* 2005;243(2):90-100.
63. Klevering BJ, Blankenagel A, Maugeri A, et al. Phenotypic spectrum of autosomal recessive cone-rod dystrophies caused by mutations in the ABCA4 (ABCR) gene. *Invest Ophthalmol Vis Sci* 2002;43(6):1980-5.
64. Rozet JM, Gerber S, Ghazi I, et al. Mutations of the retinal specific ATP binding transporter gene (ABCR) in a single family segregating both autosomal recessive retinitis pigmentosa RP19 and Stargardt disease: evidence of clinical heterogeneity at this locus. *J Med Genet* 1999;36(6):447-51.
65. Allikmets R, Shroyer NF, Singh N, et al. Mutation of the Stargardt disease gene (ABCR) in age-related macular degeneration. *Science* 1997;277(5333):1805-7.
66. Chen Y, Okano K, Maeda T, et al. Mechanism of all-trans-retinal toxicity with implications for stargardt disease and age-related macular degeneration. *J Biol Chem* 2012;287(7):5059-69.
67. Radu RA, Mata NL, Bagla A, Travis GH. Light exposure stimulates formation of A2E oxiranes in a mouse model of Stargardt's macular degeneration. *Proc Natl Acad Sci U S A* 2004;101(16):5928-33.
68. Teussink MM, Lee MD, Smith RT, et al. The effect of light deprivation in patients with Stargardt disease. *Am J Ophthalmol* 2015;159(5):964-72.e2.
69. Radu RA, Yuan Q, Hu J, et al. Accelerated accumulation of lipofuscin pigments in the RPE of a mouse model for ABCA4-mediated retinal dystrophies following Vitamin A supplementation. *Invest Ophthalmol Vis Sci* 2008;49(9):3821-9.
70. Han Z, Conley SM, Naash MI. Gene therapy for Stargardt disease associated with ABCA4 gene. *Adv Exp Med Biol* 2014;801:719-24.
71. Binley K, Widdowson P, Loader J, et al. Transduction of photoreceptors with equine infectious anemia virus lentiviral vectors: safety and biodistribution of StarGen for Stargardt disease. *Invest Ophthalmol Vis Sci* 2013;54(6):4061-71.
72. Kong J, Kim SR, Binley K, et al. Correction of the disease phenotype in the mouse model of Stargardt disease by lentiviral gene therapy. *Gene Ther* 2008;15(19):1311-20.

73. Audo IS, Weleber RG, Stout T, et al. Early findings in a Phase I/IIa clinical program for Stargardt disease (STGD1, MIM #248200). *Investigative Ophthalmology & Visual Science* 2015;56(7):3819-.
74. Schwartz SD, Hubschman JP, Heilwell G, et al. Embryonic stem cell trials for macular degeneration: a preliminary report. *Lancet* 2012;379(9817):713-20.
75. Schwartz SD, Regillo CD, Lam BL, et al. Human embryonic stem cell-derived retinal pigment epithelium in patients with age-related macular degeneration and Stargardt's macular dystrophy: follow-up of two open-label phase 1/2 studies. *Lancet* 2015;385(9967):509-16.
76. Saad L, Washington I. Can Vitamin A be Improved to Prevent Blindness due to Age-Related Macular Degeneration, Stargardt Disease and Other Retinal Dystrophies? *Adv Exp Med Biol* 2016;854:355-61.
77. Charbel Issa P, Barnard AR, Herrmann P, et al. Rescue of the Stargardt phenotype in Abca4 knockout mice through inhibition of vitamin A dimerization. *Proc Natl Acad Sci U S A* 2015;112(27):8415-20.
78. Radu RA, Mata NL, Nusinowitz S, et al. Treatment with isotretinoin inhibits lipofuscin accumulation in a mouse model of recessive Stargardt's macular degeneration. *Proc Natl Acad Sci U S A* 2003;100(8):4742-7.
79. Sackett DL, Rosenberg WM, Gray JA, et al. Evidence based medicine: what it is and what it isn't. *BMJ* 1996;312(7023):71-2.
80. Evidence-Based Medicine Working G. Evidence-based medicine. A new approach to teaching the practice of medicine. *JAMA* 1992;268(17):2420-5.
81. Daniel 1:12-13. In: *The Holy Bible*. King James Version.
82. Collier R. Legumes, lemons and streptomycin: a short history of the clinical trial. *CMAJ* 2009;180(1):23-4.
83. Zarshenas MM, Mehdizadeh A, Zargaran A, Mohagheghzadeh A. Rhazes (865-925 AD). *J Neurol* 2012;259(5):1001-2.
84. Tibi S. Al-Razi and Islamic medicine in the 9th century. *J R Soc Med* 2006;99(4):206-7.
85. Nasser M, Tibi A, Savage-Smith E. Ibn Sina's Canon of Medicine: 11th century rules for assessing the effects of drugs. *J R Soc Med* 2009;102(2):78-80.
86. Bhatt A. Evolution of clinical research: a history before and beyond James Lind. *Perspect Clin Res* 2010;1(1):6-10.
87. Fox L. Immediate capsulotomy following the removal of cataract. read before the medical society of the state of Pennsylvania, May 17, 1894. *Journal of the American Medical Association* 1894;XXII(22):837-9.
88. Patz A, Hoek LE, De La Cruz E. Studies on the effect of high oxygen administration in retrolental fibroplasia: I. Nursery observations. *American journal of ophthalmology* 1952;35(9):1248-53.
89. Preliminary report on effects of photocoagulation therapy. The Diabetic Retinopathy Study Research Group. *Am J Ophthalmol* 1976;81(4):383-96.
90. Chalmers I, Dukan E, Podolsky S, Davey Smith G. The advent of fair treatment allocation schedules in clinical trials during the 19th and early 20th centuries. *J R Soc Med* 2012;105(5):221-7.
91. Temple R. Are surrogate markers adequate to assess cardiovascular disease drugs? *JAMA* 1999;282(8):790-5.
92. Berger W, Kloeckener-Gruissem B, Neidhardt J. The molecular basis of human retinal and vitreoretinal diseases. *Prog Retin Eye Res* 2010;29(5):335-75.
93. Griggs RC, Batshaw M, Dunkle M, et al. Clinical research for rare disease: opportunities, challenges, and solutions. *Mol Genet Metab* 2009;96(1):20-6.
94. Schulz KF, Grimes DA. Blinding in randomised trials: hiding who got what. *Lancet* 2002;359(9307):696-700.
95. Cornu C, Kassai B, Fisch R, et al. Experimental designs for small randomised clinical trials: an algorithm for choice. *Orphanet J Rare Dis* 2013;8:48.
96. Bell SA, Tudur Smith C. A comparison of interventional clinical trials in rare versus non-rare diseases: an analysis of ClinicalTrials.gov. *Orphanet J Rare Dis* 2014;9:170.



CHAPTER 2

Natural history of Stargardt disease



"In its natural course, early-onset Stargardt disease initially presents with variable full-field electroretinographic abnormalities and fundusoscopic findings. As this retinal degeneration progresses, the spectrum of phenotypes eventually converges, causing profound chorioretinal atrophy and severe vision loss."

Stanley Lambertus

Ramon A.C. van Huet

Nathalie M. Bax

Lies H. Hoefsloot

Frans P.M. Cremers

Camiel J.F. Boon

B. Jeroen Klevering

Carel B. Hoyng

Ophthalmology, 2015 Feb;122(2):335-44. doi: 10.1016/j.ophtha.2014.08.032.

The authors thank Jelina Ye and Ellen van den Wittenboer for their contribution, without which this study could not have been completed.

2.1 Early-onset Stargardt disease: phenotypic and genotypic characteristics

OBJECTIVE: To describe the phenotype and genotype of patients with early-onset Stargardt disease.

DESIGN: Retrospective cohort study.

PARTICIPANTS: Fifty-one Stargardt patients with age at onset ≤ 10 years.

METHODS: We reviewed patient medical records for age at onset, medical history, initial symptoms, best-corrected visual acuity (BCVA), ophthalmoscopy, fundus photography, fundus autofluorescence (FAF), fluorescein angiography (FA), spectral-domain optical coherence tomography (SD-OCT), and full-field electroretinography (ffERG). The ABCA4 gene was screened for mutations.

MAIN OUTCOME MEASURES: Age at onset, BCVA, fundus appearance, FAF, FA, SD-OCT, ffERG, and presence of ABCA4 mutations.

RESULTS: The mean age at onset was 7.2 years (range, 1–10). The median times to develop BCVA of 20/32, 20/80, 20/200, and 20/500 were 3, 5, 12, and 23 years, respectively. Initial ophthalmoscopy in 41 patients revealed either no abnormalities or foveal retinal pigment epithelium (RPE) changes in 10 and 9 patients, respectively; the other 22 patients had foveal atrophy, atrophic RPE lesions, and/or irregular yellow-white fundus flecks. On FA, there was a “dark choroid” in 21 out of 29 patients. In 14 out of 50 patients, foveal atrophy occurred before flecks developed. On FAF, there was centrifugal expansion of disseminated atrophic spots, which progressed to the eventual profound chorioretinal atrophy. Spectral-domain OCT revealed early photoreceptor damage followed by atrophy of the outer retina, RPE, and choroid. On ffERG in 26 patients, 15 had normal amplitudes, and 11 had reduced photopic and/or scotopic amplitudes at their first visit. We found no correlation between ffERG abnormalities and the rate of vision loss. Thirteen out of 25 patients had progressive ffERG abnormalities. Finally, genetic screening of 44 patients revealed ≥ 2 ABCA4 mutations in 37 patients and single heterozygous mutations in 7.

CONCLUSIONS: In early-onset Stargardt, initial ophthalmoscopy can reveal no abnormalities or minor retinal abnormalities. Yellow-white flecks can be preceded by foveal atrophy and may be visible only on FAF. Although ffERG is insufficient for predicting the rate of vision loss, abnormalities can develop. Over time, visual acuity declines rapidly in parallel with progressive retinal degeneration, resulting in profound chorioretinal atrophy. Thus, early-onset Stargardt lies at the severe end of the spectrum of ABCA4-associated retinal phenotypes.

Introduction

Stargardt disease (STGD1) is the most prevalent inherited juvenile-onset retinal dystrophy, with a mean age at onset of 15.2 years.^{1, 2} The inheritance pattern of STGD1 is autosomal recessive, and the disease is characterized by the presence of irregular yellow-white fundus flecks in the posterior pole.^{2–4} Over time, the disease progresses to include macular depigmentation and chorioretinal atrophy. Typical STGD1 patients have normal—or near-normal—panretinal cone and rod function on full-field electroretinography (ffERG); however, progressive abnormalities in photopic and scotopic amplitudes have been reported.^{5–7} Blockage of choroidal fluorescence (the so-called dark choroid sign) on fluorescein angiography is present in 80% of STGD1 patients.^{8–10} The aforementioned yellow-white fundus flecks are hyperautofluorescent on fundus autofluorescence (FAF), presumably owing to an accumulation of lipofuscin fluorophores in the retinal pigment epithelium (RPE).^{11, 12} Spectral-domain optical coherence tomography (SD-OCT) can reveal changes in the outer nuclear layer, as well as photoreceptor loss, RPE abnormalities, and a general thinning of the retina.¹³

Mutations in the *ABCA4* gene have been associated with a spectrum of retinal diseases ranging from mild phenotypes (e.g., late-onset STGD1 with relatively preserved visual function) to severe, early-onset retinitis pigmentosa accompanied by a rapid loss of central and peripheral photoreceptors.^{14–16} The *ABCA4* gene encodes the retinal-specific adenosine triphosphate-binding cassette transporter.¹⁷ *ABCA4* is expressed in both cones and rods. In rod cells, the *ABCA4* protein is localized at the rim of the outer segment discs, where *ABCA4* transports all-trans-retinal from the lumen of the outer segment disc to the cytoplasm of the photoreceptor cell.¹⁸ The accumulation of all-trans-retinal—and its toxic derivatives—eventually results in the death of RPE cells and photoreceptor cells.^{19–21} The *ABCA4* gene has high mutation heterogeneity; >700 distinct mutations have been identified to date, with a wide range of effects on *ABCA4* protein function. A model to correlate the phenotype with the functional severity of the *ABCA4* mutation has been proposed.^{22, 23} According to this model, STGD1 results from mild to moderate *ABCA4* impairment.

Among patients who are diagnosed with STGD1, the disease has remarkably wide clinical variability with respect to the general course of the disease, the retinal features, and the electrophysiologic findings.^{5, 8, 14, 15} Stargardt disease has both genetic and clinical overlap with cone-rod dystrophy, and this may cause confusion among general ophthalmologists; indeed, diagnosing STGD1 can be challenging at an early age. Therefore, obtaining an accurate description of the full spectrum of *ABCA4*-associated retinal dystrophies—including STGD1—is essential for providing appropriate patient counseling

and adequate disease management, and may have important implications for selecting patients to participate in gene therapy trials. Although clinical features of STGD1 patients with a very young onset have been described in heterogeneous cohorts,^{5, 7, 24, 25} there is lack of studies concerning the natural history of these patients. Herein, we have provided a comprehensive description of the initial and longitudinal clinical and genetic characteristics of a large number of patients with early-onset Stargardt, which we defined as an age at onset ≤ 10 years.

Methods

Patients and genetic analysis

The database of the Department of Ophthalmology at Radboud university medical center (Nijmegen, the Netherlands) contains 426 patients with a clinical diagnosis of STGD1. For 258 of these patients, the ABCA4 gene was analyzed by the Department of Human Genetics at Radboud university medical center (Nijmegen, the Netherlands). Known mutations were screened using the arrayed-primer extension microarray (Asper Biotech, Tartu, Estonia), and exon duplications and/or deletions were detected using multiplex ligation-dependent probe amplification (MRC-Holland P151/P152). If no mutations or only a single heterozygous mutation was identified, the exons and intron-exon boundaries were sequenced using the Sanger method to screen for mutations in the other allele. All identified mutations were confirmed using Sanger sequencing. In total, 199 patients contained ≥ 1 mutation in the ABCA4 gene.

Age at onset of disease was defined as the age at which symptoms were first noticed by the patient. If this information was not available, we used the patient's age at which he or she first visited an ophthalmologist.

In this study, we included 51 patients with an age at onset of ≤ 10 years and one of the following criteria: ≥ 2 ABCA4 mutations ($n = 37$); 1 ABCA4 mutation and the presence of yellow-white flecks ($n = 7$); or in the absence of ABCA4 analysis, the presence of yellow-white flecks, and either a dark choroid or an atrophic macular lesion ($n = 7$).

This study was approved by the Institutional Ethics Committee and was performed in accordance with the Declaration of Helsinki. All patients provided informed consent before giving a blood sample and receiving additional ophthalmologic examinations.

Clinical Evaluation

We defined the duration of disease as the time interval between the patient's age at onset (defined as described) and the age at the last visit. Best-corrected visual acuity

(BCVA) was measured using a Snellen chart, then transformed into the logarithm of the minimum angle of resolution (logMAR) for subsequent analysis. A logMAR value of 1.9, 2.3, or 2.7 was assigned to the patient's ability to count fingers, detect hand movements, or perceive light, respectively.²⁶

Fundus characteristics were documented for 41 patients using fundus photography (Topcon TRC-50IX, Topcon Corporation, Tokyo, Japan). Fundus autofluorescence was performed in 32 patients using a confocal scanning laser ophthalmoscope (Spectralis, Heidelberg Engineering, Heidelberg, Germany) fitted with an optically pumped solid-state laser (488-nm excitation). Atrophic chorioretinal lesions outside the fovea were stratified into 2 groups: (1) a patchy pattern consisting of mild disseminated hypo-autofluorescent spots and (2) sharply demarcated chorioretinal atrophic lesions with an absence of autofluorescence; the extent of these lesions was then classified as either (1) lesions that were limited to the posterior pole, or (2) lesions that extended beyond the vascular arcades. Cross-sectional images were obtained for 30 patients using SD-OCT (Spectralis, Heidelberg Engineering). Fluorescein angiography (Topcon TRC-50IX, Topcon Corporation; Spectralis, Heidelberg Engineering) was performed in 32 patients to determine the presence or absence of the "dark choroid" sign.

Full-field ERG was performed in 43 patients in accordance with the guidelines established by the International Society for Clinical Electrophysiology of Vision (ISCEV)²⁷ using either Dawson-Trick-Litzkow electrodes or contact lens electrodes together with the RETI-port system (Roland Consults, Stasche & Finger GmbH, Brandenburg an der Havel, Germany). Dawson-Trick-Litzkow and contact lens electrodes have similarly high signal stability.²⁸ Based on the ffERG results, the patients were assigned to 3 groups as described previously⁵: group 1 consisted of patients with normal ffERG amplitudes, group 2 consisted of patients with reduced photopic amplitude (<5% of normal range, <78 μ V [B-wave]) and normal scotopic amplitude, and group 3 consisted of patients with reduced photopic and scotopic amplitudes (<5% of normal range, <263 μ V [B-wave]).

Statistical analysis

Data were analyzed using SPSS version 20.0 (IBM Corp, Armonk, NY). Kaplan-Meier "survival" curves were used to analyze the interval between the age at onset and the age at which the following endpoints were achieved: Mild visual impairment (≥ 0.2 logMAR; Snellen $\leq 20/32$), moderate visual impairment (≥ 0.6 logMAR; Snellen $\leq 20/80$), severe visual impairment (≥ 1.0 logMAR; Snellen $\leq 20/200$), and blindness (≥ 1.4 logMAR; Snellen $\leq 20/500$).²⁹ Cox regression analysis was used to compare the ffERG groups. Differences with a *P* value of ≤ 0.05 were considered significant.

Results

Initial clinical characteristics

A total of 51 patients (28 men and 23 women) were included in this study. The mean (\pm standard deviation) age at onset was 7.2 ± 2.2 years (median, 8; range, 1–10).

Visual acuity

In each case, the initial symptom of the disease was a decline in visual acuity noticed by the patient, the patient's parents, or the school physician. Where available ($n = 41$ patients), the mean BCVA at the first visit to an ophthalmologist was 0.51 ± 0.36 logMAR (median, 0.48; range, 0–1.15), Snellen 20/65. In 13 patients, the vision loss was initially unexplained. Six of these 13 patients were diagnosed with functional vision loss, and 6 other patients were diagnosed initially with cone–rod dystrophy. Of the 51 patients, 22 were diagnosed with STGD1 ≥ 3 years after the initial symptoms appeared (range, 3–30).

Retinal features

Ophthalmoscopy performed at the first visit revealed no retinal abnormalities in 10 out of 41 patients. Nine additional patients had foveal RPE changes, and the remaining 22 patients had foveal atrophy, atrophic RPE lesions that were not limited to the fovea,

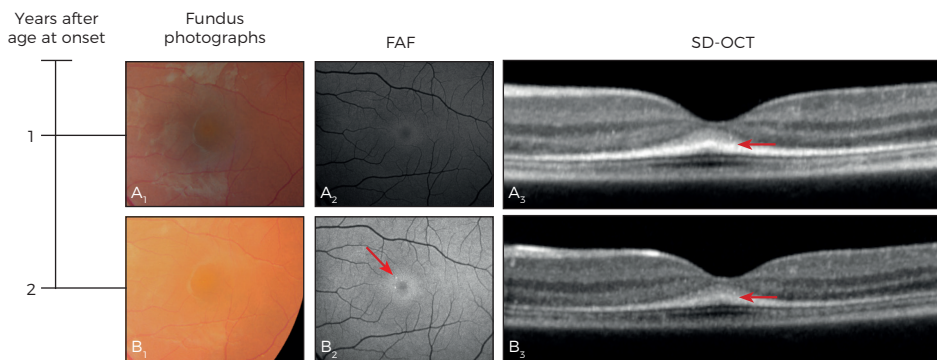


Figure 1. Retinal imaging of patient 4 (age at onset, 6 years; best-corrected visual acuity, 0.24 logMAR, Snellen 20/35; *ABCA4* genotype, p.Thr983Ala and c.5461-10T>C (p.?) at 7 ($A_{1,2,3}$) and 8 ($B_{1,2,3}$) years of age. Initially, only subtle foveal hyperautofluorescence was present (A_2); 1 year later, small parafoveal hyperautofluorescent flecks were present (the arrow in B_2), despite a lack of apparent abnormalities on ophthalmoscopy. Spectral-domain optical coherence tomography (SD-OCT) revealed foveal thickening of the band representing the external limiting membrane (the arrows in A_3 – B_3). FAF = fundus autofluorescence; logMAR = logarithm of the minimum angle of resolution.

and/or irregular yellow-white fundus flecks. Fluorescein angiography in 29 patients revealed an absence of choroidal fluorescence (the so-called dark choroid) in 21 patients. In patient 4, FAF revealed subtle hyperautofluorescence of the fovea, and SD-OCT revealed thickening of what appeared to be the external limiting membrane (Figure 1A_{1,2,3}). One year later, this patient developed several small parafoveal hyperautofluorescent flecks with no apparent abnormalities on ophthalmoscopy (Figure 1B₂).

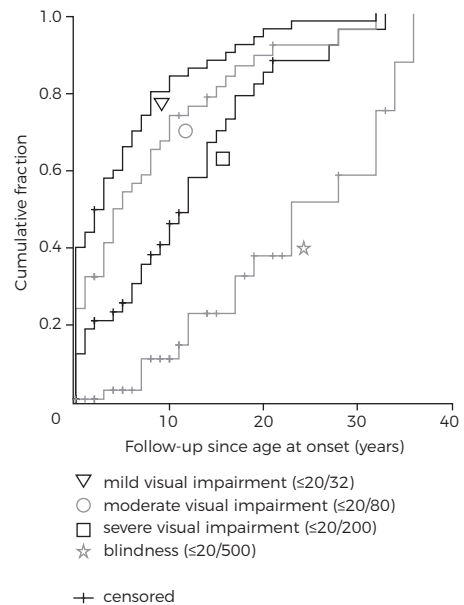
Electrophysiologic findings

At their first visit, ffERG data were collected for 26 patients, and the patients were classified based on their findings. Group 1 (patients with normal photopic and scotopic amplitudes) contained 15 patients (58%), group 2 (patients with reduced photopic amplitude and normal scotopic amplitudes) contained 4 patients (15%), and group 3 (patients with reduced photopic and scotopic amplitudes) contained 6 patients (23%). One patient could not be classified into 1 of these 3 groups because only the scotopic amplitudes were reduced moderately, although no pigmentary retinopathy was observed. We found no correlation between the ffERG group classification at the first visit and progression toward mild visual impairment ($P = 0.485$), moderate visual impairment ($P = 0.309$), severe visual impairment ($P = 0.203$), or blindness ($P = 0.647$).

Natural course

The mean disease duration was 17.1 ± 14.5 years (median, 11; range, 0–56). The follow-up period ranged from a single examination in 3 patients to 47 years (mean, 12.4 ± 12.6 ; median, 9). The clinical and genetic characteristics of the patient cohort at the last examination are summarized in Table 1.

Figure 2. Kaplan-Meier curves showing the cumulative fraction in early-onset Stargardt with the following clinical endpoints: mild visual impairment (≥ 0.2 logarithm of the minimum angle of resolution [$\log\text{MAR}$], Snellen $\leq 20/32$, triangle), moderate visual impairment (≥ 0.6 $\log\text{MAR}$; Snellen $\leq 20/80$, circle), severe visual impairment (≥ 1.0 $\log\text{MAR}$, Snellen $\leq 20/200$, square), and blindness (≥ 1.4 $\log\text{MAR}$, Snellen $\leq 20/500$, star). Censored observations are depicted as vertical bars.



Patient	Age at onset (y)	Age (y)*	BCVA (logMAR [Snellen])*	Fundus findings		ffERG*†		Mutations	
				Flecks	Dark choroid	Photopic	Scotopic	Allele 1	Allele 2
1	7‡	18	0.30 (20/40)	Yes	Yes	NP	NP	c.2588G>C. c.656G>C. c.1822T>A	
2	8	14	0.89 (20/155)	Yes	NP	NP	NP	c.5461-10T>C	c.5461-10T>C
3	6	17	1.90 (CF)	Yes	Yes	N	MR	c.5461-10T>C	c.5461-10T>C
4	6	8	0.20 (20/32)	Yes	Yes	MR	N	c.2947A>G	c.5461-10T>C
5	6	57	2.30 (HM)	Yes	Yes	ND	ND	c.768G>T	c.443-?-570+?del
6	9	10	0.40 (20/50)	Yes	Yes	SR	N	c.768G>T	NI
7	6	40	1.30 (20/400)	Yes	NP	NP	NP	c.5461-10T>C	c.5714+5G>A
8	4	35	1.90 (CF)	Yes	Yes	MR	N	c.4462T>C	c.2919-?-3328+?del
9	9	25	1.90 (CF)	Yes	Yes	NP	NP	c.768G>T	NI
10	3	36	1.90 (CF)	Yes	Yes	SR	SR	c.3813G>C	NI
11	5	52	2.30 (HM)	Yes	NP	MR	MR	c.6411T>A	NI
12	7	8	1.22 (20/333)	Yes	Yes	MR	MR	c.768G>T	c.5461-10T>C
13	7	7	0.33 (20/43)	Yes	Yes	MR	MR		NP
14	9	17	1.15 (20/286)	Yes	No	N	N	c.3874C>T	c.6543_6578del
15	3	14	1.00 (20/200)	Yes	NP	N	N	c.4539+1G>T	c.768G>T
16	9	11	1.10 (20/250)	Yes	No	MR	N		NP
17	10	47	1.90 (CF)	Yes	Yes	SR	SR		NP
18	7	48	2.30 (HM)	Yes	NP	SR	SR	c.768G>T	c.5461-10T>C
19	6	43	1.90 (CF)	Yes	NP	SR	SR	c.768G>T	c.5461-10T>C
20	8	33	1.10 (20/250)	Yes	No	N	N	c.5161-5162delAC	c.5882G>A
21	8	64	1.90 (CF)	Yes	NP	ND	ND	c.2947A>G	c.4506C>A
22	8	31	1.90 (CF)	Yes	NP	SR	SR		NP
23	9	51	1.90 (CF)	Yes	Yes	ND	ND	c.768G>T	c.5461-10T>C
24	3	19	1.00 (20/200)	Yes	No	ND	N	c.5461-10T>C	c.6320G>A
25	9	16	1.30 (20/400)	Yes	NP	MR	N	c.214G>A	c.5461-10T>C
26	5	10	1.10 (20/250)	Yes	NP	NP	NP	c.5762_5763dup	c.2919-?-3328+?del
27	10	31	0.40 (20/50)	NP§	NP§	NP	NP	c.455G>A	c.5461-10T>C
28	9	19	0.72 (20/105)	Yes	NP	N	N	c.5461-10T>C	NI
29	1	28	1.90 (CF)	Yes	Yes	SR	N	c.5585-10T>C	NI
30	8	26	1.30 (20/400)	Yes	Yes	N	N	c.5312+1G>A	c.286A>G
31	10	22	1.90 (CF)	Yes	Yes	SR	N	c.2588G>C	c.4539+1G>T
32	9	15	0.80 (20/125)	Yes	Yes	NP	NP	c.2588G>C	c.4539+1G>T
33	7	18	1.15 (20/286)	Yes	NP	N	N	c.1957C>T. c.6320G>A. c.3449G>A	
34	10	31	1.15 (20/286)	Yes	Yes	N	N	c.5461-10T>C	c.5537T>C
35	7	11	0.80 (20/125)	Yes	NP	N	N	c.818G>A	NI
36	7	7	0.80 (20/125)	No	Yes	N	N	c.872C>T.4224G>T	c.2947A>G
37	8	22	1.15 (20/286)	Yes	NP	N	N	c.1822T>A	c.5882G>A
38	10	13	0.52 (20/67)	No	No	N	N	c.5882G>A	c.5882G>A
39	10	16	1.15 (20/286)	Yes	No	N	N	c.768G>T	c.1822T>A
40	5	24	1.30 (20/400)	Yes	Yes	MR	MR	c.768G>T	c.5461-10T>C
41	6	22	1.90 (CF)	Yes	Yes	ND	ND	c.1622T>C.3113C>T	c.1622T>C.3113C>T
42	10	22	1.30 (20/400)	Yes	Yes	MR	N		NP
43	7	19	1.10 (20/250)	Yes	NP	N	N		NP
44	8	19	1.00 (20/200)	Yes	NP	SR	N		NP
45	5	15	1.00 (20/200)	Yes	Yes	MR	N	c.3335C>A	c.5461-10T>C
46	7	31	2.30 (HM)	Yes	No	ND	MR	c.1822T>A	c.5461-10T>C
47	9	20	0.85 (20/143)	Yes	NP	N	N	c.122G>A	c.286A>G
48	4	32	1.00 (20/200)	Yes	NP	NP	NP	c.5882G>A	NI
49	8	18	1.00 (20/200)	Yes	No	SR	ND	c.286A>G	c.286A>G
50	9	14	0.80 (20/125)	No	No	ND	SR	c.4773+1G>A	c.5461-10T>C
51	8	43	1.90 (CF)	Yes	No	ND	ND	c.768G>T	c.5113C>T

Table 1. Clinical and genetic characteristics of 51 early-onset Stargardt patients.

* Age, BCVA, and ffERG at last examination.

† The abbreviations reflect the B-wave amplitude: N = normal (equal to or above the lower 5% of the range for a normal population; photopic ≥ 78 μV , scotopic ≥ 263 μV); MR = moderately reduced (1%-5% or normal range; photopic ≥ 69 μV and < 78 μV , scotopic ≥ 195 μV and < 263 μV); SR = severely reduced ($< 1\%$ of normal range; photopic < 69 μV , scotopic < 195 μV); ND = not detectable (flat amplitudes).

Visual acuity

A survival analysis yielded a median interval and 95% CI between age at onset and a decline in BCVA to mild visual impairment, moderate visual impairment, severe visual impairment, and blindness of 3 (95% CI, 1.1–4.9), 5 (95% CI, 2.2–7.8), 12 (95% CI, 9.3–14.7), and 23 (95% CI, 13.2–32.8) years, respectively (Figure 2). Mean patient age at the last recorded visit was 24.9 ± 14.0 years (median, 20; range, 7–64), and mean BCVA was 1.29 ± 0.58 logMAR (median, 1.15; range, 0.20–2.30), Snellen 20/386.

Retinal features

We observed irregular yellow-white fundus flecks in 47 out of 50 patients. These flecks were not always evident at the first examination, but they developed within an average of 2.9 ± 4.1 years (median, 0; range, 0–17) of the first visit. The location of these flecks varied among the patients: In 10 patients, the flecks were present exclusively in the central macula; in 17 patients, the flecks were scattered throughout the posterior pole, but did not extend beyond the vascular arcades; and the remaining 20 patients presented with a fundus flavimaculatus pattern with numerous flecks in the central and mid-peripheral retina. Foveal atrophy was reported in 38 patients and occurred within 1.9 ± 3.3 years (median, 0; range, 0–13) of the initial visit. Finally, 14 patients developed foveal atrophy before the appearance of fundus flecks (Figure 3A_{1,2}).

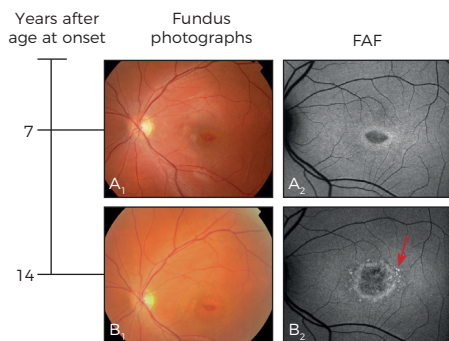


Figure 3. Fundus photographs and autofluorescence (FAF) imaging of patient 37 (age at onset, 8 years; ABCA4 genotype, p.Phe608Ile and p.Gly1961Glu) at 15 (A_{1,2}) and 22 years (B_{1,2}) of age showing isolated foveal pigment alterations and a hypoautofluorescent lesion (BCVA, 0.52 logMAR, Snellen 20/66). Seven years later (B_{1,2}), yellow-white parafoveal fundus flecks (the arrow in B₂) developed (BCVA 1.15 logMAR; Snellen 20/283). BCVA = best-corrected visual acuity; logMAR = logarithm of the minimum angle of resolution.

Long-term follow-up data revealed that the initial foveal atrophy progressed to more widespread chorioretinal atrophy. Over time, FAF imaging revealed centrifugal expansion of disseminated spots in 30 out of 32 patients with a mean timeframe of

‡ Mean age at onset of the total cohort is used.

§ In the patient's medical records fundus findings were described "in accordance with Stargardt," but no detailed description or imaging was made and thus were excluded from imaging analysis.

BCVA = best-corrected visual acuity; CF = counting fingers; del = deletion; dup = duplication; fERG = full-field electroretinography; HM = hand movements; logMAR = logarithm of the minimum angle of resolution; NI = not identified; NP = not performed.

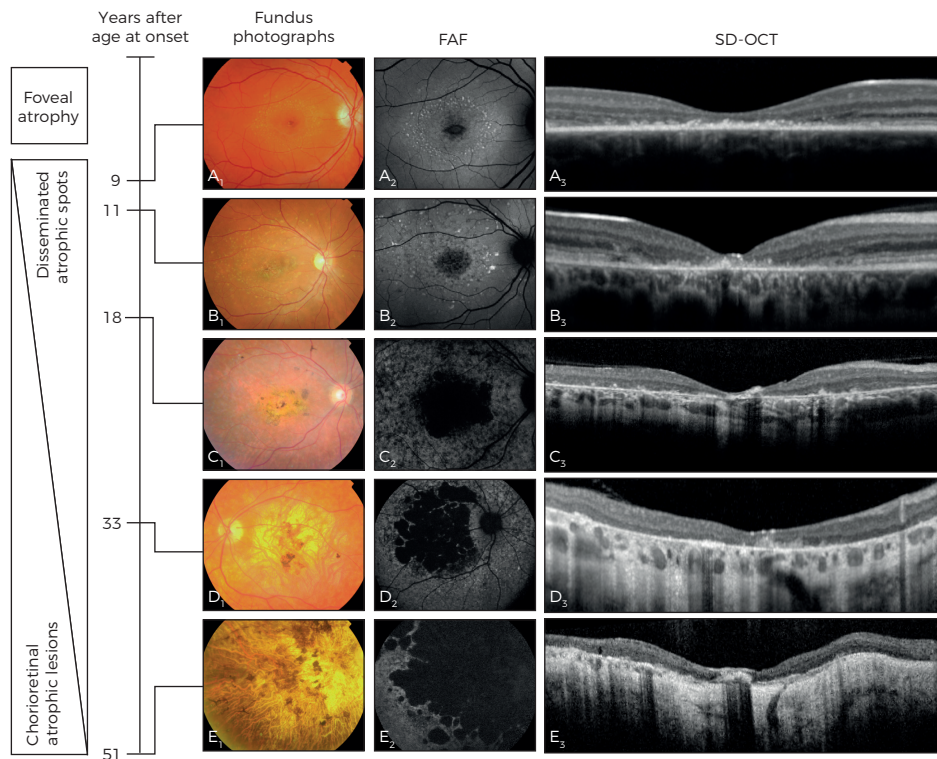


Figure 4. Overview of the natural course of retinal disease in early-onset Stargardt based on findings obtained from 5 separate patients using fundus photography, FAF, and SD-OCT. Early-onset Stargardt includes foveal atrophy and parafoveal hyperautofluorescent fundus flecks ($A_{1,2}$) in an early disease stage. On SD-OCT, there is hyperreflective abnormalities in the outer retina, loss of the ellipsoid zone, and thinning of the outer nuclear layer (A_3). The initial foveal atrophy and parafoveal flecks then extend centrifugally ($B_{1,2}$), and disseminated hypoautofluorescent spots appear (B_2). On SD-OCT, there is progression of the foveal atrophy, with thinning of the retinal pigment epithelium/Bruch's membrane complex (B_3). Further in the course of the disease, the disseminated hypoautofluorescent spots become chorioretinal atrophic lesions, the central atrophy expands further ($C_{1,2}$), and pigmentations (C_1) are visible as hyperreflective deposits on SD-OCT (C_3). Over time, confluence of these lesions evolves centrifugally ($D_{1,2}$), extending beyond the vascular arcades ($E_{1,2}$), with further retinal thinning and atrophy of the choriocapillaris (D_3 – E_3) visible on SD-OCT. $A_{1,2,3}$, Patient 1 at age 17; $B_{1,2,3}$, patient 31 at age 22; $C_{1,2,3}$, patient 40 at age 24; $D_{1,2,3}$, patient 8 at age 36; $E_{1,2,3}$, patient 5 at age 57. FAF = fundus autofluorescence; SD-OCT = spectral-domain optical coherence tomography.

9.8 ± 10.5 years (median, 8; range, 0–40; **Figure 4B₂**). These spots extended beyond the vascular arcades in 24 of these 30 patients with a mean of 11.2 ± 11.0 years (median, 9.5; range, 0–40) after the first visit (**Figure 4C₂**). In 22 out of 32 patients, the spots progressed to chorioretinal atrophic lesions after a mean period of 13.5 ± 12.3 years (median, 10.5; range, 0–40; **Figure 4C₂–D₂**). In 11 of these 22 patients, the confluence of these lesions extended beyond the vascular arcades after a mean period of 23.0 ± 0.3 years (median, 23; range, 5–40; **Figure 4E₂**). The 11 patients who presented

with the common phenotype of chorioretinal lesions beyond the vascular arcades at the final examination initially presented with flecks ($n = 3$), foveal atrophy ($n = 4$), or both flecks and atrophy ($n = 4$) at their first examination.

Over time, SD-OCT showed thinning of the outer nuclear layer and loss of the ellipsoid zone, which preceded loss of the RPE/Bruch's membrane complex. In addition, hyper-reflective abnormalities in the outer retina were present (Figure 4A₃). Progression occurred as an expanding loss of the outer nuclear layer, ellipsoid zone, RPE, and choriocapillaris (Figure 4B₃–E₃). Hyperreflective deposits in the inner layers of the fovea developed, corresponding with intraretinal pigmentations on fundus photography (Figure 4C₁–C₃).

Electrophysiologic findings

Follow-up data for 25 patients showed that 4 patients progressed from ffERG group 1 to group 2 within a mean of 10.5 ± 4.4 years (range, 7–16), and 9 patients progressed from group 1 to group 3 within a mean of 27.7 ± 14.4 years (range, 3–47).

Mutation analysis

The ABCA4 gene was screened for mutations in 44 of the 51 patients; the remaining 7 patients refused genetic analysis for personal reasons. In these 44 patients, mutations in the ABCA4 gene were identified in 81 of the 88 alleles (92%). Thirty-three of these patients had 2 ABCA4 mutations, 7 patients had 1 mutation, 3 patients had 3 mutations, and 1 patient had 4 mutations. In total, 37 distinct mutations were identified; these mutations are summarized in Table 2.

The c.768G>T mutation was identified in 25% of the 44 patients and accounted for 13% of all identified mutations. The c.5461-10T>C mutation was identified in 36% of the patients and accounted for 22% of all identified mutations. The most prevalent ABCA4 mutation among Dutch patients with STGD1 (c.2588G>C)²³ was identified in only 4% of the alleles. Table 3 summarizes the non-missense mutations that were identified in this study.

Discussion

In this study, we examined the clinical and genetic characteristics of patients with early-onset Stargardt, a disease that lies within the spectrum of retinal phenotypes linked with mutations in the ABCA4 gene. Whenever a spectrum of disorders contains overlapping phenotypes as the rule rather than an exception, any cutoff point used to define a particular disease within that spectrum will be arbitrary. Therefore, we

Mutation	Effect	Allele		References
		Frequency	Percentage	
c.122G>A	p.Trp41*	1	1	35
c.214G>A	p.Gly72Arg	1	1	32
c.286A>G	p.Asn96Asp	4	5	36
c.443-?_570+?del	p.Arg149fs	1	1	This study
c.455G>A	p.Arg152Gln	1	1	32, 37
c.656G>C	p.Arg219Thr	1	1	38
c.768G>T	p.Val256Val/p.?	11	13	16, 23, 32, 39
c.818G>A	p.Trp273*	1	1	This study
c.872C>T	p.Pro291Leu	1	1	34
c.1622T>C	p.Leu541Pro	2	2	1, 16, 32, 40
c.1822T>A	p.Phe608Ile	4	5	1, 23
c.1957C>T	p.Arg653Cys	1	1	32, 41
c.2588G>C	p.Gly863Ala/p.DelGly863	3	4	16, 18, 23, 32, 42
c.2919-?_3328+?del	p.Ser974_Gly1110delinsCys	2	2	23
c.2947A>G	p.Thr983Ala	3	4	34
c.3113C>T	p.Ala1038Val	2	2	16, 31, 32, 40, 43
c.3335C>A	p.Thr1112Asn	1	1	23
c.3449G>A	p.Cys1150Tyr	1	1	This study
c.3813G>C	p.Glu1271Asp	1	1	This study
c.3874C>T	p.Gln1292*	1	1	34
c.4224G>T	p.Trp1408Cys	1	1	This study
c.4462T>C	p.Cys1488Arg	1	1	1, 8, 44, 45
c.4506C>A	p.Cys1502*	1	1	34
c.4539+1G>T	p.?	3	4	1, 23, 43, 44
c.4773+1G>A	p.?	1	1	This study
c.5113C>T	p.Arg1705Trp	1	1	34
c.5161_5162del	p.Thr1721fs	1	1	23, 36
c.5312+1G>A	p.?	1	1	46
c.5461-10T>C	p.?	19	22	16, 23, 47
c.5537T>C	p.Ile1846Thr	1	1	23, 45
c.5585-10T>C	p.?	1	1	48
c.5714+5G>A	p.?	1	1	1, 23, 32, 41, 43
c.5762_5763dup	p.Ala1922fs	1	1	34
c.5882G>A	p.Gly1961Glu	5	6	18, 31, 32, 44, 49
c.6320G>A	p.Arg2107His	2	2	8, 31, 40, 45, 50
c.6411T>A	p.Cys2137*	1	1	34
c.6543_6578del	p.Leu2182_Phe2193del	1	1	1

Table 2. ABCA4 mutations in early-onset Stargardt patients. References are shown for mutations that have been reported previously. del = deletion; dup = duplication; fs = frameshift; ins = insertion; * stop signal.

Mutation	Protein effect	SIFT	Polyphen-2	Grantham	PhyloP
c.3449G>A	p.Cys1150Tyr	Not tolerated	Benign	194	3.19
c.3813G>C	p.Glu1271Asp	Not tolerated	Possibly damaging	45	6.10
c.4224G>T	p.Trp1408Cys	Not tolerated	Probably damaging	215	5.86

Table 3. Characteristics of the non-missense ABCA4 mutations identified in our cohort study.

The outcome of 2 protein prediction programs (SIFT = tolerated or not tolerated; PolyPhen = benign, possibly damaging, probably damaging), together with Grantham (>60 pathogenic) and PhyloP conservation score (>2.5 pathogenic), were used to form the final conclusion. Mutations are proposed to be pathogenic when ≥ 2 categories point to pathogenicity.

arbitrarily defined “early-onset Stargardt” as occurring with an age at onset of ≤ 10 years of age; this definition enabled us to avoid including patients with a more typical STGD1 phenotype. Only 4% of the 51 patients in our early-onset Stargardt cohort had visual

acuity of ≤ 0.30 logMAR, Snellen $< 20/40$ (measured at age 8 and 18 years of age in these 2 patients), compared with 14% to 37% of patients with typical STGD1 and 59% of patients with late-onset STGD1.^{5, 14, 24} Because patients with a relatively good visual acuity tended to return less often than those with progressive problems, these data may have overrepresented more severe cases. The majority of our patients for whom ffERG data were available developed abnormal ffERG amplitudes, consistent with a previous report by Fujinami et al.⁷ However, we found no correlation between the ffERG group classifications (which were based on the nature of the ffERG abnormalities) at the age of onset and the speed of vision loss in this early-onset Stargardt cohort. This finding differs from STGD1 cohorts that included patients with later ages at onset.^{5, 6} Our findings indicate that early-onset Stargardt can be considered a distinct severe subtype of STGD1 that is characterized by early foveal abnormalities and the rapid loss of visual function; in contrast, in late-onset STGD1, foveal sparing is common, and visual acuity is often preserved to a relatively advanced age.¹⁴

Diagnosis

The natural course of early-onset ABCA4-related retinal disease in our cohort reflects a broad clinical spectrum both at the time of onset and at follow-up, with varying degrees of ffERG abnormalities and yellow-white flecks and/or atrophy at a variety of locations. Thus, each combination of electrophysiologic and fundus findings could be considered a unique phenotype at a specific time point. Moreover, these phenotypes changed during the course of the disease, suggesting progression of the disease. Because both fundus and electrophysiologic criteria have been proposed for establishing a descriptive diagnosis (e.g., Stargardt disease and cone-rod dystrophy), each individual patient can potentially receive several diagnoses at 1 time point and at follow-up. Importantly, receiving several diagnoses can be extremely confusing to both the patient and the referring ophthalmologist.

Nevertheless, we found that the spectrum of fundus presentations in this early-onset retinal dystrophy ultimately converges to a single clinical and functional endpoint that includes profound chorioretinal atrophy and severe vision loss. Therefore, we propose that one diagnosis of “early-onset Stargardt” should be given to patients with early-onset central retinal dystrophy and ABCA4 gene mutations. This approach provides the patient with the benefit of receiving a single diagnosis throughout his or her entire life.

Genotype-phenotype correlation

Because early-onset Stargardt can be considered a severe phenotype, severe combinations of mutations are expected in these patients. In our cohort, the c.768G>T and c.5461-10T>C mutations were significantly more prevalent (present in 25% and 36% of

our patients, respectively) than in other STGD1 cohorts (8% and 5%, respectively).^{30, 31} The c.768G>T mutation is predicted to cause a splice defect that leads to nonsense-mediated decay owing to absence of the corresponding messenger ribonucleic acid; this mutation is therefore considered to be a severe pathogenic mutation. In addition, a founder effect has been suggested for this mutation owing to the allele frequency of 8% among Dutch patients with STGD1.³⁰ On the other hand, the c.5461-10T>C mutation does not seem to be pathogenic, because heterologous expression of this mutation failed to reveal a splicing defect.³² This mutation is rare among control patients, but is present in 5% of patients with general STGD1. Therefore, the c.5461-10T>C mutation may be in linkage disequilibrium with another, currently unidentified, severe pathogenic mutation.³¹ Equally important, the most prevalent ABCA4 mutation among Dutch patients with STGD1—c.2588G>C, which was reported in approximately one third of typical STGD1 cases³³—was present in only 4% of the ABCA4 alleles in our cohort of patients with early-onset Stargardt. To date, no homozygous carriers of this mutation have been identified,²³ supporting the hypothesis that this is a relatively mild mutation. The low prevalence of this presumably mild mutation in our cohort is consistent with a previously proposed genotype–phenotype model that correlates the degree of residual ABCA4 activity with the severity of the phenotype.^{17, 23}

We identified ABCA4 mutations in all of our patients who received genetic screening; in contrast, the detection rate in routine clinical practice is 73%.³⁴ This difference can be explained—at least in part—by the inclusion criteria; patients who lacked a detected ABCA4 mutation only would have been included if yellow-white flecks and either a dark choroid or an atrophic macular lesion were present. However, our database did not contain such patients who received genetic screening and had an early-onset disease. This finding supports the notion that early onset is highly predictive for identifying ABCA4 mutations,³⁴ possibly because of the relatively higher percentage of severe mutations, which are more readily identified and/or recognized.

It remains unclear why the fovea is affected early in the course of STGD1 in some patients, whereas it can be spared—even for many decades—in other patients carrying compound heterozygous mutations, including 1 severe ABCA4 mutation.^{14, 15} Other factors must therefore play a role in the development of foveal atrophy in early-onset Stargardt; possible factors can include pathogenic mutations or single nucleotide polymorphisms in genes other than ABCA4, as well as aberrant cellular processes. For example, the accumulation of all-trans-retinal in photoreceptor cells can directly increase cellular stress, thereby triggering apoptotic signaling pathways.³⁵ Next-generation sequencing of all retina-specific genes may help to identify the genetic factors that determine whether or not the fovea is involved early in the course of STGD1.

Clinical Significance

Although diagnosing STGD1 at an early age is challenging, delaying diagnosis can have serious consequences. For example, 22 patients in our study did not receive the correct diagnosis for ≥ 3 years, and vision loss was initially unexplained in 13 patients. Recognizing early-onset Stargardt early in the disease course enables the timely start of potential measures—such as sunlight protection and low-vision counseling—and can prevent the inappropriate prescription of vitamin A supplements. Therefore, patients who are suspected of having early-onset Stargardt should be examined thoroughly using FAF and SD-OCT, particularly when no abnormalities (or mild foveal abnormalities) are present in a child with central vision loss that is otherwise unexplained. This diagnosis should also be confirmed by screening for the presence of *ABCA4* mutations. Finally, in light of future therapeutic options, such as gene therapy for treating *ABCA4*-related retinal disorders, obtaining a thorough understanding of the phenotypic spectrum and clinical course of STGD1 is essential for identifying the patients who will benefit most from these treatments.

References

1. Lewis RA, Shroyer NF, Singh N, et al. Genotype/Phenotype analysis of a photoreceptor-specific ATP-binding cassette transporter gene, ABCR, in Stargardt disease. *Am J Hum Genet* 1999;64(2):422-34.
2. Stargardt K. Über familiäre, progressive Degeneration in der Maculagegend des Auges. *Graefes Arch Clin Exp Ophthalmol* 1909(71):534-50.
3. Franceschetti A. A special form of tapetoretinal degeneration: fundus flavimaculatus. *Trans Am Acad Ophthalmol Otolaryngol* 1965;69(6):1048-53.
4. Klevering BJ, Blankenagel A, Maugeri A, et al. Phenotypic spectrum of autosomal recessive cone-rod dystrophies caused by mutations in the ABCA4 (ABCR) gene. *Investigative Ophthalmology & Visual Science* 2002;43(6):1980-5.
5. Lois N, Holder GE, Bunce C, et al. Phenotypic subtypes of Stargardt macular dystrophy-fundus flavimaculatus. *Arch Ophthalmol* 2001;119(3):359-69.
6. Zahid S, Jayasundera T, Rhoades W, et al. Clinical phenotypes and prognostic full-field electroretinographic findings in Stargardt disease. *American Journal of Ophthalmology* 2013;155(3):465-73 e3.
7. Fujinami K, Lois N, Davidson AE, et al. A longitudinal study of stargardt disease: clinical and electrophysiologic assessment, progression, and genotype correlations. *American Journal of Ophthalmology* 2013;155(6):1075-88 e13.
8. Fishman GA, Stone EM, Grover S, et al. Variation of clinical expression in patients with Stargardt dystrophy and sequence variations in the ABCR gene. *Arch Ophthalmol* 1999;117(4):504-10.
9. Armstrong JD, Meyer D, Xu S, Elfervig JL. Long-term follow-up of Stargardt's disease and fundus flavimaculatus. *Ophthalmology* 1998;105(3):448-57; discussion 57-8.
10. Querques G, Leveziel N, Benhamou N, et al. Analysis of retinal flecks in fundus flavimaculatus using optical coherence tomography. *British Journal of Ophthalmology* 2006;90(9):1157-62.
11. Sparrow JR, Gregory-Roberts E, Yamamoto K, et al. The bisretinoids of retinal pigment epithelium. *Progress in Retinal and Eye Research* 2012;31(2):121-35.
12. Charbel Issa P, Barnard AR, Singh MS, et al. Fundus autofluorescence in the Abca4(-/-) mouse model of Stargardt disease--correlation with accumulation of A2E, retinal function, and histology. *Investigative Ophthalmology & Visual Science* 2013;54(8):5602-12.
13. Ergun E, Hermann B, Wirtitsch M, et al. Assessment of central visual function in Stargardt's disease/fundus flavimaculatus with ultrahigh-resolution optical coherence tomography. *Invest Ophthalmol Vis Sci* 2005;46(1):310-6.
14. Westeneng-van Haaften SC, Boon CJ, Cremers FP, et al. Clinical and Genetic Characteristics of Late-onset Stargardt's Disease. *Ophthalmology* 2012;119(6):1199-210.
15. Fujinami K, Sergouniotis PI, Davidson AE, et al. Clinical and molecular analysis of stargardt disease with preserved foveal structure and function. *Am J Ophthalmol* 2013;156(3):487-501 e1.
16. Maugeri A, Klevering BJ, Rohrschneider K, et al. Mutations in the ABCA4 (ABCR) gene are the major cause of autosomal recessive cone-rod dystrophy. *Am J Hum Genet* 2000;67(4):960-6.
17. Klevering BJ, Deutman AF, Maugeri A, et al. The spectrum of retinal phenotypes caused by mutations in the ABCA4 gene. *Graefes Arch Clin Exp Ophthalmol* 2005;43(2):90-100.
18. Allikmets R, Singh N, Sun H, et al. A photoreceptor cell-specific ATP-binding transporter gene (ABCR) is mutated in recessive Stargardt macular dystrophy. *Nat Genet* 1997;15(3):236-46.
19. Molday LL, Rabin AR, Molday RS. ABCR expression in foveal cone photoreceptors and its role in Stargardt macular dystrophy. *Nat Genet* 2000;25(3):257-8.
20. Sun H, Smallwood PM, Nathans J. Biochemical defects in ABCR protein variants associated with human retinopathies. *Nat Genet* 2000;26(2):242-6.
21. Sparrow JR, Wu Y, Kim CY, Zhou J. Phospholipid meets all-trans-retinal: the making of RPE bisretinoids. *J Lipid Res* 2010;51(2):247-61.
22. van Driel MA, Maugeri A, Klevering BJ, et al. ABCR unites what ophthalmologists divide(s). *Ophthalmic Genet* 1998;19(3):117-22.

23. Maugeri A, van Driel MA, van de Pol DJ, et al. The 2588G-->C mutation in the ABCR gene is a mild frequent founder mutation in the Western European population and allows the classification of ABCR mutations in patients with Stargardt disease. *Am J Hum Genet* 1999;64(4):1024-35.
24. Rotenstreich Y, Fishman GA, Anderson RJ. Visual acuity loss and clinical observations in a large series of patients with Stargardt disease. *Ophthalmology* 2003;110(6):1151-8.
25. Burke TR, Yzer S, Zernant J, et al. Abnormality in the external limiting membrane in early Stargardt Disease. *Ophthalmic Genet* 2012.
26. Schulze-Bonsel K, Feltgen N, Burau H, et al. Visual acuities "hand motion" and "counting fingers" can be quantified with the freiburg visual acuity test. *Investigative Ophthalmology & Visual Science* 2006;47(3):1236-40.
27. Marmor MF, Fulton AB, Holder GE, et al. ISCEV Standard for full-field clinical electroretinography (2008 update). *Doc Ophthalmol* 2009;118(1):69-77.
28. Kuze M, Uji Y. Comparison between Dawson, Trick, and Litzkow electrode and contact lens electrodes used in clinical electroretinography. *Japanese Journal of Ophthalmology* 2000;44(4):374-80.
29. Colenbrander A. Visual standards: aspects and ranges of vision loss with emphasis on population surveys. Report prepared for the International Council of Ophthalmology (ICO) at the 29th International Congress of Ophthalmology, Sydney, 2002. San Francisco: Pacific Vision Foundation; 2002.
30. Cremers FP, Maugeri A, den Hollander AI, Hoyng CB. The expanding roles of ABCA4 and CRB1 in inherited blindness. *Novartis Found Symp* 2004;255:68-79; discussion -84, 177-8.
31. Webster AR, Heon E, Lotery AJ, et al. An analysis of allelic variation in the ABCA4 gene. *Invest Ophthalmol Vis Sci* 2001;42(6):1179-89.
32. Rivera A, White K, Stohr H, et al. A comprehensive survey of sequence variation in the ABCA4 (ABCR) gene in Stargardt disease and age-related macular degeneration. *Am J Hum Genet* 2000;67(4):800-13.
33. Maugeri A, Flothmann K, Hemmrich N, et al. The ABCA4 2588G>C Stargardt mutation: single origin and increasing frequency from South-West to North-East Europe. *Eur J Hum Genet* 2002;10(3):197-203.
34. Ernest PJ, Boon CJ, Klevering BJ, et al. Outcome of ABCA4 microarray screening in routine clinical practice. *Molecular Vision* 2009;15:2841-7.
35. Cideciyan AV, Swider M, Aleman TS, et al. ABCA4 disease progression and a proposed strategy for gene therapy. *Hum Mol Genet* 2009;18(5):931-41.
36. Papaioannou M, Ocaka L, Bessant D, et al. An analysis of ABCR mutations in British patients with recessive retinal dystrophies. *Invest Ophthalmol Vis Sci* 2000;41(1):16-9.
37. September AV, Vorster AA, Ramesar RS, Greenberg LJ. Mutation spectrum and founder chromosomes for the ABCA4 gene in South African patients with Stargardt disease. *Investigative Ophthalmology & Visual Science* 2004;45(6):1705-11.
38. Jaakson K, Zernant J, Kulm M, et al. Genotyping microarray (gene chip) for the ABCR (ABCA4) gene. *Hum Mutat* 2003;22(5):395-403.
39. Yatsenko AN, Shroyer NF, Lewis RA, Lupski JR. Late-onset Stargardt disease is associated with missense mutations that map outside known functional regions of ABCR (ABCA4). *Hum Genet* 2001;108(4):346-55.
40. Rozet JM, Gerber S, Souied E, et al. Spectrum of ABCR gene mutations in autosomal recessive macular dystrophies. *European Journal of Human Genetics* 1998;6(3):291-5.
41. Fumagalli A, Ferrari M, Soriani N, et al. Mutational scanning of the ABCR gene with double-gradient denaturing-gradient gel electrophoresis (DG-DGGE) in Italian Stargardt disease patients. *Human Genetics* 2001;109(3):326-38.
42. Allikmets R, Shroyer NF, Singh N, et al. Mutation of the Stargardt disease gene (ABCR) in age-related macular degeneration. *Science* 1997;277(5333):1805-7.
43. Cremers FP, van de Pol DJ, van Driel M, et al. Autosomal recessive retinitis pigmentosa and cone-rod dystrophy caused by splice site mutations in the Stargardt's disease gene ABCR. *Hum Mol Genet* 1998;7(3):355-62.

44. Stone EM, Webster AR, Vandeburgh K, et al. Allelic variation in ABCR associated with Stargardt disease but not age-related macular degeneration. *Nature Genetics* 1998;20(4):328-9.
45. Briggs CE, Rucinski D, Rosenfeld PJ, et al. Mutations in ABCR (ABCA4) in patients with Stargardt macular degeneration or cone-rod degeneration. *Invest Ophthalmol Vis Sci* 2001;42(10):2229-36.
46. Zernant J, Schubert C, Im KM, et al. Analysis of the ABCA4 gene by next-generation sequencing. *Invest Ophthalmol Vis Sci* 2011;52(11):8479-87.
47. Roberts LJ, Nossek CA, Greenberg LJ, Ramesar RS. Stargardt macular dystrophy: common ABCA4 mutations in South Africa--establishment of a rapid genetic test and relating risk to patients. *Mol Vis* 2012;18:280-9.
48. Lenassi E, Jarc-Vidmar M, Glavac D, Hawlina M. Pattern electroretinography of larger stimulus field size and spectral-domain optical coherence tomography in patients with Stargardt disease. *British Journal of Ophthalmology* 2009;93(12):1600-5.
49. Simonelli F, Testa F, de Crecchio G, et al. New ABCR mutations and clinical phenotype in Italian patients with Stargardt disease. *Investigative Ophthalmology & Visual Science* 2000;41(3):892-7.
50. Paloma E, Martinez-Mir A, Vilageliu L, et al. Spectrum of ABCA4 (ABCR) gene mutations in Spanish patients with autosomal recessive macular dystrophies. *Human Mutation* 2001;17(6):504-10.

"The natural course of late-onset Stargardt features expanding areas of retinal pigment epithelium atrophy. These can serve as a robust surrogate outcome measure for disease progression in therapeutic trials to determine their potential effect."

Stanley Lambertus*

Moritz Lindner*

Nathalie M. Bax

Matthias M. Mauschitz

Jennifer Nadal

Matthias Schmid

Steffen Schmitz-Valckenberg

Anneke I. den Hollander

Bernhard H.F. Weber

Frank G. Holz

Gert Jan van der Wilt

Monika Fleckenstein†

Carel B. Hoyng†

for the Foveal sparing Atrophy Study Team (FAST)

* S.L. and M.L. are joint first authors.

† M.F. and C.B.H. contributed equally to the work presented here and should therefore be regarded as equivalent authors.

Invest Ophthalmol Vis Sci. 2016 Oct 1;57(13):5186-519

The authors thank Stéphanie Cornelis and Frans Cremers for their analysis of *ABCA4* mutations, and Hans Groenewoud for his statistical help and advice.

2.2 Progression of late-onset Stargardt disease

PURPOSE: Identification of sensitive biomarkers is essential to determine potential effects of emerging therapeutic trials for Stargardt disease. This study aimed to describe the natural history of late-onset Stargardt, and demonstrates the accuracy of retinal pigment epithelium (RPE) atrophy progression as an outcome measure.

METHODS: We performed a retrospective cohort study collecting multicenter data from 47 patients (91 eyes) with late-onset Stargardt, defined by clinical phenotype, at least one *ABCA4* mutation, and age at disease onset ≥ 45 years. We analyzed RPE atrophy progression on fundus autofluorescence and near-infrared reflectance imaging using semiautomated software and a linear mixed model. We performed sample size calculations to assess the power in a simulated 2-year interventional study and assessed visual endpoints using time-to-event analysis.

RESULTS: Over time, progression of RPE atrophy was observed (mean, 0.22 mm/year; 95% confidence interval [CI], 0.19–0.27). By including only patients with bilateral RPE atrophy in a future trial, 32 patients are needed to reach a power of 83.9% (95% CI, 83.1–84.6), assuming a fixed therapeutic effect size of 30%. We found a median interval between disease onset and visual acuity decline to 20/32, 20/80, and 20/200 of 2.74 (95% CI, 0.54–4.41), 10.15 (95% CI, 6.13–11.38), and 11.38 (95% CI, 6.13–13.34) years, respectively.

CONCLUSIONS: We show that RPE atrophy represents a robust biomarker to monitor disease progression in future therapeutic trials. In contrast, the variability in terms of the course of visual acuity was high.

Introduction

Stargardt disease is an autosomal recessive retinal dystrophy caused by mutations in the ABCA4 gene, and affects 1:8000 to 1:10,000 people worldwide.¹ Patients generally develop central loss of vision in childhood or early adulthood.²⁻⁴ However, late-onset Stargardt can be diagnosed at age ≥ 45 years, and has been associated with carrying one or two mutant ABCA4 alleles.^{5,6} Patients with this late-onset variant may first present with metamorphopsia or oscillopsia without any decrease in visual acuity. Occasionally, these patients are asymptomatic and are coincidentally diagnosed during screening tests for other retinal diseases, such as glaucoma, diabetes or thyroid disease.

The natural course of late-onset Stargardt includes a typical phenotype of yellow-white flecks and retinal pigment epithelium (RPE) atrophy. Patches of atrophy initially occur in the parafoveal retina and radially expand in size over time. New atrophic areas can arise; multifocal atrophic areas coalesce. Atrophic areas can form a ring encircling the intact and still-functioning fovea. Then, it is only until late in the disease course that the fovea will be involved in the atrophic process.⁷⁻⁹ The patient's fixation point eventually shifts eccentrically, which leads to a substantial loss of visual acuity.¹⁰ However, central atrophy can also develop early in the disease course, and only minor disease progression has been described in other patients.⁵ Indeed, substantial variations in RPE atrophy progression have been reported before in small groups of typical Stargardt patients.¹¹ Yet analyses of the natural course of large late-onset Stargardt cohorts are missing.

In light of recently upcoming therapeutic options for Stargardt disease,¹²⁻¹⁴ accurate biomarkers to determine their potential effects are crucial. The well-defined area of RPE atrophy is a frequent feature of late-onset Stargardt, showing similarities to geographic atrophy in age-related macular degeneration (AMD). Fundus autofluorescence (FAF) imaging can clearly visualize such areas of RPE atrophy,^{15,16} and change in RPE atrophy over time by FAF has already been accepted as a clinical endpoint by the U.S. Food and Drug Administration in AMD.¹⁷ We hypothesize that areas of RPE atrophy could also serve to sensitively monitor the effect of a drug trial in late-onset Stargardt. This would make patients with late-onset Stargardt appropriate candidates for upcoming therapeutic trials. In this study, we describe the natural history in late-onset Stargardt patients, and identify cohorts based on imaging parameters that determine the visual course in these patients. We quantify atrophy progression with semiautomated software, previously validated for AMD,¹⁸ showing the accuracy of this outcome measure, and include sample size calculations that are valuable for the design of upcoming therapeutic trials.

Methods

Patient selection

We identified patients from the Stargardt database of the Department of Ophthalmology at Radboud university medical center (Nijmegen, the Netherlands) and from the participants in the prospective natural history study Fundus Autofluorescence in Age-related Macular Degeneration (FAM; ClinicalTrials.gov, NCT00393692).

We included 47 patients with a late disease onset, defined by an age ≥ 45 years at which symptoms were first noticed.⁵ If the patient did not report any symptoms, we used the age at which the patient was diagnosed by an ophthalmologist. We clinically considered patients to have late-onset Stargardt when typical yellow-white flecks or dots were seen that correlated with hyperautofluorescent flecks on 488-nm FAF imaging.

Patients were analyzed for the presence of mutations in the adenosine triphosphate-binding cassette, subfamily A, member 4 (ABCA4, NM_000350.2) gene. Clinical diagnosis was confirmed by genetic testing if at least one ABCA4 mutation was found. We excluded patients without evidence of ABCA4 mutations. In patients carrying only one ABCA4 mutation, we performed additional sequencing of the peripherin-2 gene (PRPH2, NM_000322.4) to exclude pseudo-Stargardt pattern dystrophy and central areolar choroidal dystrophy.^{19, 20}

This cohort study was carried out with approval from the Institutional Ethics Committee at Radboud university medical center (Nijmegen, the Netherlands) and the University Hospital of Bonn (Bonn, Germany), and adhered to the tenets of the Declaration of Helsinki. All patients provided informed consent before giving a blood sample and receiving additional ophthalmologic examinations to complete the clinical assessment.

Clinical assessment

We reviewed the patients' records for ophthalmologic history and available technical examinations, including sex, age at disease onset, and age at baseline. Best-corrected visual acuity (BCVA) was measured using a Snellen or Early Treatment Diabetic Retinopathy Study (ETDRS) chart, then transformed into the logarithm of the minimum angle of resolution (logMAR) for subsequent analysis. Fundus characteristics were documented using fundus photography (Topcon TRC-50IX; Topcon Corporation, Tokyo, Japan; or Visucam 500; Carl Zeiss Meditec, Jena, Germany). Fundus autofluorescence ($\lambda = 488$ nm; emission 500–700 nm) and near-infrared reflectance (NIR; $\lambda = 820$ nm) imaging were performed using a confocal scanning laser ophthalmoscope (Spectralis HRA+OCT or HRA2; Heidelberg Engineering, Heidelberg, Germany) in a subset of visits. The field of

view was set at 30°×30° or 55°×55° and was centered on the macula. Eyes with signs of choroidal neovascularization were excluded from further analysis.

Image grading and cohorts

For each visit, two independent graders (M.F. and M.L.), blinded to each other's results, evaluated the status of the fovea and the presence of clearly demarcated RPE atrophy (analogous to “definitely decreased autofluorescence,” the term recently used by Kuehlewein et al.²¹) on all available imaging modalities. Atrophy was graded as follows: (1) no RPE atrophy with an intact fovea, (2) extrafoveal (but not fovea encircling) RPE atrophy, (3) a typical “foveal sparing” phenotype in which RPE atrophy encircled the fovea by $\geq 180^\circ$,¹⁰ or (4) foveal involvement. Foveal involvement was indicated by a mottled or absent autofluorescent signal (equaling what was ultimately termed “well-/poorly demarcated questionably decreased autofluorescence”²¹). In cases of discrepancy, a third grader (S.L.) evaluated the images. His agreement with one of the independent graders was finally used. Based on this grading, eyes were exploratively analyzed in order to form cohorts that might be predictive for visual acuity loss.

Quantitative measurements of retinal pigment epithelium atrophy

Two independent graders (M.F. and M.L.), blinded to each other's results, performed measurements of the area of RPE atrophy using the RegionFinder software (version 2.5.5.0, Heidelberg Engineering) on FAF images, as previously established for AMD.¹⁸ In cases in which the foveal borders of the atrophy could not be well determined in FAF images, NIR images were included in the analysis wherever available.²² The final value was defined as the average of the two measurements between the readers, provided that the two measurements did not differ by $>0.15 \text{ mm}^2$. If the difference exceeded 0.15 mm^2 , a senior reader (M.M.M.) additionally performed the measurement.¹⁸ We calculated the final value by averaging the senior reader measurement along with the closer of the two other reader measurements.

Statistical analysis

We analyzed data using SAS Statistical Analysis Software Version 9.2 (SAS Institute, Cary, NC, USA) and R Version 3.1.2.23. [Supplemental Figure S₁](#) gives an overview of the analytical process applied in this work. Changes in visual acuity over time were assessed by time-to-event curves (cumulative distribution functions), and atrophy progression was analyzed using linear mixed-effects models. We performed a simulation study for power calculation for possible future interventional trials. Unless otherwise stated, all values given in the text represent median, minimum, and maximum values. Groups were compared by Mann–Whitney U tests. Details on the statistical procedures can be found in [Supplemental Text S₁](#).

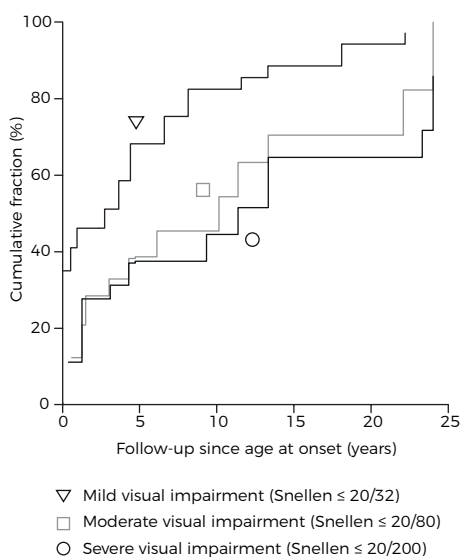
Results

Patient features and initial symptoms

A total of 91 eyes of 47 patients (19 men, 28 women) were included in this study. Two mutations in the *ABCA4* gene were found in 20 patients (42.6%) and one mutation in 27 (57.4%; [Supplemental Table S₁](#)). The median age at disease onset was 54 years (range, 45–84). Self-reported initial symptoms were obtained for 42 patients and included a decrease in visual acuity ($n = 24$; 50%), metamorphopsia ($n = 12$; 29%), nyctalopia ($n = 5$; 12%), paracentral scotomas ($n = 4$; 10%), or oscillopsia ($n = 1$; 2%). Twelve patients (29%) did not report any visual complaints. In five patients, initial symptoms were not unequivocally denoted in the patient's file.

Course of visual acuity

Overall, visual acuity data were available from 632 eye visits. At the first presentation after disease onset, the median disease duration was 0.9 years (range, 0–25.6) with a median BCVA of 0.10 logMAR (range, -0.14 to 1.70; Snellen 20/25). The median follow-up time of the patients with more than a single visit (45 out of 47 patients) was 4.8 years (range, 0.04–25.0). Time-to-event analysis yielded a median and 95% confidence interval (CI) between the age at onset and a decline in BCVA to mild visual impairment ($n = 62$), moderate visual impairment ($n = 39$), and severe visual impairment ($n = 35$) of 2.74 (0.54–4.41), 10.15 (6.13–11.38), and 11.38 (9.34–13.34) years, respectively ([Figure 1](#)). The median disease duration at the final visit was 6.8 years (range, 0–30.9). The median BCVA at the final visit was 0.37 logMAR (range, -0.10 to 1.80; Snellen 20/47).



Assessment of retinal features

For each patient, clinical imaging data were available for a subset of visits (241 eye visits of 91 eyes). At baseline (first visit with imaging data available), yellow-white flecks were observed in all but one patient, in whom small yellowish

Figure 1. Time-to-event curve (computed as 1 minus the Turnbull estimates) showing the cumulative fraction of eyes in late-onset Stargardt patients reaching the following clinical endpoints: mild visual impairment (≥ 0.2 logMAR, Snellen $\leq 20/32$; triangle), moderate visual impairment (≥ 0.6 logMAR, Snellen $\leq 20/80$; square), and severe visual impairment (≥ 1.0 logMAR, Snellen $\leq 20/200$; circle). logMAR = logarithm of the minimum angle of resolution.

spots were noted. An apparently intact fovea (Figure 2A) without mottled or sharply decreased autofluorescence indicating RPE atrophy was present in 58 eyes. Out of these 58 eyes without foveal involvement, 22 had no RPE atrophy (Figure 2B), 16 had extrafoveal (but not fovea encircling) atrophy (Figure 2C), and 20 had a foveal sparing pattern of RPE atrophy encircling the fovea $\geq 180^\circ$ (Figure 2D). The other 32 eyes had an involved fovea by either a mottled appearance (23 eyes; Figure 2E) or central RPE atrophy (9 eyes; Figure 2F). One eye was excluded because it was inconclusive if the fovea appeared mottled. There was no significant difference in patient's age between eyes that initially had foveal involvement and those that did not (median, 60.4 [n = 32] and 61.0 years [n = 58] respectively; $P = 0.421$).

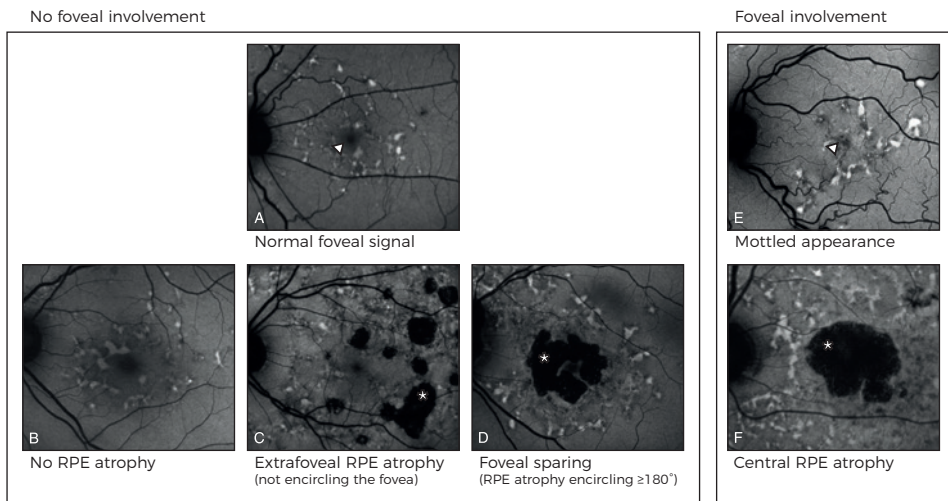


Figure 2. The assessment of retinal features in late-onset Stargardt patients was done by grading foveal involvement and RPE atrophy. The foveal signal (triangles) was graded as either (A) “uninvolved/normal” or (E) “involved” (mottled or absent). RPE atrophy (asterisks) was graded as (B) none, (C) extrafoveal but not fovea encircling, (D) foveal sparing $\geq 180^\circ$ encircling the fovea, or (F) central RPE atrophy. RPE = retinal pigment epithelium.

Cohorts

Assessment of retinal features over the entire imaging interval (Table 1) enabled us to categorize the eyes into four clearly distinctive cohorts. During the entire follow-up period, 20 eyes (22.2%) showed only flecks without any mottled foveal alterations or RPE atrophy (cohort I). Eleven eyes (12.2%) showed extrafoveal (but not fovea encircling) RPE atrophy (cohort II). Twenty-six eyes (28.9%) developed foveal sparing (RPE atrophy encircling the fovea $\geq 180^\circ$; cohort III). In four of these 26 eyes, the fovea eventually involved in the atrophic process at the last visit. Thirty-three eyes (36.7%) had eventual foveal involvement without passing through a foveal sparing phenotype during the observational interval (cohort IV).

At baseline			Clinical course		Resulting cohort
Initial features	Eyes	Median visual acuity, logMAR (range)	Change in features	Median visual acuity, final visit, logMAR (range)	
No foveal involvement					
No RPE atrophy	22	0.10 (-0.20 to 0.64)	20 unchanged 2 eyes developed extrafoveal atrophy	0.06 (-0.06 to 0.58) -0.02 (-0.06 to 0.02)	I II
Extrafoveal but not fovea encircling	16	0.05 (-0.10 to 0.72)	9 unchanged 6 progressed to foveal sparing 1 developed foveal involvement	0.12 (0 to 1.54) 0.44 (-0.06 to 0.74) 0.36	II III IV
Foveal sparing encircling $\geq 180^\circ$	20	0.12 (0 to 0.52)	16 unchanged 4 eyes loss of foveal sparing	0.22 (-0.04 to 1.80) 1.25 (0.94 to 1.50)	III III
Foveal involvement					
Central RPE atrophy	9	0.98 (0.30 to 1.50)			IV
Mottled	23	0.30 (-0.08 to 1.80)	20 eyes unchanged 3 eyes changed to central RPE atrophy		IV IV

Table 1. Retinal features in late-onset Stargardt over the entire observational interval. Cohort I had only flecks without any mottled foveal alterations or RPE atrophy. Cohort II had extrafoveal (but not fovea encircling) RPE atrophy until the last visit. Cohort III developed foveal sparing (RPE atrophy encircling the fovea $\geq 180^\circ$), and cohort IV had foveal involvement by either a mottled fovea or central RPE atrophy without passing through a foveal sparing phenotype during the observational interval. logMAR = logarithm of minimum angle of resolution; RPE = retinal pigment epithelium.

Cohort	Mild impairment $\leq 20/32, \geq 0.2$ logMAR	Moderate impairment $\leq 20/80, \geq 0.6$ logMAR	Severe impairment $\leq 20/200, \geq 1.0$ logMAR
Foveal sparing (cohort III)	0.95 (NA*–6.61)	10.15 (3.09–13.34)	23.3 (13.6–NA*)
Foveal involvement (cohort IV)	0.51 (NA*–4.41)	7.73 (4.30–22.89)	NA* (24.0–NA*)
Log-rank test	0.57	0.07	0.06

Table 2. Median times (years; 95% confidence interval) of best-corrected visual acuity decline since the age at onset compared between eyes of late-onset Stargardt patients who developed foveal sparing and those who had early foveal involvement. logMAR = logarithm of the minimum angle of resolution; NA = not available. *Values could not be calculated, as too many events occurred outside the observational interval.

The median follow-up periods of the entire imaging interval of cohorts I, II, III, and IV were 3.4 (range, 0–10.4), 3.3 (range, 0.1–11.7), 8.7 (range, 2.1–30.9), and 11.4 (range, 0.3–30.9) years, respectively. Eyes in cohorts I and II had a median disease duration of 3.4 years (range, 0–11.7), which was shorter ($P = 1.0 \times 10^{-6}$) than in cohort III and IV (median, 11.0 years; range, 0.3–30.9).

Based on the morphologic observation of distinct cohorts among collective late-onset Stargardt patients, we further analyzed eyes with long follow-up grouped into the “foveal sparing” (cohort III) and “foveal involvement” (cohort IV) cohorts for possible distinctive long-term visual courses among these cohorts. Eyes that formed foveal sparing cohort III took an overall favorable visual course when compared to eyes from foveal involvement cohort IV. Survival analysis for the endpoints ≥ 0.2 logMAR, ≥ 0.6 logMAR,

and ≥ 1.0 logMAR showed a notably later, though not significant, occurrence of each of these events in eyes from foveal sparing cohort III (Table 2).

Modeling of retinal pigment epithelium atrophy

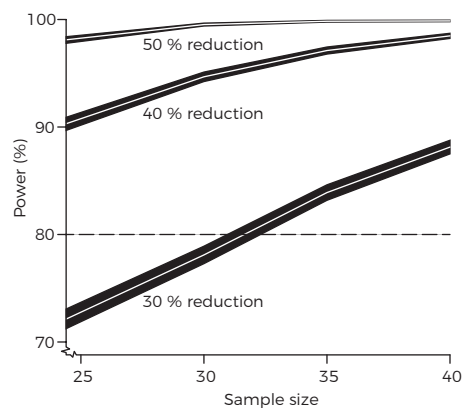
We assessed changes in RPE atrophy area over time in a subset of visits from 66 eyes (from 21 female and 17 male patients). The median follow-up time with FAF imaging was 2.3 years (range, 0.07–7.7). Measurement of RPE atrophy size was possible with high agreement between two independent readers (Supplemental Figure S₂). At the first visit, the mean (\pm standard deviation) RPE atrophy size was 6.26 ± 7.3 mm². Square root transformed data were used for all further analysis. Modeling RPE atrophy over time revealed an annual atrophy progression rate (slope) of 0.22 mm/year (95% CI: 0.19–0.27).

For 28 patients, data on RPE atrophy progression were available from both eyes for the same observational interval, and revealed that atrophy progression rates moderately correlated between the two eyes of a single patient (Pearson's $r = 0.52$; Supplemental Figure S₃).

Sample Size Calculations

Based on the observed progression kinetics and the agreement between two eyes of a single individual, we were able to perform sample size calculations for possible future therapeutic trials. The assumption of a trial duration of 2 years and inclusion of only patients with bilateral RPE atrophy resulted in the sample size–power relationship depicted in Figure 3, with expected effect sizes of 50%, 40%, and 30% reduction in RPE atrophy progression. For effect sizes of 50% and 40%, fewer than 25 patients would be needed to obtain a statistical power of 0.9 at the 5% significance level, while for an effect size of 30%, a power of 0.8 would be reached if at least 32 patients were included.

Figure 3. Statistical power as a function of sample size. Calculations were performed for expected effect sizes of 50%, 40%, and 30% reduction of atrophy progression. The figure shows the power values \pm 95% confidence intervals for each value of the effect size, as estimated from a simulation study with 10,000 runs. The significance level was set to 0.05. A trial duration of 2 years was assumed.



Discussion

The natural history of late-onset Stargardt features expanding, well-demarcated areas of RPE atrophy, which can be a promising clinical biomarker to monitor disease progression. Although clinical features have been previously described,⁵ we comprehensively report on visual course and specific RPE atrophy progression rates in a large multicenter cohort that was well defined by clinical, genetic, and validated imaging parameters. In addition, we used advanced statistical methods to deliver robust results,²⁴ as these are required for planning and conducting clinical trials. These measures ensured the highest levels of data integrity. As a result, this work showed that a future therapeutic trial can be realized with sufficient statistical power with a cohort of as few as 35 patients (Figure 3).

In contrast, visual acuity loss may not be a useful outcome measure in clinical trials due to its high interindividual variance² and overall slow decline; this would result in unrealistic large cohorts and long follow-up. Surrogate biomarkers may be more convenient, ideally predicting long-term changes in functional disease progression by detecting small short-term changes.²⁵ Indeed, both visual acuity loss and atrophic RPE lesions, in which small changes are measurable, progress over time. Although this relationship may justify using RPE atrophy as a surrogate, there is a profound disconnect, particularly in late-onset Stargardt, between the area of RPE atrophy and vision. This discordance can be explained by clinically distinct progression subtypes: progression to either a foveal sparing phenotype in which RPE atrophy encircles the fovea in a horseshoe- or donut-like fashion (cohort III),^{7,8,10,22} or a subtype in which no such foveal sparing occurs (cohort IV). Foveal involvement can determine the eventual vision loss, either early when the eye has an initially involved fovea, or late when it exhibits a foveal sparing phenotype.

As discussed above, visual acuity can vary widely, and for now, unpredictably, depending on the eventual foveal involvement. As the present data show, a large group of 37% with foveal involvement will do poorly, the rest relatively well. To determine those patients that would benefit most from therapy in terms of future clinical trials, analysis of additional imaging modalities could be helpful. While mottled decreased areas are difficult to quantify,²¹ other imaging biomarkers, in particular, spectral-domain optical coherence tomography, could indicate what drives the disease process toward foveal involvement. It has been demonstrated that outer retinal involvement precedes RPE loss. Specifically, outer nuclear layer and ellipsoid zone thinning can occur in regions of normal RPE thickness, suggesting that photoreceptor thinning may precede RPE degeneration.²⁶ Hence, outer retinal damage on spectral-domain optical coherence tomography would precede recognition on FAF. In addition, environmental and genetic factors could significantly

influence the development of RPE atrophy as identified in atrophic AMD.^{27, 28} Such data were not included in this study and need to be addressed in future work.

Further limitations include the retrospective nature of the study and the resulting heterogeneity of the patients' data, which may have been the reason for failing to show significance between different subtypes of late-onset Stargardt. For instance, some patients did not report any symptoms, and were more likely to have no RPE atrophy or only extrafoveal RPE atrophy not encircling the fovea. These patients would need a longer follow-up to identify in which direction the disease will develop. Analogously, heterogeneity within the imaging data, for example, the fields of view in NIR and FAF imaging, might have led to the nondetection of more peripheral atrophic lesions in patients with a 30° field of view, while such lesions would have been detected in eyes imaged with a 55° objective.

In recent years, identifying biomarkers in retinal disease has become a central issue for therapeutic trials that aim to test the efficacy of a drug. A surrogate outcome measure accepted by the U.S. Food and Drug Administration is geographic atrophy in AMD,¹⁷ to which areas of RPE atrophy show close similarities. As this study now has shown that RPE atrophy can also be used as an outcome measure in late-onset Stargardt, it may even be valuable in other retinal diseases affecting the RPE. Of special interest is the precise characterization of late-onset Stargardt patients; their adult age makes them ethically more appropriate candidates to participate in clinical trials than patients who are of minor age. This study provides important knowledge on the natural history of late-onset Stargardt, quantitatively describing the course of visual loss and atrophy progression. In addition, it provides fundamental information necessary to conduct clinical trials in patients with Stargardt disease.

References

1. Blacharski PA. Fundus flavimaculatus. In: Newsome DA, ed. *Retinal dystrophies and degenerations*. New York: Raven Press, 1988.
2. Rotenstreich Y, Fishman GA, Anderson RJ. Visual acuity loss and clinical observations in a large series of patients with Stargardt disease. *Ophthalmology* 2003;110(6):1151-8.
3. Fujinami K, Zernant J, Chana RK, et al. Clinical and molecular characteristics of childhood-onset Stargardt disease. *Ophthalmology* 2015;122(2):326-34.
4. Lambertus S, van Huet RA, Bax NM, et al. Early-onset stargardt disease: phenotypic and genotypic characteristics. *Ophthalmology* 2015;122(2):335-44.
5. Westeneng-van Haafte SC, Boon CJ, Cremers FP, et al. Clinical and genetic characteristics of late-onset Stargardt's disease. *Ophthalmology* 2012;119(6):1199-210.
6. Fritsche LG, Fleckenstein M, Fiebig BS, et al. A subgroup of age-related macular degeneration is associated with mono-allelic sequence variants in the ABCA4 gene. *Invest Ophthalmol Vis Sci* 2012;53(4):2112-8.
7. Sunness JS. The natural history of geographic atrophy, the advanced atrophic form of age-related macular degeneration. *Mol Vis* 1999;5:25.
8. Sunness JS, Gonzalez-Baron J, Applegate CA, et al. Enlargement of atrophy and visual acuity loss in the geographic atrophy form of age-related macular degeneration. *Ophthalmology* 1999;106(9):1768-79.
9. Sarks JP, Sarks SH, Killingsworth MC. Evolution of geographic atrophy of the retinal pigment epithelium. *Eye (Lond)* 1988;2 (Pt 5):552-77.
10. van Huet RA, Bax NM, Westeneng-Van Haafte SC, et al. Foveal sparing in Stargardt disease. *Invest Ophthalmol Vis Sci* 2014;55(11):7467-78.
11. McBain VA, Townend J, Lois N. Progression of retinal pigment epithelial atrophy in stargardt disease. *Am J Ophthalmol* 2012;154(1):146-54.
12. Han Z, Conley SM, Naash MI. Gene therapy for Stargardt disease associated with ABCA4 gene. *Adv Exp Med Biol* 2014;801:719-24.
13. Schwartz SD, Hubschman JP, Heilwell G, et al. Embryonic stem cell trials for macular degeneration: a preliminary report. *Lancet* 2012;379(9817):713-20.
14. Charbel Issa P, Barnard AR, Herrmann P, et al. Rescue of the Stargardt phenotype in *Abca4* knockout mice through inhibition of vitamin A dimerization. *Proc Natl Acad Sci U S A* 2015;112(27):8415-20.
15. Cukras CA, Wong WT, Caruso R, et al. Centrifugal expansion of fundus autofluorescence patterns in Stargardt disease over time. *Arch Ophthalmol* 2012;130(2):171-9.
16. Lois N, Halfyard AS, Bird AC, et al. Fundus autofluorescence in Stargardt macular dystrophy-fundus flavimaculatus. *Am J Ophthalmol* 2004;138(1):55-63.
17. Csaky KG, Richman EA, Ferris FL, 3rd. Report from the NEI/FDA Ophthalmic Clinical Trial Design and Endpoints Symposium. *Invest Ophthalmol Vis Sci* 2008;49(2):479-89.
18. Schmitz-Valckenberg S, Brinkmann CK, Alten F, et al. Semiautomated image processing method for identification and quantification of geographic atrophy in age-related macular degeneration. *Invest Ophthalmol Vis Sci* 2011;52(10):7640-6.
19. Boon CJ, van Schooneveld MJ, den Hollander AI, et al. Mutations in the peripherin/RDS gene are an important cause of multifocal pattern dystrophy simulating STGD1/fundus flavimaculatus. *Br J Ophthalmol* 2007;91(11):1504-11.
20. Boon CJ, Klevering BJ, Cremers FP, et al. Central areolar choroidal dystrophy. *Ophthalmology* 2009;116(4):771-82, 82 e1.
21. Kuehlewein L, Hariri AH, Ho A, et al. Comparison of manual and semiautomated fundus autofluorescence analysis of macular atrophy in Stargardt disease phenotype. *Retina* 2016;36(6):1216-21.
22. Lindner M, Boker A, Mauschitz MM, et al. Directional Kinetics of Geographic Atrophy Progression in Age-Related Macular Degeneration with Foveal Sparing. *Ophthalmology* 2015;122(7):1356-65.
23. R Development Core Team. *R: A Language and Environment for Statistical Computing*. Vienna, Austria: R Foundation for Statistical Computing, 2012.

24. Turnbull BW. The empirical distribution function with arbitrary grouped censored and truncated data. *J R Stat Soc Series B Stat Methodol* 1976;38:290-5.
25. Brooks DJ, Frey KA, Marek KL, et al. Assessment of neuroimaging techniques as biomarkers of the progression of Parkinson's disease. *Exp Neurol* 2003;184 Suppl 1:S68-79.
26. Burke TR, Rhee DW, Smith RT, et al. Quantification of peripapillary sparing and macular involvement in Stargardt disease (STGD1). *Invest Ophthalmol Vis Sci* 2011;52(11):8006-15.
27. Finger RP, Chong E, McGuinness MB, et al. Reticular Pseudodrusen and Their Association with Age-Related Macular Degeneration: The Melbourne Collaborative Cohort Study. *Ophthalmology* 2016;123(3):599-608.
28. Reynolds R, Rosner B, Seddon JM. Dietary omega-3 fatty acids, other fat intake, genetic susceptibility, and progression to incident geographic atrophy. *Ophthalmology* 2013;120(5):1020-8.



“A lack of obvious fundus abnormalities left an alarming number of children with Stargardt disease without the correct diagnosis. We hope that greater awareness of this subtype avoids misdiagnosis and years of inappropriate treatment.”

Nathalie M. Bax
Stanley Lambertus
Frans P.M. Cremers
B. Jeroen Klevering
Carel B. Hoyng

Submitted

3.1 The absence of fundus abnormalities in Stargardt disease

PURPOSE: To raise awareness of Stargardt disease (STGD1) patients without fundus abnormalities.

DESIGN: Retrospective cohort study.

PARTICIPANTS: Thirty-one STGD1 patients with ≥ 1 ABCA4 variants in whom no fundus abnormalities were described at first ophthalmic consultation.

METHODS: Medical records were evaluated for age at onset, initial symptoms and diagnosis, delay reason for delay of diagnosis, age at STGD1 diagnosis, best-corrected visual acuity (BCVA), ophthalmoscopy, fundus photography, fundus autofluorescence (FAF), fluorescein angiography (FA), spectral-domain optical coherence tomography (SD-OCT), full-field electroretinography (ffERG), color vision test, and the presence of ABCA4 variants.

MAIN OUTCOME MEASURES: Age at onset, reason for delay of diagnosis, initial diagnosis, age at STGD1 diagnosis, presence of ABCA4 variants.

RESULTS: In 11.1% of our STGD1 cohort, no fundus abnormalities were observed at first ophthalmic consultation. The median age at onset was 8 years (range, 1–18). There was a median delay in diagnosis of 3 years (range, 0–19) in 27 out of 31 patients, which resulted in a median age at diagnosis of 12 years (range, 7–26). Patients were misdiagnosed with amblyopia, myopia, optic disk pathology, mental health problems, tension headache, neuritis bulbaris, and uveitis. Subtle abnormalities, such as lipofuscin accumulation, were seen on FAF at an earlier disease stage than in ophthalmoscopy. On SD-OCT, this included a thickened external limiting membrane. Color vision tests showed red-green insufficiency in 79% of patients. Reduced ffERG amplitudes were only present in 26%, and a dark choroid sign in 65% of the patients. Visual acuity considerably fluctuated in the first 5 years after onset. The majority of the patients (65%) carried a least one variant with a severe effect on ABCA4 function.

CONCLUSIONS: A high number of childhood-onset STGD1 patients were diagnosed with a major delay. The presence of accurate competence, equipment and the possibility for genetic screening is required, therefore we recommend to refer children with visual complaints without initial fundus abnormalities to a specialized ophthalmologic center. In particular, to diagnose patients at an early stage of disease is of increased importance with the advent of new therapeutic possibilities.

Introduction

Stargardt disease (STGD1) is arguably the most common retinal dystrophy and affects 1:10000 people worldwide.¹ This autosomal recessive disease is caused by variants in the ABCA4 gene that encodes for a retinal-specific adenosine triphosphate-binding cassette transporter protein. Dysfunction of the ABCA4 protein leads to toxic accumulation of byproducts from the visual cycle in the photoreceptor cell and retina pigment epithelium (RPE), which eventually leads to irreversible damage of the outer retinal layers.^{2,3}

Up to 5,962 variants in the ABCA4 gene have been identified; the specific combinations of variants in conjunction with largely unknown modifying factors in each patient result in a highly heterogenic phenotype. Patients with STGD1 present with progressive vision loss, which typically occurs in the second decade but early and late forms have been well recognized.⁴⁻⁶ In general, the fundus picture is characterized by the presence of irregular yellow-white fundus flecks in the posterior pole. During the course of the disease, macular atrophy develops, sometimes with a 'beaten bronze' aspect; in other patients a bull's eye pattern can be observed. Lipofuscin accumulates in the outer retinal layers, which results in a 'dark choroid' on the fluorescein angiogram in approximately 80% of the patients.⁷⁻¹⁰ In early forms with a disease onset ≤ 10 years of age, atrophy of the macula is a prominent and early feature; the yellow flecks may be absent or hardly notable.^{4,11,12} The flecks are much more common in the classic form of STGD1 with an age of onset in the early teens, sometimes extending beyond the vascular arcades resulting in the fundus flavimaculatus phenotype.^{13,14} Late-onset forms of the disease are characterized by atrophy of the retinal pigment epithelium, subtle flecks, and foveal sparing.^{5,15,16}

The diagnosis of STGD1 can be challenging in early disease especially, as no apparent changes may be present on ophthalmoscopy despite the loss of visual function.⁴ This lack of clinical signs in combination with the limited capabilities for expression in young children may delay the correct diagnosis. Not only is early identification of these patients essential for the emotional aspect of a timely diagnosis, it is also important in the light of emerging therapeutic options for STGD1 disease, such as gene augmentation (ClinicalTrials.gov, NCT01367444 and NCT01736592), stem cell therapy (ClinicalTrials.gov, NCT01469832), and small-molecule drugs (ClinicalTrials.gov, NCT02402660).

In this study, we describe—in detail—the clinical and molecular genetic findings in a group of STGD1 patients, which presents without initial fundus abnormalities in ophthalmoscopy. We hope that a heightened awareness avoids misdiagnosis, such as functional visual loss in these children and, in worst case scenarios, years of inappropriate treatment.

Methods

Patients

The database with STGD1 patients of the Department of Ophthalmology, Radboud university medical center (Nijmegen, the Netherlands) contains 448 patients of all ages and disease onset, of whom 294 were screened for variants in the ABCA4 gene. In 280 patients, ≥ 1 ABCA4 variants could be identified. We included 31 patients who did not show obvious fundus abnormalities at the first presentation. This study was approved by the Institutional Ethics Committee and was performed in accordance with the Declaration of Helsinki.

Clinical evaluation

We collected the clinical data from the medical records. These included age at onset, initial symptoms, initial diagnosis and examinations or therapy, age at STGD1 diagnosis, delay of diagnosis and reason for this delay, number of referrals before diagnosis, and general medical history. Age at onset was defined as the first manifestation of the disease, these symptoms could have been noticed by the patient, but also their family members and/or the school physician.

The standard ophthalmic examination included best-corrected visual acuity (BCVA) using Early Treatment Diabetic Retinopathy Study (ETDRS) or Snellen charts, slit-lamp biomicroscopy and detailed fundus examination. Best-corrected visual acuity was transformed into the logarithm of the minimum angle of resolution (logMAR) for statistical analysis. For fundus photography, we used the Topcon TRC50IX (Topcon Corporation, Tokyo, Japan). Fluorescein angiography and cross-sectional images using spectral-domain optical coherence tomography (SD-OCT) centered at the macula were obtained with the Spectralis (HRA+OCT, Heidelberg Engineering, Heidelberg, Germany). Short-wave fundus autofluorescence (FAF) imaging ($\lambda = 488$ nm, emission 500–700 nm) was performed using a confocal scanning laser ophthalmoscope (Spectralis HRA+OCT or HRA2, Heidelberg Engineering, Heidelberg, Germany). The field of view was set at $30^\circ \times 30^\circ$ or $55^\circ \times 55^\circ$, centered at the macula. For evaluation of color vision, we employed the Ishihara or Panel D-15 test. Full-field electroretinography (ffERG) was performed using Dawson-Trick-Litzkow electrodes and the RETI-port system (Roland Consults, Stasche & Finger GmbH, Brandenburg an der Havel, Germany). The recordings were performed in accordance with the guidelines of the International Society for Clinical Electrophysiology of Vision (ISCEV).¹⁷ We grouped ffERG results as described by Lois et al.¹⁸: group 1, patients with normal ffERG responses; group 2, patients with reduced photopic amplitudes (<5% of normal range); and group 3, patients with reduced photopic and scotopic amplitudes (<5% of normal range).

Genetic analysis

Genetic analysis of the ABCA4 gene was performed at the Department of Human Genetics at the Radboud university medical center (Nijmegen, the Netherlands) using arrayed primer extension analysis (Asper Biotech, Tartu, Estonia). If the Asper microarray screening revealed only one ABCA4 variant, exon and intron-exon boundaries were sequenced in the ABCA4 gene to identify additional variants. All variants were confirmed with Sanger sequencing. The following variants were defined as severe: protein-truncating, canonical splice-site variants, as well as deletions spanning at least one exon.

Statistical analysis

We used SPSS version 22.0 (IBM Corp, Armonk, NY) for statistical data analysis, using descriptive statistics by median and range for continuous variables, and percentages for categorical variables. We employed Kaplan-Meier estimators to analyze the interval between age at onset and age at which four different visual endpoints were reached. These four points were based on the classification of visual impairment of the World Health Organization: (near-)normal to mild visual impairment ≥ 0.2 logMAR ($\leq 20/32$ Snellen), moderate visual impairment ≥ 0.6 logMAR ($\leq 20/80$ Snellen), severe visual impairment ≥ 1.0 logMAR ($\leq 20/200$ Snellen), and blindness ≥ 1.4 logMAR ($\leq 20/500$ Snellen).

Results

Clinical characteristics

In 31 of 280 (11.1%) STGD1 patients, no obvious fundus abnormalities were observed at the first ophthalmic consultation. The group consisted of 15 males and 16 females with six siblings from three different families, and 25 isolated cases. An overview of the clinical findings and the diagnostic process is given in [Table 1](#). In one-third of cases, symptoms of a decreased visual acuity were not noticed by the patient but by the parents or a school physician. Age at onset occurred at a median age of 8 years (range, 1–18). In 87% of the patients, there was a delay in diagnosis: a median delay of 3 years (range, 0–19), which resulted in a median age at diagnosis of 12 years (range, 7–26). The main reason for delayed STGD1 diagnosis was misdiagnosis, in particular amblyopia treated with occlusion therapy (6 patients) and mental health issues (5 patients). The majority of patients (94%) visited more than two hospitals before the correct diagnosis was made. All patients were finally diagnosed with STGD1 in tertiary referral centers. The first fundus abnormalities were observed at a median time of 3 years (range, 0.5–16) after first symptoms. These included central RPE alterations (43%), bull's eye maculopathy (33%), and/or parafoveal flecks (24%). Once these features had been observed, STGD1

ID	Gender	Age at onset (years)	Decreased VA noticed by	Number of other hospitals before correct diagnosis	Reason for delay of diagnosis	Initial diagnosis and examinations or therapy	Age at STCD1 diagnosis (years)	Fundus abnormalities at the time of diagnosis	BCVA at diagnosis (Snellen)
1	m	1	family	2	Wrong diagnosis	Mental health problem or unknown syndrome	14	Bull's eye	20/200
2	m	5	patient	2	Wrong diagnosis	Amblyopia with occlusion therapy	11	Bull's eye	20/125
3	f	16	family	2	Wrong diagnoses	Amblyopia with occlusion therapy. Retinobulbar optic neuritis. Neuro-imaging (CT) was performed (no abnormalities). Cone dystrophy	20	RPE alterations	20/100
4	m	7	patient	2	No delay (mother insisted on a referral to an academic hospital)	Cone dystrophy	7	RPE alterations	20/125
5	f	7	family	3	Wait and see	No diagnosis	26	Bull's eye	20/125
6	f	7	patient	3	Wrong diagnosis	Diagnosed with a mental health problem, in view of the variable VA between visits.	23	RPE alterations	20/50
7	f	9	patient	1	Wait and see	No diagnosis	15	Bull's eye	20/125
8	m	10	patient	2	Wrong diagnosis	Myopia	13	Central fundus flecks	20/35
9	m	4	patient	2	Wrong diagnoses	Initially, amblyopia with occlusion therapy. Complaints of headache lead to neuro-imaging (MRI) followed by physiotherapy. Eventually diagnosed with cone dystrophy.	8	RPE alterations	20/70
10	f	7	patient	2	Wrong diagnosis	Mental health problem	10	RPE alterations	20/20
11	m	6	public health service	2	Delayed referral to ophthalmologist	Cone dystrophy	8	RPE alterations	20/125
12	m	3	school physician	2	Wrong diagnosis	Amblyopia with occlusion therapy	10	Bull's eye	20/35
13	f	17	patient	2	Delayed referral to ophthalmologist	Cone dystrophy	20	Bull's eye	20/80
14	f	13	patient	2	Wrong diagnosis	Amblyopia with occlusion therapy. Also neuro-imaging (MRI) via neurologist.	15	RPE alterations	20/70
15	m	8	patient	2	Wrong diagnosis	Optic neuropathy. A brain MRI and lumbar puncture revealed no abnormalities.	10	RPE alterations	20/80
16	f	8	patient	3	Wrong diagnosis	Myopia	23	Central fundus flecks	20/35
17	m	15	patient	2	Wait and see	No diagnosis	18	Central fundus flecks	20/100
18	f	10	school physician	4	Other disease overshadowed STCD1	Diagnosis of optic drusen overshadowed diagnosis STCD1	26	RPE alterations	20/200
19	f	9	patient	2	Wait and see	No diagnosis	12	Bull's eye	20/400
20	m	16	patient	2	Wait and see	No diagnosis	21	RPE alterations	20/70
21	f	9	school physician	2	Wrong diagnosis	Uveitis	10	RPE alterations	20/40
22	m	6	patient	2	No delay, due to timely referral to academic hospital	Immediate referral to academic center for additional examinations. Because of extreme low VA (20/400 Snellen)	7	RPE alterations	20/400

23	f	11	patient	2	Wrong diagnosis	Tension headache, consulting neurologist	13	Central fundus flecks	20/125
24	m	3	school physician and family	2	Wrong diagnosis	Amblyopia, received occlusion therapy (decrease in VA due to lack of therapy)	9	Bull's eye	20/125
25	f	11	patient	2	Delayed referral	No diagnosis	13	Bull's eye	20/100
26	m	7	patient	2	Little delay, due to referral to academic hospital	Cone dystrophy	8	Bull's eye	20/125
27	f	8	patient	1	Wrong diagnosis	Mental health problem	11	RPE alterations	20/70
28	m	6	patient	2	Minor delay, due to timely referral to academic hospital	Cone dystrophy	7	Central fundus flecks	20/35
29	f	18	patient	2	Delayed referral	Cone dystrophy	20	Bull's eye	20/35
30	f	3	public health service	2	Wrong diagnosis	"Schoolgirl amblyopia"	12	Central fundus flecks	20/250
31	m	13	school physician	2	Minor delay due to timely referral to academic hospital	Cone dystrophy	14	RPE alterations	20/70

Table 1. Clinical characteristics and diagnostic process in Stargardt disease (STGD1) patients without initial fundus abnormalities.

ID = patient identification in this study; m = male; f = female; VA = visual acuity; BCVA = best-corrected visual acuity; RPE = retinal pigment epithelium.

was generally diagnosed relatively quickly in the majority of patients (median, 0.7 years; range, 0.1–3).

We could retrieve the BCVA at the first ophthalmic visit in 21 out of 31 patients; the median BCVA at that time was 20/32 Snellen (20/20–20/400). The median interval and 95% confidence interval (CI) between the age at onset and decline in BCVA to mild, moderate, severe visual impairment and blindness was 1 year (95% CI, 0.0–2.25), 4 years (95% CI, 3.1–4.9) and 12 years (95% CI, 7.8–16.2). One patient reached blindness 34 years after the first symptoms of onset at age 9. In many patients, the visual acuity findings were quite variable early in the course of the disease as shown in [Figure 1](#).

In 29 out of 31 patients, fundus flecks were eventually noticed at a median time of 3.5 years (range, 0.1–16.5) after the initial ophthalmic consultation. In 17 patients (59%), subtle parafoveal flecks could be seen, in 5 patients (17%) flecks were noticed within the vascular arcades, and in 7 patients (24%) flecks extended to the periphery. In 2 patients, no fundus flecks were reported at any time during the course of the disease (follow-up time, 1 and 10 years).

In 23 of 31 patients, the first SD-OCT scan was performed at 9 years (range, 0.1–24) after disease onset. No SD-OCT scans were performed in the remaining 8 patients. All SD-OCT scans showed abnormalities by disorganized or absent RPE. A thickened external limiting membrane (ELM) was seen in 2 patients (0.5 and 1 year after disease

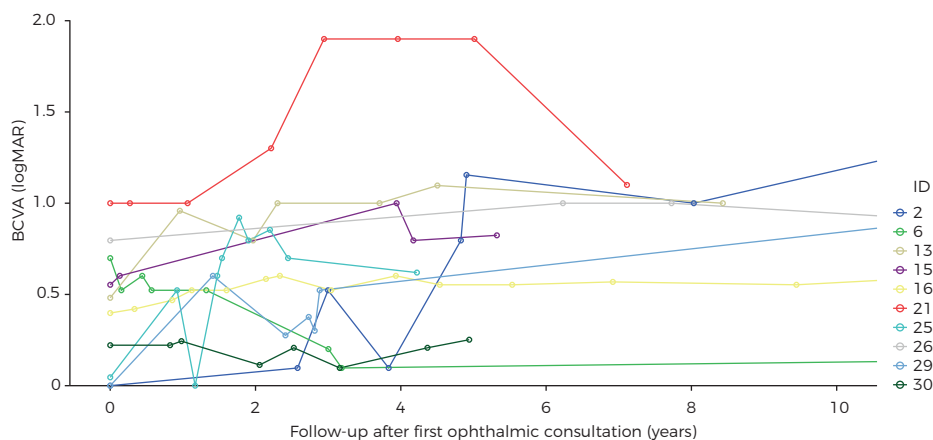


Figure 1. Course of the best-corrected visual acuity (BCVA) in logMAR in ten patients. The visual acuity varies greatly during the first five years after first ophthalmic consultation. LogMAR 0 = 20/20 Snellen, LogMAR 0.5 = 20/63 Snellen, LogMAR 1.00 = 20/200 Snellen, LogMAR 1.50 ≈ 20/630 Snellen, LogMAR 2.00 = 20/2000 Snellen. Each patient (ID = patient identification) is shown in a different color.

onset). A dark choroid was observed in 15 of 23 (65%) patients in whom fluorescein angiography was performed. In 22 patients, the first FAF was performed 3.5 years (0.5–24) after onset. No atrophy was seen (median, 1 year after onset) in 5 patients, (peri)foveal atrophy in 9 (median, 4 years after onset), atrophy within the vascular arcades in 7 (median, 15 years after onset), and panretinal atrophy (15 years after onset) in 1. In 4 patients, abnormalities were seen on FAF, but were missed on ophthalmoscopy.

The first ffERG was performed 2 years (0.1–27) after onset in 27 patients. Normal ffERG recordings (group 1) were present in 20 patients (74%), 2 years (0.1–21) after disease onset. We found group 2 ffERGs in 4 patients (15%) with 1 year (0.1–3.5) after onset, and group 3 recordings in 3 patients (11%) with 18 years (6–27) after onset. Follow-up for ffERG recordings was available in 21 patients. In 4 of these patients progressed from group 1 to group 2 (median time, 8 years; range, 7–16), 2 patients progressed from group 2 to group 3 (within 2 and 3 years), and 1 patient progressed from group 1 to group 3 in 6 years. In 17 patients, color vision was tested. In 15 patients (79%) abnormalities were noticed, red-green defects in 14 patients and a blue-yellow defect in 1 patient.

Various imaging modalities of patient 28 and patient 21 are depicted in [Figure 2 and 3](#), respectively.

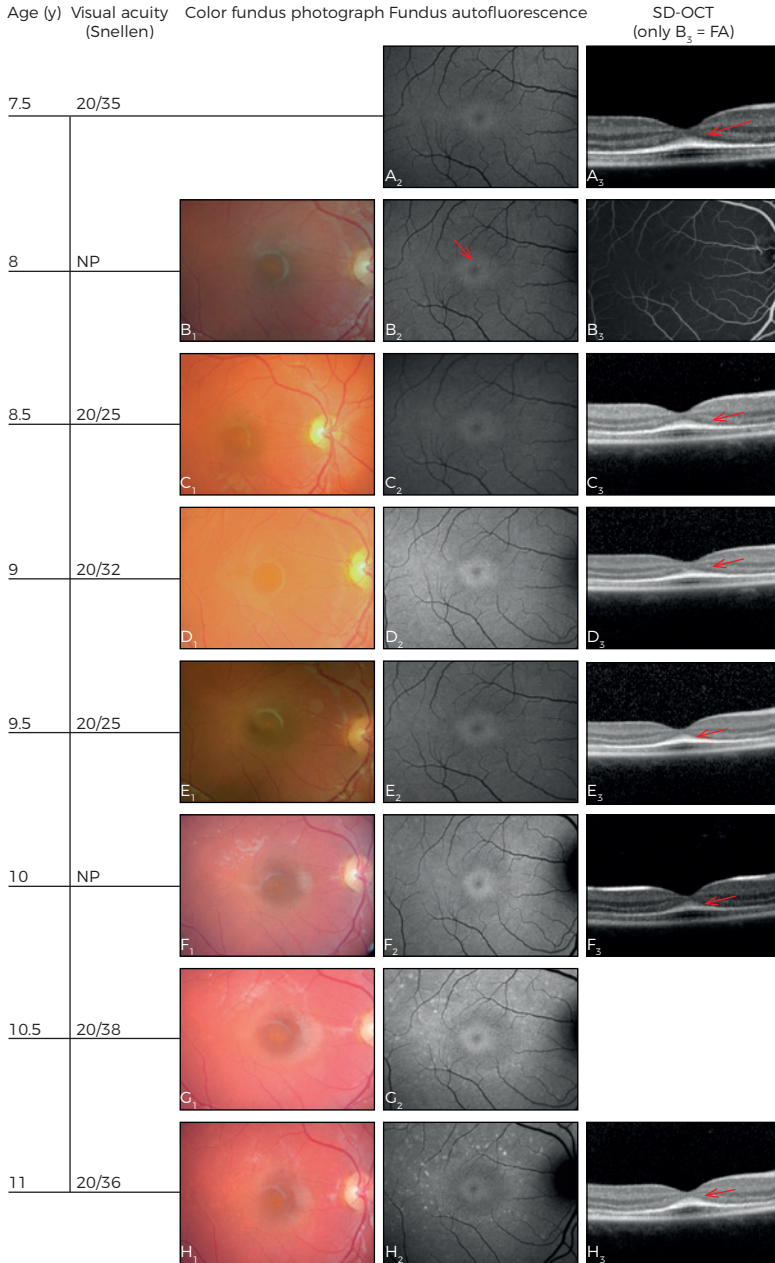


Figure 2. Three-and-a-half-year follow-up in patient 28. Age at onset: 6.5 years. One year later, fundus autofluorescence (FAF) imaging showed a perifoveal ring of hyperautofluorescence (A₂), and on spectral-domain optical coherence tomography (SD-OCT), a discrete thickening of the external limiting membrane (ELM) can be seen (arrow, A₃). Only 6 months later, a subtle hyperautofluorescent perifoveal lesion developed (arrow, B₂). Over time, the hyperautofluorescent flecks become more visible on FAF imaging. In addition, the flecks became noticeable on color fundus photographs. The thickened ELM remained present during the entire follow-up time (arrows, A₃, C₃-H₃). FA = fluorescein angiography. NP = not performed.

Genetic characteristics

Overall, genetic analysis was not performed at first visit, but with a median delay of five years (range, 0–30) after first visit. An overview of *ABCA4* variants in our cohort is described in [Table 2](#).

Variants in the *ABCA4* gene were identified in 59 of 62 alleles (95%). Three variants were found in one patient, two *ABCA4* variants in 27, and one variant in three. In total, 32 distinct variants were detected. The majority of the patients (65%) carried at least one variant with a severe effect on *ABCA4* function ([Table 2, bold](#)).

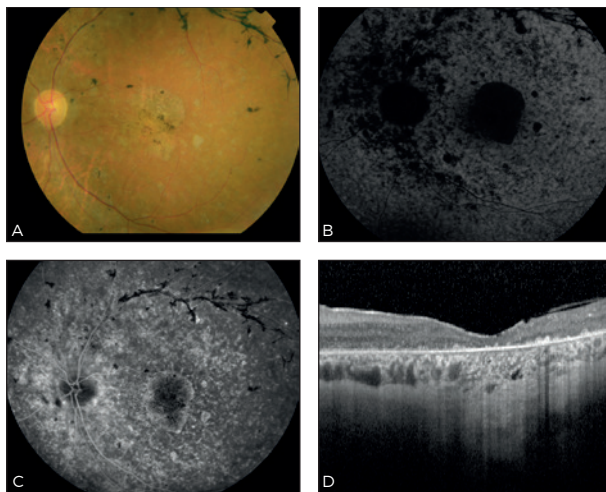


Figure 3. Multimodal imaging in patient 21 at age 25, 15 years after the first symptoms. The visual acuity is 20/1000 Snellen. Color fundus photography (A) shows attenuated retinal vessels (especially the veins), para-arteriolar pigmentations and diffuse chorioretinal atrophy. Fundus autofluorescence imaging (B) shows widespread hypoautofluorescence, especially at the macula, indicating RPE cell loss. Fluorescein angiography (C) shows widespread granular hyperfluorescent lesions as a result of RPE damage, and on spectral-domain optical coherence tomography, (D) loss of the outer retinal layers, as well as the choriocapillaris, can readily be observed.

Discussion

A lack of obvious fundus abnormalities left a high number of children with STGD1 disease without the correct diagnosis. Instead, these patients underwent unnecessary investigations, such as psychic evaluations, brain MRIs or CTs, and lumbar punctures. Many of these children were treated for mental illness and/or amblyopia with pointless and possibly harmful treatments, including years of occlusion therapy.

In patients with adult-onset STGD1, initial ophthalmoscopic features typically include yellow-white flecks and central macular atrophy, and cases without fundus abnormalities have not been described.⁵ In young children, the clinical presentation can be confusing for the general ophthalmologist. Fujinami et al. noticed that one third of their child cohort (<17 years) initially had a normal fundus appearance.⁶ Lambertus et al. described a cohort of 41 STGD1 patients younger than 10 years, and 10 of these patients (24%)

ID	Variant 1	Protein	Type of variant	Variant 2	Protein	Type of variant
1	c.5585-10T>C	p.(?)	Splice-site (non-canonical)			
2	c.[1622T>C:3113C>T]	p.(Leu541Pro:Ala1038Val)	Missense, missense	c.[1622T>C:3113C>T]	p.(Leu541Pro:Ala1038Val)	Missense, missense
3	c.5882G>A	p.(Gly1961Glu)	Missense	c.3305A>T	p.(Asp1102Val)	Missense
4	c.4539+1C>T	p.(?)	Splice-site (canonical)	c.5762_5763dup	p.(Ala1922Trpfs*18)	Frameshift
5	c.6089G>A	p.(Arg230Gln)	Missense	c.5461-10T>C	p.(Thr1821Valfs*13, Thr1821Aspfs*6)	Frameshift
6	c.2588G>C	p.(Gly863Ala, Gly863del)	Missense, splice defect	c.4539+1G>T	p.(?)	Splice-site (canonical)
7	c.2588G>C	p.(Gly863Ala, Gly863del)	Missense, splice defect	c.4539+1G>T	p.(?)	Splice-site (canonical)
8	c.2588G>C	p.(Gly863Ala, Gly863del)	Missense, splice defect	c.4128+1G>A	p.(?)	Splice-site (canonical)
9	c.3259G>A	p.(Glu1087*)	Nonsense	c.2919-?_3328+?del	p.(Ser974Clnfs*64)	Frameshift; deletion
10	c.3259G>A	p.(Glu1087*)	Nonsense	c.768G>T	p.(?)	Splice-site (non-canonical)
11	c.5762_5763dup	p.(Ala1922Trpfs*18)	Frameshift	c.6320G>A	p.(Arg2107His)	Missense
12	c.4539+1C>T	p.(?)	Splice-site (canonical)			
13	c.3874C>T	p.(Gln1292*)	Nonsense			
14	c.5196+1137G>A	p.(?)	Deep-intronic, splicing			
15	c.5312+1G>A	p.(?)	Splice-site (canonical)	c.286A>G	p.(Asn96Asp)	Missense
16	c.5161_5162del	p.(Thr1721Hisfs*65)	Frameshift	c.5882G>A	p.(Gly1961Glu)	Missense
17	c.3874C>T	p.(Gln1292*)	Nonsense	c.5196+1137G>A	p.(?)	Deep-intronic, splicing
18	c.5461-10T>C	p.(Thr1821Valfs*13, Thr1821Aspfs*6)	Frameshift	c.5537T>C	p.(Ile1846Thr)	Missense
19	c.214G>A	p.(Gly72Arg)	Missense	c.5461-10T>C	p.(Thr1821Valfs*13, Thr1821Aspfs*6)	Frameshift
20	c.4773+1C>A	p.(?)	Splice-site (canonical)	c.5537T>C	p.(Ile1846Thr)	Missense
21	c.768G>T	p.(?)	Splice-site (non-canonical)	c.2919?_*3328+?del	p.(Ser974Clnfs*64)	Frameshift; deletion
22	c.768G>T	p.(?)	Splice-site (non-canonical)	c.1804C>T	p.(Arg602Trp)	Missense
23	c.[1622T>C:3113C>T]	p.(Leu541Pro:Ala1038Val)	Missense, missense	c.6316C>T	p.(Arg2106Cys)	Missense
24	c.5714+5G>A	p.(?)	Splice-site (non-canonical)	c.3033-?_3364+?del	p.(?)	Frameshift; deletion
25	c.5714+5G>A	p.(?)	Splice-site (non-canonical)	c.3033-?_3364+?del	p.(?)	Frameshift; deletion
26	c.[872C>T:424C>T]	p.(Pro291Leu:Trp1408Cys)	Missense, missense	c.2947A>C	p.(Thr983Ala)	Missense
27	c.768G>T	p.(?)	Splice-site (non-canonical)	c.5113C>T	p.(Arg1705Trp)	Missense
28	c.2947A>C	p.(Thr983Ala)	Missense	c.5461-10T>C	p.(Thr1821Valfs*13, Thr1821Aspfs*6)	Frameshift
29	c.768G>T	p.(?)	Splice-site (non-canonical)	c.872C>T	p.(Pro291Leu)	Missense
30	c.5461-10T>C	p.(Thr1821Valfs*13, Thr1821Aspfs*6)	Frameshift	c.6320G>A	p.(Arg2107His)	Missense
31	c.5882G>A	p.(Gly1961Glu)	Missense	c.4352+1G>A	p.(?)	Splice-site (canonical)

Table 2. Variant, protein notation, and type of variant in the ABCA4 gene of Stargardt disease patients without fundus abnormalities.

del = deletion; dup = duplication; dup = duplication; fs = frameshift; NI = not identified; * stop signal.

also did not have fundus abnormalities.⁴ These studies show that the absence of readily observable fundus abnormalities in young STGD1 patients is not an isolated finding, but a relative common part of the clinical spectrum.

In our cohort, when fundus abnormalities did occur, these were often not the typical yellowish flecks but rather RPE alterations, often in a bull's eye pattern. A hypothesis for the absence of typical fundus flecks may lie in the relative high pathogenicity of ABCA4 variants. As the majority of our cohort (65%) carried at least one severe variant, there may be little ABCA4 function left in these patients, leading to a very early manifestation of the disease. The built-up of toxic *N*-retinylidene-*N*-retinylethanolamine in RPE cells develops rapidly, thereby causing early cell death without the opportunity for lipofuscin to accumulate and subsequent fleck formation.

Blocking of the choroidal vessels on FA resulting a dark or silent choroid is frequently used as diagnostic marker for STGD1. The prevalence of this FA finding in STGD1 patients has been described in up to 86% of patients.¹⁹ A dark choroid was present in 65% in our relatively small cohort. A correlation has been described between the presence of yellow-white fundus flecks and the appearance of dark choroid,^{8, 20} which might account for the relative low percentage of patients with a dark choroid in this cohort. Fundus autofluorescence imaging is a relative new modality that may be used to identify early and subtle lipofuscin.²¹ In addition, a thickened ELM on SD-OCT may also serve as an early marker for STGD1.²² However, in the study of Lee et al, this distinct ELM thickening was described to occur in all (26/26) cases. In our cohort, only 2/23 cases with performed SD-OCT were observed to have this feature. The delay of performing an SD-OCT (mean, 9 years after disease onset) could be an explanation of the difference in appearance of ELM thickening in both cohorts. The two cases of our cohort with this distinct feature was SD-OCT performed 0.5 and 1 year after disease onset, so suggestive for early disease marker. Abnormal color vision was observed in 79% of our STGD1 patients, which corresponds with the previously reported percentages.²³

Although STGD1 is the most common juvenile macular dystrophy, it remains a relative rare disorder. Clinicians in a general ophthalmic practice may lack the experience to identify and interpret the subtle abnormalities in these young children. When we consider the relative difficulty associated with the ophthalmic examination of (very) young children, the high number of misdiagnoses in the early-onset STGD1 patient group may not come as a surprise. Therefore, we want to make ophthalmologists aware of early findings in STGD1, especially appearing in children. First, visual acuity often fluctuates in these patients which should not automatically rule out the possibility of a photoreceptor disease. Second, a fundus photograph can be helpful in discerning very subtle fundus

abnormalities and may be useful in follow-up. Third, non-invasive investigations such as SD-OCT (thickening of the ELM), FAF (subtle lipofuscin accumulation) and color vision tests may help in the diagnostic process. Fluorescein angiography is invasive, apart from the oral variant, but may also be less helpful in patients without fundus abnormalities in the light of the relative low percentage of dark choroids in these patients.

In children with visual disturbances, retinal dystrophies should be considered and ruled out when possible, even in the absence of fundus abnormalities on ophthalmoscopy. Instead of wait and see, we would recommend referring these children to a tertiary ophthalmic center and performing SD-OCT and FAF to define early findings of STGD1. A correct and early diagnosis of STGD1 prevents a lot of distress, unnecessary investigations and harmful therapies; in addition, early identification may prove important in the light of emerging therapeutic options.

References

1. Blacharski P. Retinal dystrophies and degenerations. Newsome DA (ed) 1988:135-59.
2. Allikmets R, Shroyer NF, Singh N, et al. Mutation of the Stargardt disease gene (ABCR) in age-related macular degeneration. *Science* 1997;277(5333):1805-7.
3. Allikmets R, Singh N, Sun H, et al. A photoreceptor cell-specific ATP-binding transporter gene (ABCR) is mutated in recessive Stargardt macular dystrophy. *Nat Genet* 1997;15(3):236-46.
4. Lambertus S, van Huet RA, Bax NM, et al. Early-onset stargardt disease: phenotypic and genotypic characteristics. *Ophthalmology* 2015;122(2):335-44.
5. Westeneng-van Haafden SC, Boon CJ, Cremers FP, et al. Clinical and genetic characteristics of late-onset Stargardt's disease. *Ophthalmology* 2012;119(6):1199-210.
6. Fujinami K, Zernant J, Chana RK, et al. Clinical and molecular characteristics of childhood-onset Stargardt disease. *Ophthalmology* 2015;122(2):326-34.
7. Klevering BJ, Blankenagel A, Maugeri A, et al. Phenotypic spectrum of autosomal recessive cone-rod dystrophies caused by mutations in the ABCA4 (ABCR) gene. *Invest Ophthalmol Vis Sci* 2002;43(6):1980-5.
8. Fishman GA, Stone EM, Grover S, et al. Variation of clinical expression in patients with Stargardt dystrophy and sequence variations in the ABCR gene. *Arch Ophthalmol* 1999;117(4):504-10.
9. Armstrong JD, Meyer D, Xu S, Elfervig JL. Long-term follow-up of Stargardt's disease and fundus flavimaculatus. *Ophthalmology* 1998;105(3):448-57; discussion 57-8.
10. Querques G, Leveziel N, Benhamou N, et al. Analysis of retinal flecks in fundus flavimaculatus using optical coherence tomography. *Br J Ophthalmol* 2006;90(9):1157-62.
11. Klevering BJ, Blankenagel A, Maugeri A, et al. Phenotypic spectrum of autosomal recessive cone-rod dystrophies caused by mutations in the ABCA4 (ABCR) gene. *Investigative Ophthalmology & Visual Science* 2002;43(6):1980-5.
12. Michaelides M, Chen LL, Brantley MA, Jr., et al. ABCA4 mutations and discordant ABCA4 alleles in patients and siblings with bull's-eye maculopathy. *Br J Ophthalmol* 2007;91(12):1650-5.
13. Stargardt K. Über familiäre, progressive Degeneration in der Maculagegend des Auges. *Graefes Arch Clin Exp Ophthalmol* 1909(71):534-50.
14. Franceschetti A. A special form of tapetoretinal degeneration: fundus flavimaculatus. *Trans Am Acad Ophthalmol Otolaryngol* 1965;69(6):1048-53.
15. van Huet RA, Bax NM, Westeneng-Van Haafden SC, et al. Foveal sparing in Stargardt disease. *Investigative Ophthalmology & Visual Science* 2014;55(11):7467-78.
16. Fujinami K, Sergouniotis PI, Davidson AE, et al. Clinical and molecular analysis of stargardt disease with preserved foveal structure and function. *Am J Ophthalmol* 2013;156(3):487-501 e1.
17. Marmor MF, Fulton AB, Holder GE, et al. ISCEV Standard for full-field clinical electroretinography (2008 update). *Doc Ophthalmol* 2009;118(1):69-77.
18. Lois N, Holder GE, Bunce C, et al. Phenotypic subtypes of Stargardt macular dystrophy-fundus flavimaculatus. *Arch Ophthalmol* 2001;119(3):359-69.
19. Fishman GA, Farber M, Patel BS, Derlacki DJ. Visual acuity loss in patients with Stargardt's macular dystrophy. *Ophthalmology* 1987;94(7):809-14.
20. Gelisken O, De Laey JJ. A clinical review of Stargardt's disease and/or fundus flavimaculatus with follow-up. *Int Ophthalmol* 1985;8(4):225-35.
21. Chun R, Fishman GA, Collison FT, et al. The value of retinal imaging with infrared scanning laser ophthalmoscopy in patients with stargardt disease. *Retina* 2014;34(7):1391-9.
22. Lee W, Noupou K, Oll M, et al. The external limiting membrane in early-onset Stargardt disease. *Invest Ophthalmol Vis Sci* 2014;55(10):6139-49.
23. Vandenbroucke T, Buyl R, De Zaeytijd J, et al. Colour Vision in Stargardt Disease. *Ophthalmic Res* 2015;54(4):181-94.

"This article reveals the differences in natural history of geographic atrophy secondary to age-related macular degeneration and atrophy of the retinal pigment epithelium in late-onset Stargardt disease by analyzing two large cohorts of patients."

Moritz Lindner*

Stanley Lambertus*

Matthias M. Mauschitz

Nathalie M. Bax

Eveline Kersten

Anna Lüning

Jennifer Nadal

Steffen Schmitz Valckenberg

Matthias Schmid

Frank G. Holz

Carel B. Hoyng

Monika Fleckenstein

for the Foveal sparing Atrophy Study Team (FAST).

*M.L. and S.L. are joint first authors.

Invest Ophthalmol Vis Sci. 2017 Feb 1;58(2):1001-1007

The authors thank Frans Cremers and Bernhard Weber for their analysis of *ABCA4* mutations; and the collaborators of the FAM-Study group.

3.2 Differential disease progression in atrophic age-related macular degeneration and late-onset Stargardt disease

PURPOSE: To compare the disease course of retinal pigment epithelium (RPE) atrophy secondary to age-related macular degeneration (AMD) and late-onset Stargardt disease (STGD1).

METHODS: Patients were examined longitudinally by fundus autofluorescence, near-infrared reflectance imaging and best-corrected visual acuity (BCVA). Areas of RPE atrophy were quantified using semi-automated software, and the status of the fovea was evaluated based on fundus autofluorescence and near-infrared reflectance images. Mixed-effects models were used to compare atrophy progression rates. BCVA loss and loss of foveal integrity were analyzed using Turnbull's estimator.

RESULTS: A total of 151 patients (226 eyes) with RPE atrophy secondary to AMD and 38 patients (66 eyes) with RPE atrophy secondary to late-onset STGD1 were examined for a median time of 2.3 years (interquartile range, 2.7). Mean baseline age was 74.2 years (SD, 7.6) in AMD and 63.4 (SD, 9.9) in late-onset STGD1 ($P = 1.1 \times 10^{-7}$). Square root atrophy progression was significantly faster in AMD when compared with late-onset STGD1 (0.28 mm/year [\pm standard error (SE), 0.01] versus 0.23 [\pm SE, 0.03]; $P = 0.030$). In late-onset STGD1, the median survival of the fovea was significantly longer when compared with eyes with AMD (8.60 versus 3.35 years; $P = 0.005$) with a trend to a later BCVA loss of ≥ 3 lines (5.97 versus 4.37 years; $P = 0.382$).

CONCLUSIONS: These natural history data indicate differential disease progression in AMD versus late-onset STGD1. The results underline the relevance of refined phenotyping in elderly patients presenting with RPE atrophy in regard to prognosis and design of interventional trials.

Introduction

Atrophy of the retinal pigment epithelium (RPE) represents a common late-stage manifestation of various retinal diseases, including late-stage dry age-related macular degeneration (AMD) and Stargardt disease (STGD1).¹ In industrialized countries, late-stage neovascular or advanced dry AMD is the leading cause of legal blindness in the elderly.² Although the exact pathogenetic mechanisms leading to geographic atrophy³ are still poorly understood, chronic inflammatory processes, excessive lipofuscin accumulation in the RPE lysosomal compartment, complement system dysregulation, and vascular factors have been implicated in the development of AMD.⁴

In contrast to the multifactorial etiology of AMD, STGD1 is an autosomal recessive retinal dystrophy caused by pathogenic sequence variants in the adenosine triphosphate-binding cassette, subfamily A, member 4 (ABCA4, MIM 601691) gene. ABCA4 encodes an integral transmembrane protein, expressed in retinal photoreceptors. It is involved in the clearance of all-trans-retinal aldehyde, a byproduct of the retinoid cycle of vision.⁵ ABCA4 dysfunction leads to the accumulation of lipofuscin and its constituent, di-retinoid-pyridinium-ethanolamine, finally resulting in RPE atrophy development.^{6,7}

Comparable ages of onset as well as fundusoscopic parallels result in a certain risk in confounding AMD and late-onset STGD1.⁸ It is well understood that distinction between both conditions is of practical relevance to an individual patient with regard to genetic counseling. Yet to what extent differentiation between both conditions also influences individual prognosis in terms of visual acuity loss and RPE atrophy progression has not been assessed. Extending our analysis on two recently described cohorts,^{9,10} in the present work we identify significant differences in the course of AMD and late-onset STGD1. These results underline the relevance of refined phenotyping in patients presenting with RPE atrophy. Furthermore, the improved understanding of the distinct kinetic of disease progression will be relevant for emerging therapeutic approaches.

Methods

Patient identification

The present study consists of the following two distinct cohorts: patients with RPE atrophy secondary to AMD and patients with RPE atrophy associated with late-onset STGD1. Inclusion criteria for the current analysis for both cohorts were the following: (1) at least one well-defined contiguous area of RPE atrophy corresponding to areas of reduced fundus autofluorescence (FAF) to an extent of ≥ 0.05 mm² (the size of the smallest atrophic area in cases of multifocality) in one or both eyes and (2) clear ocular

media allowing for acquisition of high-quality FAF images. For inclusion into the AMD cohort, soft drusen and/or retinal pigment abnormalities consistent with the diagnosis of AMD had to be present. For inclusion into the late-onset STGD1 cohort, patients had to exhibit typical yellow-white flecks or dots correlating with hyperautofluorescent flecks on 488-nm FAF imaging. This FAF pattern had previously been termed “fine granular pattern with peripheral punctate spots (GPS[+])”.^{11, 12} The clinical phenotype of late-onset STGD1 was supported by at least one (likely) pathogenic variant in the *ABCA4* (NM_000350.2) gene. The peripherin-2 gene (*PRPH2*; NM_000322.4) was additionally sequenced in patients with fewer than two *ABCA4* (likely) pathogenic variants to exclude autosomal-dominant multifocal pattern dystrophy or central areolar choroidal dystrophy.^{13, 14} Patients had to be at least 45 years of age at self-reported symptom onset. Both eyes of a patient were included in the analysis if the inclusion criteria were met. General exclusion criteria for both cohorts were the presence of retinal disease that could possibly confound observations (e.g., diabetic retinopathy, present or past exudative events, idiopathic serous chorioretinopathy).

All of the patients were recruited in the context of the Fundus Autofluorescence in Age-Related Macular Degeneration (FAM) Study or at the outpatient department of Radboud university medical center. The study followed the tenets of the Declaration of Helsinki. Approval by the institutional review boards was obtained by each of the participating centers. Informed consent was obtained from each participant after an explanation of the study's nature and possible consequences of participation. Both cohorts have previously been reported elsewhere.^{8–10, 12, 15}

Assessment of visual acuity

At each visit, best-corrected visual acuity (BCVA) was determined using a Snellen or Early Treatment Diabetic Retinopathy Study (ETDRS) chart. Visual acuity is reported in logarithm of the minimum angle of resolution (logMAR) notation. Visual acuity of counting fingers was set to 1.8 logMAR and hand motions to 2.2 logMAR.¹⁶

Image acquisition and grading

Fundus autofluorescence images were acquired using HRA2 or Spectralis HRA+OCT (Heidelberg Engineering, Heidelberg, Germany) with an excitation wavelength of 488 nm and an emission spectrum of 500 to 700 nm using the high-speed mode. Near-infrared (NIR) reflectance images were obtained with an excitation wavelength of 820 nm. The field of view was centered on the fovea and set to 30°×30° or 55°×55° to fit the entire area of atrophy. Images were acquired with a minimum resolution of 512×512 pixels and single FAF images were automatically aligned and averaged to maximize the signal-to-noise ratio using the manufacturer's software.

Areas of RPE atrophy were measured on FAF images applying image processing software based on gray value detection for semi-automated identification of atrophic RPE areas. Only areas of decreased autofluorescence $>0.05 \text{ mm}^2$ were considered to represent RPE atrophy.^{17–20} The involvement of the fovea by the atrophic process was determined based on FAF and NIR reflectance images and was graded as follows: definitely involved, probably involved, probably not involved, and definitely not involved. For further analysis, these gradings were summarized to “involved” and “not involved.” A representative example of an eye with RPE atrophy secondary to AMD and RPE atrophy secondary to late-onset STGD1 is provided in [Figure 1](#).

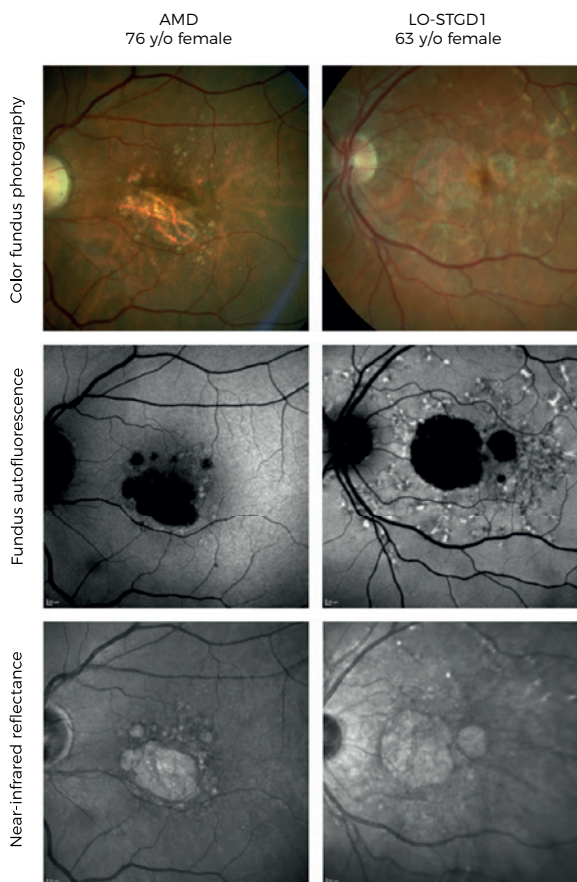


Figure 1. Multimodal imaging as performed in this study of representative left eyes of a patient with retinal pigment epithelium atrophy secondary to age-related macular degeneration (AMD) and a patient with retinal pigment epithelium atrophy secondary to late-onset Stargardt disease (LO-STGD1).

Statistical analysis

The total atrophy size measured for each visit was square-root transformed to reduce the dependency of enlargement rates on baseline lesion size ($\sqrt{\text{area [mm]}}$) as previously suggested.²¹ To quantify atrophy progression rates within the patient collective, a linear mixed-effects model was used as described earlier.^{22, 23} The two-level, random-effects model used here separates eye-specific and patient-specific effects and accounts for dependencies between measurements that were obtained from the same patient and/or eye.

The factor “AMD” versus “LO-STGD1” was included as a fixed effect in the model. Backward selection of the other covariates, including higher order interactions, was used to build the final linear mixed-effects model.

Turnbull's estimator²⁴ was used to estimate the percentages of eyes with BCVA loss ≥ 0.3 logMAR (≥ 3 ETDRS chart lines) and ≥ 0.6 logMAR (≥ 6 ETDRS chart lines) from baseline, as previously reported.⁹ A similar approach was used to estimate the percentage of eyes with loss of foveal integrity over time (status transition of the fovea from “not involved” to “involved”). A comparison of the course of BCVA and of the foveal status between AMD versus late-onset STGD1 was performed using the log-rank test.

Results

Patients

A total of 226 eyes (151 patients; 55 males, 96 females) with RPE atrophy secondary to AMD and 66 eyes (38 patients; 17 males, 21 females) with RPE atrophy secondary to late-onset STGD1 were examined over time. At baseline, 113 patients exhibited bilateral RPE atrophy (86 patients with AMD and 27 patients with late-onset STGD1). In 24 patients, the fellow eye had early changes, that is, disease-related alterations without atrophy or neovascularization (15 patients with AMD and nine patients with late-onset STGD1; $P = 0.117$), and 41 patients exhibited neovascularization in the fellow eye (39 patients with AMD and two patients with late-onset STGD1; $P = 0.006$). In 11 patients, only one eye was included because the fellow eyes fulfilled any of the exclusion criteria (e.g., insufficient imaging quality). One eye did not contribute to the analysis because neovascularization developed right after the first visit.

Baseline characteristics

Mean age at baseline was 74.2 years (SD, 7.6) in the AMD and 63.4 years (SD, 9.9) in the late-onset STGD1 patient cohort. At first presentation, RPE atrophy size in AMD patients was 6.3 mm^2 (SD, 5.0) and 6.2 mm^2 (SD, 7.3) in late-onset STGD1 ($P = 0.914$). At baseline, the fovea was graded as “not involved” in 54.0% of eyes (122 of 226 eyes) with AMD and in 86.4% of eyes (57 of 66 eyes) with late-onset STGD1 ($P = 4.1 \times 10^{-6}$). BCVA at baseline was significantly different between both cohorts with 0.6 logMAR (SD, 0.4) in AMD and 0.4 logMAR (SD, 0.5) in late-onset STGD1 ($P = 1.3 \times 10^{-3}$). An overview on baseline characteristics is given in [Table 1](#).

Characteristic	AMD		Late-onset STGD1		P value
	Patients, n (%)	Mean ± SD	Patients, n (%)	Mean ± SD	
Gender					
Male	55 (36.4%)		17 (44.7%)		0.449*
Female	96 (63.6%)		21 (55.3%)		
Disease status					
Bilateral RPE atrophy	86 (61.4%)		27 (71.1%)		
RPE atrophy + CNV in fellow eye	39 (27.9%)		2 (5.2%)		0.006*
RPE atrophy + "early" changes in fellow eye	15 (10.7%)		9 (23.7%)		0.117*
Follow-up time, years		2.2 (IQR, 2.6)†			0.774‡
Age, years		74.2 ± 7.6			<0.001§
Atrophy size, mm ²					
Eyes, n (%)	226	6.3 ± 5.0	66	6.2 ± 7.3	0.914§
Status of the fovea at baseline					
Not involved	122 (54%)		57 (86.4%)		<0.001*
Involved	104 (46%)		9 (13.6%)		
Visual acuity, logMAR	226	0.6 ± 0.4	66	0.4 ± 0.4	0.001§

Table 1. Baseline characteristics of patients with age-related macular degeneration and late-onset Stargardt. * χ^2 -Test; † median; ‡ Mann-Whitney U; § t-test.

AMD = age-related macular degeneration; CNV = choroidal neovascularization; IQR = interquartile range; RPE = retinal pigment epithelium; SD = standard deviation; STGD1 = Stargardt disease.

Disease Progression

Data of a total of 897 eye visits were included in the analysis. The median follow-up time was 2.2 years (interquartile range [IQR], 2.6) in AMD and 2.5 years (IQR, 3.6) in late-onset STGD1 ($P = 0.774$). To compare atrophy progression kinetics between AMD and late-onset STGD1, a linear mixed-effects model was used. Average square-root transformed atrophy progression was 0.28 mm/year (SE, 0.01) in AMD, and 0.23 mm/year (SE, 0.03) in late-onset STGD1 ($P = 0.030$). Model results were corrected for distinct age structures between the cohorts by including age as a fixed effect (coefficient estimate, 0.02 ± 0.00 ; $P = 0.011$).

Transition of the status of the fovea from "not involved" to "involved" during the observational period was observed in 48 eyes with AMD (39.3% of eyes with "not involved" fovea at baseline) and in only 5 eyes with late-onset STGD1 (8.8% of eyes with "not involved" fovea at baseline). Notably, the follow-up period in late-onset STGD1 patients was longer than in AMD patients (see earlier). Time-to-event analyses revealed a median time from noninvolvement of the fovea at baseline to foveal involvement of 3.35 years (95% confidence interval [CI], 2.50–4.15) in AMD and 8.60 years (CI, not available) in late-onset STGD1 (Table 2). In parallel, a visual acuity loss of ≥ 3 and ≥ 6 lines, respectively, occurred consistently, although not significantly later in late-onset STGD1 when compared with AMD (Table 2). Figure 2 shows two representative disease courses in an eye with late-onset STGD1 and an eye with AMD.

Event	AMD		Late-onset STGD1		P value
	Median, years	CI	Median, years	CI	Log-rank
Fovea becomes involved	3.35	2.50-4.15	8.60	NA	0.005
Visual acuity loss ≥ 3 lines	4.37	2.96-4.37	5.97		0.449*
Visual acuity loss ≥ 6 lines	7.52	7.52- ∞	33.2% had event after 7.50 years		0.320

Table 2. Median times to event for foveal involvement and vision loss in age-related macular degeneration and late-onset Stargardt. CI = confidence interval; NA = not available.

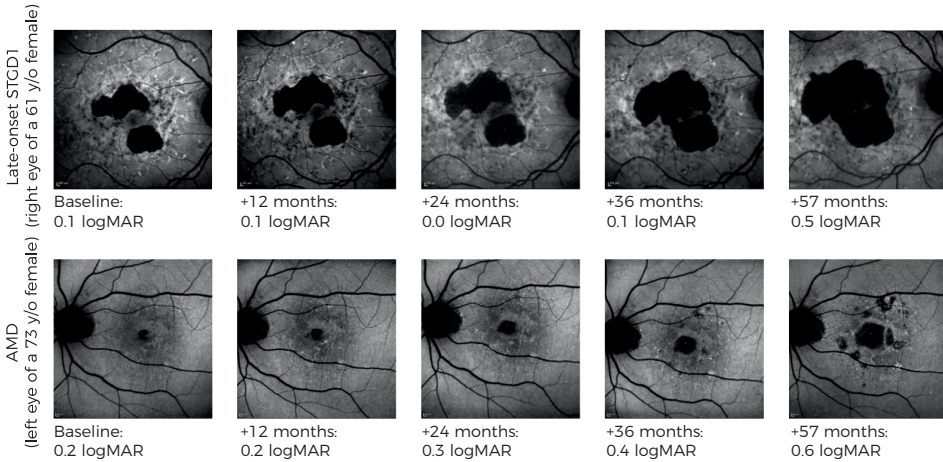


Figure 2. Fundus autofluorescence and corresponding visual acuity values of an exemplary course of late-onset STGD1 (upper row) and AMD (lower row). Square root atrophy progression rate in the late-onset STGD1 eye shown is 0.25 mm/year, whereas it is 0.58 mm/year in the age-related macular degeneration (AMD) eye. Note that the eye with late-onset STGD1 shown has a larger non-square root transformed progression as a result of the larger baseline atrophy size. AMD = age-related macular degeneration; logMAR = logarithm of the minimum angle of resolution; STGD1 = Stargardt disease.

Discussion

This study reveals differences between AMD and late-onset STGD1 with respect to both atrophy progression and changes in visual acuity. We found a significantly faster atrophy progression in eyes with AMD along with significantly lower BCVA scores at baseline and faster, albeit not significant, loss of BCVA.

Atrophy progression and visual acuity courses have been previously assessed independently in both AMD and STGD1. Although distinct analytic strategies preclude direct comparisons, our data are overall compatible with previously published values.^{10, 25-28} Despite similar lesion size at baseline, patients with late-onset STGD1 had a better BCVA, presumably because their fovea was more frequently intact (86.4% versus 54% of eyes with AMD). Moreover, they had both atrophy progression kinetics and survival times of the fovea in favor, but the difference in decline in BCVA when compared with AMD was less pronounced. We have recently reported that the parameters “status of

the fovea”, “total lesion size”, and the “age at baseline” in eyes with atrophy as a result of AMD have a significant impact on BCVA and that these factors together explain 65% of BCVA variability.⁹ The remaining 35% of BCVA variability may be explained by other factors, such as media opacities and the general mental status. In addition, it may be explained by BCVA test variability itself.⁹

Foveal sparing is observed in several retinal diseases,^{8, 10, 15, 20, 29–33} exhibiting a specific pattern of RPE atrophy surrounding an intact foveal island. Although the present study did not differentiate between this typical pattern of foveal sparing and general foveal noninvolvement, patients with a long-term preservation of foveal integrity may develop eventual foveal sparing. Interestingly, eyes with an uninvolved fovea at baseline progressed to foveal atrophy during the review period in almost 40% of eyes with AMD, but only 8.8% of eyes with late-onset STGD1, despite their slightly longer follow-up. Atrophy being more closely to the fovea at first presentation may be a reason for requiring less time to involve the fovea into the atrophic process in AMD. Another explanation may be a longer foveal survival because of the protecting mechanisms in late-onset STGD1. Yet foveal sparing can be present in phenotypes that are independent of ABCA4 sequence variants, including AMD,^{8, 15, 20, 29–33} and is infrequent in a general STGD1 population.¹⁵ Therefore, other genetic factors and distinct anatomical, metabolic, and/or biochemical aspects are likely involved.

A further hallmark contrast between both cohorts was the frequency of neovascularization observed in fellow eyes, which was less frequent in late-onset STGD1. For AMD, it has been described that atrophy progression is slower in eyes with a fellow eye exhibiting neovascularization.³⁴ We did not correct for this factor in the linear mixed-effects model. Yet from the available data on AMD,³⁴ we would expect the difference between AMD and late-onset STGD1 to become even larger when correcting for this factor.

Our patients with biallelic—but also with mono-allelic—ABCA4 variants share an identical phenotype that exhibits typical flecks of increased FAF surrounding the atrophic lesion; it resembles the FAF pattern in patients with typical STGD1. Given the high carrier frequency up to 1:25,³⁵ it is highly unlikely that a single pathogenic ABCA4 variant can cause this phenotype on its own. In analog, several cases with typical STGD1 are to date also genetically still unsolved by failing to detect a second pathogenic ABCA4 variant. However, these second “missing” pathogenic variants are now increasingly being found with recent genetic techniques.³⁶ We postulate that either a second sequence variant affecting ABCA4 function or other genetic factors that lower the total ABCA4 function are still to be found in our patients with mono-allelic ABCA4 variants. They may be sufficient to cause this distinct phenotype at the mild end of STGD1 and in

the disease spectrum of AMD. With regard to these hypotheses, recent studies are of particular interest quantifying normal levels of lipofuscin in parents of patients with STGD1.^{37,38} Furthermore, it has also been reported that *abca4*^{+/-} mice show increased levels of some bis-retinoids.³⁹ Overall, the pathogenesis of cases with a typical STGD1 phenotype and only one identified pathogenic *ABCA4* variant remains controversial. Nonetheless, it appears reasonable to require detection of at least one pathogenic *ABCA4* variant in patients with this distinct late-onset phenotype to assign the clinical diagnosis late-onset STGD1.

One may argue about how this distinct late-onset atrophy phenotype associated with *ABCA4* should be entitled. In the FAM Study, this phenotype was originally termed “fine granular pattern with peripheral punctate spots” (GPS[+]) and was classified as a subtype of AMD.^{11,12} In two independent approaches, we found an association of this late-onset phenotype with mono- and biallelic *ABCA4* variants.^{8,11} Here, we postulate that late-onset STGD1 and GPS[+] describe the same entity. Analyses of *ABCA4* gene variants in AMD were not performed in this study. Several earlier works have addressed the issue of *ABCA4* in large cohorts from a genetic point of view, giving controversial results.⁴⁰⁻⁴² A recent study in AMD did not detect increased lipofuscin levels, which should be expected in retinal disease associated with *ABCA4*.⁴³ However, further contributing to this controversy will require (1) a clinically well-phenotyped AMD cohort where late-onset STGD1/GPS[+] patients are excluded, (2) a well-matched control cohort, and (3) state-of-the-art genetic approaches to identify relevant variants, which was beyond the scope of this work.

Optical coherence tomography was not included in this study, which may have caused uncertainty to the grading of foveal involvement. In particular, only the definite gradings “involved” versus “not involved” were compared in contrast to other works.^{9,44} Another limitation included the two cohorts being unequal in number of patients; because of the smaller late-onset STGD1 cohort, time-to-event curves were affected more strongly by the potential loss of follow-up here when compared with a dropout of an AMD patient. Yet time-to-event analyses are robust against such dropouts as long as patients who are more likely to suffer the event early during follow-up are not more (or less) likely to drop out. These limitations are balanced by the large cohorts of both AMD and late-onset STGD1 patients who were included into this study and followed during a long period of time.

Differential disease progression between AMD and late-onset STGD1 are particularly important to emerging therapeutic trials. Strategies in multifactorial AMD range from choroidal perfusion enhancers over neuroprotective agents to complement inhibitors.⁴

Preclinical data suggest that complement activation is a final common pathway leading to RPE cell death in both conditions^{45, 46}; for AMD, the MAHALO trial also shows therapeutic effects in human.⁴⁷ Yet patients with ABCA4-related late-onset STGD1 will rather benefit if earlier and more specific disease processes are targeted, for example, by focusing on the visual cycle or retinal ABCA4-gene delivery (e.g., ClinicalTrials.gov, NCT01367444 and ref.⁴⁸). Therefore, it appears prudent to carefully distinguish between late-onset STGD1 and AMD. Inclusion of late-onset STGD1 patients into interventional AMD trials, and vice versa, would blur the therapeutic effect under observation and potentially lead to a fail in proving efficacy.

Furthermore, although the clinical diagnosis of late-onset STGD1 can be supported by the detection of one disease-causing ABCA4 variant, it would be prudent to require the identification of two disease-causing variants before enrollment in early therapeutic trials involving late-onset STGD1 patients.

In summary, the present analysis reveals distinct progression characteristics in eyes with RPE atrophy associated with AMD and late-onset STGD1. These results underscore the relevance of refined phenotyping to predict the course of disease in a patient presenting with RPE atrophy. The results enable more sophisticated prognosis for the individual patient and should be considered when designing future interventional trials for both.

References

1. Saksens NT, Fleckenstein M, Schmitz-Valckenberg S, et al. Macular dystrophies mimicking age-related macular degeneration. *Prog Retin Eye Res.* 2014; 39: 23–57.
2. Lim LS, Mitchell P, Seddon JM, Holz FG, Wong TY. Age-related macular degeneration. *Lancet.* 2012; 379: 1728–1738.
3. Schmitz-Valckenberg S, Sadda S, Staurengi G, Chew E, Fleckenstein M, Holz FG. “Geographic atrophy”: semantic considerations and literature review. *Retina.* 2016; 36: 2250–2264.
4. Holz FG, Strauss EC, Schmitz-Valckenberg S, van Lookeren Campagne M. Geographic atrophy: clinical features and potential therapeutic approaches. *Ophthalmology.* 2014; 121: 1079–1091.
5. Cideciyan AV, Swider M, Aleman TS, et al. ABCA4 disease progression and a proposed strategy for gene therapy. *Hum Mol Genet.* 2009; 18: 931–941.
6. Sparrow JR, Boulton M. RPE lipofuscin and its role in retinal pathobiology. *Exp Eye Res.* 2005; 80: 595–606.
7. Bergmann M, Schutt F, Holz FG, Kopitz J. Inhibition of the ATP-driven proton pump in RPE lysosomes by the major lipofuscin fluorophore A2-E may contribute to the pathogenesis of age-related macular degeneration. *FASEB J.* 2004; 18: 562–564.
8. Westeneng-van Haften SC, Boon CJ, Cremers FP, Hoefsloot LH, den Hollander AI, Hoyng CB. Clinical and genetic characteristics of late-onset Stargardt’s disease. *Ophthalmology.* 2012; 119: 1199–1210.
9. Schmitz-Valckenberg S, Nadal J, Fimmers R, et al. Modeling visual acuity in geographic atrophy secondary to age-related macular degeneration. *Ophthalmologica.* 2016; 235: 215–224.
10. Lambertus S, Lindner M, Bax NM, et al. Progression of late-onset Stargardt disease. *Invest Ophthalmol Vis Sci.* 2016; 57: 5186–5191.
11. Holz FG, Bindewald-Wittich A, Fleckenstein M, et al. Progression of geographic atrophy and impact of fundus autofluorescence patterns in age-related macular degeneration. *Am J Ophthalmol.* 2007; 143: 463–472.
12. Fritsche LG, Fleckenstein M, Fiebig BS, et al. A subgroup of age-related macular degeneration is associated with mono-allelic sequence variants in the ABCA4 gene. *Invest Ophthalmol Vis Sci.* 2012; 53: 2112–2118.
13. Boon CJ, van Schooneveld MJ, den Hollander AI, et al. Mutations in the peripherin/RDS gene are an important cause of multifocal pattern dystrophy simulating STGD1/fundus flavimaculatus. *Br J Ophthalmol.* 2007; 91: 1504–1511.
14. Boon CJ, den Hollander AI, Hoyng CB, Cremers FP, Klevering BJ, Keunen JE. The spectrum of retinal dystrophies caused by mutations in the peripherin/RDS gene. *Prog Retin Eye Res.* 2008; 27: 213–235.
15. van Huet RA, Bax NM, Westeneng-Van Haften SC, et al. Foveal sparing in Stargardt disease. *Invest Ophthalmol Vis Sci.* 2014; 55: 7467–7478.
16. Lange C, Feltgen N, Junker B, Schulze-Bonsel K, Bach M. Resolving the clinical acuity categories “hand motion” and “counting fingers” using the Freiburg Visual Acuity Test (FrACT). *Graefes Arch Clin Exp Ophthalmol.* 2009; 247: 137–142.
17. Schmitz-Valckenberg S, Brinkmann CK, Alten F, et al. Semiautomated image processing method for identification and quantification of geographic atrophy in age-related macular degeneration. *Invest Ophthalmol Vis Sci.* 2011; 52: 7640–7646.
18. Deckert A, Schmitz-Valckenberg S, Jorzik J, Bindewald A, Holz FG, Mansmann U. Automated analysis of digital fundus autofluorescence images of geographic atrophy in advanced age-related macular degeneration using confocal scanning laser ophthalmoscopy (cSLO). *BMC Ophthalmol.* 2005; 5: 8.
19. Fleckenstein M, Adrion C, Schmitz-Valckenberg S, et al. Concordance of disease progression in bilateral geographic atrophy due to AMD. *Invest Ophthalmol Vis Sci.* 2010; 51: 637–642.
20. Lindner M, Boker A, Mausnitz MM, et al. Directional kinetics of geographic atrophy progression in age-related macular degeneration with foveal sparing. *Ophthalmology.* 2015; 122: 1356–1365.

21. Feuer WJ, Yehoshua Z, Gregori G, et al. Square root transformation of geographic atrophy area measurements to eliminate dependence of growth rates on baseline lesion measurements: a reanalysis of age-related eye disease study report no. 26. *JAMA Ophthalmol.* 2013; 131: 110–111.
22. Fleckenstein M, Schmitz-Valckenberg S, Adrion C, et al. Tracking progression with spectral-domain optical coherence tomography in geographic atrophy caused by age-related macular degeneration. *Invest Ophthalmol Vis Sci.* 2010; 51: 3846–3852.
23. Dreyhaupt J, Mansmann U, Pritsch M, Dolar-Szczasny J, Bindewald A, Holz FG. Modelling the natural history of geographic atrophy in patients with age-related macular degeneration. *Ophthalmic Epidemiol.* 2005; 12: 353–362.
24. Turnbull BW. The empirical distribution function with arbitrary grouped, censored and truncated data. *J R Stat Soc Series B Stat Methodol.* 1976; 38: 290–295.
25. Schmitz-Valckenberg S, Sahel JA, Danis R, et al. Natural history of geographic atrophy progression secondary to age-related macular degeneration (Geographic Atrophy Progression Study). *Ophthalmology.* 2016; 123: 361–368.
26. Yehoshua Z, de Amorim Garcia Filho CA, Nunes RP, et al. Systemic complement inhibition with eculizumab for geographic atrophy in age-related macular degeneration: the COMPLETE study. *Ophthalmology.* 2014; 121: 693–701.
27. McBain VA, Townend J, Lois N. Progression of retinal pigment epithelial atrophy in stargardt disease. *Am J Ophthalmol.* 2012; 154: 146–154.
28. Chen B, Tosha C, Gorin MB, Nusinowitz S. Analysis of autofluorescent retinal images and measurement of atrophic lesion growth in Stargardt disease. *Exp Eye Res.* 2010; 91: 143–152.
29. Fujinami K, Sergouniotis PI, Davidson AE, et al. Clinical and molecular analysis of Stargardt disease with preserved foveal structure and function. *Am J Ophthalmol.* 2013; 156: 487–501.e1.
30. Sunness JS, Rubin GS, Zuckerbrod A, Applegate CA. Foveal-sparing scotomas in advanced dry age-related macular degeneration. *J Vis Impair Blind.* 2008; 102: 600–610.
31. de Laat P, Smeitink JA, Janssen MC, Keunen JE, Boon CJ. Mitochondrial retinal dystrophy associated with the m.3243A>G mutation. *Ophthalmology.* 2013; 120: 2684–2696.
32. Klevering BJ, Deutman AF, Maugeri A, Cremers FP, Hoyng CB. The spectrum of retinal phenotypes caused by mutations in the ABCA4 gene. *Graefes Arch Clin Exp Ophthalmol.* 2005; 243: 90–100.
33. Schmitz-Valckenberg S, Fleckenstein M, Helb HM, Charbel Issa P, Scholl HP, Holz FG. In vivo imaging of foveal sparing in geographic atrophy secondary to age-related macular degeneration. *Invest Ophthalmol Vis Sci.* 2009; 50: 3915–3921.
34. Fleckenstein M, Schmitz-Valckenberg S, Adrion C, et al. Progression of age-related geographic atrophy: role of the fellow eye. *Invest Ophthalmol Vis Sci.* 2011; 52: 6552–6557.
35. Maugeri A, van Driel MA, van de Pol DJ, et al. The 2588G->C mutation in the ABCR gene is a mild frequent founder mutation in the Western European population and allows the classification of ABCR mutations in patients with Stargardt disease. *Am J Hum Genet.* 1999; 64: 1024–1035.
36. Bax NM, Sangermano R, Roosing S, et al. Heterozygous deep-intronic variants and deletions in ABCA4 in persons with retinal dystrophies and one exonic ABCA4 variant. *Hum Mutat.* 2015; 36: 43–47.
37. Delori F, Greenberg JP, Woods RL, et al. Quantitative measurements of autofluorescence with the scanning laser ophthalmoscope. *Invest Ophthalmol Vis Sci.* 2011; 52: 9379–9390.
38. Duncker T, Stein GE, Lee W, et al. Quantitative fundus autofluorescence and optical coherence tomography in ABCA4 carriers. *Invest Ophthalmol Vis Sci.* 2015; 56: 7274–7285.
39. Muller PL, Gliem M, Mangold E, et al. Monoallelic ABCA4 mutations appear insufficient to cause retinopathy: a quantitative autofluorescence study. *Invest Ophthalmol Vis Sci.* 2015; 56: 8179–8186.
40. Allikmets R, Shroyer NF, Singh N, et al. Mutation of the Stargardt disease gene (ABCR) in age-related macular degeneration. *Science.* 1997; 277: 1805–1807.
41. Stone EM, Webster AR, Vandenburgh K, et al. Allelic variation in ABCR associated with Stargardt disease but not age-related macular degeneration. *Nat Genet.* 1998; 20: 328–329.
42. Rivera A, White K, Stohr H, et al. A comprehensive survey of sequence variation in the ABCA4 (ABCR) gene in Stargardt disease and age-related macular degeneration. *Am J Hum Genet.* 2000; 67: 800–813.

43. Gliem M, Muller PL, Finger RP, McGuinness MB, Holz FG, Charbel Issa P. Quantitative fundus autofluorescence in early and intermediate age-related macular degeneration. *JAMA Ophthalmol.* 2016; 134: 817–824.
44. Sayegh RG, Simader C, Scheschy U, et al. A systematic comparison of spectral-domain optical coherence tomography and fundus autofluorescence in patients with geographic atrophy. *Ophthalmology.* 2011; 118: 1844–1851.
45. Radu RA, Hu J, Jiang Z, Bok D. Bisretinoid-mediated complement activation on retinal pigment epithelial cells is dependent on complement factor H haplotype. *J Biol Chem.* 2014; 289: 9113–9120.
46. Radu RA, Hu J, Yuan Q, et al. Complement system dysregulation and inflammation in the retinal pigment epithelium of a mouse model for Stargardt macular degeneration. *J Biol Chem.* 2011; 286: 18593–18601.
47. Roche. Lempalizumab: Potentially first treatment in geographic atrophy, an advanced form of dry AMD. Investor Update. Basel and London: Roche; 2013.
48. Charbel Issa P, Barnard AR, Herrmann P, Washington I, MacLaren RE. Rescue of the Stargardt phenotype in *Abca4* knockout mice through inhibition of vitamin A dimerization. *Proc Natl Acad Sci U S A.* 2015; 112: 8415–8420.



“Asymmetric inter-eye progression in Stargardt disease is most likely observed in patients with a later onset and patients carrying lower pathogenic ABCA4 combinations. This needs to be considered in novel therapeutic trials with a fellow-eye paired controlled design to optimize the power of a study.”

Stanley Lambertus

Nathalie M. Bax

Joannes M.M. Groenewoud

Frans P.M. Cremers

Gert Jan van der Wilt

B. Jeroen Klevering

Thomas Theelen

Carel B. Hoyng

Invest Ophthalmol Vis Sci. 2016 Dec 1;57(15):6824-6830.

The authors thank the Diagnostic Image Analysis Group, Department of Radiology and Nuclear Medicine, Radboud university medical center (Nijmegen, the Netherlands) for providing the image analysis algorithm.

4.1 Asymmetric inter-eye progression in Stargardt disease

PURPOSE: Asymmetry in disease progression between left and right eyes can occur in Stargardt disease (STGD1) and this needs to be considered in novel therapeutic trials with a fellow-eye paired controlled design. This study investigated the inter-eye discordance of best-corrected visual acuity (BCVA) and progression of retinal pigment epithelium (RPE) atrophy in STGD1.

METHODS: We performed a retrospective cohort study collecting 68 STGD1 patients (136 eyes) with ≥ 1 ABCA4 variants and ≥ 0.5 year follow-up on BCVA and fundus auto-fluorescence. We compared inter-eye correlations of RPE atrophy progression between early-onset (≤ 10 years), intermediate-onset (11–44), and late-onset (≥ 45) STGD1 and ABCA4 variant combinations by χ^2 -tests. We identified associations of discordant baseline BCVA and RPE atrophy with discordant RPE atrophy progression by odds ratios (OR). We defined discordance by differences >1.5 interquartile ranges \pm first/third interquartiles.

RESULTS: Progression of RPE atrophy correlated moderately between eyes ($p = 0.766$), which decreased with later onset ($P = 9.8 \times 10^{-7}$) and lower pathogenicity of ABCA4 combinations ($P = 0.007$). Twelve patients (17.6%) had discordant inter-eye RPE atrophy progression, associated with baseline discordance of RPE atrophy (OR, 6.50 [1.35–31.34]), but not BCVA (OR, 0.33 [0.04–2.85]).

CONCLUSIONS: Lower inter-eye correlations are more likely found in late-onset STGD1 and patients carrying low pathogenic ABCA4 combinations. To achieve the highest power in a therapeutic trial, early-phase studies should minimize inter-eye discordance by selecting early-onset STGD1 patients carrying severe ABCA4 variants without evidence of asymmetry at baseline.

Introduction

Stargardt disease (STGD1) is one of the most common retinal dystrophies. Loss of macular function causes bilateral loss of visual acuity—usually at childhood.^{1, 2} The first manifestations of the disease may also occur in older patients, up to the seventh decade.^{3, 4} In general, the severity of the disease is associated with the age of onset: young patients tend to do worse.⁵ The variation in age of onset and rate of progression is, for the most part, the result of combinations of over 900 variants in the *ABCA4* gene.⁶

ABCA4 encodes the adenosine triphosphate-binding cassette, subfamily A, member 4 transporter protein, which actively removes all-trans-retinal with its conjugate N-retinylidene-phosphatidylethanolamine from the photoreceptor outer segment disks.⁷ Impaired removal results in condensation reactions, which lead to toxic levels of bisretinoids in the outer segment disks. Through phagocytosis of these outer segments, bisretinoids accumulate as lipofuscin deposits in the retinal pigment epithelium (RPE). These lipofuscin deposits are observed as yellowish-white flecks in the posterior pole.⁸ The accumulation of toxic lipofuscin eventually leads to atrophy of the retinal pigment epithelium (RPE) and photoreceptors with subsequent loss of the neurosensory retina and choriocapillaris.⁹

Over time, RPE atrophy progresses, as uni- or multifocal areas enlarge and coalesce. However, there is considerable variability in these patterns of atrophy; they range from large central atrophic areas in early-onset STGD1 patients that can be seen at adolescence² to relatively small atrophic lesions encircling the fovea in older patients with late-onset STGD1.³ The difference in atrophic lesion not only varies between patients,¹⁰ but also the patterns of RPE loss may differ significantly between eyes of one patient. Even though the extent of abnormalities is often similar between left and right eyes,^{11, 12} some cases with remarkable differences have been described.¹³

Profound inter-eye differences in disease progression have impact on the statistical power in clinical trials; treated and untreated eyes must demonstrate a larger difference than do the inter-eye differences by their natural course. Otherwise, the required sample size will be unreasonably large. However, in early-phase clinical trials for novel treatments of STGD1¹⁴⁻¹⁶ and other retinal dystrophies, small therapeutic effects have to be evaluated generally within two years with no more than a few dozen patients. Thus, better knowledge of inter-eye correlations is needed for fellow-eye paired controlled trials in which the untreated eyes of participants serve as a control.

In view of these upcoming interventional trials, we have studied the extent of asymmetric inter-eye progression of RPE atrophy in patients with STGD1. Fundus autofluorescence (FAF) imaging is a valuable tool to evaluate progression of RPE atrophy over time.¹⁷⁻²⁰ We therefore analyzed inter-eye discordance of RPE atrophy progression using FAF imaging along with visual acuity. We hypothesized that a later disease onset and less pathogenic combinations of ABCA4 variants contribute to asymmetric inter-eye progression, and that the asymmetry will increase when asymmetry at baseline is already present.

Methods

Patient selection

We selected patients from the STGD1 database, containing 454 cases, of the Department of Ophthalmology at Radboud university medical center (Nijmegen, the Netherlands). We included patients in whom the clinical diagnosis of STGD1 was supported by the presence of ≥ 1 (likely) pathogenic ABCA4 variants with a follow-up data of ≥ 6 months on FAF imaging. Ninety-three STGD1 patients met these inclusion criteria.

Ten cases were excluded because no RPE atrophy had developed during the entire follow-up time. Nine cases displayed RPE atrophy to such a degree that the lesions extended beyond the limits of the FAF image. One case was excluded because choroidal neovascularization occurred in one eye. Five cases were excluded because they participated in an interventional trial.²¹ The remaining 68 cases were included in this study. The patient inclusion process is shown in [Supplemental Figure 1](#). This retrospective cohort study was approved by the Institutional Ethics Committee and was performed in accordance with the Declaration of Helsinki.

Measurements

We documented sex, age at onset, age at baseline, and follow-up time. Age at onset was defined as either the age at which visual complaints were first noted, or, if unavailable, the age when the diagnosis was made. Disease onset groups were based on previously reported cut-off points: early-onset STGD1, ≤ 10 years² and late-onset STGD1, ≥ 45 years.³ The remaining patients were grouped as intermediate-onset STGD1, 11 to 44 years. The age at baseline was the first visit with available imaging and visual acuity tests.

Best-corrected visual acuity (BCVA) was measured with a Snellen or Early Treatment Diabetic Retinopathy Study chart, then transformed into the logarithm of the minimum angle of resolution (logMAR) for analysis. Fundus autofluorescence ($\lambda = 488$ nm,

emission 500–700 nm) imaging was performed using a confocal scanning laser ophthalmoscope (Spectralis HRA+OCT; Heidelberg Engineering, Heidelberg, Germany). The field of view was set at 30°×30° or 55°×55° and was centered on the macula.²²

Image quantification

The total RPE atrophy area was automatically quantified in FAF images by an observer-independent image analysis algorithm. The algorithm automatically segmented the area starting from an arbitrarily selected seed point inside the atrophic area. This method was based on a combination of a region growing algorithm and a dynamic, user-independent threshold selection procedure using Otsu thresholding. Areas were square-root ($\sqrt{}$) transformed to correct for baseline RPE atrophy area.²³ A good agreement has previously been observed between manual area measurements and the automatically quantified values (C.I. Sanchez et al. IOVS 2015;56:ARVO E-Abstract 5258), and was found to be consistent with the agreement within this cohort (intra-class correlation coefficient, 0.977; 95% confidence interval [CI], 0.951–0.987).

Genetic analysis

All reported ABCA4 variants ([Supplemental Table 1](#)) were classified as follows: 1) pathogenic: truncating alleles, significantly enriched in ABCA4-LOVD (LOVD. nI/ABCA4), which contains 6903 variants (861 unique variants) reported in 3987 persons with STGD1 or autosomal recessive cone-rod dystrophy (S.S. Cornelis and F.P.M. Cremers, unpublished data, 2016); 2) likely pathogenic: non-truncating alleles, significantly enriched in ABCA4-LOVD; 3) likely benign: allele frequency (AF) ABCA4-LOVD/AF ExAC non-Finnish Caucasian <1; 4) benign: ExAC AF >0.006; 5) unknown pathogenicity: AF ABCA4-LOVD/AF ExAC non-Finnish Caucasian >1, however not significantly enriched. Patients were then grouped by combinations of ABCA4 pathogenicity: 1) pathogenic/pathogenic, 2) pathogenic/likely pathogenic, 3) likely pathogenic/likely pathogenic, 4) pathogenic in combination with unknown pathogenicity, (likely) benign, or a variant that was not published until 31 December 2015, 5) likely pathogenic in combination with unknown pathogenicity or (likely) benign (S.S. Cornelis and F.P.M. Cremers, unpublished data, 2016).

Statistical analysis

We analyzed BCVA and RPE atrophy measurements using SPSS version 22 (IBM Corp., IBM SPSS Statistics, Chicago, IL, USA) with parametric tests. Retinal pigment atrophy progression rates were calculated by the difference at the baseline and last follow-up visit divided by the follow-up time. Differences in disease duration and follow-up time between disease onset groups were analyzed with the Kruskal-Wallis test.

We used Pearson's correlation coefficients (ρ) to assess inter-eye correlations of baseline BCVA, baseline RPE atrophy, and RPE atrophy progression. We compared these correlations between disease-onset groups and ABCA4 variant combination groups by first performing a Fisher transformation:

$$z' = \frac{1}{2} \ln \frac{1 + \rho}{1 - \rho}$$

Then, these z' -scores were compared for homogeneity. The test for homogeneity employs the χ^2 -distribution for two and four degrees of freedom:

$$\chi^2 = \sum (n_i - 3) (z'_i)^2 - \frac{[\sum (n_i - 3) (z'_i)]^2}{n_i}$$

where the summation is over the three disease-onset groups and five ABCA4 variant combination groups, respectively.²⁴

Baseline BCVA and RPE atrophy differences between measurements and the average measurements of both eyes were calculated and plotted according to the method of Bland and Altman to assess the intra-individual agreement graphically.²⁵ Limits of agreement between eyes were plotted for each disease-onset group.

Lin's concordance correlation coefficient ρ_c was calculated to evaluate the extent of inter-eye symmetry of baseline BCVA, baseline RPE atrophy, and RPE atrophy progression.²⁶⁻²⁸ The ρ_c consists of the product of a precision coefficient (Pearson's ρ) and an accuracy coefficient χ_a . The accuracy coefficient χ_a indicates how far the best-fit line of all paired left- and right-eye measurements deviates from the 45° line on a square scatter plot, and is defined as $\frac{2}{\omega + 1/\omega + v^2}$, where scale shift $\omega = \frac{\sigma_{OD}}{\sigma_{OS}}$ and location shift relative to the scale $v = \frac{\mu_{OD} - \mu_{OS}}{\sqrt{\sigma_{OD} \sigma_{OS}}}$ (OD, right eye; OS, left eye).²⁹ If all paired measurements exactly lie on the 45° line, a coefficient of 1 would be found, indicating perfect symmetry. Strength-of-agreement criteria were as follows: almost perfect, >0.90; substantial, 0.80–0.90; moderate, 0.65–0.80; poor, <0.65.³⁰

As standard deviations can be affected by extreme differences and rely on distributional assumptions, box-and-whisker plots were used to identify outliers by differences >1.5 interquartile ranges (IQR) below the first (Q_1) or above the third (Q_3) interquartiles in baseline BCVA, baseline RPE atrophy, and RPE atrophy progression. Odds ratios were calculated to identify associations of discordant BCVA and RPE atrophy at baseline with RPE atrophy progression.

We performed sample size calculations and a sensitivity analysis for a theoretical intervention using nQuery Advisor 7.0 (Statistical Solutions, Boston, MA). We used

a two-sided paired t-test for differences in means of RPE atrophy progression with a test significance level (α) of 0.05 and a power of $(1 - \beta)$ of 0.80. Standard deviations of differences between RPE atrophy progression of treated and nontreated eyes were obtained from the standard deviations and correlations of left and right eyes using the formula: $\sigma_d = \sqrt{(\sigma_1^2 + \sigma_2^2 - 2\rho\sigma_1\sigma_2)}$.

Results I: Patient characteristics

A total of 68 patients (136 eyes) were included in this study (26 men, and 42 women). The median age at onset was 8.5 (range, 4–10), 20 (range, 11–42), and 50 (range, 45–69) years for 14 early-onset STGD1, 33 intermediate-onset STGD1, and 21 late-onset STGD1 patients, respectively. At baseline, the median disease duration was 5 years (range, 0–39). The distribution did not differ between the three disease-onset categories. Details of patient characteristics and inter-eye correlations at baseline and follow-up are depicted in [Table 1](#).

Baseline inter-eye correlations of best-corrected visual acuity

At baseline, the mean (\pm standard deviation) BCVA in the right and left eyes was 0.66 ± 0.51 logMAR and 0.72 ± 0.53 logMAR, respectively. Twenty-four right eyes and 23 left eyes were identified as the better seeing eye; 21 pairs of eyes had equal BCVA. The overall inter-eye correlation (ρ) in BCVA at baseline was 0.756 and did not differ between disease onset groups, although a trend of decreasing correlations at later disease onset was also observed at follow-up.

Next, we compared the average and differences of baseline BCVA between the left and right eyes by a Bland-Altman plot ([Supplemental Figure 2A](#)), revealing discordance up to 1.70 logMAR. This discordance was most pronounced in 13 patients (two early-onset STGD1, seven intermediate-onset STGD1, and four late-onset STGD1), as defined by outlying differences below $Q_1 - 1.5 \times \text{IQR}$ or above $Q_3 + 1.5 \times \text{IQR}$ ([Supplemental Figure 2B](#)). Overall, this resulted in an inter-eye agreement (ρ_c) in baseline BCVA of 0.751 (95% confidence interval (CI), 0.626–0.838).

Baseline inter-eye correlations of retinal pigment epithelium atrophy

At baseline, the mean $\sqrt{\text{RPE atrophy area}}$ in the right and left eyes was 1.56 ± 1.36 mm and 1.45 ± 1.36 mm, respectively. Twenty-nine right eyes and 34 left eyes had the smallest RPE atrophy area; 5 pairs of eyes had no RPE atrophy. Although baseline RPE atrophy between the left and right eyes was highly correlated ($\rho = 0.878$), the correlation was significantly decreased in late-onset STGD1 patients.

Patient characteristics	Early-onset STGD1	Intermediate-onset STGD1	Late-onset STGD1	P value
Sex	7 male 7 female	9 male 24 female	10 male 11 female	
Age at onset, years (median and range)	8.5 (4–10)	20 (11–42)	50 (45–69)	
Baseline				
Disease duration, years (median and range)	7 (0–27)	4 (0–39)	5 (0–26)	0.768*
Age, years (median and range)	14.5 (9–31)	36 (13–56)	59 (45–81)	
BCVA, logMAR (mean and SD)				0.419†
OD	1.08 ± 0.41	0.67 ± 0.50	0.36 ± 0.39	
OS	1.09 ± 0.28	0.77 ± 0.49	0.40 ± 0.55	
Correlation, ρ	0.830	0.723	0.619	
$\sqrt{\text{RPE atrophy}}$, mm (mean and SD)				$5.5 \times 10^{-8}\dagger$
OD	1.79 ± 1.29	1.31 ± 1.52	1.79 ± 1.10	
OS	1.76 ± 1.27	1.28 ± 1.58	1.51 ± 1.03	
Correlation, ρ	0.992	0.931	0.601	
Follow-up				
Follow-up time, years (median and range)	5.7 (1.1–9.7)	3.1 (0.9–9.5)	3.8 (0.5–7.6)	0.220*
Age, years (median and range)	21 (11–36)	33 (15–59)	64 (47–86)	
BCVA, logMAR (mean and SD)				0.0497†
OD	1.23 ± 0.29	0.93 ± 0.44	0.63 ± 0.60	
OS	1.23 ± 0.29	0.88 ± 0.52	0.54 ± 0.60	
Correlation, ρ	0.897	0.767	0.527	
$\sqrt{\text{RPE atrophy}}$, mm (mean and SD)				$6.1 \times 10^{-4}\dagger$
OD	2.73 ± 1.23	1.89 ± 1.69	2.29 ± 1.55	
OS	2.77 ± 1.26	1.86 ± 1.62	2.17 ± 1.49	
Correlation, ρ	0.974	0.938	0.670	

Table 1. Characteristics and inter-eye correlations at baseline and at follow-up in 68 Stargardt patients. Median and ranges are shown for time variables. Mean and standard deviations (SD) are shown for best-corrected visual acuity (BCVA) and $\sqrt{\text{RPE atrophy}}$.

* Kruskal-Wallis test for differences in disease duration and follow-up.

† χ^2 with two degrees of freedom for differences in inter-eye correlations.

The Bland-Altman plot (Supplemental Figure 3A) showed inter-eye differences up to 2.49 mm of baseline $\sqrt{\text{RPE atrophy}}$ area. An inter-eye difference below $Q_1 - 1.5 \times \text{IQR}$ or above $Q_3 + 1.5 \times \text{IQR}$ (Supplemental Figure 3B), that is, discordant RPE atrophy at baseline, was identified in eight patients (intermediate-onset STGD1, four patients; late-onset STGD1, four patients). The overall inter-eye agreement (ρ) of baseline RPE atrophy was 0.876 (95% CI, 0.806–0.921).

Results II: Discordance of RPE atrophy progression rates

Inter-eye correlations of retinal pigment epithelium atrophy progression

The median follow-up time was 3.9 years (range, 0.5–9.7), of which the distribution did not differ between all disease-onset categories. The mean $\sqrt{\text{RPE atrophy}}$ progression rates in the right and left eyes were 0.21 ± 0.20 mm/year and 0.20 ± 0.21 mm/year, respectively. Thirty-five right eyes and 31 left eyes were identified as the eye with the

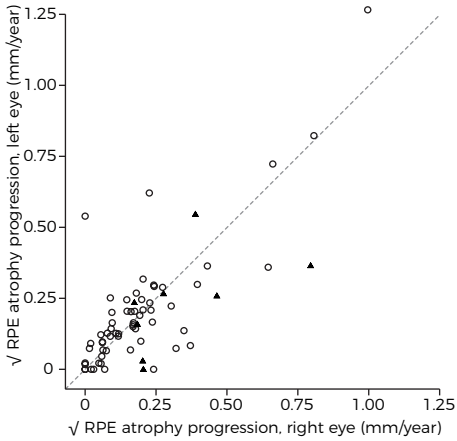


Figure 1. A square scatter plot of inter-eye $\sqrt{\text{RPE}}$ progression. Circles are patients with differences in baseline $\sqrt{\text{RPE}}$ atrophy between their eyes within $Q_{1.3} \pm 1.5 \times \text{IQR}$. Triangles are patients who fall outside the $Q_{1.3} \pm 1.5 \times \text{IQR}$ for differences in baseline $\sqrt{\text{RPE}}$ atrophy. Dashed line: 45° line of perfect agreement. Q_1 , first interquartile; Q_3 , third interquartile; IQR, interquartile range.

rates between their eyes by differences below $Q_1 - 1.5 \times \text{IQR}$ or above $Q_3 + 1.5 \times \text{IQR}$. In four of these patients, the eye with the largest RPE atrophy area progressed faster than the other eye, thus increasing inter-eye discordance of RPE atrophy over time (mean difference, 0.26 ± 0.10 mm/year; **Figure 2A**). In the other eight patients, the eye with the smallest RPE atrophy area progressed faster than the other eye, therefore reducing inter-eye discordance of RPE atrophy (mean difference, 0.30 ± 0.12 mm/year; **Figure 2B**). The remaining 56 patients had similar progression rates between their eyes (mean difference, 0.05 ± 0.04 mm/year, within $Q_{1.3} \pm 1.5 \times \text{IQR}$; **Figure 2C**).

Baseline RPE atrophy and genetic associations with discordant RPE atrophy progression
Discordant RPE atrophy at baseline was associated with discordant RPE atrophy progression (odds ratio, 6.50; 95% CI, 1.35–31.34); this association was not found for discordant BCVA at baseline (odds ratio, 0.33 (95% CI, 0.04–2.85).

Furthermore, decreasing pathogenicity of ABCA4 variant combinations were significantly associated with increasing discordant inter-eye progression ($P = 0.007$). Proportions and correlations are depicted in **Table 2**.

slowest progression rate. Two pairs of eyes showed no progression in 3.0 and 3.4 years, respectively. The progression rates of $\sqrt{\text{RPE}}$ atrophy correlated between the left and right eyes with $\rho = 0.766$, and increased with earlier disease-onset groups ($P = 9.8 \times 10^{-7}$). Evaluating the inter-eye agreement in progression of RPE atrophy, the agreement between the eyes was $\rho_c = 0.765$ (95% CI, 0.645–0.847) (**Figure 1**).

Discordant progression rates of RPE atrophy

Twelve out of 68 patients (early-onset STGD1, two patients (14%); intermediate-onset STGD1, four patients (12%); late-onset STGD1, six patients (29%)) had discordant RPE atrophy progression

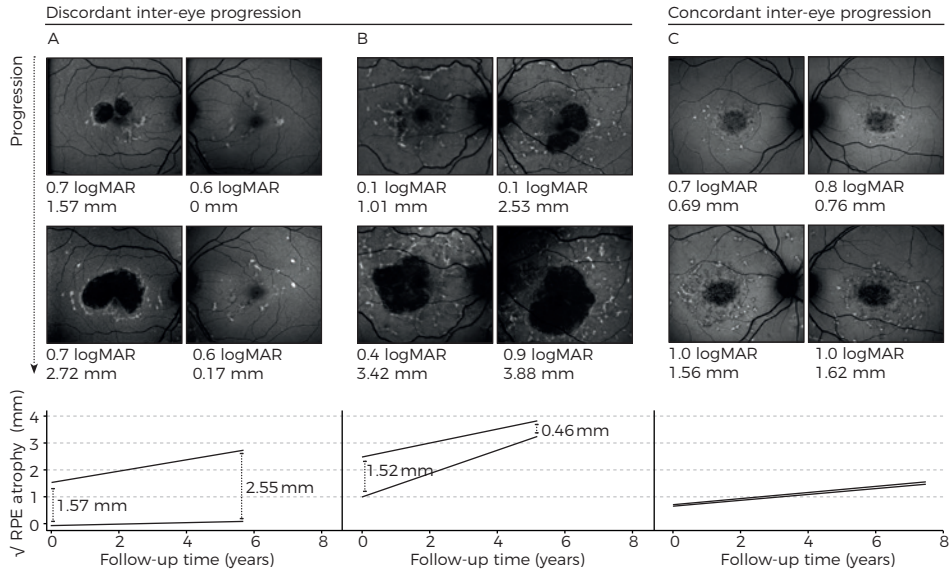


Figure 2. Concordant and discordant inter-eye progression in Stargardt disease. (A) 60-year old female with a disease duration of 1 year and increasing inter-eye differences. *ABCA4* variants: c.5461-10T>C;p.[Thr1821Valfs*13,Thr1821Aspfs*6]/c.2757A>C;p.(Glu919Asp). (B) Eighty-one-year old female with a disease duration of 26 years and decreasing inter-eye differences. *ABCA4* variants: c.5196+1G>T;p.(?)/+. (C) Twenty-six-year old female with a disease duration of 6 years and similar progression rates between eyes. *ABCA4* variants: c.1853G>A;4297G>A;p.(Gly618Glu;Val1433Ile)/c.2588G>C;p.[Gly863Ala;Gly863del].

<i>ABCA4</i> variant combination	RPE Atrophy Progression		
	No discordance	Discordant	Inter-eye correlation (Pearson's <i>p</i>)
1. Pathogenic/pathogenic	3	1	0.995
2. Pathogenic/likely pathogenic	21	4	0.790
3. Likely pathogenic/likely pathogenic	9	0	0.597
4. Pathogenic/*	12	3	0.079
5. Likely pathogenic/*	11	4	0.346

Table 2. Proportions of combinations of *ABCA4* variants and discordant RPE atrophy progression.

* The second *ABCA4* variant was likely benign, of unknown pathogenicity, or not found.

Results III: Power calculations of a theoretical intervention trial

The power of a paired-control intervention trial will depend on the strength of correlations between pairs, that is, the left and right eye of each patient, and the expected treatment effect. For each two-fold increase in expected treatment effect, approximately a four-fold decrease in patient numbers is needed for a study at equal power. Stronger inter-eye correlations will have a linear beneficial effect on the number needed to include. The impact on these numbers is highest when a relatively modest treatment effect is expected. For instance, a correlation of $\rho = 0.766$ would require 44 patients,

whereas this number is reduced to 20 in the case of a correlation of $\rho = 0.9$ (Figure 3). The specific inclusion criteria, for example, disease onset, ABCA4 variant combinations, and baseline discordance can significantly affect the number needed to include.

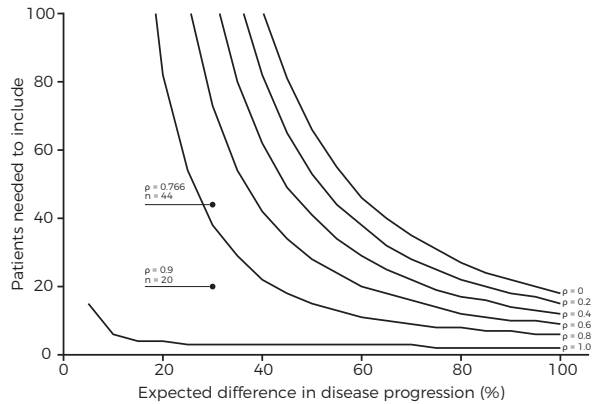


Figure 3. A sensitivity analysis for the power calculation of a theoretical intervention trial. Assuming a 30% reduction in disease progression (treatment effect), 44 patients are needed (inter-eye correlation $\rho = 0.766$; $p = 0.20$, $p = 0.05$, two-sided paired samples t-test). The sample size will decrease to 20 in the case of an inter-eye correlation of 0.9. In the case of a correlation in disease progression of 1, 0.8, 0.6, 0.4, 0.2, and 0 between left and right eyes, 3, 38, 73, 108, 143, or 178 patients are needed, respectively.

Discussion

Based on longitudinal FAF data in our current study, the overall agreement of inter-eye RPE atrophy progression in STGD1 was

only moderate; it was highest in early-onset STGD1 and lowest in late-onset STGD1. Discordant progression rates were found in 12 out of 68 (17.6%) patients—which is surprisingly high—given that STGD1 is assumed to be a symmetrical inherited retinal disease. Discordant progression rates resulted in eyes either converging or diverging in atrophy size. Discrepancies of RPE atrophy progression rates were associated with discrepancies of RPE atrophy at baseline and less pathogenic ABCA4 variant combinations.

Autosomal retinal dystrophies are expected to be symmetrical owing to the similar genetic and environmental background of both eyes. The majority of STGD1 patients exhibit bilateral symmetry in retinal features. Chen et al. illustrated this symmetry in left and right eyes of 24 STGD1 patients; they had highly correlated areas of RPE atrophy (Pearson's $\rho = 0.998$).¹² McBain et al. studied the atrophy progression rates in 12 STGD1 patients, reporting a strong inter-eye correlation (Spearman's $\rho = 0.846$).¹¹ In our cohort, these inter-eye correlations of RPE atrophy were substantially lower, but they can be explained by inclusion of late-onset STGD1 patients, which decreased the overall correlation. Inter-eye correlations of late-onset STGD1 were previously estimated to be moderate ($\rho = 0.52$).²⁰ When late-onset STGD1 patients are excluded, our inter-eye correlations were similar to those reported by others.

Previous studies were limited by standard analyses of correlations, which cannot address the absolute symmetry within a patient. In contrast, we used Lin's concordance correlation coefficients and descriptive Bland-Altman plots, which are more appropriate and previously described in age-related macular degeneration.²⁷ In addition, there is an inherent increase in variability of inter-eye differences when the magnitude of atrophic areas increases. We corrected this by expressing the inter-eye differences as the square root, thus the differences were proportional to the magnitude of measurements. Moreover, square-root transformation corrected baseline dependence, which was reported previously with an average atrophy enlargement increase of 0.016 mm²/year for each month of follow-up.¹⁰

Although we found that progression rates for atrophy are more likely to be discordant in eyes that differ more at baseline, progression rates are rather unpredictable between patients and between eyes within a patient. McBain et al. suggested that electroretinography could predict the rate of atrophy progression, but they did not account for baseline atrophy size. It would be interesting if discordance in electroretinography between eyes of a patient would also predict inter-eye differences in progression, independent of their baseline atrophy size.¹⁰ Burke et al. indicated that changes on optical coherence tomography would precede RPE atrophy and may thus predict the rates of atrophy progression.³¹ These potential predictors for disease progression need to be addressed in future work.

The lower inter-eye correlations in older patients could be explained by the increased time within which stochastic factors, for example, small initial differences leading to significant differences later, can influence phenotypic expression. Differences in ABCA4 variant expression may alter disease severity between eyes with mild variants, which can have a slightly different pathogenicity. In contrast, differences in expression would not influence progression speed much in severe ABCA4 combinations as both variants would cause an equally severe phenotype.

The statistical power of a randomized controlled trial increases when differences are measured between correlated left and right eyes. To this extent, we recommend a fellow-eye paired trial design for retinal dystrophies, for example, as applied in a phase II gene therapy trial for choroideremia with 30 patients enrolled (ClinicalTrials.gov, NCT02407678). To achieve 80% statistical power in this trial, an effect size of at least 0.53 is required.³² For the same expected effect size, a patient-controlled trial would need 58 patients in each arm.³³ Even in multicenter trials, such high sample sizes are difficult to obtain in rare retinal dystrophies. However, it is important to bear in mind that a fellow-eye paired control is impossible for pharmaceutical strategies in which both eyes of a patient are being treated (ClinicalTrials.gov, NCT02402660). Furthermore, it is

preferred that an effect on relatively slow retinal degeneration is detected to identify a potential long-term benefit rather than a temporary gain of visual function.³⁴

A therapeutic trial will gain a major advantage from a fellow-eye control in early-onset STGD1 because of their high inter-eye correlations. However, discordance was also present in some of these younger patients. As the progression can be better predicted in similar rather than in discordant eyes, retinal asymmetry needs to be considered as an exclusion criterion for small early-phase trials. Such stringent criteria will increase the chance of detecting efficacy with fewer patients. Criteria would include early-onset STGD1 patients with concordant retinal abnormalities between their eyes carrying severe ABCA4 variants; not only do these patients have the highest inter-eye symmetry in disease progression, but they are also expected to have the most severe disease course.^{1, 2} In these patients, therapy will potentially provide the most benefit, and in these patients, its effect has the highest chance to be detected.

References

1. Fujinami K, Zernant J, Chana RK, et al. Clinical and molecular characteristics of childhood-onset Stargardt disease. *Ophthalmology* 2015;122(2):326-34.
2. Lambertus S, van Huet RA, Bax NM, et al. Early-onset stargardt disease: phenotypic and genotypic characteristics. *Ophthalmology* 2015;122(2):335-44.
3. Westeneng-van Haaften SC, Boon CJ, Cremers FP, et al. Clinical and genetic characteristics of late-onset Stargardt's disease. *Ophthalmology* 2012;119(6):1199-210.
4. Yatsenko AN, Shroyer NF, Lewis RA, Lupski JR. Late-onset Stargardt disease is associated with missense mutations that map outside known functional regions of ABCR (ABCA4). *Hum Genet* 2001;108(4):346-55.
5. Rotenstreich Y, Fishman GA, Anderson RJ. Visual acuity loss and clinical observations in a large series of patients with Stargardt disease. *Ophthalmology* 2003;110(6):1151-8.
6. Allikmets R, Singh N, Sun H, et al. A photoreceptor cell-specific ATP-binding transporter gene (ABCR) is mutated in recessive Stargardt macular dystrophy. *Nat Genet* 1997;15(3):236-46.
7. Weng J, Mata NL, Azarian SM, et al. Insights into the function of Rim protein in photoreceptors and etiology of Stargardt's disease from the phenotype in *abcr* knockout mice. *Cell* 1999;98(1):13-23.
8. Stargardt K. Über familiäre, progressive degeneration in der makulagegend des auges. *Graefes Arch Clin Exp Ophthalmol* 1909;71:534-50.
9. Armstrong JD, Meyer D, Xu S, Elfervig JL. Long-term follow-up of Stargardt's disease and fundus flavimaculatus. *Ophthalmology* 1998;105(3):448-57; discussion 57-8.
10. Fishman GA, Stone EM, Grover S, et al. Variation of clinical expression in patients with Stargardt dystrophy and sequence variations in the ABCR gene. *Arch Ophthalmol* 1999;117(4):504-10.
11. McBain VA, Townend J, Lois N. Progression of retinal pigment epithelial atrophy in stargardt disease. *Am J Ophthalmol* 2012;154(1):146-54.
12. Chen B, Tosha C, Gorin MB, Nusinowitz S. Analysis of autofluorescent retinal images and measurement of atrophic lesion growth in Stargardt disease. *Exp Eye Res* 2010;91(2):143-52.
13. Fujinami K, Sergouniotis PI, Davidson AE, et al. Clinical and molecular analysis of Stargardt disease with preserved foveal structure and function. *Am J Ophthalmol* 2013;156(3):487-501.e1.
14. Han Z, Conley SM, Naash MI. Gene therapy for Stargardt disease associated with ABCA4 gene. *Adv Exp Med Biol* 2014;801:719-24.
15. Schwartz SD, Hubschman JP, Heilwell G, et al. Embryonic stem cell trials for macular degeneration: a preliminary report. *Lancet* 2012;379(9817):713-20.
16. Charbel Issa P, Barnard AR, Herrmann P, et al. Rescue of the Stargardt phenotype in *Abca4* knockout mice through inhibition of vitamin A dimerization. *Proc Natl Acad Sci U S A* 2015;112(27):8415-20.
17. Cukras CA, Wong WT, Caruso R, et al. Centrifugal expansion of fundus autofluorescence patterns in Stargardt disease over time. *Arch Ophthalmol* 2012;130(2):171-9.
18. Fujinami K, Lois N, Mukherjee R, et al. A longitudinal study of Stargardt disease: quantitative assessment of fundus autofluorescence, progression, and genotype correlations. *Invest Ophthalmol Vis Sci* 2013;54(13):8181-90.
19. Lois N, Halfyard AS, Bird AC, et al. Fundus autofluorescence in Stargardt macular dystrophy-fundus flavimaculatus. *Am J Ophthalmol* 2004;138(1):55-63.
20. Lambertus S, Lindner M, Bax NM, et al. Progression of Late-Onset Stargardt Disease. *Invest Ophthalmol Vis Sci* 2016;57(13):5186-91.
21. Teussink MM, Lee MD, Smith RT, et al. The effect of light deprivation in patients with Stargardt disease. *Am J Ophthalmol* 2015;159(5):964-72.e2.
22. Boon CJ, Jeroen Klevering B, Keunen JE, et al. Fundus autofluorescence imaging of retinal dystrophies. *Vision Res* 2008;48(26):2569-77.
23. Feuer WJ, Yehoshua Z, Gregori G, et al. Square root transformation of geographic atrophy area measurements to eliminate dependence of growth rates on baseline lesion measurements: a reanalysis of age-related eye disease study report no. 26. *JAMA Ophthalmol* 2013;131(1):110-1.

24. Cohen J, & Cohen, P. Chapter: 2.8.3 Fisher's z' Transformation and Comparisons between independent rs. *Applied multiple regression/correlation analysis for the behavioral sciences*, Second edition ed. Hillsdale, NJ: Erlbaum 1983.
25. Bland JM, Altman DG. Statistical Methods for Assessing Agreement between Two Methods of Clinical Measurement. *Lancet* 1986;1(8476):307-10.
26. Lin LI. A Concordance Correlation-Coefficient to Evaluate Reproducibility. *Biometrics* 1989;45(1):255-68.
27. Fleckenstein M, Adrion C, Schmitz-Valckenberg S, et al. Concordance of disease progression in bilateral geographic atrophy due to AMD. *Invest Ophthalmol Vis Sci* 2010;51(2):637-42.
28. Lin L, Hedayat AS, Sinha B, Yang M. Statistical methods in assessing agreement: Models, issues, and tools. *Journal of the American Statistical Association* 2002;97(457):257-70.
29. Lin LI. A note on the concordance correlation coefficient. *Biometrics* 2000;56:324-5.
30. McBride GB. A proposal for strength-of-agreement criteria for Lin's Concordance Correlation Coefficient. NIWA Client Report: HAM2005-06. 2005.
31. Burke TR, Rhee DW, Smith RT, et al. Quantification of peripapillary sparing and macular involvement in Stargardt disease (STGD1). *Invest Ophthalmol Vis Sci* 2011;52(11):8006-15.
32. O'Brien RG, Muller KE. Unified Power Analysis for t-Tests Through Multivariate Hypotheses. In: Edwards LK, ed. *Applied Analysis of Variance in Behavioral Science*. New York: Marcel Dekker, 1993.
33. Dixon WJ, Massey FJJ. *Introduction to Statistical Analysis*, Fourth Edition ed. New York: McGraw Hill, 1983.
34. Cideciyan AV, Jacobson SG, Beltran WA, et al. Human retinal gene therapy for Leber congenital amaurosis shows advancing retinal degeneration despite enduring visual improvement. *Proc Natl Acad Sci U S A* 2013;110(6):E517-25.

“Weighted composite endpoints can be powerful in the evaluation of the efficacy of new treatment modalities with small cohorts in a timely fashion. Potentially, it can reduce costs and duration of pivotal clinical trials and can also reduce beta errors in data analysis, thereby hopefully facilitating effective treatments being identified more readily and rapidly for patients with rare diseases.”

Stanley Lambertus

Nathalie M. Bax

Ana Fakin

Joannes M.M. Groenewoud

B. Jeroen Klevering

Anthony T. Moore

Michel Michaelides

Andrew R. Webster

Gert Jan van der Wilt

Carel B. Hoyng

PLoS One. 2017 Mar 29;12(3):e0174020.

We thank Frans Cremers and John (Pei-Wen) Chiang for performing the genetic analysis; and Willem Woertman and Jelle Goeman for their fruitful discussions that helped to develop the methods used in this study.

4.2 Highly sensitive measurements of disease progression in rare disorders: developing and validating a multimodal model of retinal degeneration in Stargardt disease

BACKGROUND: Each inherited retinal disorder is rare, but together, they affect millions of people worldwide. No treatment is currently available for these blinding diseases, but promising new options—including gene therapy—are emerging. Arguably, the most prevalent retinal dystrophy is Stargardt disease. In each case, the specific combination of ABCA4 variants (>900 identified to date) and modifying factors is virtually unique. It accounts for the vast phenotypic heterogeneity including variable rates of functional and structural progression, thereby potentially limiting the ability of phase I/II clinical trials to assess efficacy of novel therapies with few patients. To accommodate this problem, we developed and validated a sensitive and reliable composite clinical trial endpoint for disease progression based on structural measurements of retinal degeneration.

METHODS AND FINDINGS: We used longitudinal data from early-onset Stargardt patients from the Netherlands (development cohort, $n = 14$) and the United Kingdom (external validation cohort, $n = 18$). The composite endpoint was derived from best-corrected visual acuity, fundus autofluorescence, and spectral-domain optical coherence tomography. Weighting optimization techniques excluded visual acuity from the composite endpoint. After optimization, the endpoint outperformed each univariable outcome, and showed an average progression of 0.41° retinal eccentricity per year (95% confidence interval, 0.30–0.52). Comparing with actual longitudinal values, the model accurately predicted progression (R^2 , 0.904). These properties were largely preserved in the validation cohort ($0.43^\circ/\text{year}$ [0.33–0.53]; prediction R^2 , 0.872). We subsequently ran a two-year trial simulation with the composite endpoint, which detected a 25% decrease in disease progression with 80% statistical power using only 14 patients.

CONCLUSIONS: These results suggest that a multimodal endpoint, reflecting structural macular changes, provides a sensitive measurement of disease progression in Stargardt disease. It can be very useful in the evaluation of novel therapeutic modalities in rare disorders.

Introduction

Inherited blindness affects millions of people worldwide—the majority suffering from retinal disease.¹ Inherited retinal disorders now represent the primary cause of blindness in the working age population in the UK, and secondary in childhood.² They are clinically and genetically heterogeneous, caused by sequence variants in more than 300 distinct genes (RetNet). Mutations in the adenosine triphosphate-binding cassette, subfamily A, member 4 (ABCA4) gene are linked to arguably the most common retinal dystrophy: autosomal recessive Stargardt disease (STGD1).³ Each case of STGD1 is, in a sense, unique by specific combinations of pathogenic ABCA4 variants (>900 variants identified to date) and modifying factors. Consequently, the natural course is highly variable, ranging from severe early-onset rapid degeneration^{4,5} to relatively mild late-onset disease.^{6,7} The eventual vision loss results from progressive impairment and degeneration of photoreceptors and their supporting retinal pigment epithelium (RPE).⁸

Recently, significant advancement has been made in the development of therapies that aim to slow disease progression, or even to restore lost photoreceptors in STGD1. These include replacement of ABCA4 by gene therapy,⁹ cell-based therapies,¹⁰ and pharmacological strategies including slowing the visual cycle or inhibition of vitamin A dimerization.^{11,12} Clinical trials are currently recruiting patients to assess safety and efficacy. However, successful evaluation of these therapies critically hinges on sensitive and reliable measures for disease progression.

To monitor efficacy of a treatment, current trials generally use functional endpoints (Supplemental Table S₁). One of the most widely used U.S. Food and Drug Administration-approved endpoints is best-corrected visual acuity (BCVA).¹³ However, the main disadvantage of BCVA lies in its extremely variable deterioration rate in patients with retinal dystrophies. Moreover, visual acuity decline can be a late phenomenon following a long period of pathophysiological changes.¹⁴ As a result, the endpoint has an unfavorable signal-to-noise ratio, which leads to a need for longer follow-up and large cohorts. This setup is impossible to achieve given the unacceptable long time frame and the rarity of these disorders.

However, studies suggest that structural abnormalities gradually expand centrifugally,^{5,15} starting from the foveal center towards the periphery. Although loss of foveal function is highly important from a patient's perspective, it is only one step in the overall pattern of retinal degeneration. This pattern is thought to initiate with melanization abnormalities in the RPE,^{16,17} and is trailed by changes in lipofuscin fluorophores,¹⁸⁻²⁰ degeneration of the RPE,²¹⁻²³ and loss of the ellipsoid zone (EZ) and external limiting membrane (ELM).²⁴⁻²⁷

However, these transition zones are not present in every case, and do not always start at the center of the macula; many are still not well understood.

A composite outcome measure is likely to outperform single candidate outcome measures²⁸ in accurately measuring short-term progression, and can therefore increase statistical power of pivotal clinical trials. In this

study, we chose to measure four structural metrics of expanding transition zones and one psychophysical metric over time in a cohort of patients with early-onset STGD1. These included questionably and definitely decreased autofluorescence (QDAF and DDAF), and loss of the EZ, ELM and BCVA. Next, we assessed intra- and inter-grader differences. Having standardized all metrics, we then calculated an optimal weighted composite. The same measurements were made in a second patient cohort, and, using the composite, we predicted and compared progression with real longitudinal values. We subsequently ran a simulation to examine the power of the composite endpoint and alternatives to detect a difference in outcome given a theoretical intervention with a significant impact on progression rate.

Results

Characteristics of the initial patient population

A cohort of 14 patients with early-onset STGD1 ascertained at the Radboud university medical center in Nijmegen had a median age at disease onset of 9 years (range, 4–11). Seventy-four eye-visits of 28 eyes were included in this study (range, 2–4 visits per eye). At the time of inclusion, all eyes had abnormal fundus autofluorescence (FAF) imaging and evidence of loss of photoreceptors on spectral-domain optical coherence tomography (SD-OCT), primarily limited to the macula at their baseline visit. Due to their early disease onset and rapidly progressive macular changes, a significant proportion of patients were expected to progress to retina-wide disease over time.^{4,5,29} The follow-up time ranged from 1.1 to 9.7 years (median, 4.7).

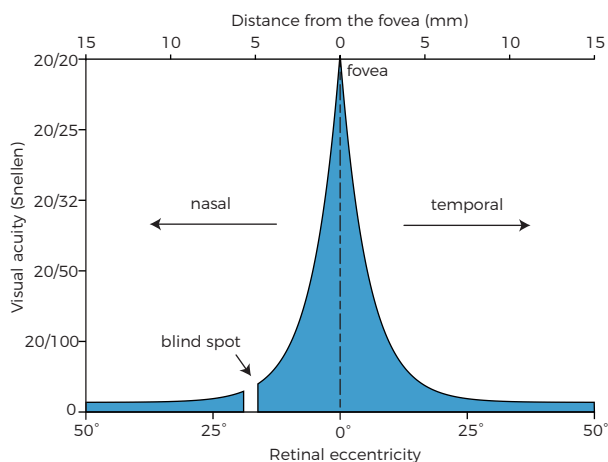


Figure 1. Visual acuity as a function of degrees of retinal eccentricity.

Visual acuity measurements indicate extra-macular dysfunction

At the first visit, the Nijmegen cohort had a median BCVA of 20/205 Snellen in both eyes. The highest BCVA can be obtained at the fovea and diminishes rapidly by retinal eccentricity (ϵ) as shown in Figure 1.³⁰ According to Figure 1, 20/205 Snellen corresponds to 12.76° of ϵ by BCVA (ϵ_{BCVA}), the equivalent diameter being 7.7 mm. Assuming a 5.5 mm diameter of the macula, the high degree of eccentricity indicated that the patients' visual function corresponded to extra-macular disease at baseline.

Structural parameters are measured with high reproducibility

To assess the accuracy and reliability of measurements on FAF imaging and SD-OCT, we analyzed inter- and intra-grader agreements. These included transition zones of QDAF and DDAF areas, and transverse loss of the EZ and ELM. The absolute mean (\pm standard deviation) differences within one grader for ϵ_{QDAF} , ϵ_{DDAF} , ϵ_{EZ} and ϵ_{ELM} were $0.19 \pm 0.18^\circ$, $0.20 \pm 0.23^\circ$, $0.10 \pm 0.12^\circ$, and $0.20 \pm 0.22^\circ$, respectively. The intra-grader measurements were highly correlated with intraclass correlation coefficients (95% confidence interval) of 0.995 (0.989–0.997), 0.994 (0.986–0.997), 0.998 (0.993–0.999), and 0.998 (0.994–0.999), respectively. The absolute mean differences between graders were $0.26 \pm 0.23^\circ$, $0.22 \pm 0.21^\circ$, $0.26 \pm 0.23^\circ$, and $0.23 \pm 0.18^\circ$, respectively. The measurements from both graders were highly correlated with intraclass correlation coefficients of 0.992 (0.986–0.995), 0.994 (0.990–0.996), 0.992 (0.971–0.998), and 0.997 (0.992–0.999), respectively.

(A) Fundus autofluorescence



(B) Spectral-domain optical coherence tomography

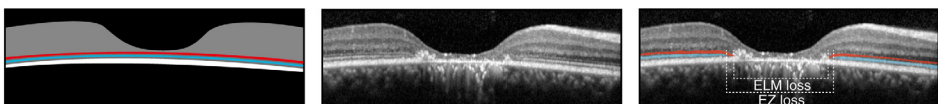


Figure 2. Schematic and representative images of measurements in fundus autofluorescence imaging and spectral-domain optical coherence tomography. Patient 9: area of questionably decreased autofluorescence (QDAF, blue), 1.37 mm²; area of definitely decreased autofluorescence (DDAF, black), 0.33 mm²; transverse loss of external limiting membrane (ELM loss, red), 1.75 mm; transverse loss of ellipsoid zone (EZ loss, blue), 2.24 mm; best-corrected visual acuity, 20/100; ABCA4 variants, c.1622T>C;3113C>T;p.[Leu541Pro;Ala1038Val] and c.6316C>T;p.(Arg2106Cys).

	Slope (mean)	Residual (SD)	MSDR
<i>Univariable outcomes</i>			
ϵ_{BCVA}	0.31°/year	3.77°/year	0.08
ϵ_{QDAF}	0.32°/year	0.14°/year	2.32
ϵ_{DDAF}	0.58°/year	0.33°/year	1.73
ϵ_{ELM}	0.34°/year	0.17°/year	1.97
ϵ_{EZ}^*	0.38°/year	*	*
<i>Composite outcomes</i>			
Unweighted ($\epsilon_{BCVA}, \epsilon_{QDAF}, \epsilon_{DDAF}, \epsilon_{ELM}, \epsilon_{EZ}$)	0.35°/year	1.24°/year	0.28
Unweighted ($\epsilon_{QDAF}, \epsilon_{DDAF}, \epsilon_{ELM}, \epsilon_{EZ}$)	0.47°/year	0.24°/year	2.00
Optimal weight (15% ϵ_{QDAF} , 5% ϵ_{DDAF} , 15% ϵ_{ELM} , 55% ϵ_{EZ})	0.41°/year	0.13°/year	3.21

Table 1. Yearly progression rate of changes in retinal eccentricity (ϵ) by visual function, fundus autofluorescence and optical coherence tomography. *There were limited measurements available because it exceeded retinal scans. BCVA = best-corrected visual acuity. QDAF = questionably decreased autofluorescence. DDAF = definitely decreased autofluorescence. ELM = external limiting membrane. EZ = ellipsoid zone. MSDR = mean-to standard deviation ratio. SD = standard deviation. ϵ = retinal eccentricity.

Initial transition zones on retinal imaging

We measured the abnormalities of lipofuscin fluorophores in the RPE by determining both the transition zones of DDAF and QDAF on FAF imaging as shown in Figure 2A.^{20,31} At the first visit, the median ϵ_{DDAF} and ϵ_{QDAF} for both eyes were 1.80° (range, 0–5.60) and 4.22° (range, 1.68–7.67), equivalent to an area of 0.92 mm² and 5.03 mm²,

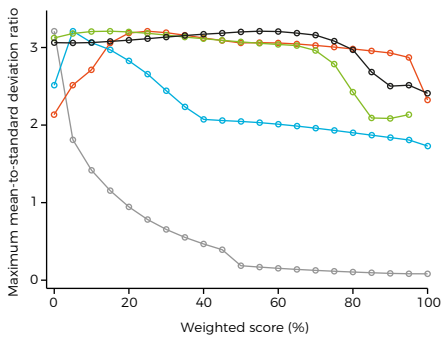


Figure 3. Highest potential mean-to-standard deviation ratio (MSDR) for each single outcome measure at different weightings with all possible weight combinations of the other metrics. MSDRs for best-corrected visual acuity (grey) decrease at increasing weight. MSDRs for transition zones of questionably decreased autofluorescence (blue) increase until 25% weight, but gradually decrease at higher weights. MSDRs for transition zones of definitely decreased autofluorescence (red) decrease at weights higher than 5%. MSDRs for loss of the ellipsoid zone (green) are constant, but decrease substantially at weights higher than approximately 70%. MSDRs for loss of the external limiting membrane (black) decrease at weights higher than approximately 80%.

respectively. Additionally, we measured the horizontal loss of the photoreceptor-related ELM and EZ through the foveal center on SD-OCT (Figure 2B). At the first visit, the median ϵ_{ELM} and ϵ_{EZ} for both eyes were 5.09° (range, 2.50–10.71) and 3.54° (range, 2.99–7.83), equivalent to a loss of 3.05 mm and 2.12 mm, respectively.

A structural composite measure of expanding transition zones outperforms univariable measures

We assessed the change of each individual parameter over time by linear mixed-effects models. The models accounted for between-patients and between-eyes effects. We then calculated the sensitivity of each parameter by the ratio of the population mean slope, i.e., overall disease progression, and the residual standard deviation (mean-to-standard-deviation ratio, MSDR). ϵ_{QDAF} had the highest sensitivity

(MSDR, 2.32), whereas $\varepsilon_{\text{BCVA}}$ had the lowest (MSDR, 0.08). The MSDR for ε_{EZ} could not be obtained as there were not sufficient measurements available. Sensitivities of all individual parameters are shown in Table 1. We constructed a composite variable from changes in ε as measured by BCVA, QDAF, DDAF, EZ, and ELM. Results from MSDR calculations of every potential weighting combination indicated that the most sensitive composite consisted of a weighted mean of changes in $\varepsilon_{\text{BCVA}}$ (0%), $\varepsilon_{\text{QDAF}}$ (25%), $\varepsilon_{\text{DDAF}}$ (5%), ε_{EZ} (55%), and ε_{ELM} (15%). We observed an overall progression rate of 0.41°/year (95% confidence interval, 0.30–0.52). Potential MSDRs for all measures with different weighting scores are shown in Figure 3. Based on the weighted composite score we predicted changes in ε of six patients with a third or fourth visit. The predicted values correlated strongly with the measured weighted composite score (R^2 , 0.904; slope, 0.90 [0.70–1.11]; intercept, 0.14 [-0.55 to 0.83]; Figure 4A).

Accurate prediction of disease progression is validated in a replication cohort

Using the identical weighted score in the mixed-effects model, we predicted the progression in a separate replication cohort of 18 Stargardt patients, ascertained at Moorfields Eye Hospital in London. One hundred and thirty-eight eye-visits were included (range, 2–6 visits per patient). The London cohort was not significantly different to the Nijmegen cohort: with a median age at disease onset of 8 years (range, 5–11; Mann-Whitney U, $P=0.419$), and follow-up from 1.0 to 11.0 years (median, 4.5; Mann-Whitney U, $P=0.722$). We observed an overall progression of 0.43°/year (95% confidence interval, 0.33–0.53).

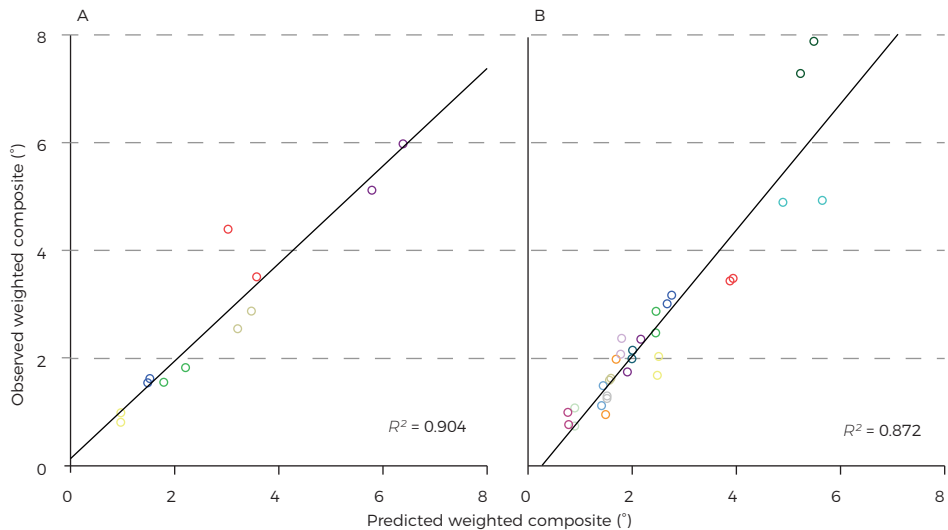


Figure 4. Weighted composite score and predicted outcome. Matching colors represent the right and left eye of the same patient. (A) Results from six early-onset Stargardt patients. (B) The predicted outcome in the replication cohort showed comparable results.

	Radboudumc	MEH
Patients	7 men 7 women	11 men 7 women
<i>Baseline characteristics</i>		
Age at onset (years)	9 (4–11)	8 (5–11)
Age at baseline (years)	13 (9–26)	14 (8–25)
ϵ BCVA ($^{\circ}$, Snellen equivalent)	12.76 (9.85–24.00), 20/200	12.62 (6.31–18.94), 20/200
ϵ_{QDAF} ($^{\circ}$, area equivalent)	4.22 (1.68–7.67), 5.03 mm ²	4.64 (1.44–9.98), 6.10 mm ²
ϵ_{DDAF} ($^{\circ}$, area equivalent)	1.80 (0–5.60), 0.92 mm ²	2.40 (0–6.41), 1.63 mm ²
ϵ_{ELM} ($^{\circ}$, transverse equivalent)	5.09 (2.50–10.71), 3.05 mm	4.82 (2.06–7.71), 2.89 mm
ϵ_{EZ} ($^{\circ}$, transverse equivalent)	3.54 (2.99–7.83), 2.12 mm	5.87 (3.86–8.58), 3.52 mm
<i>Disease progression</i>		
Follow-up (years)	4.73 (1.13–9.71)	4.47 (1.0–10.99)
Progression ($^{\circ}$ /year)	0.41 (95% CI, 0.30–0.52)	0.43 (95% CI, 0.33–0.53)

Table 2. Characteristics of early-onset Stargardt cohorts from Radboud university medical center (Radboudumc) and Moorfields Eye Hospital (MEH). Median and range are shown for baseline characteristics and follow-up. BCVA = best-corrected visual acuity. CI = confidence interval. QDAF = questionably decreased autofluorescence, DDAF = definitely decreased autofluorescence, ϵ = retinal eccentricity. ELM = external limiting membrane, EZ = ellipsoid zone, SE = standard error, ϵ = retinal eccentricity.

Cohort characteristics compared to the Nijmegen cohort are further described in [Table 2](#). Predicted values correlated with the measured weighted composite score (R^2 , 0.872; slope, 1.17 [0.99–1.34]; intercept, -0.29 [-0.77–0.18]; [Figure 4B](#)).

Simulation reveals high statistical power despite small numbers of patients and short follow-up

Finally, to assess the value of the composite biomarker in an interventional trial, we simulated a randomized-controlled paired trial in 14 patients, with a two-year follow-up period, and different treatment effects ([Figure 5](#)). Using the optimized weighted composite score as the primary endpoint, we obtained a statistical power of >80% (with a significance level of 0.05) in the case of a 25% treatment effect. Unweighted structural scores decreased the power by approximately 50%.

Discussion

The genotypic and phenotypic heterogeneity of rare diseases are a challenge for designing therapeutic clinical trials using conventional parameters. This affects many patients; current estimates are between 6.5 and 9.9 million inhabitants of the EU28 countries (1.3–2.0%). Jointly, these diseases represent a relevant public health issue,³² and to evaluate novel treatments, better strategies are needed. Current strategies use biomarkers, which are often insufficient to provide appropriate sample size calculations, or require long-term follow-up ([Supplemental Table S₁](#)). However, an

integrated approach of these individual biomarkers can result in a reliable and sensitive marker for disease progression. In this paper, we showed that such markers can be developed using composite endpoints and weighting optimization techniques.

The composite endpoint that we developed to sensitively measure disease progression in patients with early-onset STGD1 was based on its spatiotemporal disease course. Although the exact pathophysiological mechanisms of the disease pattern are still not completely understood, natural history studies suggest a centrifugal expansion from macula-only to potentially retina-wide disease.^{5, 15, 16, 29, 33} Visual acuity failed to detect this gradual expansion due to its low signal-to-noise ratio in the composite model. In the final model, the expansion of different transition zones is analyzed by two widely available imaging techniques. SD-OCT can visualize photoreceptor damage, represented by loss of the ellipsoid zone, followed by loss of the external limiting membrane,³⁴⁻³⁶ and FAF imaging can detect RPE atrophy associated with photoreceptor dysfunction/loss.²⁶

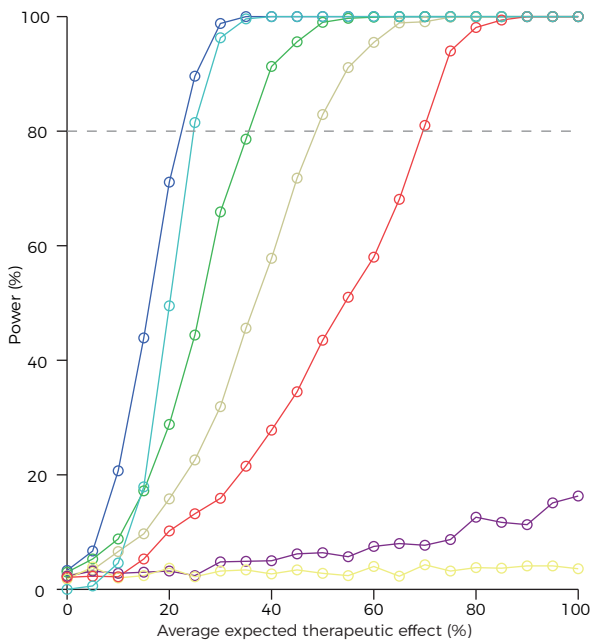


Figure 5. Power calculations of a simulated therapeutic trial based on fourteen early-onset Stargardt patients. Dark blue line: a power of 80% is reached with a 25% overall treatment effect and a two-year follow-up period. Purple line: the power will drastically decrease when best-corrected visual acuity is included in the outcome measure. Turquoise line: worse eye treated. Green line: one-year follow-up. Ocher line: unweighted structural composite. Red line: non-paired trial design. Yellow line: best-corrected visual acuity as a single outcome measure.

In the future, the composite model may be further optimized by incorporating more sophisticated retinal imaging techniques such as adaptive optics scanning light ophthalmoscopy which affords *in-vivo* cellular imaging. Parameters derived from electrophysiological assessment could also potentially strengthen the composite model, although it is limited by significantly greater test-retest variability than aforementioned structural testing.³⁷⁻³⁹

We are aware that, ultimately, the value of novel therapeutic modalities should be inferred from their impact on outcomes that matter to patients. In

the context of eye disease, these would certainly include vision and the impact that visual impairments have on daily life (patient-reported outcome measures). In addition, the long-term safety of such novel treatments should be safeguarded. For these purposes, the metric that we have developed in this study is unlikely to be appropriate in isolation, since its focus lies on structural abnormalities alone. We believe its value mainly derives from the ability to rationally select promising novel treatment modalities and also potentially facilitate patient selection for recruitment to clinical trials. Consequently, it will need to be demonstrated that the employed structural parameters correlate with functional outcome in the long term.

Multimodal analysis is a powerful technique, potentially reducing costs and duration of clinical trials and also likely reducing beta errors in data analysis, thereby hopefully facilitating effective treatments being identified more readily and rapidly for patients with rare diseases. There is also the possibility of further improvements with the inclusion of other biomarkers in the future, and the potential to be extrapolated to other disorders.

Materials and methods

Patient selection

We selected patients from the Stargardt databases of the Departments of Ophthalmology at Radboud university medical center (Nijmegen, the Netherlands) and Moorfields Eye Hospital (London, United Kingdom). We used the patient data from Radboud university medical center to develop the progression model, and the data from Moorfields Eye Hospital to replicate the study. We included patients with the faster progressive early-onset form of STGD1, harboring ≥ 2 likely disease-causing sequence variants in ABCA4 (Table 3), and with at least one year follow-up with FAF imaging and/or SD-OCT. The early-onset phenotype typically presents with foveal atrophy that may precede the development of yellow-white fundus flecks. Early-onset STGD1 is associated with the most rapid deterioration of all patients with STGD1.⁵ We only included patients with a reported disease onset < 12 years of age.^{4,5} We excluded (1) patients with very early disease in which only thickening of the external limiting membrane was present, because this would preclude the OCT measurements, (2) patients with advanced disease characterized by RPE atrophy beyond the vascular arcades at first presentation, and (3) patients who participated in an interventional trial.⁴⁰ This study was approved by the relevant Institutional Ethics Committees and was performed in accordance with the Declaration of Helsinki. All patients provided informed consent prior to receiving additional ophthalmologic examinations.

Radboudumc				
Patient	Variant 1		Variant 2	
1	c.5461-10T>C	p.[Thr1821Valfs*13, Thr1821Aspfs*6]	c.5461-10T>C	p.[Thr1821Valfs*13, Thr1821Aspfs*6]
2	c.5461-10T>C	p.[Thr1821Valfs*13, Thr1821Aspfs*6]	c.214G>A	p.(Gly72Arg)
3	c.5461-10T>C	p.[Thr1821Valfs*13, Thr1821Aspfs*6]	c.5537T>C	p.(Ile1846Thr)
4	c.768G>T	p.(?)	c.1822T>A	p.(Phe608Ile)
5	c.3033-?_3364+?del	p.(?)	c.5714+5G>A	p.(?)
6	c.5461-10T>C	p.[Thr1821Valfs*13, Thr1821Aspfs*6]	c.5337C>A	p.(Tyr1779*)
7	c.286A>G	p.(Asn96Asp)	c.286A>G	p.(Asn96Asp)
8	c.5461-10T>C	p.[Thr1821Valfs*13, Thr1821Aspfs*6]	c.4773+1G>A	p.(?)
9	c.1622T>C;3113C>T	p.[Leu541Pro;Ala1038Val]	c.6316C>T	p.(Arg2106Cys)
10	c.768G>T	p.(?)	c.768G>T	p.(?)
11	c.3033-?_3364+?del	p.(?)	c.5714+5G>A	p.(?)
12	c.4128+1G>A	p.(?)	c.3259G>A	p.(Glu1087Lys)
13	c.4128+1G>A	p.(?)	c.3259G>A	p.(Glu1087Lys)
14	c.4139C>T	p.(Pro1380Leu)	c.2160+1G>T	p.(?)
MEH				
Patient	Variant 1		Variant 2	
1	c.3191-1G>T	p.(?)	c.4139C>T	p.(Pro1380Leu)
2	c.4462T>C	p.(Cys1488Arg)	c.4462T>C	p.(Cys1488Arg)
3	c.6079C>T	p.(Leu2027Phe)	c.3322C>T	p.(Arg1108Cys)
4	c.6479+1G>A	p.(?)	c.6479+1G>A	p.(?)
5	c.6479+1G>A	p.(?)	c.6479+1G>A	p.(?)
6	c.4469G>A	p.(Cys1490Tyr)	c.3197T>G	p.(Met1066Arg)
7	c.4253+4C>T	p.(?)	c.4253+4C>T	p.(?)
8	c.5461-10T>C	p.[Thr1821Valfs*13, Thr1821Aspfs*6]	c.3299T>A	p.(Ile1100Asn)
9	c.768G>T	p.(?)	c.4139C>T	p.(Pro1380Leu)
10	c.3081T>G	p.(Tyr1027*)	c.3081T>G	p.(Tyr1027*)
11	c.6286G>A	p.(Glu2096Lys)	c.2894A>G	p.(Asn965Ser)
12	c.4577C>T	p.(Thr1526Met)	c.3322C>T	p.(Arg1108Cys)
13	c.93G>A	p.(Trp31*)	c.2522A>C	p.(Gln841Pro)
14	c.4139C>T	p.(Pro1380Leu)	c.1957C>T	p.(Arg653Cys)
15	c.6729+4_6729+18del AGTTGGCCCTGGGGC	p.(?)	c.6729+4_6729+18del AGTTGGCCCTGGGGC	p.(?)
16	c.5714+5G>A	p.(?)	c.1622T>C;3113C>T	p.[Leu541Pro;Ala1038Val]
17	c.6729+4_6729+18del AGTTGGCCCTGGGGC	p.(?)	c.6729+4_6729+18del AGTTGGCCCTGGGGC	p.(?)
18	c.2912C>A	p.(Thr971Asn)	c.2912C>A	p.(Thr971Asn)

Table 3. ABCA4 variants in early-onset Stargardt patients from Radboud university medical center (Radboudumc) and Moorfields Eye Hospital (MEH).

del = deletion, fs = frameshift, ins = insertion, * = stop codon.

Clinical examinations

We reviewed the records and imaging databases to extract information including BCVA, FAF imaging, and SD-OCT. Best-corrected visual acuity was measured using a Snellen or Early Treatment Diabetic Retinopathy Study chart. Short-wave FAF imaging ($\lambda = 488$ nm, emission 500–700 nm) was performed using a confocal scanning laser ophthalmoscope (Spectralis HRA+OCT or HRA2, Heidelberg Engineering, Heidelberg, Germany). The field of view was set at 30°×30° or 55°×55° and was centered at the

macula. Cross-sectional images were obtained using SD-OCT (Spectralis HRA+OCT, Heidelberg Engineering, Heidelberg, Germany) centered at the macula ([Supplemental Dataset S₁](#)).

Functional measurements

We analyzed data with SAS Statistical Analysis Software Version 9.2 (SAS Institute, Cary, NC). Best-corrected visual acuity can be expressed in retinal eccentricity (ϵ) to estimate the spatial extent of retinal dysfunction spatially. It has been calculated previously that an object must grow by 0.2° in size to maintain BCVA for each degree of eccentricity.³⁰ The BCVA is therefore reduced by a factor of $1/1.2$ for each degree. This results in a transformed BCVA to the estimated equivalent of ϵ :

$$BCVA = \left(\frac{1}{1.2}\right)^\epsilon \quad (1) \text{ which can be written as } \epsilon_{BCVA} = \log_{1/1.2} BCVA \quad (2)$$

Quantitative measurements on imaging

Abnormalities that were expected to consistently increase over time were included for quantification. Two independent authors (S.L. and N.M.B.), blinded to the each other's findings, manually delineated areas of abnormal autofluorescence signals based on darkness levels on FAF imaging, and the loss of retinal layers on SD-OCT. These included areas of questionably decreased autofluorescence (QDAF), definitely decreased autofluorescence (DDAF), transverse loss of the external limiting membrane (ELM) and ellipsoid zone (EZ) on the OCT scan through the fovea. All measurements were standardized to retinal eccentricity. One degree of eccentricity corresponds to approximately 0.3 mm on the retina.⁴¹ Therefore, the eccentricity can be calculated as the radius of the circular equivalents of the sum of QDAF and DDAF areas using the previously reported conversion factor:

$$\epsilon_{QDAF} = 0,3^{-1} \sqrt{\frac{QDAF}{\pi}} \quad (3) \text{ and } \epsilon_{DDAF} = 0,3^{-1} \sqrt{\frac{DDAF}{\pi}} \quad (4)$$

As the transverse horizontal loss of retinal layers represents the diameter of a circular equivalent, the eccentricities of ELM loss and EZ loss could be calculated as follows:

$$\epsilon_{EZ} = 0,3^{-1} \frac{EZ}{2} \quad (5) \text{ and } \epsilon_{ELM} = 0,3^{-1} \frac{ELM}{2} \quad (6)$$

Reproducibility of measurements

If the discrepancy between graders exceeded 1° , the graders were asked to reach consensus on the location and extent of the transition zone. To assess the intra-grader reproducibility, one of the two graders (S.L.) measured each image by each method twice, with a two-month interval between gradings of the same image. We calculated

the absolute inter- and intrarater agreement of ε_{QDAF} , ε_{DDAF} (5%), ε_{ELM} , and ε_{EZ} by intraclass correlation coefficients with 95% confidence intervals. Averaged values of the graders were used for final analyses.

Modelling disease progression

The composite ΔC was constructed from changes in ε as measured in all univariable biomarkers:

$$\begin{aligned} \Delta C_{ij}(\Delta t_{ik}) = & (a \times [\varepsilon_{BCVA_{ij}}(t_{ik}) - \varepsilon_{BCVA_{ij}}(t_{i,0})] + b \times [\varepsilon_{QDAF_{ij}}(t_{ik}) - \varepsilon_{QDAF_{ij}}(t_{i,0})] \\ & + c \times [\varepsilon_{DDAF_{ij}}(t_{ik}) - \varepsilon_{DDAF_{ij}}(t_{i,0})] + d \times [\varepsilon_{EZ_{ij}}(t_{ik}) - \varepsilon_{EZ_{ij}}(t_{i,0})] \quad (7) \\ & + e \times [\varepsilon_{ELM_{ij}}(t_{ik}) - \varepsilon_{ELM_{ij}}(t_{i,0})]) / (a + b + c + d + e) \end{aligned}$$

a, b, c, d, and e are weighting scores for each biomarker.

The composite biomarker was used to detect disease progression in a linear two-level random effects mixed model, which can describe expansion rates of a transition zone quite well within a short period. It accounts for variations between patients and between the eyes of each patient, and can thus incorporate a potential non-linear process in the variance components of these random effects⁴²:

$$\Delta C_{ij}(\Delta t_{ik}) = [s + s_i + s_{ij}] \times \Delta t_{ik} + E_{ijk} \quad (8)$$

- $\Delta C_{ij}(\Delta t)$ is the change of the composite score from baseline for the i^{th} patient in eye j at time since baseline Δt ,
- Δt_{ik} is the k^{th} follow-up time for patient i ,
- s is the mean population slope (first level fixed effect),
- s_i are the deviations of the i^{th} patient's slope from the population value (independent second level random effects),
- s_{ij} are the deviations of the slope of both eyes in patient i from his mean regression line (independent third level random effects),
- E_{ijk} is the residual error.

The intercept of the model was set to zero, because differences from baseline were used.

Weighting scores optimization

Weighting scores were subsequently chosen by an optimization criterion,²⁸ which was constructed by the ratio of the population mean slope and the residual standard deviation (MSDR). The criterion was empirically evaluated for different combinations of weighting scores of parameters:

MSDR = s / RMSE (9)

- s is the mean population slope,
- RMSE (root-mean-square error) is the residual standard deviation, a scale-dependent measure for accuracy.

The total number of unique combinations follows a binomial coefficient $\binom{n+a-1}{n}$, where n is the number of intervals, and a is the number of biomarkers. Five biomarkers with 5% intervals (20 steps from 0 to 100%) resulted $\frac{24!}{20!4!} = 10626$ in combinations, which could be tested within reasonable computational time. A weighting of zero resulted in exclusion of that particular biomarker. When a certain biomarker was missing or not measurable, the ΔC was calculated by the changes in the other biomarkers with their respective weighting scores. The combination with the highest MSDR was eventually used in the final model ([Supplemental Dataset S₂](#) and [Appendix S₁](#)).

Validation and replication of the model

In a subset of patients (six), in which three or more visits were available, we calculated disease progression of the last visit. These final visits were excluded in the construction of the weighted composite. We compared these scores with the predicted scores based on the mixed model. Using identical weighting scores, we replicated the study in another cohort.

Trial simulations

Based on these calculations, the optimal composite score difference was used to perform simulations of a two-year interventional trial with the change in retinal eccentricity as primary outcome measured by the composite biomarker. By introducing a potential treatment effect, we calculated the expected power of a trial with these patients. The treated eye was randomly assigned by a Bernoulli distribution. The progression was then simulated as follows:

(10)

$$\text{Difference of } \Delta C_{ij}(\Delta t_{i,t+x}) = [\Delta C_{ij}(\Delta t_{i,t+x}) \pm \text{adjusted RMSE} - \delta] - \Delta C_{ij}(\Delta t_{i,t})$$

where

(11)

$$\delta = \text{effect size } (\pm 0.1) \times [\text{predicted } \Delta C_{ij}(\Delta t_{i,t+x}) - \text{predicted } \Delta C_{it}(\Delta t_{i,t})]$$

- difference of $\Delta C_{i,t}(\Delta t_{i,t+x})$ is the difference of the change of the composite score from baseline for the i^{th} patient in the j^{th} eye t at x years after the last visit l , compared to the last visit.
- the adjusted RMSE was calculated for residual errors of follow-up measurements without baseline measurements ($\Delta t_{i,0}$), where E_{ij} is zero in all patients,
- the treatment effect δ was simulated from 0 to 1 by steps of 0.05 in treated eyes.

As the degree of abnormalities are highly correlated between left and right eyes,^{21,23} the power can be increased considerably when the fellow eye serves as the paired control. A paired-samples T-test was therefore performed to assess the differences between eyes in progression of changes in retinal eccentricity. Power calculations were performed by 10000 simulations for each data point (Supplemental Appendix S₂).

References

1. Berger W, Kloeckener-Gruissem B, Neidhardt J. The molecular basis of human retinal and vitreoretinal diseases. *Prog Retin Eye Res* 2010;29(5):335-75.
2. Liew G, Michaelides M, Bunce C. A comparison of the causes of blindness certifications in England and Wales in working age adults (16-64 years), 1999-2000 with 2009-2010. *BMJ Open* 2014;4(2):e004015.
3. Kaplan J, Gerber S, Larget-Piet D, et al. A gene for Stargardt's disease (fundus flavimaculatus) maps to the short arm of chromosome 1. *Nat Genet* 1993;5(3):308-11.
4. Fujinami K, Zernant J, Chana RK, et al. Clinical and molecular characteristics of childhood-onset Stargardt disease. *Ophthalmology* 2015;122(2):326-34.
5. Lambertus S, van Huet RA, Bax NM, et al. Early-onset stargardt disease: phenotypic and genotypic characteristics. *Ophthalmology* 2015;122(2):335-44.
6. Westeneng-van Haften SC, Boon CJ, Cremers FP, et al. Clinical and genetic characteristics of late-onset Stargardt's disease. *Ophthalmology* 2012;119(6):1199-210.
7. Fujinami K, Sergouniotis PI, Davidson AE, et al. Clinical and molecular analysis of Stargardt disease with preserved foveal structure and function. *Am J Ophthalmol* 2013;156(3):487-501.e1.
8. Armstrong JD, Meyer D, Xu S, Elfervig JL. Long-term follow-up of Stargardt's disease and fundus flavimaculatus. *Ophthalmology* 1998;105(3):448-57; discussion 57-8.
9. Binley K, Widdowson P, Loader J, et al. Transduction of photoreceptors with equine infectious anemia virus lentiviral vectors: safety and biodistribution of StarGen for Stargardt disease. *Invest Ophthalmol Vis Sci* 2013;54(6):4061-71.
10. Schwartz SD, Regillo CD, Lam BL, et al. Human embryonic stem cell-derived retinal pigment epithelium in patients with age-related macular degeneration and Stargardt's macular dystrophy: follow-up of two open-label phase 1/2 studies. *Lancet* 2015;385(9967):509-16.
11. Radu RA, Mata NL, Nusinowitz S, et al. Treatment with isotretinoin inhibits lipofuscin accumulation in a mouse model of recessive Stargardt's macular degeneration. *Proc Natl Acad Sci U S A* 2003;100(8):4742-7.
12. Charbel Issa P, Barnard AR, Herrmann P, et al. Rescue of the Stargardt phenotype in *Abca4* knockout mice through inhibition of vitamin A dimerization. *Proc Natl Acad Sci U S A* 2015;112(27):8415-20.
13. Csaky KG, Richman EA, Ferris FL, 3rd. Report from the NEI/FDA Ophthalmic Clinical Trial Design and Endpoints Symposium. *Invest Ophthalmol Vis Sci* 2008;49(2):479-89.
14. Rotenstreich Y, Fishman GA, Anderson RJ. Visual acuity loss and clinical observations in a large series of patients with Stargardt disease. *Ophthalmology* 2003;110(6):1151-8.
15. Cukras CA, Wong WT, Caruso R, et al. Centrifugal expansion of fundus autofluorescence patterns in Stargardt disease over time. *Arch Ophthalmol* 2012;130(2):171-9.
16. Cideciyan AV, Swider M, Schwartz SB, et al. Predicting Progression of ABCA4-Associated Retinal Degenerations Based on Longitudinal Measurements of the Leading Disease Front. *Invest Ophthalmol Vis Sci* 2015;56(10):5946-55.
17. Kellner S, Kellner U, Weber BH, et al. Lipofuscin- and melanin-related fundus autofluorescence in patients with ABCA4-associated retinal dystrophies. *Am J Ophthalmol* 2009;147(5):895-902. .e1.
18. Smith RT, Gomes NL, Barile G, et al. Lipofuscin and autofluorescence metrics in progressive STGD. *Invest Ophthalmol Vis Sci* 2009;50(8):3907-14.
19. Lois N, Halfyard AS, Bird AC, et al. Fundus autofluorescence in Stargardt macular dystrophy-fundus flavimaculatus. *Am J Ophthalmol* 2004;138(1):55-63.
20. Kuehlewein L, Hariri AH, Ho A, et al. COMPARISON OF MANUAL AND SEMIAUTOMATED FUNDUS AUTOFLUORESCENCE ANALYSIS OF MACULAR ATROPHY IN STARGARDT DISEASE PHENOTYPE. *Retina* 2016;36(6):1216-21.
21. McBain VA, Townend J, Lois N. Progression of retinal pigment epithelial atrophy in stargardt disease. *Am J Ophthalmol* 2012;154(1):146-54.

22. Fujinami K, Lois N, Mukherjee R, et al. A longitudinal study of Stargardt disease: quantitative assessment of fundus autofluorescence, progression, and genotype correlations. *Invest Ophthalmol Vis Sci* 2013;54(13):8181-90.
23. Chen B, Tosha C, Gorin MB, Nusinowitz S. Analysis of autofluorescent retinal images and measurement of atrophic lesion growth in Stargardt disease. *Exp Eye Res* 2010;91(2):143-52.
24. Ritter M, Zotter S, Schmidt WM, et al. Characterization of stargardt disease using polarization-sensitive optical coherence tomography and fundus autofluorescence imaging. *Invest Ophthalmol Vis Sci* 2013;54(9):6416-25.
25. Ergun E, Hermann B, Wirtitsch M, et al. Assessment of central visual function in Stargardt's disease/fundus flavimaculatus with ultrahigh-resolution optical coherence tomography. *Invest Ophthalmol Vis Sci* 2005;46(1):310-6.
26. Gomes NL, Greenstein VC, Carlson JN, et al. A comparison of fundus autofluorescence and retinal structure in patients with Stargardt disease. *Invest Ophthalmol Vis Sci* 2009;50(8):3953-9.
27. Anastasakis A, Fishman GA, Lindeman M, et al. Infrared scanning laser ophthalmoscope imaging of the macula and its correlation with functional loss and structural changes in patients with stargardt disease. *Retina* 2011;31(5):949-58.
28. Langbaum JB, Hendrix SB, Ayutyanont N, et al. An empirically derived composite cognitive test score with improved power to track and evaluate treatments for preclinical Alzheimer's disease. *Alzheimers Dement* 2014;10(6):666-74.
29. Cideciyan AV, Swider M, Aleman TS, et al. ABCA4 disease progression and a proposed strategy for gene therapy. *Hum Mol Genet* 2009;18(5):931-41.
30. Anstis SM. Letter: A chart demonstrating variations in acuity with retinal position. *Vision Res* 1974;14(7):589-92.
31. Strauss RW, Ho A, Munoz B, et al. The Natural History of the Progression of Atrophy Secondary to Stargardt Disease (ProgStar) Studies: Design and Baseline Characteristics: ProgStar Report No. 1. *Ophthalmology* 2016;123(4):817-28.
32. Mazzucato M, Visona Dalla Pozza L, Manea S, et al. A population-based registry as a source of health indicators for rare diseases: the ten-year experience of the Veneto Region's rare diseases registry. *Orphanet J Rare Dis* 2014;9:37.
33. Walia S, Fishman GA. Natural history of phenotypic changes in Stargardt macular dystrophy. *Ophthalmic Genet* 2009;30(2):63-8.
34. Lazow MA, Hood DC, Ramachandran R, et al. Transition zones between healthy and diseased retina in choroideremia (CHM) and Stargardt disease (STGD) as compared to retinitis pigmentosa (RP). *Invest Ophthalmol Vis Sci* 2011;52(13):9581-90.
35. Lee W, Noupou K, Oll M, et al. The External Limiting Membrane in Early-Onset Stargardt Disease. *Invest Ophthalmol Vis Sci* 2014.
36. Staurengi G, Satta S, Chakravarthy U, et al. Proposed lexicon for anatomic landmarks in normal posterior segment spectral-domain optical coherence tomography: the IN³OCT consensus. *Ophthalmology* 2014;121(8):1572-8.
37. Kretschmann U, Seeliger MW, Ruether K, et al. Multifocal electroretinography in patients with Stargardt's macular dystrophy. *Br J Ophthalmol* 1998;82(3):267-75.
38. Praidou A, Hagan R, Newman W, Chandna A. Early diagnosis of Stargardt disease with multifocal electroretinogram in children. *Int Ophthalmol* 2014;34(3):613-21.
39. Kuniyoshi K, Terasaki H, Arai M, Hirose T. Multifocal electroretinograms in Stargardt's disease/fundus flavimaculatus. *Ophthalmologica* 2014;232(2):118-25.
40. Teussink MM, Lee MD, Smith RT, et al. The effect of light deprivation in patients with Stargardt disease. *Am J Ophthalmol* 2015;159(5):964-72.e2.
41. Drasdo N, Fowler CW. Non-linear projection of the retinal image in a wide-angle schematic eye. *Br J Ophthalmol* 1974;58(8):709-14.
42. Dreyhaupt J, Mansmann U, Pritsch M, et al. Modelling the natural history of geographic atrophy in patients with age-related macular degeneration. *Ophthalmic Epidemiol* 2005;12(6):353-62.

“This paper addresses concerns that exposure to the 488-nm excitation light used in fundus autofluorescence imaging may be harmful in patients with elevated retinal lipofuscin (i.e., Stargardt disease). With age, fundus autofluorescence imaging causes more oxidative stress than does daylight; moreover, this effect is amplified 3.3-fold in patients with Stargardt disease. This quantitative information contributes to our understanding of potential harm caused during fundus autofluorescence imaging and provides grounds for aforementioned concerns.”

Michel M. Teussink

Stanley Lambertus

Frits F. de Mul

Malgorzata B. Rozanowska

Carel B. Hoyng

B. Jeroen Klevering

Thomas Theelen

PLoS One. 2017 Feb 24;12(2):e0172635

The authors are grateful to Eiko de Jong for insightful discussions about the study concept and methods.

4.3 Lipofuscin-associated photo-oxidative stress during fundus autofluorescence imaging

PURPOSE: Current standards and guidelines aimed at preventing retinal phototoxicity during intentional exposures do not specifically evaluate the contribution of endogenous photosensitizers. However, certain retinal diseases are characterized by abnormal accumulations of potential photosensitizers such as lipofuscin bisretinoids in the retinal pigment epithelium (RPE). We sought to determine these contributions by a numerical assessment of *in-vivo* photo-oxidative stress during irradiation of RPE lipofuscin.

METHODS: Based on the literature, we calculated the retinal exposure levels, optical filtering of incident radiation by the ocular lens, media, photoreceptors, and RPE melanin, light absorption by lipofuscin, and photochemical effects in the RPE in two situations: exposure to short-wavelength ($\lambda = 488$ nm) fundus autofluorescence (SW-AF) excitation light and exposure to indirect (diffuse) sunlight.

RESULTS: In healthy persons at age 20, 40, and 60, respectively, the rate of oxygen photoconsumption by lipofuscin increases by 1.3, 1.7, and 2.4-fold during SW-AF imaging as compared to diffuse sunlight. In patients with STGD1 below the age of 30, this rate was 3.3-fold higher compared to age-matched controls during either sunlight or SW-AF imaging.

CONCLUSIONS: Our results suggest that the RPE of patients with STGD1 is generally at increased risk of photo-oxidative stress, while exposure during SW-AF imaging amplifies this risk. These theoretical results have not yet been verified with *in-vivo* data due to a lack of sufficiently sensitive *in-vivo* measurement techniques.

Introduction

Fundus autofluorescence (AF) imaging visualizes the accumulation of fluorophores that constitute a substantial fraction of lipofuscin in the retinal pigment epithelium (RPE).¹ The pigments of lipofuscin are produced in the membranes of photoreceptor outer segments from non-enzymatic reactions of vitamin A aldehyde.²⁻⁵ This fluorescent material is transferred to RPE cells within phagocytosed outer segment disks,^{6, 7} and becomes deposited in the lysosomal compartment of the cells. As a result, RPE lipofuscin accumulates with age⁸ and fundus AF increases linearly with age although subjects vary in terms of intensities.⁹ Short-wavelength AF (SW-AF, $\lambda_{\text{exc}} = 488 \text{ nm}$, unless stated otherwise) is commonly regarded as a way to monitor the status of RPE cells, with areas of high AF indicating increased lipofuscin levels and areas of absent AF indicating loss of RPE cells.

The retinal radiant exposure of the SW-AF excitation light is far below American National Standards Institute (ANSI) safety thresholds:¹⁰ SW-AF imaging with the widely used Spectralis device is safe for up to 8 hours ($9 \text{ J}\cdot\text{cm}^{-2}$) whereas typical examinations irradiate the retina for less than 5 minutes ($<0.1 \text{ J}\cdot\text{cm}^{-2}$). These thresholds were based on cross-sectional data of the effects of light on a cellular level, designed to protect the eye and skin from accidental light exposure. To reduce ocular exposures, the International Commission of Non-Ionizing Radiation Protection has also provided guidelines for ophthalmic instruments.¹¹ Commercial or experimental ophthalmic instruments adhere to these standards with additional constraints for intentional exposures,¹² and may thus be considered safe with regard to short-term effects.

However, the ANSI thresholds and Commission guidelines do not specifically evaluate the contribution of endogenous photosensitizers in enhancing a patient's susceptibility to retinal phototoxicity. In fact, patients with certain retinal diseases may be highly susceptible to phototoxicity.^{13, 14} This has led to concerns that patients with recessive Stargardt disease (STGD1) may be at risk for light toxicity during SW-AF imaging.¹⁵ In patients with STGD1, photochemical damage may involve changes in molecules within the visual cycle such as all-trans-retinal.^{14, 16} Additionally, removal of all-trans-retinal from the photoreceptor outer segment disks is impaired,¹⁷ which leads to an accelerated accumulation of lipofuscin bisretinoids in the RPE. Some of these bisretinoids have been identified as potent photosensitizers in animal studies. In *Abca4*^{-/-} mice, very high intensities ($50 \text{ mW}/\text{cm}^2$) of blue light ($\lambda = 430 \pm 20 \text{ nm}$) irradiation for 30 minutes caused severe atrophy of photoreceptors and RPE cells with elevated lipofuscin, which was less pronounced in age-matched wild type controls.¹⁸ Conversely, there was no photoreceptor atrophy in *Rpe65*^{rd12} mice without RPE lipofuscin.¹⁸ Whether the mechanism

of photochemical damage involves changes in either lipofuscin or molecules within the visual cycle such as all-trans-retinal, patients with STGD1 will be highly susceptible to photic injury.^{14, 16} Consistent with this notion, even chronic exposure to normal daylight appears to increase the progression of RPE damage in STGD1.¹⁹

We aimed to determine the extent to which the endogenous photosensitizer lipofuscin makes humans more susceptible to photic injury, for which there is lack of empirical evidence. Extrapolation from results from animal studies to humans is difficult because of their considerable differences in light susceptibility. Therefore, we numerically simulated *in-vivo* photo-oxidative stress in the human RPE subsequent to irradiation of endogenous RPE lipofuscin, allowing us to estimate this extent. More precisely, we simulated exposure during either SW-AF imaging in common clinical practice or diffuse sunlight, in healthy individuals of different ages and in patients with STGD1. Daylight exposure is not known to cause retinal injury to healthy people except for unintentional and excessive exposures,²⁰ which thus can provide a reference frame of normally harmless effects. Such an approach may yield considerable insight, because it facilitates the identification of gaps in our knowledge of all aspects involved in retinal photo-oxidative stress.

Methods

Retinal exposures

Exposure to daylight

We used the solar spectrum of the American Society of Testing and Materials (ASTM G173-03) as a reference for terrestrial solar irradiation.²¹ It was measured under atmospheric conditions considered a reasonable average over a period of one year, and pointing to the sun at an inclination of 37°. This inclination corresponds to the approximate average latitude of the 48 contiguous states of the USA. This spectrum includes light scattered by the atmosphere and light reflected off the earth's surface (Figure 1). In such a scenario of free or Newtonian illumination,²² a distant light source—the sun—irradiates an area A larger than the pupil of the eye. The retinal radiant exposure H_r ($\text{J}\cdot\text{cm}^{-2}$) can then be expressed as a function of corneal radiant exposure H_c ($\text{J}\cdot\text{cm}^{-2}$).¹²

$$H_r = H_c \frac{A_{pupil}}{A_{retina}} \approx H_c \tau \frac{d_p^2}{f_e^2 \alpha^2} = L_s \tau \frac{\pi}{4} \left(\frac{d_p}{f_e} \right)^2 \quad (1)$$

with the pupil diameter (d_p), the eye's focal length (f_e), the visual angle of the source (α), and the ocular media transmission (τ). For free illumination, the retinal radiant exposure H_r can also be expressed as a function of the irradiance of the source (L_s , unit $\text{J}\cdot\text{sr}^{-1}$), independent of α (Eq. [1], third term).¹² Using normative data of the pupil diameter at different ages measured under various lighting conditions,²³ we calculated an average

pupil diameter d_p at age 20, 40, and 60 of 3.8, 3.5, and 3.2 mm, respectively (Section A in Supplemental Text S₁). We assumed that the pupil is adapted to daylight luminance without pharmacological dilation and we used an average focal length f_e of the eye of 17 mm.

Because a person will usually not stare directly into the sun, the referenced solar spectrum is an overestimation of the actual solar irradiation entering the eye. We therefore subtracted the ‘direct and circumsolar’ spectrum that measures a 2.5° circle around the solar disk from the aforementioned (‘global tilt’) solar spectrum as an indication of indirect solar irradiation, i.e., diffuse insolation (Figure 1). To determine the irradiance

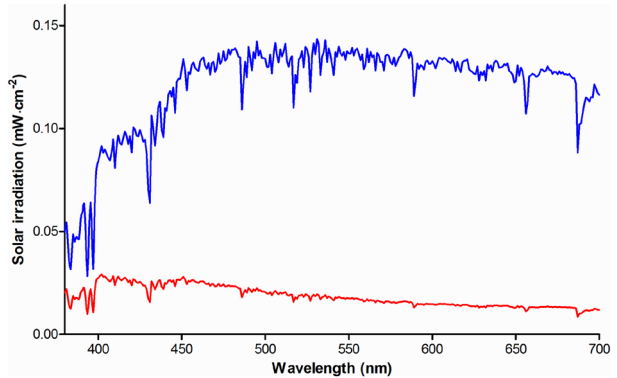


Figure 1. Solar irradiance spectra. Visible range of the American Society of Testing and Materials G173-03 solar irradiance spectrum, measured at a global tilt of 37° pointing to the sun (blue). The solar irradiance spectrum when not staring directly at the sun, including light scattered by the atmosphere and light reflected off the earth's surface, is also shown (red).

L_s ($\text{W}\cdot\text{cm}^{-2}\cdot\text{sr}^{-1}$) of this diffuse scattered light, we used the solid angle Ω of radiation specified for the ASTM reference spectrum, which equals that of diffuse light scattered in a full hemisphere ($\Omega = 2\pi$ steradian).²¹ Consequently, $L_s \approx H_c/2\pi$. To account for absorption in the ocular media, we employed an algorithm that predicts the average media optical density at a given age and wavelength.^{24, 25} The algorithm of Van de Kraats and Van Norren is based on six optical density components with the optical density D_λ depending only on wavelength and age.²⁵ We obtain:

$$H_r = \frac{H_c}{2\pi} \exp(-D_\lambda) \frac{\pi}{4} \left(\frac{d_p}{f_e} \right)^2 \quad (2)$$

We used Eq. (2) to predict retinal exposures to diffuse insolation at age 20, 40, and 60.

Autofluorescence imaging

In SW-AF by confocal scanning laser ophthalmoscopy, the imaging beam enters the eye with a known angle α through an entrance pupil smaller than the pharmacologically dilated pupil. In this scenario of Maxwellian illumination, the retinal radiant exposure is the power entering the pupil Φ , divided by the retinal exposed area¹²:

$$H_r = \Phi\tau \frac{4}{\pi(f_e\alpha)^2} \quad (3)$$

The blue autofluorescence imaging mode of the widely used Spectralis HRA+OCT employs an optically pumped solid-state continuous wave laser with a wavelength of 488 ± 2 nm and a recommended maximum optical power of 260 μW to excite lipofuscin fluorophores in the fundus. Emitted fluorescence in the wavelength range of 500–680 nm is detected after passing through a barrier filter. We assumed that during AF imaging in a clinical setting, the retina is scanned at the high-speed mode (768×768 pixels; 8.9 frames·s⁻¹) in square 30° fields. Imaging of 55° fields is performed frequently, although the resulting average retinal exposure will be lower, and it therefore should be safer. Although the Spectralis also offers the possibility of imaging at the ‘high-resolution’-mode with a doubled sampling rate (i.e., each imaged area is probed twice by the imaging beam), the average retinal exposure will remain the same since the beam power, imaging speed, and size of the imaged area remain equal. Under our assumptions, the average retinal radiant exposure in perfectly transparent media is 328 $\mu\text{W}\cdot\text{cm}^{-2}$.²⁶ Taking media absorption in a healthy 20-year old person²⁵ into account, it is 190.4 $\mu\text{W}\cdot\text{cm}^{-2}$.

Optical screening in the fundus

Photoreceptors

The absorption of light in the neural retina is orders of magnitude lower than that in the RPE.²⁷ Since our study is focused on the paramacula (about 10° retinal eccentricity), we neglect the influence of macular pigments. Visual pigments in the photoreceptors, however, may contribute to the absorption of light. Therefore, we estimated the visual pigment optical density versus wavelength during daylight exposure.

A luminance of 2.9 photopic cd·m⁻² is already sufficient to saturate rod electroretinographic responses,²⁸ and therefore the unbleached fraction of rod visual pigment at an illuminance of 4400 cd·m⁻² (Section A in Supplemental Text S₁) will be very low—we consequently neglect absorption by rods during either daylight or SW-AF imaging. We used data on the normalized wavelength-dependent optical density of visual pigments in photoreceptor outer segments, measured by microspectrophotometry on ex-vivo human samples.²⁹ We fitted these data with polynomial functions to obtain the optical density of the entire 380–700 nm wavelength range. These normalized data, expressed in normalized optical density per micron outer segment length, were multiplied by the mean dark-adapted double-pass optical density of each of the photoreceptor types, divided by two to obtain single-pass optical density. These numbers were multiplied by the mean length of photoreceptors at 10° retinal eccentricity.³⁰ Next, we multiplied the result by the retinal area fraction occupied by cone photoreceptors at

9.2° retinal eccentricity, as derived from electron microscopy data obtained by Curcio et al.,³¹ and by the relative numbers of the different cone types as published by Dartnall et al.²⁹ Finally, we used data on the steady-state bleach fraction of visual pigments at an illuminance of 4400 cd·m⁻² to derive the fraction of unbleached visual pigments. We multiplied the wavelength-dependent optical density of cones with this fraction, which was determined to be 0.080374.

Melanin in the retinal pigment epithelium

The flux of photons impinging on lipofuscin is reduced due to optical screening by melanin granules situated apically in RPE cells. RPE melanin consists largely of eumelanin,³² which is able to dissipate approximately 90% of incident UV energy as heat.³³ We performed a Monte-Carlo (MC) simulation of light scattering and absorption by melanin in the RPE to investigate optical screening by melanin in healthy people of different ages and in patients with STGD1. Monte-Carlo methods are a standard approach in numerical simulation and the basic methodology in simulating scattering of light in human tissues is, by now, strongly established. Monte-Carlo methods have been employed with great success in order to predict the properties of light scattering in human tissues.³⁴⁻³⁷ Our calculation of light scattering by melanosomes was similar to an earlier study by Cracknell et al., who used MC methods to investigate iris melanosomes.³⁸ Our calculation of light absorption by melanin was different from the calculation by Cracknell et al.; we based it on empirical data of the absorption spectrum of melanin. Details of this MC simulation of *in-vivo* optical attenuation by RPE melanin in the paramacular RPE cells are depicted in [Section B in Supplemental Text S₁](#). We modeled the paramacular RPE as a single 9 μm thick sheet,³⁹ and RPE melanin could occupy the apical ≤33% of the RPE cell (inward positive, i.e., the optical path length l_{melanin} ranged from 0 to +3 μm). An infinitely thin and non-divergent beam of light ('pencil beam') injected 5·10⁵ photons into the system. We varied the thickness of the layer in which the scatterers (melanosomes) are present with age and/or the presence of STGD1, as specified in [Section B in Supplemental Text S₁](#).

Monte-Carlo simulations of optical screening by RPE melanin were performed for specified wavelengths ($\lambda = 380, 405, \dots, 705$) for each of four different scenarios: healthy 20-, 40-, and 60- year old paramacular RPE, and 20-year old non-atrophic RPE of a patient with STGD1. MontCarl© counted the number of photons that were either absorbed, backscattered (upon refractive passage at the interface between two layers and directed towards negative depth values), or transmitted (the inverse of backscattering; this could therefore include non-scattered and forward scattered photons). From these fractions and the total number of incident photons, we calculated attenuation coefficients ($\mu_{\text{a, melanin}}$ and $\mu'_{\text{s, melanin}}$) and the optical density ($\text{OD}_{\text{melanin}}$) as:

$$\mu_{a, \text{melanin}} = \frac{-\log\left(1 - \frac{[\text{Absorbed photons}]}{[\text{Total injected photons}]}\right)}{l_{\text{melanin}}} \quad (4)$$

$$\mu'_{s, \text{melanin}} = \frac{-\log\left(1 - \frac{[\text{Backscattered photons}]}{[\text{Total injected photons}]}\right)}{l_{\text{melanin}}} \quad (5)$$

$$OD_{\text{melanin}} = (\mu_{a, \text{melanin}} + \mu'_{s, \text{melanin}}) \cdot l_{\text{melanin}} \quad (6)$$

Optical absorption by lipofuscin

The high optical density of each lipofuscin granule may give rise to significant internal optical screening.⁴⁰ Granules in the basal part of the cell may therefore receive little or no light; resulting in a poor correlation between the RPE lipofuscin concentration and total light absorbed. This may explain why—at present—we have no evidence that lipofuscin bisretinoid photo-oxidation varies with the lipofuscin bisretinoid concentration.

Calibrated SW-AF measurements have shown that patients with STGD1 exhibit substantially increased fluorescence from RPE lipofuscin.⁴¹⁻⁴³ This may be ascribed to either increased fluorescence efficiency of lipofuscin bisretinoids, increased absorption of excitation energy, or both. The ‘dark’ or ‘silent’ choroid sign on fluorescein angiography, present in 37–50% of patients,^{44, 45} indicates a considerable reduction in light transmission ($\lambda = 488 \text{ nm}$) through the RPE.^{44, 46, 47} Increased backscatter and/or absorption from lipofuscin may underlie this phenomenon; however, increased backscatter is highly unlikely to be the sole cause. Finally, mouse studies have shown that the amount of the lipofuscin bisretinoid *N*-retinylidene-*N*-retinylethanolamine (A2E) decreases *in vivo* when retinal light exposure increases, due to lipofuscin oxidation and subsequent degradation.⁴⁸

We incorporated light absorption by lipofuscin into our simulation because of these indications. Although an accurate approximation of the fraction of light absorbed could be obtained with an MC simulation, as far as we know there are no empirical data on certain optical parameters of lipofuscin granules. These parameters include the granule size distribution, wavelength-dependent absorption- and scattering cross-sections, and empirical data on the angular scattering function. We therefore took a different approach, based on the principle that light absorption tends to correlate with the granule concentration (n_g) and the optical path length (l) through these granules. Hence, we considered their product ($n_g \cdot l$) indicative of light absorption.

Although electron microscopy of the RPE of patients with STGD1 shows massive accumulations of lipofuscin in the posterior pole,⁴⁹ it is difficult to obtain an exact value of ($n_g \cdot l$) based on these images. In mice, however, the concentration of a major fluorophore of

lipofuscin (A2E)⁵⁰ was found to correlate with the calibrated fluorescence intensity from RPE cells.⁵¹ Since similar data²⁶ are available both in healthy people⁴² and patients with STGD1,⁴³ estimations of $(n_g \cdot I)$ in STGD1 based on fundus AF would be an alternative. We tested the feasibility of such estimations by determining the correlation between $(n_g \cdot I)$ and SW-AF intensity (detailed in [Section C \[a\] in Supplemental Text S₁](#)). The individual of whom a SW-AF image is depicted in [Figure 6](#) has given written informed consent (as outlined in the PLOS consent form) to publish this image.

Oxygen photoconsumption by lipofuscin granules

The goal of our simulation was to compute oxygen uptake by lipofuscin granules *in vivo* under the considered exposure regimes, because oxygen photoconsumption by lipofuscin can serve as an indicator of lipofuscin oxidation.⁵² We considered *in-vitro* oxygen uptake measurements on isolated human RPE lipofuscin granules by Rozanowska et al.⁵² to be—at present—the most appropriate basis for this calculation. Firstly, their measurement setup and results were described in sufficient detail to allow for meaningful and quantitative comparisons with *in-vivo* exposure conditions. Second, isolated—but intact—human RPE lipofuscin granules of different ages were used, and the pH of the medium is comparable to that *in vivo*. As such, these two factors are representative of physiological conditions. The results obtained in [Sections 3.1 and 3.2](#) allow us to estimate the flux of photons impinging on RPE lipofuscin granules *in vivo*, and studies on photosensitizers have shown a strong relationship between total light absorbed and oxygen uptake.^{53, 54} Therefore, the results obtained in [Sections 3.1 to 3.3](#) can be regarded as variables influencing oxygen uptake by lipofuscin, and are applicable to an *in-vivo* milieu. We determined the corresponding values of these variables applicable to the *in-vitro* measurements by Rozanowska et al.⁵² By normalizing for differences in these variables *in vivo*, we predicted the rates of oxygen uptake, were they measured *in vivo* in the RPE. Details on this normalization are described in [Section D in Supplemental Text S₁](#).

Results

Retinal exposures

The retinal exposure ($\text{mW} \cdot \text{cm}^{-2}$) during daylight or typical SW-AF imaging sessions was corrected for absorption and scattering in the lens and media (plotted in [Figure 2](#)).

Optical screening in the fundus

Photoreceptors

The calculated visual pigment optical densities during daylight exposure, at a luminance of $4400 \text{ photopic } \text{cd} \cdot \text{m}^{-2}$, are shown in [Figure 3](#). Under this condition, the optical

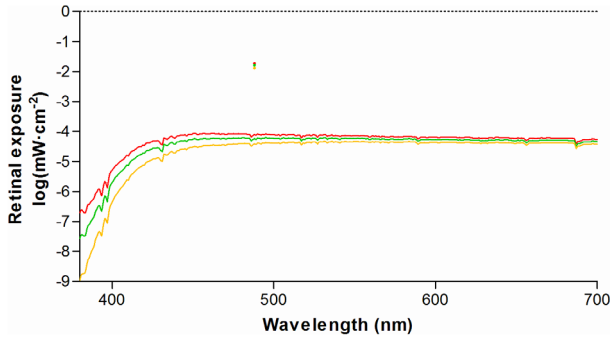


Fig 2. Retinal exposure from diffuse solar irradiation compared to excitation light of short-wavelength retinal autofluorescence. At $\lambda = 488$ nm, the peak height is indicated by single colored dots. Exposures were calculated by Eqs. (2) and (3), respectively. Exposures in ocular media of different ages are plotted: 20 year-old (red), 40 year-old (green), and 60 year-old (orange).

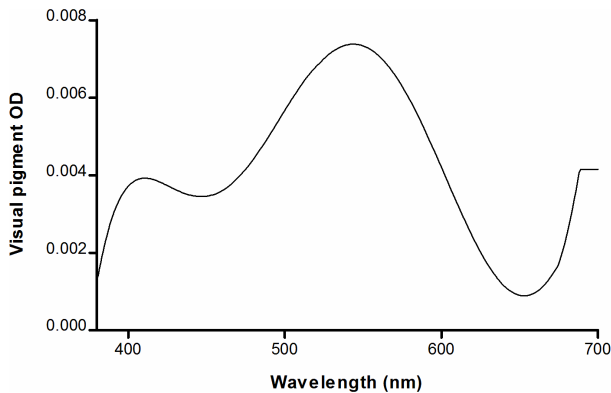


Figure 3. Optical screening by visual pigments in the outer segments of paramacular photoreceptors. The wavelength-dependent single-pass optical density (OD) of light passing through the outer segments was calculated under conditions of daylight illuminance, amounting to 4400 photopic $\text{cd}\cdot\text{m}^{-2}$. See text for details.

scattering (backscattering) coefficient can be calculated by including the scattering anisotropy factor (g). It varies from -1 for complete backscattering, through 0 for isotropic scattering, to +1 for complete forward scattering. We calculated the backscattering coefficient by $\mu'_{s, \text{melanin}} = \mu_{s, \text{melanin}} \cdot (1 - g)$. An estimate of light attenuation due to absorption ($OD_{a, \text{melanin}} = \mu_{a, \text{melanin}} \cdot l_{\text{melanin}}$), backscattering ($OD_{s, \text{melanin}} = \mu'_{s, \text{melanin}} \cdot l_{\text{melanin}}$), and the total optical density (Eq. 6) can then be made. As can be seen in Figure 4A, scattering is expected to dominate over absorption for all wavelengths under investigation, which is in contrast to the MC simulation results. In addition, the MC results show several fold lower attenuation for both scattering and absorption.

screening by photoreceptors in the paramacula ranges between 0.002 to 0.008 optical density units (0.46–1.83%), and is therefore negligible.

Melanin in the retinal pigment epithelium

The MC results are plotted in Figure 4. It can be seen that absorption dominates over scattering at $\lambda < 505$ nm. We evaluated whether this phenomenon is caused by wavelength-dependent differences in the absorption and scattering properties of the melanosomes. By taking the product of each granule class' concentration and absorption/scattering cross-section, and taking the arrhythmic sum of all granule classes in the medium, the theoretical absorption coefficient ($\mu_{a, \text{melanin}}$) and scattering coefficient ($\mu_{s, \text{melanin}}$) can be determined. The reduced

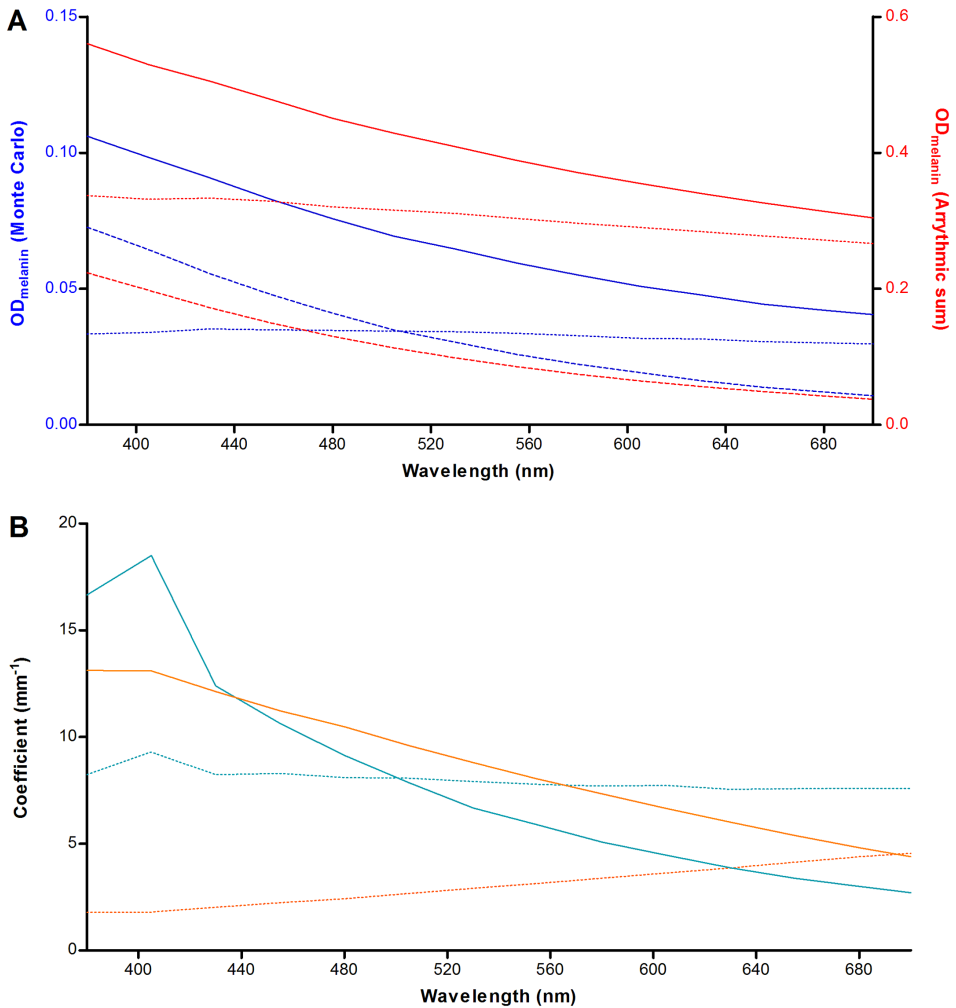


Figure 4. Relative contributions of light scattering and absorption by retinal pigment epithelium (RPE) melanin. (A) Agreement between Monte-Carlo simulation and theory, plotted based on conditions in the paramacular RPE of a healthy 20-year old person. The optical density (OD) was calculated based on the product of the attenuation coefficient and the melanosome layer thickness (l_{melanin}). Attenuation by absorption (*striped line*), scattering (*dotted line*), and total attenuation (*straight line*) are plotted separately. The MC results are shown in blue (*left Y-axis*) and the theoretical result is shown in red (*right Y-axis*). See text for details. (B) Simulations of a thin ($3 \mu\text{m}$; *blue*) and thick ($52.5 \mu\text{m}$; *orange*) layer of melanosomes. In case of thicker layers, there is a dominance of the absorption coefficient ($\mu'_{\text{a, melanin}}$; *straight lines*) over the backscattering coefficient ($\mu'_{\text{s, melanin}}$; *striped lines*) for all tested wavelengths.

We found that both of these phenomena can be explained by two aspects: our simulation was performed for a thin layer ($3 \mu\text{m}$) in combination with a strong tendency for forward scattering in this layer of melanosomes. In this system, photons will deviate from their path by about 30° on average ($\cos^{-1} \langle g \rangle = \cos^{-1}(0.865) = 30.3^\circ$) at each

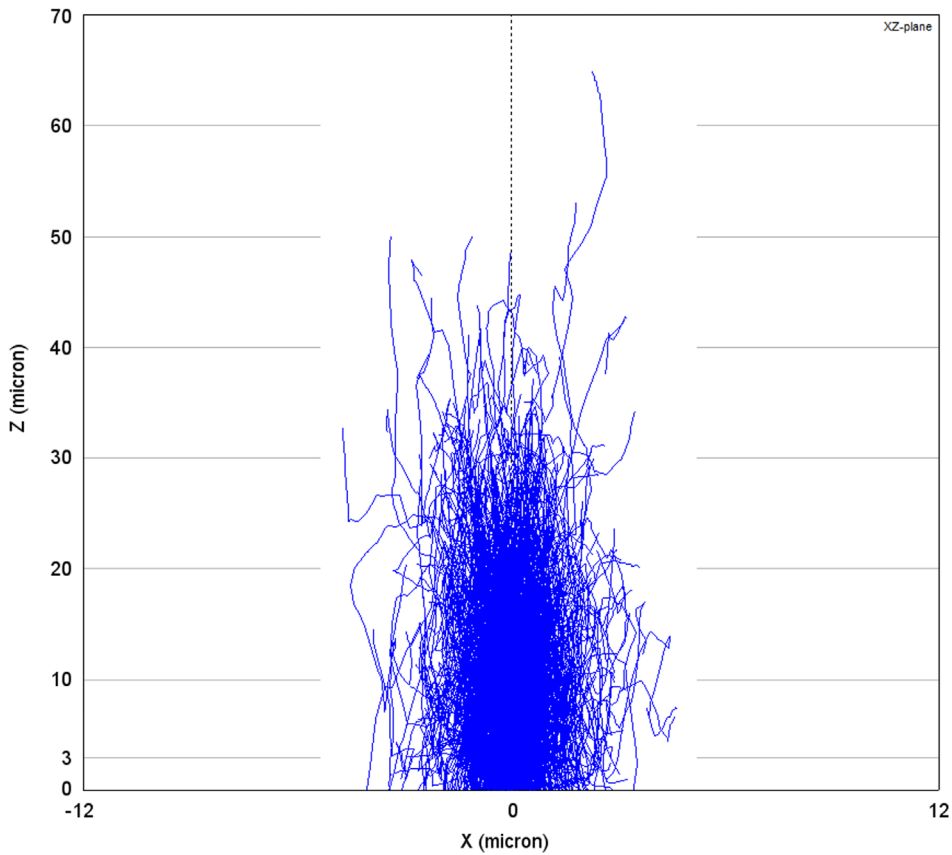


Figure 5. Monte-Carlo simulation of light scattering and absorption in a thick layer of melanosomes. In this plot generated by MontCarl, the optical paths (blue lines) of 3000 photons are ray-traced through a relatively thick layer of retinal pigment epithelium (RPE) melanosomes at the concentration *in vivo*. Photons are injected by an infinitely thin light beam at $X/Y = 0/0$. The X- and Z-axes, respectively, indicate the lateral and vertical (depth) location in the sample. Most photons are either absorbed or scattered back at $Z = 30 \mu\text{m}$. At the assumed maximum *in-vivo* layer ‘thickness’ of RPE melanosomes ($3 \mu\text{m}$), a small proportion of photons are backscattered or absorbed.

scattering event, which indicates that randomization of the direction of scattering occurs only after several scattering events. This would suggest that more backscattering occurs when the melanosome layer is thicker. We tested this suggestion by simulating a melanosome layer of either $3 \mu\text{m}$ or $52.5 \mu\text{m}$ with an average transmission of photons of 89.4% and 6.6%, respectively (Figure 4B). We found that, in the case of the thicker sample, absorption actually dominates over scattering for all tested wavelength and an overall reduction in the backscattering coefficient $\mu'_{s, \text{melanin}}$. This suggests that, although a photon may only backscatter after a given number of scattering events, it becomes increasingly more likely that the photon will be absorbed before it reaches that point. The effect of simulating a thin sample is also illustrated in Figure 5. Thus, in our MC

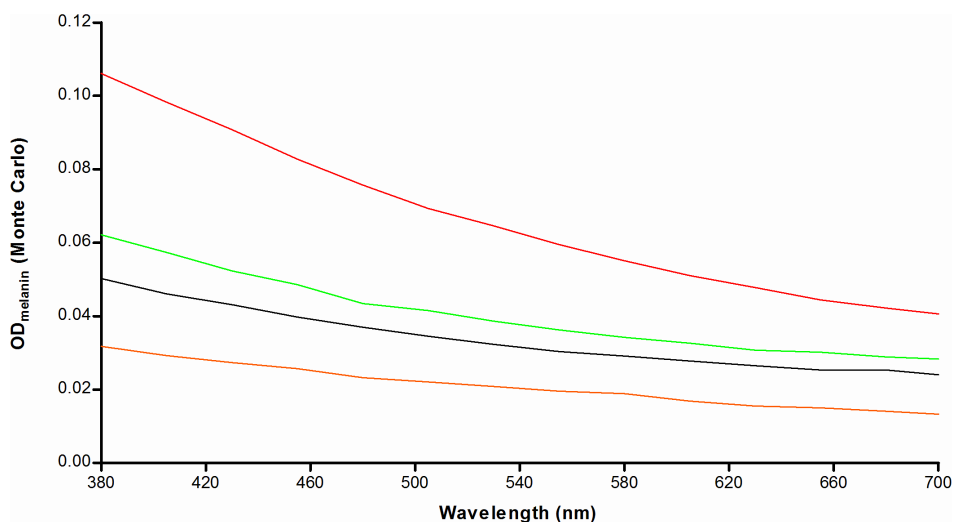


Figure 6. Light attenuation by retinal pigment epithelium (RPE) melanin *in vivo* varies with age and the presence of Stargardt disease. We calculated the total optical density (OD) of paramacular RPE melanin versus wavelength of incident radiation with Eqs. 4–6 based on results of Monte Carlo simulations. Colored lines indicate attenuation in healthy people of different ages: 20 (red), 40 (green), and 60 (orange). The same is shown for a 20-year old patient with Stargardt disease (black).

simulation (3 μm), photons have a greater tendency for absorption as compared to backscattering at shorter wavelengths. The MC results for the various scenarios tested are shown in Figure 6. We found optical screening by melanin in 20-year old patients with STGD1 to be less than half of that in age-matched controls, with the difference diminishing at longer wavelengths.

Light absorption by lipofuscin

As shown in Figure 7, we found a strong correlation between calibrated SW-AF measurements (qAF_g) and values we consider indicative of light absorption by lipofuscin ($ng \cdot l$). Based on a linear regression model and our calculated average qAF_g value of patients with STGD1, we interpolated the value of ($ng \cdot l$) in these patients.

Oxygen photoconsumption by lipofuscin

We used the results obtained in Sections 3.1 - 3.3 together with data on the oxygen concentration in the RPE *in vivo* to normalize for differences with *in-vitro* studies on isolated lipofuscin granules (Eq. S7 in Supplemental Text S₁).⁵² Figure 8 shows age-related differences in the rate of oxygen uptake ($\text{pM} \cdot \text{cm}^{-2} \cdot \text{s}^{-1}$) during sunlight exposure. This is particularly evident for short-wavelength visible light. However, in patients with STGD1, we found an amplification of the rate of oxygen photoconsumption regardless of wavelength. We integrated the results along λ to better compare results for different

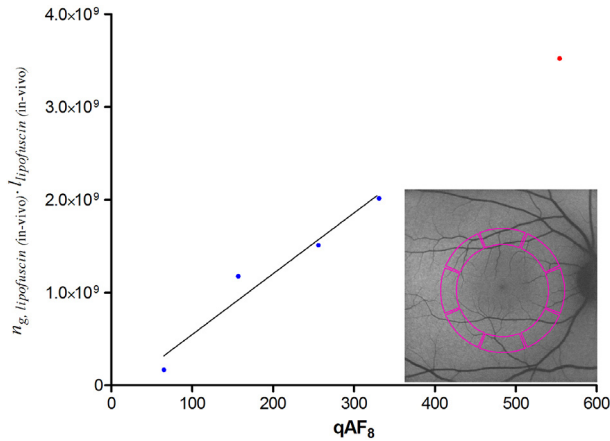


Figure 7. Correlation between calibrated short-wave autofluorescence (SW-AF) measurements and histologic data on lipofuscin granules. We considered the product of optical path length (l) and granule concentration (n_g) to be indicative of light absorption by lipofuscin granules. Here, we tested whether this product correlates with calibrated SW-AF measurements published earlier (qAF_8).^{28,44,45} possibly allowing an estimation of this product ($n_g \cdot l$) in patients with Stargardt disease (STGD1) based on their qAF_8 values. qAF_8 values were measured in the posterior pole of the fundus (colored area in the inset). Blue dots represent average values of healthy people of different age-ranges; the red dot represents average values of patients with STGD1 (age <30 years). Pearson's correlation ($r = 0.97$) was significant ($P = 0.0259$); therefore, a linear regression analysis was performed with data from healthy people (solid line). With the average value of patients with STGD1, we extrapolated the value of ($n_g \cdot l$) in STGD1 prior to atrophy of the retinal pigment epithelium. (red dot).

this fold-increase is 3.292 and 3.264, respectively. When comparing oxygen uptake during either exposure to diffuse sunlight or to the SW-AF excitation light, we found a 1.33-, 1.70-, and 2.39-fold increase for healthy individuals aged 20, 40, and 60, respectively. For patients with STGD1, we found a 1.32-fold increase, i.e., close to that in age-matched controls.

Discussion

Herein, we performed a comprehensive simulation of photo-oxidative stress in the RPE *in vivo*, which suggests that lipofuscin granules had a 3-fold higher oxygen uptake and light absorption in patients with STGD1 compared to age-matched controls. To our knowledge, this is the first study to report STGD1 patients' relative sensitivity to light. We incorporated all known factors influencing light-induced oxygen consumption by RPE lipofuscin, insofar sufficient empirical data was available.

ages, and healthy versus STGD1 (Figure 9). This also facilitates a comparison of low-intensity, broadband radiation (diffuse sunlight) and high-intensity narrowband laser light (SW-AF excitation light). Interestingly, the total rate of oxygen uptake during diffuse sunlight exposure *in vivo* varies little with age according to our simulation. During SW-AF, however, oxygen uptake increases considerably with advancing age. The results suggest that oxygen uptake by lipofuscin is increased by about 3.3-fold in 20-year old patients with STGD1 as compared to age-matched controls. To be more specific, during diffuse sunlight and SW-AF imaging,

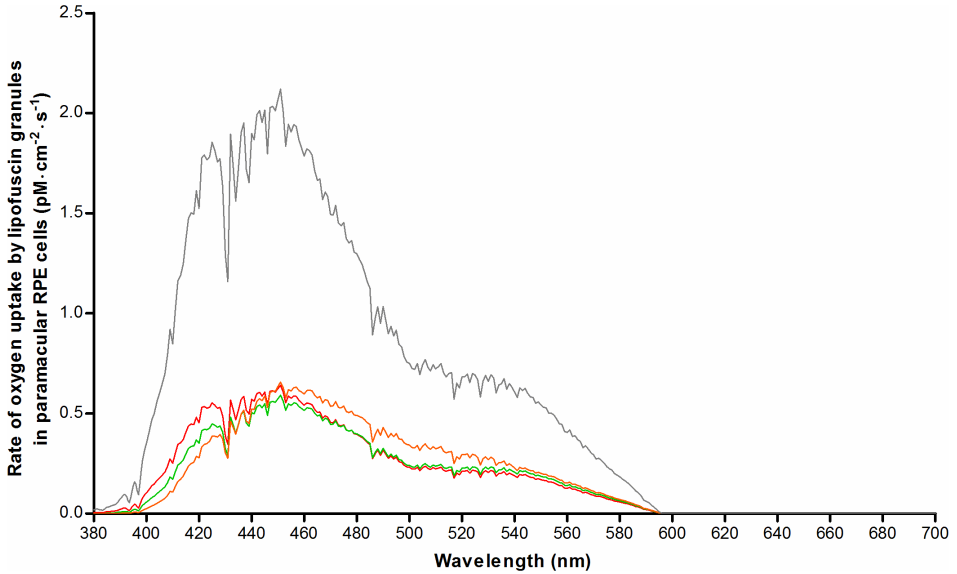


Figure 8. Numerical simulation of oxygen uptake by lipofuscin in paramacular retinal pigment epithelium *in vivo* during exposure to diffuse sunlight. Oxygen uptake was calculated based on results from a previous investigation of oxygen uptake by isolated human lipofuscin granules,²⁰ after correction for factors affecting retinal exposure levels *in vivo* (see text). Results were plotted for healthy people of different ages: 20-year old (red), 40-year old (green), and 60-year old (orange). Results for 20-year old patients with Stargardt disease are also shown (grey).

Optical screening in the fundus

We identified differences in optical attenuation ($\mu_{a, \text{melanin}}$) by RPE melanosomes between our simulated *in-vivo* data and earlier *ex-vivo* studies. Weiter et al.³⁹ found a total attenuation of $0.022 \pm 0.008 \text{ OD}\cdot\mu\text{m}^{-1}$ in the apical part of RPE cells ($\lambda = 500\text{-}600 \text{ nm}$). This agrees well with the pooled average result of our MC simulation for healthy people aged 20-60 ($0.020 \pm 0.002 \text{ OD}\cdot\mu\text{m}^{-1}$). The difference in μ_{melanin} may lie in two facts. First, Weiter et al. could not distinguish between melanin and melanolipofuscin in their

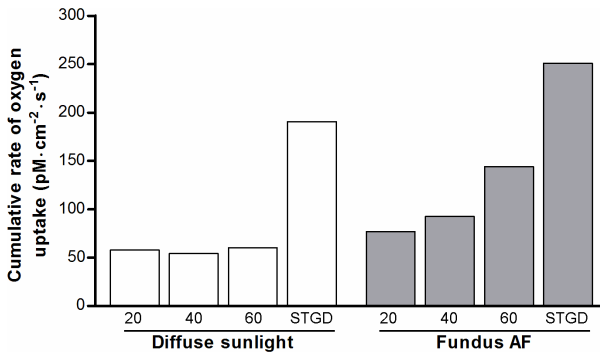


Figure 9. Total rates of oxygen uptake by lipofuscin during light exposure. Rates of oxygen uptake (Figure 8) were integrated along the wavelength of incident radiation to obtain the total rate of O_2 -uptake, as an indication of cellular oxidative stress *in vivo* during exposure to diffuse sunlight (white bars) or during SW-AF imaging (grey bars). X-axes: age of healthy individuals, or patients with Stargardt disease (age, 20).

measurements.³⁹ Our MC simulation would probably have shown a higher μ_{melanin} if we had included melanolipofuscin granules, since the latter granules are known to accumulate with advancing age concomitant with reductions in melanosomes.⁵⁵ Second, our simulated ‘layer’ of melanosomes (1–3 micron) was thinner than the histologic sections used by Weiter et al. (8 micron).³⁹ As we showed in [Figure 5](#), there is a higher proportion of backscattered photons in our simulation as compared to their study, causing an overall higher μ_{melanin} . Therefore, these two facts taken together might explain the aforementioned slight difference with histologic data, in terms of optical attenuation by melanin in the RPE.

However, optical screening by melanin only marginally protects lipofuscin against irradiation. At an $\text{OD}_{\text{melanin}}$ of 0.05, only about 11% of incident light is filtered. Assuming that optical parameters of melanosomes are unchanged in STGD1—as indicated by their normal morphological appearance⁴⁹—the MC simulation showed a 50% lesser screening effect as compared to age-matched controls ([Figure 6](#)). Therefore, our data indicates that the apical displacement of melanin in RPE cells of patients with STGD1⁴⁹ is of little consequence with regard to intracellular optical screening.

Light absorption by lipofuscin

Comparison of light-induced oxidative stress in patients with STGD1 versus healthy controls requires correction for differences in light absorption. Earlier studies used lipofuscin AF as an indication of the concentration of fluorophores.^{8,39} Because calibrated SW-AF measurements²⁶ are the only quantitative *in-vivo* indication of the fluorophore concentration, we investigated its correlation with histologic data of the concentration of lipofuscin granules. The fraction of light absorbed (A) can be calculated by the formula $A = n_g \cdot l \cdot \sigma_a$,⁵⁶ and as shown in [Figure 7](#), we found calibrated SW-AF and ($n_g \cdot l$) to be linearly proportional. We considered the latter directly related to the amount of light absorption, because of two indications of an age-invariant absorption cross-section (σ_a). First, our image analysis of previously published⁴⁰ electron microscopy images shows no age-related difference in granule size ([Section C \[b\] in S1 text](#)), ruling out a change in the amount of light scattering. Second, the optical density of lipofuscin granules decreases only slightly (0 - 14%) with age.⁴⁰ In the context of unchanged scattering by these granules, absorption will only marginally change with age. One aspect of note is the increased fluorescence efficiency of oxidized bisretinoids,⁵⁷ with the oxidized form of A2E being the strongest fluorophore among them.⁵⁸ Also, in lipofuscin granules, the ratio of oxidized A2E versus unoxidized A2E increases considerably with age.⁵⁸ These results indicate that increased qAF may not correspond with equally increased light absorption. Another aspect to consider is the effect of internal optical screening among lipofuscin granules at high concentrations, due to the high optical density of

each granule.⁴⁰ This would also cause a lack of linear proportionality between total light absorbed and the granule concentration, especially at high concentrations. Since these two aspects would lead to an overestimation of the amount of light absorbed at high qAF_g or high granule concentrations, a linear relationship between qAF_g and $(n_g \cdot l)$ may be expected. On the other hand, this means that light absorption in patients with STGD1 is probably increased by less than 3-fold.

Oxygen uptake

Our results suggest that RPE cells of patients with STGD1 are at increased risk of oxidative stress. During SW-AF imaging, the potential for oxidation almost doubles from age 20 to age 60 (Figure 9). We found a 3.3-fold increase in the rate of oxygen uptake in 20-year old patients with STGD1 relative to that in age-matched controls, regardless of the exposure regime. However, we cannot conclude whether the oxidant/anti-oxidant balance is affected, and if permanent impairment will occur to the RPE or photoreceptor cells. RPE cells are highly resistant to oxidative stress,⁵⁹ but survival of RPE cells under light stress is largely determined by the relative concentrations of lipofuscin and melanosomes.⁶⁰ This balance is clearly less favorable in patients with STGD1; the limited anti-oxidative capacity afforded by melanosomes may prove insufficient to cope with situations of increased oxidative stress when it would normally suffice. In any case, indirect effects of oxidative stress that likely cause damage to photoreceptors have been proven, in terms of a decrease of outer segment phagocytosis by RPE cells.^{61, 62} Impairments in this key function of RPE cells can result in retinal degenerations.⁶³

Limitations and perspectives

This study had several limitations. First, melanosomes can reduce iron-mediated oxidation in RPE *in vitro* by protecting against redox-active metal ion-mediated oxidation.^{64, 65} However, whether the net result of this process is anti- or even pro-oxidant depends on many factors, such as relative concentrations of metal ions, small molecular weight ion chelators and melanin-binding sites, presence of oxygen, and irradiation conditions.⁶⁵ Due to lack of related *in-vivo* data on these parameters and their interactions, we omitted this part from our simulation of oxidative stress. Second, the aerobic photoreactivity of melanosomes and melanolipofuscin was not taken into account. These granules display about 6- and 3-fold less oxygen uptake upon irradiation,⁶⁶ respectively. In addition, in comparison to lipofuscin, they have a relatively high yield of hydrogen peroxide,⁶⁶ which has a long half-life,⁶⁷ and thus is less prone to cause unwanted oxidative damage. Also, melanolipofuscinogenesis involves a gradual fusion of two granule types,⁶⁸ and optical characteristics and oxygen uptake may differ with advanced progression which may be difficult to model accurately in an MC simulation.

Although we calculated oxygen uptake in STGD1 under the assumption that the photophysical characteristics of RPE lipofuscin remain unchanged, this may prove incorrect considering the ‘abnormal form of lipofuscin’ noted in a histological study of STGD1.⁴⁹ Furthermore, we have not evaluated the consequences of the consumed oxygen; that requires future work that is able to culture RPE cells under replicated *in-vivo* conditions. We anticipate that this will yield insights into the tolerance of RPE cells to oxidative stress under physiological cell culturing—and light exposure—conditions. It is of interest to note that AF imaging in patients with STGD1 at $\lambda = 532$ nm, instead of 488 nm, leads to less oxygen uptake at equal optical power: a 0.98-fold versus a 1.32-fold increased uptake relative to daylight, respectively.

Conclusions

Our numerical simulation of susceptibility to phototoxicity in health and disease indicated a substantial increase in the rate of oxygen uptake by lipofuscin in patients with STGD1. However, sufficient empirical data is lacking on the molecular dynamics of the interplay between increased oxygen uptake, synthesis of oxygen radicals, anti-oxidants, and mechanisms leading to permanent retinal damage. Unfortunately, current *in-vivo* measurement techniques are insufficiently sensitive to show any effect of subthreshold light damage in patients. Considerable insight into these dynamics can be gained by numerical simulation and comparisons with empirical data obtained in cells cultured in replicated (patho)physiological conditions. Simulations can also elucidate the relative vulnerability of various retinal areas with different characteristics. We anticipate that this can eventually lead to personalized risk assessments of patients undergoing retinal light exposure in various settings. In high risk patients it may be advisable to largely avoid chronic exposure to light with wavelengths less than 500 nm and to choose auto-fluorescence excitation above this wavelength.

References

1. Delori FC, Dorey CK, Staurenghi G, et al. In vivo fluorescence of the ocular fundus exhibits retinal pigment epithelium lipofuscin characteristics. *Invest Ophthalmol Vis Sci* 1995;36(3):718-29.
2. Eldred GE, Katz ML. Fluorophores of the human retinal pigment epithelium: separation and spectral characterization. *Exp Eye Res* 1988;47(1):71-86.
3. Katz ML, Eldred GE, Robison WG, Jr. Lipofuscin autofluorescence: evidence for vitamin A involvement in the retina. *Mech Ageing Dev* 1987;39(1):81-90.
4. Ben-Shabat S, Parish CA, Vollmer HR, et al. Biosynthetic studies of A2E, a major fluorophore of retinal pigment epithelial lipofuscin. *J Biol Chem* 2002;277(9):7183-90.
5. Liu J, Itagaki Y, Ben-Shabat S, et al. The biosynthesis of A2E, a fluorophore of aging retina, involves the formation of the precursor, A2-PE, in the photoreceptor outer segment membrane. *J Biol Chem* 2000;275(38):29354-60.
6. Katz ML, Drea CM, Eldred GE, et al. Influence of early photoreceptor degeneration on lipofuscin in the retinal pigment epithelium. *Exp Eye Res* 1986;43(4):561-73.
7. Young RW, Bok D. Participation of the retinal pigment epithelium in the rod outer segment renewal process. *J Cell Biol* 1969;42(2):392-403.
8. Wing GL, Blanchard GC, Weiter JJ. The topography and age relationship of lipofuscin concentration in the retinal pigment epithelium. *Invest Ophthalmol Vis Sci* 1978;17(7):601-7.
9. Delori FC, Goger DG, Dorey CK. Age-related accumulation and spatial distribution of lipofuscin in RPE of normal subjects. *Invest Ophthalmol Vis Sci* 2001;42(8):1855-66.
10. ANSI. American national Standard for Safe Use of Lasers (ANSI 136.1). ANSI 1361-2007: The Laser Institute of America, 2007.
11. Sliney D, Aron-Rosa D, DeLori F, et al. Adjustment of guidelines for exposure of the eye to optical radiation from ocular instruments: statement from a task group of the International Commission on Non-Ionizing Radiation Protection (ICNIRP). *Applied Optics* 2005;44(11):2162-76.
12. Delori FC, Webb RH, Sliney DH. Maximum permissible exposures for ocular safety (ANSI 2000), with emphasis on ophthalmic devices. *Journal of the Optical Society of America a-Optics Image Science and Vision* 2007;24(5):1250-65.
13. Cideciyan AV, Jacobson SG, Aleman TS, et al. In vivo dynamics of retinal injury and repair in the rhodopsin mutant dog model of human retinitis pigmentosa. *Proc Natl Acad Sci U S A* 2005;102(14):5233-8.
14. Paskowitz DM, LaVail MM, Duncan JL. Light and inherited retinal degeneration. *British Journal of Ophthalmology* 2006;90(8):1060-6.
15. Cideciyan AV, Swider M, Aleman TS, et al. Reduced-illuminance autofluorescence imaging in ABCA4-associated retinal degenerations. *Journal of the Optical Society of America a-Optics Image Science and Vision* 2007;24(5):1457-67.
16. Hunter JJ, Morgan JJ, Merigan WH, et al. The susceptibility of the retina to photochemical damage from visible light. *Prog Retin Eye Res* 2012;31(1):28-42.
17. Weng J, Mata NL, Azarian SM, et al. Insights into the function of Rim protein in photoreceptors and etiology of Stargardt's disease from the phenotype in *Abcr* knockout mice. *Cell* 1999;98(1):13-23.
18. Wu L, Ueda K, Nagasaki T, Sparrow JR. Light damage in *Abca4* and *Rpe65rd12* mice. *Invest Ophthalmol Vis Sci* 2014;55(3):1910-8.
19. Teussink MM, Lee MD, Smith RT, et al. The effect of light deprivation in patients with stargardt disease. *Am J Ophthalmol* 2015;159(5):964-72 e2.
20. Yannuzzi LA, Fisher YL, Krueger A, Slakter J. Solar retinopathy: a photobiological and geophysical analysis. *Trans Am Ophthalmol Soc* 1987;85:120-58.
21. American Society for Testing and Materials A. Standard Tables for Reference Solar Spectral Irradiance at Air mass 1.5: Direct Normal spectrum for a 37 Degree Tilted Surface (ASTM G173-03 Global Tilt), ISO 9845-1, 1992. . 1999.
22. Burns SA, Webb RH. Optical generation of the visual stimulus. In: Bass M, van Stryland EW, Williams DR, Wolfe WL, eds. *Handbook of Optics*: McGrawhill, 1994.

23. Winn B, Whitaker D, Elliott DB, Phillips NJ. Factors affecting light-adapted pupil size in normal human subjects. *Invest Ophthalmol Vis Sci* 1994;35(3):1132-7.
24. Pokorny J, Smith VC, Lutze M. Aging of the human lens. *Appl Opt* 1987;26(8):1437-40.
25. van de Kraats J, van Norren D. Optical density of the aging human ocular media in the visible and the UV. *J Opt Soc Am A Opt Image Sci Vis* 2007;24(7):1842-57.
26. Delori F, Greenberg JP, Woods RL, et al. Quantitative measurements of autofluorescence with the scanning laser ophthalmoscope. *Invest Ophthalmol Vis Sci* 2011;52(13):9379-90.
27. Hammer M, Roggan A, Schweitzer D, Muller G. Optical properties of ocular fundus tissues--an in vitro study using the double-integrating-sphere technique and inverse Monte Carlo simulation. *Phys Med Biol* 1995;40(6):963-78.
28. Mahroo OA, Lamb TD. Recovery of the human photopic electroretinogram after bleaching exposures: estimation of pigment regeneration kinetics. *J Physiol* 2004;554(Pt 2):417-37.
29. Dartnall HJ, Bowmaker JK, Mollon JD. Human visual pigments: microspectrophotometric results from the eyes of seven persons. *Proc R Soc Lond B Biol Sci* 1983;220(1218):115-30.
30. Sharpe T. Length (μm) of outer segments of human photoreceptors. v. 2015.
31. Curcio CA, Sloan KR, Kalina RE, Hendrickson AE. Human photoreceptor topography. *J Comp Neurol* 1990;292(4):497-523.
32. Dryja TP, O'Neil-Dryja M, Albert DM. Elemental analysis of melanins from bovine hair, iris, choroid, and retinal pigment epithelium. *Invest Ophthalmol Vis Sci* 1979;18(3):231-6.
33. Nofsinger JB, Forest SE, Simon JD. Explanations for the disparity among absorption and action spectra of eumelanin *J Phys Chem* 1999;103:11428-32.
34. Prah SA, Keijzer SL, Jacques SL, Welch AJ. A Monte Carlo model of light propagation in tissue. *SPIE Inst Ser IS 5* 1989:102-11.
35. Wang L, Jacques SL, Zheng L. MCML--Monte Carlo modeling of light transport in multi-layered tissues. *Comput Methods Programs Biomed* 1995;47(2):131-46.
36. Bergougnoux L, Misguich-Ripault J, Firpo JL, Andre J. Monte Carlo calculation of backscattered light intensity by suspension: comparison with experimental data. *Appl Opt* 1996;35(10):1735-41.
37. Tran NT, Campbell CG, Shi FG. Study of particle size effects on an optical fiber sensor response examined with Monte Carlo simulation. *Appl Opt* 2006;45(29):7557-66.
38. Cracknell KP, Farnell DJ, Grierson I. Monte Carlo simulation of latanoprost induced iris darkening. *Comput Methods Programs Biomed* 2007;87(2):93-103.
39. Weiter JJ, Delori FC, Wing GL, Fitch KA. Retinal pigment epithelial lipofuscin and melanin and choroidal melanin in human eyes. *Invest Ophthalmol Vis Sci* 1986;27(2):145-52.
40. Boulton M, Docchio F, Dayhaw-Barker P, et al. Age-related changes in the morphology, absorption and fluorescence of melanosomes and lipofuscin granules of the retinal pigment epithelium. *Vision Res* 1990;30(9):1291-303.
41. Delori FC, Staurenghi G, Arend O, et al. In vivo measurement of lipofuscin in Stargardt's disease--Fundus flavimaculatus. *Invest Ophthalmol Vis Sci* 1995;36(11):2327-31.
42. Greenberg JP, Duncker T, Woods RL, et al. Quantitative fundus autofluorescence in healthy eyes. *Invest Ophthalmol Vis Sci* 2013;54(8):5684-93.
43. Burke TR, Duncker T, Woods RL, et al. Quantitative fundus autofluorescence in recessive Stargardt disease. *Invest Ophthalmol Vis Sci* 2014;55(5):2841-52.
44. Fish G, Grey R, Sehmi KS, Bird AC. The dark choroid in posterior retinal dystrophies. *Br J Ophthalmol* 1981;65(5):359-63.
45. Uliss AE, Moore AT, Bird AC. The dark choroid in posterior retinal dystrophies. *Ophthalmology* 1987;94(11):1423-7.
46. Bonnin MP. [The choroidal silence sign in central tapetoretinal degenerations examined by fluorescein]. *Bull Soc Ophthalmol Fr* 1971;71(3):348-51.
47. Bonnin MP, Passot M, Triolaire-Cotten T. Le signe du silence choroidien dans les degenerescences tapeto-retiennes posterieures. In: De Laey JJ, ed. *International Symposium on Fluorescein Angiography Doc Ophthalmol* 1976.

48. Ueda K, Zhao J, Kim HJ, Sparrow JR. Photodegradation of retinal bisretinoids in mouse models and implications for macular degeneration. *Proc Natl Acad Sci U S A* 2016;113(25):6904-9.
49. Eagle RC, Jr., Lucier AC, Bernardino VB, Jr., Yanoff M. Retinal pigment epithelial abnormalities in fundus flavimaculatus: a light and electron microscopic study. *Ophthalmology* 1980;87(12):1189-200.
50. Eldred GE, Lasky MR. Retinal age pigments generated by self-assembling lysosomotropic detergents. *Nature* 1993;361(6414):724-6.
51. Sparrow JR, Blonska A, Flynn E, et al. Quantitative fundus autofluorescence in mice: correlation with HPLC quantitation of RPE lipofuscin and measurement of retina outer nuclear layer thickness. *Invest Ophthalmol Vis Sci* 2013;54(4):2812-20.
52. Rozanowska M, Pawlak A, Rozanowski B, et al. Age-related changes in the photoreactivity of retinal lipofuscin granules: role of chloroform-insoluble components. *Invest Ophthalmol Vis Sci* 2004;45(4):1052-60.
53. van Gemert JC, Berenbaum MC, Gijssbers GH. Wavelength and light-dose dependence in tumour phototherapy with haematoporphyrin derivative. *Br J Cancer* 1985;52(1):43-9.
54. Kawachi S, Sato S, Morimoto Y, Kikuchi M. Correlation between oxygen consumption and photobleaching during in vitro photodynamic treatment with ATX-S10.Na(II) using pulsed light excitation: dependence of pulse repetition rate and irradiation time. *Photochem Photobiol* 2004;80(2):216-23.
55. Feeney-Burns L, Hilderbrand ES, Eldridge S. Aging human RPE: morphometric analysis of macular, equatorial, and peripheral cells. *Invest Ophthalmol Vis Sci* 1984;25(2):195-200.
56. Jacques SL. Optical properties of biological tissues: a review. *Phys Med Biol* 2013;58(11):R37-61.
57. Kim SR, Jang YP, Sparrow JR. Photooxidation of RPE lipofuscin bisretinoids enhances fluorescence intensity. *Vision Res* 2010;50(7):729-36.
58. Feldman TB, Yakovleva MA, Arbukhanova PM, et al. Changes in spectral properties and composition of lipofuscin fluorophores from human-retinal-pigment epithelium with age and pathology. *Anal Bioanal Chem* 2015;407(4):1075-88.
59. Kurz T, Karlsson M, Brunk UT, et al. ARPE-19 retinal pigment epithelial cells are highly resistant to oxidative stress and exercise strict control over their lysosomal redox-active iron. *Autophagy* 2009;5(4):494-501.
60. Zareba M, Skumatz CM, Sarna TJ, Burke JM. Photic injury to cultured RPE varies among individual cells in proportion to their endogenous lipofuscin content as modulated by their melanosome content. *Invest Ophthalmol Vis Sci* 2014;55(8):4982-90.
61. Qin S, De Vries GW. alpha2 But not alpha1 AMP-activated protein kinase mediates oxidative stress-induced inhibition of retinal pigment epithelium cell phagocytosis of photoreceptor outer segments. *J Biol Chem* 2008;283(11):6744-51.
62. Olchawa MM, Herrnreiter AM, Skumatz CM, et al. Photosensitized oxidative stress to ARPE-19 cells decreases protein receptors that mediate photoreceptor outer segment phagocytosis. *Invest Ophthalmol Vis Sci* 2013;54(3):2276-87.
63. Mullen RJ, LaVail MM. Inherited retinal dystrophy: primary defect in pigment epithelium determined with experimental rat chimeras. *Science* 1976;192(4241):799-801.
64. Zadlo A, Burke JM, Sarna T. Effect of untreated and photobleached bovine RPE melanosomes on the photoinduced peroxidation of lipids. *Photochem Photobiol Sci* 2009;8(6):830-7.
65. Rozanowski B, Burke JM, Boulton ME, et al. Human RPE melanosomes protect from photosensitized and iron-mediated oxidation but become pro-oxidant in the presence of iron upon photodegradation. *Invest Ophthalmol Vis Sci* 2008;49(7):2838-47.
66. Rozanowska M, Korytowski W, Rozanowski B, et al. Photoreactivity of aged human RPE melanosomes: a comparison with lipofuscin. *Invest Ophthalmol Vis Sci* 2002;43(7):2088-96.
67. Winkler BS, Boulton ME, Gottsch JD, Sternberg P. Oxidative damage and age-related macular degeneration. *Mol Vis* 1999;5:32.
68. Feeney L. Lipofuscin and melanin of human retinal pigment epithelium. Fluorescence, enzyme cytochemical, and ultrastructural studies. *Invest Ophthalmol Vis Sci* 1978;17(7):583-600.



Over 7000 rare diseases exist, and together, they represent a relevant public health issue. They afflict up to 10 million European Union citizens, about half of which being children.¹ For these patients, the scientific landscape attests to the promising and encouraging progress in finding a cure. We would not only be intervening in behavior and environment, for example, avoiding excessive sun light exposure and dietary restrictions in Stargardt disease, but we will also have opportunities to alter disease progression and possibly even to restore vision. Optimists may envision therapies becoming available within the next five years,² but the scientific process generally proves to be a “long and winding road”. Each step on this road to a cure is essential for the eventual success.

Eventually, a potential cure needs to be approved by the U.S. Food and Drug Administration (FDA) and/or European Medicines Agency (EMA). To be approved by these official agencies, a clinical trial is required to prove that a potential cure is effective. To be able to prove this, clinical endpoints that represent a measurable and significant effect are needed. In turn, the FDA/EMA must also consent with these chosen endpoints. This thesis directly addresses the specific challenges associated with treatment evaluation for rare diseases, specifically for Stargardt disease. The general aims of this thesis are to: [1] evaluate the effect of nature's time by characterizing the natural history of distinct patient groups within the spectrum of Stargardt disease [2] identify the diagnostic challenges in distinct patient groups within Stargardt disease to be able to select the right patients in the right trial, and [3] choose the appropriate method for outcome evaluation by developing a model to measure disease progression with high accuracy. These steps provide a strategy for future studies which aim to identify the effect of novel treatments in rare and heterogeneous diseases, in which Stargardt disease serves as a model.

This discussion will outline the main findings and put the results in a broad and future perspective. The main findings were as follows: in **Chapter 2**, we described phenotypic and genotypic characteristics of early-onset Stargardt and late-onset Stargardt. Early-onset Stargardt can be considered a distinct severe subtype of Stargardt disease that is characterized by early foveal abnormalities and the rapid loss of visual function. In contrast, late-onset Stargardt frequently demonstrates foveal sparing in which visual acuity is often preserved to a relatively advanced age. This difference in natural history provides the basis to create models that describe disease progression. **Chapter 3** reveals the challenges in the clinical diagnosis of Stargardt disease. Increased awareness of the absence of retinal abnormalities in certain young Stargardt patients helps finding the correct diagnosis. It can prevent distress, unnecessary investigations and harmful therapies and may prove important in early inclusion in future trials. Inclusion in future trials is also challenging in older patients because of retinal abnormalities mimicked by age-related disease; both age-related macular degeneration and late-onset Stargardt can exhibit

progressive foveal sparing atrophy. However, they differ in etiology and progression speed. Finally, **Chapter 4** creates models of disease progression in Stargardt disease. The inter-eye concordance decreases as the age at onset increases. This has important consequences for clinical trial design; potential treatment effects are best assessed in young patients. Moreover, there is substantial benefit of using a composite outcome measure to assess efficacy in clinical trials for Stargardt disease with small cohorts in a timely fashion. In all of these assessments, fundus autofluorescence imaging is used as a main tool to measure disease progression. However, we need to bear in mind that patients with Stargardt disease are generally at increased risk of photo-oxidative stress.

5.1 Relevance of disease classification

Etiological and prognostic and homogeneity

To classify patients to a specific disease or disease group that is clinically relevant, both sufficient prognostic and etiological homogeneity between patients are required.³ Such a classification is necessary for appropriate patient counselling as well as treatment selection. Moreover, appropriate patient selection is a prerequisite to be able to evaluate a treatment effect in clinical trials. Patients are to be selected with sufficient prognostic and etiologic homogeneity when few patients are included. Otherwise, an effect may be observed while there is none, or it may not be observed while in fact there is. The degree of etiologic and prognostic homogeneity in subgroups of Stargardt disease according to phenotype, genotype and electrophysiology is discussed in the subsequent paragraphs.

Phenotypical similarity

Four distinct retinal features reflecting stages of Stargardt disease were previously described by Fishman: an atrophic-appearing macular lesion with localized perifoveal flecks, retinal flecks throughout the posterior pole, resorbed flecks, and extensive atrophic-appearing changes of the retinal pigment epithelium and choroid.^{4, 5} These phenotypes represent stages in the natural history of Stargardt disease, although not all patients go through these stages and some appear to halt at a certain stage. This classification thus only addresses phenotypical similarity at a given time point, but do not take etiological and prognostic similarity into account.

Patterns on electroretinography

Stargardt disease demonstrates vast prognostic heterogeneity, that is, differences in disease course. A classification that addresses prognostic homogeneity involves three patterns on electroretinography (ERG) identified by Lois: severe pattern ERG abnormality with normal full-field ERG, additional loss of photopic function consistent with a clinical diagnosis of cone dystrophy, or loss of both photopic and scotopic function,

i.e., cone-rod dystrophy.⁶ The latter would have the worst prognosis. Although these patterns are suggested to have this prognostic value, a transition over time from one to another pattern can still occur within a patient.⁷ For instance, a patient can have a severely abnormal pattern ERG but an otherwise normal full-field ERG at his initial presentation. This would indicate a maculopathy consistent with Stargardt disease. However, additional loss of photopic and scotopic function is likely to occur over time. As this pattern is consistent with a cone-rod dystrophy, this patient's prognosis changes as his disease progresses.

Genotype-phenotype correlations

The etiology in Stargardt disease is clearly apparent: disease-causing variants in the ABCA4 gene. A classification was developed by genotype: the expected residual function of the ABCA4 protein resulting in the mildest phenotype of age-related macular degeneration (one mild ABCA4 variant) to the most severe retinitis pigmentosa-like phenotype (two severe ABCA4 variants).⁸ This model by Van Driel may hold for the average of genotypic groups, but discrepancies can be observed in individual patients. For instance, occasionally only one variant is detected in severe retinal dystrophy,⁹ whereas a combination of a severe and a mild variant can be detected in mild foveal sparing disease.^{10, 11} Comprehensive genotype-phenotype correlations may further help identify those patients who are expected to have prognostic homogeneity. In case of homozygous variants with no ABCA4 function (null variants), a rather simple correlation can be made with severe disease. Furthermore, specific missense variants are now associated with disease severity classes ranging from a mild phenotype to a severe null-like phenotype based on electroretinographic findings.¹² Straightforward conclusions still cannot be made; each combination of ABCA4 variants will have a unique combined effect on disease severity. Moreover, the variations in phenotype can be caused by loss or alteration of contiguous genes, transporter proteins and activator proteins. Such modifiers have become increasingly recognized as an important source of phenotypic variation. Arrayed primer extension genotyping and Sanger sequencing are now standard methods of genetic analysis, but next-generation sequencing is increasingly changing the diagnostic workflow of retinal specialists to identify novel variants in approximately 250 retinal genes.^{13, 14} As the entire genome sequence can now be determined, challenges lay ahead to interpret newly detected variants. Genotype-phenotype correlations can further unravel the heterogeneity of Stargardt disease, and let us better understand potential differences in the effect of new treatments.¹⁵

The age of onset

Multiple types of subgroups have now been proposed resulting in multiple possibilities of classifications, some of which confusingly can change over time within the same patient.

Each combination of genotypic, funduscopy and electrophysiologic findings could be considered a unique type at a specific time point. Hence, the multitude of descriptive classifications and stages does not identify specific diagnostic subgroups of Stargardt disease with sufficient clinically relevant prognostic homogeneity. Prognostic homogeneity can be identified by long-term follow-up that carefully evaluates the natural history of patients. The approach of grouping patients based on their natural history has led to a division of Stargardt disease into three groups based on the age at onset. Age dependency on the eventual visual prognosis has indeed been previously described,¹⁶ and now translates itself into subgroups of Stargardt disease described in **Chapter 2**: [1] early-onset Stargardt (≤ 10 years of age) with minor initial abnormalities, early foveal loss, and a fast progression toward retina-wide chorioretinal atrophy with severe vision loss,^{9, 17} and [2] late-onset Stargardt (≥ 45 years of age) with a relatively intact fovea surrounded by yellow-white fundus flecks and gradually expanding, well-demarcated areas of atrophic retinal pigment epithelium lesions.^{10, 18} This age-specific incidence distribution allows at least a third subgroup of intermediate-onset Stargardt patients

1. Evaluate the effect of time

Challenge: Rare diseases inherently have small populations. Moreover, they demonstrate a wide range of severity in their natural progression.

Case: Three subgroups of Stargardt disease that are based on the age of onset converges to an identical single clinical and functional endpoint, demonstrating prognostic homogeneity: early-onset Stargardt, intermediate-onset Stargardt and late-onset Stargardt.

Conclusion: Knowledge of the effect of time provides the basis to identify any intervention that aims to change the natural course of the disease. Classification of disease is therefore required to have patient groups with etiologic as well as prognostic homogeneity. Thus, natural history studies are essential to be performed prior to the initiation of any clinical trial.

with an incidence between 10 and 45 of age. A comparable bimodal pattern occurs in acute lymphoblastic leukemia, with an initial incidence rate peak among infants, a decline in childhood, and an exponential rise with advancing age beginning in young adulthood.¹⁹ These subgroups within Stargardt disease still contain a broad clinical spectrum of their natural courses by differences of electroretinographic abnor-

malities, retinal abnormalities in terms of the spatiotemporal distribution of yellow-white flecks, as well as combinations of ABCA4 variants. Further refinement of differential prognosis may therefore still lie in the severity of loss of ABCA4 function, ERG findings, or other imaging modalities.^{6, 7, 20} Nonetheless, each of the three subgroups that are based on the age of onset converges to an identical single clinical and functional endpoint—thus demonstrating prognostic homogeneity.

5.2 Identification and selection of patients

Rare diseases are generally difficult to recognize and diagnose, because of their wide range of severity both at clinical presentation and natural progression. This also accounts for Stargardt disease, particularly in early-onset and late-onset Stargardt disease.

Early diagnostics

In young patients, the retinal abnormalities may be very subtle despite major visual complaints (**Chapter 3.1**).

In such cases, there are no obvious yellow-white flecks or evident atrophic macular lesion that would help direct the clinician to the diagnosis of Stargardt disease. The fluctuating severity of visual acuity loss further impedes a correct diagnosis. Color vision tests and electroretinography²¹ may help in screening in the early disease stages. However, a thorough examination by fundus autofluorescence imaging and spectral-domain optical coherence tomography will enable to detect subtle abnormalities that point to the right diagnosis, which are otherwise left undetected. This includes parafoveal hyperautofluorescence,²² and a thickened external limiting membrane.²³ Thickening of this hyperreflective band is more recently being hypothesized to represent a structural change at the level of the foveal cone nuclei, sparing the foveolar region.²⁴ Early diagnostics remains challenging, but essential if a potential treatment requires the earliest possible intervention, i.e., in gene therapy.

Similar diagnostic challenges arise in late-onset Stargardt patients. Here, the challenge lies in distinguishing late-onset Stargardt^{10, 25} with atrophic age-related macular degeneration (**Chapter 3.2**).^{25, 26} Both include a progressive foveal sparing atrophy of the retinal pigment epithelium, but the underlying pathophysiologic process differs. Consequently, potential treatments are different as well because of different mechanisms; in age-related macular degeneration, multiple factors play a role. Strategies in multifactorial age-related macular degeneration may better involve final common pathways

2. Select the right patients

Challenge: Rare diseases generally have a clinical presentation that is often incompletely described and difficult to be recognized.

Case: In Stargardt disease, young patients initially have limited retinal abnormalities, while the visual acuity loss is quite severe. Subtle abnormalities can be detected by optical coherence tomography and fundus autofluorescence imaging. Patients with late-onset Stargardt disease can demonstrate abnormalities mimicking age-related macular degeneration and need to be carefully distinguished.

Conclusion: Inclusion of wrong patients in clinical trials would blur the therapeutic effect under observation and potentially lead to a fail in proving efficacy. Appropriate diagnostic tools and information will help early and correct diagnosis to select the right patients for a specific trial at the right time.

leading to cell death from choroidal perfusion enhancers over neuroprotective agents to complement inhibitors.^{27, 28} In contrast, ABCA4 will remain the main factor in late-onset Stargardt, and thus the primary target for interventions.²⁹

Timely interventions

The potential delay in diagnosis has important clinical implications; not only does it delay appropriate counseling and interventions, but also will it be important to have an early diagnosis when it comes to early disease-modifying interventions by inclusion in gene therapy trials. Moreover, those patients are preferably included before the disease is expected to rapidly progress further, increasing the chance to detect differences when progression is slowed down. These features have been shown to be present in early-onset Stargardt patients (**Chapter 2.1**). Finally, misdiagnosis risks patients being selected in trials with a suboptimal therapeutic effect.

5.3 Endpoints in clinical trials

Visual function tests, such as best-corrected visual acuity or visual field may be suitable endpoints in clinical trials with large cohorts and long follow-up. However, when cohorts are small, other strategies are needed. Alternative designs in clinical trials and endpoints can potentially decrease the time and cost required to assess the safety and effect of new drugs.³⁰ Although many of these techniques are not new, an integral approach can optimize clinical trials in rare diseases like Stargardt. In this thesis, such strategies are provided.

Surrogate endpoints

The choice of an appropriate endpoint can drastically affect the power of a study. Loss of visual acuity has been the primary clinical endpoint in many ocular clinical trials since the advent of the Early Treatment for Diabetic Retinopathy Studies. However, functional endpoints such as visual acuity have been shown not to be the optimal outcome measure in small clinical trials due to its high interindividual variance,¹⁶ test variability^{31, 32} and overall slow decline. This high variance can result in unrealistic large cohorts and long follow-up required when used in a trial.

In contrast, structural parameters on fundus autofluorescence and optical coherence tomography provide better characteristics in terms of detectable small short-term change as the disease progresses (**Chapter 4.1 and 4.2**). These surrogate measurements can reflect changes in functional disease progression, which are otherwise only detectable with long follow-up.³³ However, there is always an unavoidable trade-off between clinical relevance of an outcome and the time frame in which it occurs.

A therapeutic effect on a surrogate endpoint does not necessarily mean that the therapy also has an effect on the functional endpoint (Figure 1).³⁴ The method for outcome evaluation need to adhere to the requirement that the endpoint lies in the causal pathway of the disease process. For example, in an upcoming trial for the treatment Stargardt disease, Remofuscin intervenes in the removal of lipofuscin.³⁵ Consequently, the endpoint need to be a measurement that rather detects a change in lipofuscin than the later stages of retinal pigment epithelium atrophy and loss of visual function. Because lipofuscin accumulation is expected to result in the eventual retinal degeneration with associated loss in vision function, such a surrogate endpoint is reasonably likely to predict clinical benefit.

A valid surrogate endpoint is not only correlated with the clinically meaningful endpoint, but also captures the net effect of treatment on the clinical outcome completely.³⁶ According to these criteria, no surrogate can possibly suffice; to show that a surrogate is a valid outcome, one would need an effective drug showing the eventual benefit on both the surrogate and a clinically meaningful endpoint. However, the surrogate is used to prevent waiting on the occurrence of the clinically meaningful endpoint in the first place—clearly a catch-22. Thus, Fleming later defined an endpoint validation hierarchy for outcome measures: level 1, clinical-efficacy endpoints; level 2, a validated surrogate endpoint (for a specific disease setting and class of interventions); level 3,

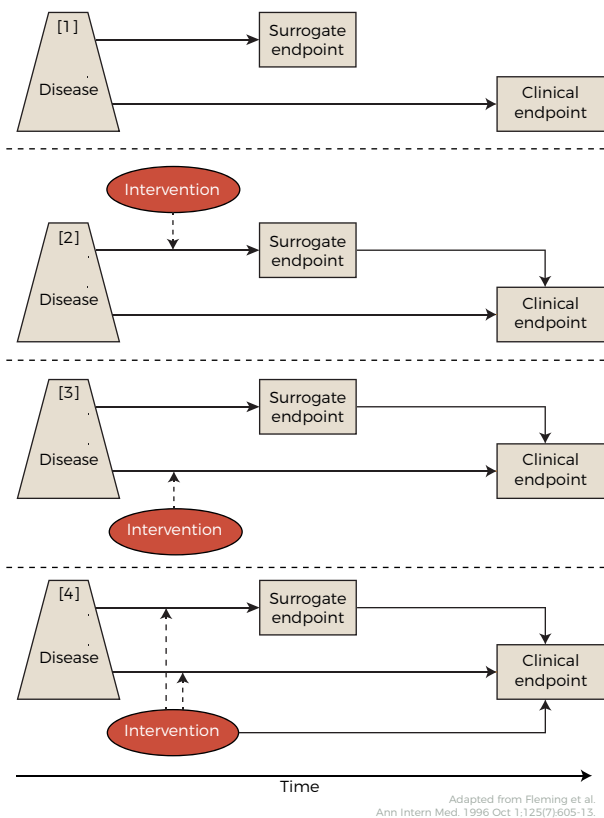


Figure 1. Reasons of possible failure of surrogate endpoints. [1] The surrogate is not in the causal pathway of the disease process. [2] of several causal pathways of disease, the intervention affects only the pathway mediated through the surrogate. [3] the surrogate is not in the pathway of the intervention's effect or is insensitive to its effect. or [4] the intervention has mechanisms of action independent of the disease process.

a nonvalidated surrogate endpoint, yet one established to be “reasonably likely to predict clinical benefit” (for a specific disease setting and class of interventions), and level 4, a correlate that is a measure of biological activity, but that has not been established to be a higher level.³⁷ **Chapter 2.2** has shown that progression of RPE atrophy can be used as a “level 3” surrogate in late-onset Stargardt. Despite having a disconnect between visual acuity and RPE atrophy because of a frequently occurring initial foveal sparing pattern,^{11, 38-40} foveal involvement can drive the eventual vision loss, and the fovea is more likely to be involved as RPE atrophy progresses, both centrifugally toward the periphery, as well as centripetally toward the fovea. A similar structural parameter, geographic atrophy has been already accepted as a surrogate outcome measure by the FDA in age-related macular degeneration,⁴¹ and may also be valuable in other retinal diseases affecting the RPE. Long-term natural history studies provide further insight into the value of surrogate endpoints reflecting disease progression which lead to the eventual clinically meaningful endpoint.

Multimodal strategy

The endpoint can be further optimized by identifying a unique combination of structural measurements that has the best signal-to-noise ratio, i.e., the largest change in disease progression with minimal variability.⁴² The downside of a composite outcome is that it increases the complexity in a trial, both for the construction as well as interpretation of the results.⁴³ The concern that many published research findings are false may particularly apply to the use of these complex outcome measurements. Moreover, research findings are less likely to be true when the sample sizes and effect sizes are smaller. Therefore, in interventional trials for rare diseases including Stargardt disease, it is even more critical that the design is prospectively defined: being randomized and blinded where possible and the primary objectives clear and the complex statistical analysis (for example, as presented in **Chapter 4.2**) to address the primary objectives prespecified. Only then will the interpretation of the results be valid.⁴⁴

Composite endpoints can be extremely valuable in highly accurate measurements of disease progression. The heterogeneity of Stargardt disease requires knowledge of which specific combination of measurements are the most important in specific patient groups to identify a response or non-response for a specific treatment. In **Chapter 4.2**, multimodal analysis of disease progression has been shown to be able to provide an appropriate composite endpoint in early-onset Stargardt disease by applying different weights,⁴⁵ i.e., importance, to individual parameters that ultimately form the composite. The importance of the rate of ellipsoid zone loss, which was automatically identified by the model, was indeed confirmed by other studies.^{46, 47} Other parameters, such as en-face optical coherence tomography, may also prove highly valuable in measuring disease progression.⁴⁸

This composite endpoint outperforms any unimodal structural endpoint in terms of signal-to-noise ratio, further facilitating the detection of potential treatment effects. Statistical models can then establish the distribution of an expected range of future outcomes. If a treatment exceeds the predicted future ranges, the intervention can be considered to have an effect (Figure 2). Such potential treatment effects can be simulated in varying patient populations and study designs. This approach can eventually optimize the trial design for the right patient group.

Other considerations in trial design

The methodology of controlled trials can be improved to facilitate patient recruitment, reduce the number of patients required to include, optimize trial duration and increase statistical power.

The standard parallel group comparisons require large sample sizes, but a factorial design, based on parallel groups, can include more than two treatment arms; patients are randomized twice—once for treatment X or placebo and then for treatment Y or placebo—can be time-saving and requires fewer patients to answer two questions. Matched-pairs parallel groups allow patients to be matched with another patient having similar characteristics, taking advantage of similarities to improve power. A major advantage

in ocular therapies is the availability of the ideal matched-pair control. When a local therapy to an eye of a patient is applied, his untreated eye is the internal matched pair. The advantage will increase when the inter-eye, i.e., within-participant, correlation is high. A fellow-eye paired trial design is therefore recommended in retinal dystrophies: a missed opportunity in general. As presented in Chapter 4.1, the high inter-eye correlation is an additional reason to prefer early-onset Stargardt patients to be

3. Choose the appropriate method for outcome evaluation

Challenge: A randomized-controlled design includes an appropriate sample size, statistical power, and methods to minimize bias. This is unfeasible with conventional methods in rare diseases.

Case: The heterogeneity of Stargardt disease requires knowledge of which specific combination of measurements are the most important in specific patient groups to identify a response or non-response for a specific treatment. In early-onset Stargardt, a unique combination of structural measurements has shown to have the best signal-to-noise ratio, i.e., the largest change in disease progression with minimal variability.

Conclusion: Clinical trials need to be adapted to small populations. A right endpoint is needed to identify any modification of the natural disease progression to evaluate the effectiveness of new treatments. This endpoint depends on the patient selection as well as the specific treatment being evaluated. Herein, composite endpoints can be extremely valuable in highly accurate measurements of disease progression. This approach can eventually optimize the trial design in rare diseases.

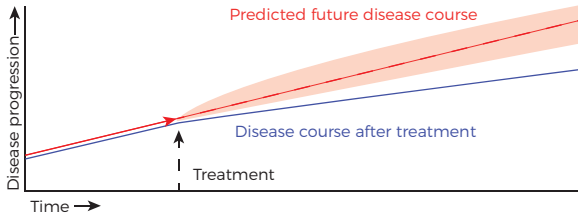


Figure 2. Model of predicted future disease course. The intervention is considered to have an effect if the disease course exceeds the expected range of predicted future measurements.

selected in clinical trials over intermediate-onset and late-onset Stargardt patients. However, this advantage does not hold for systemic pharmacological strategies, in which both eyes are inherently treated. Moreover, when the outcome is measured at the patient level, the untreated eye cannot serve as a control.⁴⁹ Nonetheless, inclusion of both eyes of a patient in a clinical trial seems to have been a missed opportunity in recent ocular therapies, and should be permitted unless it is not appropriate for the study design.⁵⁰

Another improvement includes a crossover design, in which patients receive the treatment and the placebo in a prespecified random sequence. Patients then serve as their own control. Similar to crossover includes a Latin square in which every treatment occurs once in each sequence and in each period, and N-of-1 trials: a within-patient randomized controlled multi-crossover trial design. Here, only 1 patient receives multiple cycles of double-blind treatment in a random sequence, which provides an estimate of individual effectiveness. For crossover trials, including within-patient designs, a relatively stationary disease is required, and a wash-out period is needed to prevent a carryover effect. Trial duration is therefore longer. Moreover, a crossover design cannot be used in case the treatment is irreversible, e.g., in case of surgical intervention with gene replacement therapy or cell-based therapy.⁵¹ To conclude, no single design is suited for all rare diseases and interventions (Table 1).

Parallel group design	Patients are assigned to treatment or control
Factorial design	Multiple treatment arms
Matched-pairs	Correlated pairs in treated and untreated arm
Crossover design	Patients receive both treatment and placebo
Latin square	Every treatment occurs once in each sequence and period
N-of-1	Within-patient multi-crossover

Table 1. Alternative designs in addition to double-blind randomization.

5.4 Meaningful outcome measures

Emerging therapies

Insight into the pathogenesis of human disease is constantly increasing, as well as potential therapeutic opportunities. Patients have indeed been provided needed therapies, but effective treatments are still unavailable for most rare diseases. The development of gene therapy has been ongoing for over 30 years, and now, the first *in-vivo* gene replacement therapy has just been approved; treatment of RPE65-mediated retinal dystrophy by voretigene neparvovec-rzyl is a major milestone and has reached three patients up to now.^{52, 53} Concurrently, early-stage experiments are already going beyond this 'conventional' gene augmentation therapy, showing that a one-time, permanent genome editing offers new ways to reverse blindness.⁵⁴ Technology is changing at such a fast pace, clinical implementation could eventually stay behind. Eventually, we risk implementing nothing into regular clinical care at all, because the treatments to be approved will be already outdated and outperformed by new state-of-the-art treatments being developed in the lab.

Regulatory reformations

The succeeding drug and device approval have been hampered by regulatory requirements which are rather stringent but necessary to protect patients from harm.⁵⁵ Important steps have been made in regulatory reformations to help speed up the discovery and delivery of new treatments. Since the U.S. Orphan Drug Act (1983) and the E.U. Regulation on Orphan Medicinal Products (2000) facilitated the development of drugs for small populations, several treatments for rare diseases have been approved. Currently, over one third of indications were already approved based on a single pivotal trial, and about three-quarters were approved on trials with a duration of less than six months, supposed to be taken for a lifetime.⁵⁶

The 21st Century Cures Act was introduced to speed up the pace of innovation further. Organizations representing patients, physicians, and researchers allied with pharmaceutical and medical device industries voting for this 21st Century Cures Act; others opposed the act because of serious concerns. The act includes funding for the National Institute of Health (NIH), facilitating collaborative research by encouraging data sharing and ensuring the reproducibility. It further reduces administrative tasks, and supports high-risk, high-reward research. However, a worrisome aspect of this act encourages the FDA to lower the standards of empirical evidence despite that the FDA already provides guidance for accelerated drug approval.⁵⁷ Less strict regulations to drug approval may sound promising but could increase the risk of misjudging that useless treatments are helpful, or that helpful treatments are useless.

For example, the recent lampalizumab phase III trial for age-related macular degeneration failed to show a therapeutic effect. Natural history studies that followed the initiation of the lampalizumab trial showed no difference in progression speed of geographic atrophy in patients with different complement profiles.⁵⁸ The role of complement activation in geographic atrophy therefore seems to be insignificant. With this knowledge, the trial probably needed to include different patients in an earlier disease stage before the development of geographic atrophy and needed to have a different primary endpoint. The treatment likely aimed at a different mechanism, which was not captured with the primary endpoint.

Rushing to our destination may end up in taking wrong turns and can set us back to where we came from. If we were to reduce the standard to anecdotes of experiences and uncontrolled, unrandomized data, we would return to 19th-century problems we thought we had left behind.^{59, 60} Although there is an urgent need to move forward to find a cure for patients with rare diseases, the solution may not lie in shortcuts which lower the standards of robust clinical evidence. Although the freedom given will require greater scrutiny, such changes to accelerate the development of novel treatments for Stargardt disease and other rare diseases are encouraging.

5.5 When present becomes history

Precision medicine

The societal need is high for efficient precision medicine: personalized healthcare being refined to have the most significant impact upon our individual needs. We want to be informed how to stay healthy, and how to manage and treat disease. Precision medicine encompasses all the information on the individual, including their environment and behavior. Disregarding the latter could create unrealistic expectations to both clinicians as well as patients, potentially changing perceptions of their risk of disease; if patients believe they are less at risk, they may feel excessively protected, worsening their behavior, putting them at increased risk. This also holds for Stargardt disease, despite being a monogenetic disease; in the future, when a successful treatment has been implemented, patients should still protect themselves from sun light and avoid vitamin A supplements, as they are likely at increased risk for phototoxic injury (**Chapter 4.3**).

To measure our health status, the medical armamentarium is expanding exponentially.⁶¹⁻⁶⁴ The massive amount of information should eventually guide us to diagnostic, therapeutic, and preventive strategies, tailored for every unique individual. However, this can give rise to a plethora of prognostic probabilities and ambiguity of the efficiency of these strategies.⁶⁵

Pursuing perfect surrogacy

Regulatory agencies have mainly focused on single primary endpoints, but there is no perfect single surrogate or clinical endpoint that could encompass the complex interactions in a patient. Slowly, we begin to understand the complex interactions of genomics, proteomics, metabolomics, behavior and environment. By thinking in these interactions rather than in single pathways,⁶⁶ we can identify new biomarkers and new targets for treatment and understand their effects.⁶⁷ The ground for drug approval should therefore arise from combined measurements within the range from biomarkers to patient-reported outcomes.

Universal measurement and reporting of core outcome sets could pave the way to further accelerate novel therapeutic strategies.⁶⁸⁻⁷⁰ An international agreement on the minimum sufficient set of outcomes would allow to collect and share natural history data more efficiently, for which The International Consortium for Health Outcomes Measurement (ICHOM) has already taken significant steps on this path. An international digital platform is furthermore needed to rapidly facilitate collecting and sharing of standardized measurements. Meaningful outcome measures should comprise the complete biological network from the molecular level to societal interactions: from molecular biomarkers to patient self-reports in real-life settings.

Chapter 4.2 integrated structural changes of the natural progression of retinal degeneration to provide a sensitive outcome measure within two years of follow-up. However, the progression detected here does not completely describe the natural progression of Stargardt disease. Outcomes that matter to patients are essential, and undoubtedly include long-term safety, vision and the impact on visual impairments in daily life. The value of the composite structural outcome measure mainly lies on rationally selecting potential novel treatments. It still needs to demonstrate how it relates to functional outcome in the long term. We could then gain insight into the effect of interventions, and how this translates to an eventual true change in disease progression. Thinking in interactions may eventually change medical practice with a deeper holistic view, offering patients the right intervention at the right time.^{71, 72}

Evolution of evidence synthesis

The productivity of drug development is decreasing, while the costs for drug development can increase up to 1.2 billion US dollars.⁷³ Evidence synthesis needs to evolve by “increasing value and reducing waste in biomedical research”.⁷⁴ Herein, outcome measures play a crucial role; they are to be standardized and need to incorporate all aspects of the human biological network.^{71, 75, 76} Lessons can be learned from studies on rare diseases; dissecting common diseases into “rare” molecularly defined subtypes helps to

capture individual variability of these common diseases.⁴⁴ As these diseases are being dissected more and more into rarer subtypes, clinical trials in common diseases will face similar challenges as studies in rare diseases: challenges such as the identification of the most important outcome measures and their ability to show potential treatment effects. Stargardt disease poses the challenges of small populations and vast heterogeneity. This thesis outlined a strategy to provide clinical trials the right outcome measurements for the right patients to identify an effective drug in Stargardt disease: [1] evaluate the effect of time, [2] select the right patients, and [3] choose the appropriate method for outcome evaluation. In the next step, standardization of outcome measures can prevent scientists and organizations continuously reinventing the wheel. The change of our daily practice should ultimately focus on interweaving clinical care with scientific research using universal measurements and reporting of core outcome sets; the borders between the clinical care, patient registries, and therapeutic trials need to dissolve. It can unleash creativity in treatment implementation without compromising safety: toward a cure for Stargardt disease.

References

1. Mazzucato M, Visona Dalla Pozza L, Manea S, et al. A population-based registry as a source of health indicators for rare diseases: the ten-year experience of the Veneto Region's rare diseases registry. *Orphanet J Rare Dis* 2014;9:37.
2. Kamenova K, Caulfield T. Stem cell hype: media portrayal of therapy translation. *Sci Transl Med* 2015;7(278):278ps4.
3. William MG, Niels GW, David F, et al. *A Paul Meehl Reader*. Routledge, 2006.
4. Fishman GA. Fundus flavimaculatus. A clinical classification. *Arch Ophthalmol* 1976;94(12):2061-7.
5. Fishman GA, Stone EM, Grover S, et al. Variation of clinical expression in patients with Stargardt dystrophy and sequence variations in the ABCR gene. *Arch Ophthalmol* 1999;117(4):504-10.
6. Lois N, Holder GE, Bunce C, et al. Phenotypic subtypes of Stargardt macular dystrophy-fundus flavimaculatus. *Arch Ophthalmol* 2001;119(3):359-69.
7. Fujinami K, Lois N, Davidson AE, et al. A longitudinal study of stargardt disease: clinical and electrophysiologic assessment, progression, and genotype correlations. *Am J Ophthalmol* 2013;155(6):1075-88.e13.
8. van Driel MA, Maugeri A, Klevering BJ, et al. ABCR unites what ophthalmologists divide(s). *Ophthalmic Genet* 1998;19(3):117-22.
9. Lambertus S, van Huet RA, Bax NM, et al. Early-onset stargardt disease: phenotypic and genotypic characteristics. *Ophthalmology* 2015;122(2):335-44.
10. Westeneng-van Haaften SC, Boon CJ, Cremers FP, et al. Clinical and genetic characteristics of late-onset Stargardt's disease. *Ophthalmology* 2012;119(6):1199-210.
11. van Huet RA, Bax NM, Westeneng-Van Haaften SC, et al. Foveal sparing in Stargardt disease. *Invest Ophthalmol Vis Sci* 2014;55(11):7467-78.
12. Fakin A, Robson AG, Chiang J, et al. The Effect on Retinal Structure and Function of 15 Specific ABCA4 Mutations: A Detailed Examination of 82 Hemizygous Patients The Disease Severity of Specific ABCA4 Alleles. *Investigative Ophthalmology & Visual Science* 2016;57(14):5963-73.
13. Consugar MB, Navarro-Gomez D, Place EM, et al. Panel-based genetic diagnostic testing for inherited eye diseases is highly accurate and reproducible, and more sensitive for variant detection, than exome sequencing. *Genet Med* 2015;17(4):253-61.
14. Daiger SP, Rossiter BJF, Greenberg J, et al. Data services and software for identifying genes and mutations causing retinal degeneration. *Invest Ophthalmol Vis Sci* 1998;39(S295).
15. Lu JT, Campeau PM, Lee BH. Genotype-phenotype correlation--promiscuity in the era of next-generation sequencing. *N Engl J Med* 2014;371(7):593-6.
16. Rotenstreich Y, Fishman GA, Anderson RJ. Visual acuity loss and clinical observations in a large series of patients with Stargardt disease. *Ophthalmology* 2003;110(6):1151-8.
17. Fujinami K, Zernant J, Chana RK, et al. Clinical and molecular characteristics of childhood-onset Stargardt disease. *Ophthalmology* 2015;122(2):326-34.
18. Fujinami K, Sergouniotis PI, Davidson AE, et al. Clinical and molecular analysis of Stargardt disease with preserved foveal structure and function. *Am J Ophthalmol* 2013;156(3):487-501.e1.
19. Dores GM, Devesa SS, Curtis RE, et al. Acute leukemia incidence and patient survival among children and adults in the United States, 2001-2007. *Blood* 2012;119(1):34-43.
20. Zahid S, Jayasundera T, Rhoades W, et al. Clinical phenotypes and prognostic full-field electroretinographic findings in Stargardt disease. *Am J Ophthalmol* 2013;155(3):465-73.e3.
21. Holder GE. Pattern electroretinography (PERG) and an integrated approach to visual pathway diagnosis. *Prog Retin Eye Res* 2001;20(4):531-61.
22. Chun R, Fishman GA, Collison FT, et al. The value of retinal imaging with infrared scanning laser ophthalmoscopy in patients with stargardt disease. *Retina* 2014;34(7):1391-9.
23. Lee W, Noupouu K, Oll M, et al. The External Limiting Membrane in Early-Onset Stargardt Disease. *Invest Ophthalmol Vis Sci* 2014.

24. Khan KN, Kasilian M, Mahroo OAR, et al. Early Patterns of Macular Degeneration in ABCA4-Associated Retinopathy. *Ophthalmology* 2018;125(5):735-46.
25. Holz FG, Bindewald-Wittich A, Fleckenstein M, et al. Progression of geographic atrophy and impact of fundus autofluorescence patterns in age-related macular degeneration. *Am J Ophthalmol* 2007;143(3):463-72.
26. Fritsche LG, Fleckenstein M, Fiebig BS, et al. A subgroup of age-related macular degeneration is associated with mono-allelic sequence variants in the ABCA4 gene. *Invest Ophthalmol Vis Sci* 2012;53(4):2112-8.
27. Holz FG, Strauss EC, Schmitz-Valckenberg S, van Lookeren Campagne M. Geographic atrophy: clinical features and potential therapeutic approaches. *Ophthalmology* 2014;121(5):1079-91.
28. Roche. Lampalizumab: Potentially first treatment in geographic atrophy, an advanced form of dry AMD. Investor Update. Basel and London: Roche, 2013; v. 28.07.2016.
29. Charbel Issa P, Barnard AR, Herrmann P, et al. Rescue of the Stargardt phenotype in Abca4 knockout mice through inhibition of vitamin A dimerization. *Proc Natl Acad Sci U S A* 2015;112(27):8415-20.
30. Dorsey ER, Venuto C, Venkataraman V, et al. Novel methods and technologies for 21st-century clinical trials: a review. *JAMA Neurol* 2015;72(5):582-8.
31. Parker MA, Choi D, Erker LR, et al. Test-Retest Variability of Functional and Structural Parameters in Patients with Stargardt Disease Participating in the SAR422459 Gene Therapy Trial. *Transl Vis Sci Technol* 2016;5(5):10.
32. Schmitz-Valckenberg S, Nadal J, Fimmers R, et al. Modeling Visual Acuity in Geographic Atrophy Secondary to Age-Related Macular Degeneration. *Ophthalmologica* 2016;235(4):215-24.
33. Brooks DJ, Frey KA, Marek KL, et al. Assessment of neuroimaging techniques as biomarkers of the progression of Parkinson's disease. *Exp Neurol* 2003;184 Suppl 1:S68-79.
34. Fleming TR, DeMets DL. Surrogate end points in clinical trials: are we being misled? *Ann Intern Med* 1996;125(7):605-13.
35. Sears AE, Bernstein PS, Cideciyan AV, et al. Towards Treatment of Stargardt Disease: Workshop Organized and Sponsored by the Foundation Fighting Blindness. *Transl Vis Sci Technol* 2017;6(5):6.
36. Prentice RL. Surrogate endpoints in clinical trials: definition and operational criteria. *Stat Med* 1989;8(4):431-40.
37. Fleming TR. Surrogate endpoints and FDA's accelerated approval process. *Health Aff (Millwood)* 2005;24(1):67-78.
38. Sunness JS. The natural history of geographic atrophy, the advanced atrophic form of age-related macular degeneration. *Mol Vis* 1999;5:25.
39. Sunness JS, Gonzalez-Baron J, Applegate CA, et al. Enlargement of atrophy and visual acuity loss in the geographic atrophy form of age-related macular degeneration. *Ophthalmology* 1999;106(9):1768-79.
40. Lindner M, Boker A, Mauschitz MM, et al. Directional Kinetics of Geographic Atrophy Progression in Age-Related Macular Degeneration with Foveal Sparing. *Ophthalmology* 2015;122(7):1356-65.
41. Csaky KG, Richman EA, Ferris FL, 3rd. Report from the NEI/FDA Ophthalmic Clinical Trial Design and Endpoints Symposium. *Invest Ophthalmol Vis Sci* 2008;49(2):479-89.
42. Gagne JJ, Thompson L, O'Keefe K, Kesselheim AS. Innovative research methods for studying treatments for rare diseases: methodological review. *BMJ* 2014;349:g6802.
43. Freemantle N, Calvert M, Wood J, et al. Composite outcomes in randomized trials: greater precision but with greater uncertainty? *JAMA* 2003;289(19):2554-9.
44. Korn EL, McShane LM, Freidlin B. Statistical challenges in the evaluation of treatments for small patient populations. *Sci Transl Med* 2013;5(178):178sr3.
45. Langbaum JB, Hendrix SB, Ayutyanont N, et al. An empirically derived composite cognitive test score with improved power to track and evaluate treatments for preclinical Alzheimer's disease. *Alzheimers Dement* 2014;10(6):666-74.
46. Cai CX, Light JG, Handa JT. Quantifying the Rate of Ellipsoid Zone Loss in Stargardt Disease. *Am J Ophthalmol* 2018;186:1-9.
47. Arepalli S, Traboulsi EI, Ehlers JP. Ellipsoid Zone Mapping and Outer Retinal Assessment in Stargardt Disease. *Retina* 2017.

48. Greenstein VC, Nunez J, Lee W, et al. A Comparison of En Face Optical Coherence Tomography and Fundus Autofluorescence in Stargardt Disease. *Invest Ophthalmol Vis Sci* 2017;58(12):5227-36.
49. Bunce C, Wormald R. Considerations for randomizing 1 eye or 2 eyes. *JAMA Ophthalmology* 2015;133(10):1221-.
50. Glassman AR, Melia M. Randomizing 1 eye or 2 eyes: A missed opportunity. *JAMA Ophthalmology* 2015;133(1):9-10.
51. Kianifard F, Islam MZ. A guide to the design and analysis of small clinical studies. *Pharm Stat* 2011;10(4):363-8.
52. Russell S, Bennett J, Wellman JA, et al. Efficacy and safety of voretigene neparvovec (AAV2-hRPE65v2) in patients with RPE65-mediated inherited retinal dystrophy: a randomised, controlled, open-label, phase 3 trial. *Lancet* 2017;390(10097):849-60.
53. Ameri H. Prospect of retinal gene therapy following commercialization of voretigene neparvovec-rzyl for retinal dystrophy mediated by RPE65 mutation. *J Curr Ophthalmol* 2018;30(1):1-2.
54. Suzuki K, Tsunekawa Y, Hernandez-Benitez R, et al. In vivo genome editing via CRISPR/Cas9 mediated homology-independent targeted integration. *Nature* 2016;540(7631):144-9.
55. Kuerner T. Essential rules and requirements for global clinical trials in rare lung diseases: A sponsor's standpoint. *Respiratory Investigation* 2015;53(1):2-6.
56. Downing NS, Aminawung JA, Shah ND, et al. Clinical trial evidence supporting FDA approval of novel therapeutic agents, 2005-2012. *JAMA* 2014;311(4):368-77.
57. Mitka M. FDA and pharma seek better ways to assess drug safety, efficacy in clinical trials. *JAMA* 2012;307(24):2576-7.
58. Holz FG, Sadda SR, Busbee B, et al. Efficacy and Safety of Lampalizumab for Geographic Atrophy Due to Age-Related Macular Degeneration: Chroma and Spectri Phase 3 Randomized Clinical Trials. *JAMA Ophthalmol* 2018.
59. Prasad V, Kim C, Burotto M, Vandross A. The Strength of Association Between Surrogate End Points and Survival in Oncology: A Systematic Review of Trial-Level Meta-analyses. *JAMA Intern Med* 2015;175(8):1389-98.
60. Avorn J, Kesselheim AS. The 21st Century Cures Act--Will It Take Us Back in Time? *N Engl J Med* 2015;372(26):2473-5.
61. Chaitankar V, Karakulah G, Ratnapriya R, et al. Next generation sequencing technology and genomewide data analysis: Perspectives for retinal research. *Prog Retin Eye Res* 2016;55:1-31.
62. Aebersold R, Mann M. Mass-spectrometric exploration of proteome structure and function. *Nature* 2016;537(7620):347-55.
63. Morgan JJ. The fundus photo has met its match: optical coherence tomography and adaptive optics ophthalmoscopy are here to stay. *Ophthalmic Physiol Opt* 2016;36(3):218-39.
64. Koh A, Kang D, Xue Y, et al. A soft, wearable microfluidic device for the capture, storage, and colorimetric sensing of sweat. *Sci Transl Med* 2016;8(366):366ra165-366ra165.
65. Hunter DJ. Uncertainty in the Era of Precision Medicine. *N Engl J Med* 2016;375(8):711-3.
66. Kelder T, Verschuren L, van Ommen B, et al. Network signatures link hepatic effects of anti-diabetic interventions with systemic disease parameters. *BMC Syst Biol* 2014;8:108.
67. den Hollander AI. Omics in Ophthalmology: Advances in Genomics and Precision Medicine for Leber Congenital Amaurosis and Age-Related Macular Degeneration. *Invest Ophthalmol Vis Sci* 2016;57(3):1378-87.
68. Gargon E, Gurung B, Medley N, et al. Choosing important health outcomes for comparative effectiveness research: a systematic review. *PLoS One* 2014;9(6):e99111.
69. Porter ME, Larsson S, Lee TH. Standardizing Patient Outcomes Measurement. *N Engl J Med* 2016;374(6):504-6.
70. Kost RG, Lee LM, Yessis J, et al. Assessing participant-centered outcomes to improve clinical research. *N Engl J Med* 2013;369(23):2179-81.
71. Barabasi AL. Network medicine--from obesity to the "diseasome". *N Engl J Med* 2007;357(4):404-7.
72. Loscalzo J, Kohane I, Barabasi AL. Human disease classification in the postgenomic era: a complex systems approach to human pathobiology. *Mol Syst Biol* 2007;3:124.

73. A. DJ, G. GH. The cost of biopharmaceutical R&D: is biotech different? *Managerial and Decision Economics* 2007;28(4-5):469-79.
74. Ioannidis JPA, Greenland S, Hlatky MA, et al. Increasing value and reducing waste in research design, conduct, and analysis. *The Lancet* 2014;383(9912):166-75.
75. Barabasi AL, Gulbahce N, Loscalzo J. Network medicine: a network-based approach to human disease. *Nat Rev Genet* 2011;12(1):56-68.
76. Al-Harazi O, Al Insaif S, Al-Ajlan MA, et al. Integrated Genomic and Network-Based Analyses of Complex Diseases and Human Disease Network. *J Genet Genomics* 2016;43(6):349-67.



6.1 Summary

Over 7000 rare diseases exist, and together, they afflict millions of patients worldwide. For these patients, there is promising and encouraging progress in finding a cure. However, no treatment is available for the majority of these diseases. Arguably the most prevalent inherited retinal disorder is Stargardt disease. In its natural course, the heterogeneity in the age at onset reflects the vast heterogeneity in variable rates of functional and structural disease progression. Herein, not only do the challenges of treatment evaluation—which have been present since ancient history—apply, but its rare nature and heterogeneity also pose additional challenges. This thesis responds to those challenges in treatment evaluation for Stargardt disease, providing a strategy for future studies which aim to identify an effect of novel treatments for rare diseases.

Chapter 1 is an introduction from the history to the current understanding of Stargardt disease and the evaluation of new treatments. The evaluation of new treatments has evolved significantly since ancient times and is nowadays known as a clinical trial. Without clinical trials, we may conclude that useless treatments are helpful, or that helpful treatments are useless.

The first step is to evaluate the effect of nature's time by characterizing the natural history of distinct patient groups within the spectrum of Stargardt disease. To classify patients to a specific group that is relevant, both sufficient prognostic as well as etiological homogeneity between patients are required. **Chapter 2** describes unique phenotypic and genotypic characteristics of subgroups within the vast heterogeneity of Stargardt disease, established in the context of previously emerged classifications and staging. The natural course of early-onset Stargardt disease initially features variable full-field electroretinographic abnormalities and early foveal changes. As this retinal degeneration progresses, the spectrum of phenotypes eventually converges, causing profound chorioretinal atrophy and severe vision loss. In contrast, the natural course of late-onset Stargardt describes expanding areas of retinal pigment epithelium atrophy that can spare the fovea associated with prolonged preservation of visual acuity to a relatively advanced age.

The second step consists of selecting the right patients by identifying the diagnostic challenges in specific patient groups. Rare diseases generally have a clinical presentation that is difficult to be recognized and diagnosed. **Chapter 3** reveals the challenges in the clinical diagnosis of Stargardt disease. The awareness of possible absence of retinal abnormalities in young patients allows early diagnosis. It can prevent distress, unnecessary investigations and harmful therapies and may prove important in early inclusion in

future trials. Inclusion in future trials is also challenged in older patients because of retinal abnormalities mimicked by age-related disease. Both age-related macular degeneration and late-onset Stargardt can exhibit progressive foveal sparing atrophy, but they differ in etiology and progression speed.

The third step comprises the choice of the appropriate method for outcome evaluation by developing a technique to measure disease progression with high accuracy. **Chapter 4** creates models of disease progression in Stargardt disease. The inter-eye concordance decreases as the age at onset increases, which has important consequences in clinical trial design. Potential treatment effects are best assessed in young patients. Moreover, a composite outcome measure can be powerful in the evaluation of treatment efficacy in clinical trials for Stargardt disease with small cohorts in a timely fashion. In this evaluation, optical coherence tomography and fundus autofluorescence imaging are used as measurements reflecting structural macular changes. However, we need to bear in mind that patients with Stargardt disease are generally at increased risk of photo-oxidative stress. Nonetheless, these structural macular changes provide a sensitive measurement of disease progression in Stargardt disease. It can be very useful in the evaluation of novel therapeutic modalities in rare disorders. Potentially, it can reduce costs and duration of pivotal clinical trials, thereby hopefully facilitating effective treatments being identified more readily and rapidly for patients with rare diseases.

Finally, **Chapter 5** puts the aforementioned results in a broad and future perspective. The productivity of drug development is decreasing, while the costs for drug development is ever increasing. Evidence synthesis needs to evolve, in which outcome measures play a crucial role. There is no perfect single surrogate or clinical endpoint, so the ground for drug approval should therefore arise from combined measurements within the range from biomarkers to patient-reported outcomes. Universal measurement and reporting of core outcome sets can further accelerate drug development and approval. The change of our daily practice should ultimately focus on interweaving clinical care with scientific research; the borders between the clinical care, patient registries, and therapeutic trials need to dissolve.

6.2 Samenvatting

Meer dan 7000 zeldzame aandoeningen treffen samen wereldwijd miljoenen patiënten. Voor hen is er de afgelopen jaren veel vooruitgang geboekt in de zoektocht naar een geneesmiddel. Een dergelijk geneesmiddel is echter nog lang niet beschikbaar voor de meeste zeldzame ziekten. De meest voorkomende erfelijke retinale aandoening is de ziekte van Stargardt. Deze ziekte kan zowel op zeer jonge leeftijd beginnen als ook op laatvolwassen leeftijd. Tussen deze patiënten kan de ziekteprogressie enorm verschillen. Dit uit zich als een enorme heterogeniteit in afwijkingen op zowel functioneel als op structureel niveau. De zeldzame aard en heterogeniteit van de ziekte van Stargardt geven nieuwe uitdagingen om het effect van een nieuwe behandeling te kunnen testen. Dit proefschrift speelt in op de uitdagingen in de evaluatie van een behandeling voor de ziekte van Stargardt. Het presenteert hiermee een strategie voor toekomstige studies die gericht zijn op het identificeren van effectieve nieuwe behandelingen voor zeldzame ziekten.

Hoofdstuk 1 is een inleiding van de geschiedenis tot aan de huidige stand van zaken over de ziekte Stargardt en het testen van nieuwe behandelingen. De evaluatie van nieuwe behandelingen is aanzienlijk veranderd sinds de oudheid en wordt nu gedaan aan de hand van een klinische trial. Deze klinische trials zijn nodig om aan te kunnen tonen of een behandeling effectief is.

De eerste stap bestaat uit het onderzoeken van het natuurlijk beloop binnen het spectrum van de ziekte van Stargardt tussen verschillende patiëntengroepen. Om patiënten te kunnen classificeren in een bepaalde groep, moet een dergelijke groep klinische relevant zijn: dat wil zeggen, een groep dat zowel voldoende prognostische als etiologische homogeniteit bevat. **Hoofdstuk 2** geeft unieke fenotypische en genotypische kenmerken van subgroepen weer binnen de enorme heterogeniteit van de ziekte van Stargardt. Dit wordt beschreven in de context van eerder ontstane classificaties en stadiëring. Het natuurlijke beloop van early-onset Stargardt vertoont in het begin subtiele foveale veranderingen met variabele afwijkingen op full-field elektroretinografie. Naarmate de degeneratie voortschrijdt, convergeert het spectrum van fenotypen en leidt dit uiteindelijk tot forse chorioretinale atrofie en ernstig gezichtsverlies. Dit in tegenstelling tot late-onset Stargardt, wat zich kenmerkt zich door uitbreiding van atrofische gebieden van het retinaal pigmentepitheel. Van deze gebieden blijft de fovea doorgaans gespaard en zorgt dat de visus tot een relatief hoge leeftijd intact blijft.

De tweede stap bestaat uit het selecteren van de juiste patiënten welke wordt ondersteund door de diagnostische uitdagingen in specifieke patiëntengroepen te kunnen identificeren. Zeldzame ziekten hebben namelijk over het algemeen een klinische

presentatie die moeilijk te herkennen en te diagnosticeren is. **Hoofdstuk 3** toont de uitdagingen in de klinische diagnose van de ziekte van Stargardt. De afwezigheid van retinale afwijkingen bij jonge patiënten maakt vroege diagnose lastig, maar wel mogelijk zodra we ons hiervan bewust zijn. Dit kan onnodige vertraging, onnodig diagnostisch onderzoek en zelfs schadelijke therapieën voorkómen. Vroege diagnose is bovendien belangrijk voor een tijdige en juiste inclusie in toekomstige klinische trials. Bij oudere patiënten is dit eveneens van belang, omdat bij deze patiënten de diagnose verward kan worden met leeftijdsgebonden maculadegeneratie. Zowel late-onset Stargardt als leeftijdsgebonden maculadegeneratie kan foveasparende atrofie van het retinaal pigmentepitheel vertonen, maar zij verschillen in etiologie en progressiesnelheid.

De derde stap omvat het kiezen van een geschikte uitkomstmaat voor een klinische trial door het ontwikkelen van een techniek om ziekteprogressie met hoge nauwkeurigheid te meten. **Hoofdstuk 4** maakt progressiemodellen bij de ziekte van Stargardt. De concordantie tussen het linker- en het rechteroog neemt af naarmate de beginleeftijd toeneemt, wat belangrijke consequenties heeft in het ontwerp van een klinische trial. Een effect wordt namelijk het makkelijkst gedetecteerd bij jonge patiënten, omdat bij hen de concordantie het hoogst ligt. Verder kan een samengestelde uitkomstmaat de power van een trial met kleine cohorten aanzienlijk verhogen. Bij de samengestelde uitkomstmaat zijn optische coherentietomografie en fundusautofluorescentie gebruikt als metingen die structurele maculaire veranderingen weerspiegelen. We moeten echter in gedachten houden dat patiënten met de ziekte van Stargardt over het algemeen een verhoogd risico op foto-oxidatieve stress hebben. Niettemin geven deze structurele veranderingen een gevoelige meting van ziekteprogressie. Het kan zeer nuttig zijn bij de evaluatie van nieuwe therapeutische behandelingen bij zeldzame aandoeningen. Uiteindelijk kan het in potentie de kosten en de duur van cruciale klinische trials verminderen, waardoor het gemakkelijker wordt om effectieve behandelingen sneller en gemakkelijker te identificeren.

Ten slotte zet **Hoofdstuk 5** de bovengenoemde resultaten in een breed toekomstperspectief. De productiviteit van de ontwikkeling van geneesmiddelen neemt af, terwijl de kosten ervoor steeds groter worden. De synthese van bewijsvoering moet evolueren, waarbij uitkomstmaten een cruciale rol spelen. Er is geen enkel perfect eindpunt; de basis voor goedkeuring van een geneesmiddel moet daarom uitgaan van gecombineerde metingen van biomarkers tot aan patiënt-gerapporteerde resultaten. Universele meetmethoden en rapportage van de belangrijkste uitkomstmaten kunnen de ontwikkeling en goedkeuring van geneesmiddelen verder versnellen. De verandering in onze dagelijkse praktijk moet uiteindelijk gericht zijn op het verweven van klinische zorg met wetenschappelijk onderzoek. De grenzen tussen de klinische zorg, patiëntenregisters en klinische trials moeten verdwijnen.

6.3 Ringkasan

Ada lebih dari 7000 penyakit langka, dan bersama-sama, penyakit-penyakit itu menimpa jutaan pasien di seluruh dunia. Untuk pasien-pasien ini, terdapat perkembangan yang menjanjikan dan memberi harapan dalam penemuan obat. Namun, tidak ada pengobatan yang tersedia untuk sebagian besar penyakit ini. Dapat dikatakan bahwa gangguan retina turunan yang paling umum adalah penyakit Stargardt. Dalam perjalanan alaminya, heterogenitas pada usia permulaan menggambarkan heterogenitas yang luas dalam tingkat variabel perkembangan penyakit fungsional dan struktural. Di sini, tidak hanya tantangan evaluasi pengobatan—yang telah ada sejak sejarah kuno—saja yang terjadi, tetapi sifat dan heterogenitasnya yang langka juga menimbulkan tantangan lainnya. Tesis ini menanggapi tantangan-tantangan dalam evaluasi pengobatan untuk penyakit Stargardt, memberikan strategi untuk studi berikutnya yang bertujuan untuk mengidentifikasi efek pengobatan baru untuk penyakit langka.

Bab 1 adalah pendahuluan mulai dari sejarah hingga pemahaman terkini tentang penyakit Stargardt dan evaluasi pengobatan baru. Evaluasi pengobatan baru telah berkembang secara signifikan sejak zaman kuno dan saat ini dikenal dengan uji klinis. Tanpa uji klinis, kita dapat menyimpulkan bahwa pengobatan yang tidak berguna justru sangat membantu, atau bahwa pengobatan yang membantu justru tidak berguna.

Langkah pertama yang diperlukan adalah mengevaluasi pengaruh waktu alam dengan mencirikan riwayat alami berbagai kelompok pasien dalam spektrum penyakit Stargardt. Untuk mengklasifikasikan pasien ke kelompok tertentu yang relevan, diperlukan prognostik yang cukup dan juga homogenitas etiologi antar pasien. **Bab 2** menjelaskan karakteristik fenotipik dan genotipik unik dari subkelompok dalam heterogenitas penyakit Stargardt, yang ditetapkan dalam konteks klasifikasi dan penahapan yang muncul sebelumnya. Perjalanan alami penyakit Stargardt tahap awal pada mulanya memiliki kelainan elektoretinografi bidang penuh dan perubahan foveal awal. Ketika degenerasi retina berlangsung, spektrum fenotipe akhirnya menyatu, menyebabkan atrofi koriorretinal dan kehilangan penglihatan yang parah. Sebaliknya, perjalanan alami Stargardt tahap lanjut menggambarkan perluasan area atrofi epitelium pigmen retina yang dapat menyelamatkan fovea yang terkait dengan pemeliharaan ketajaman visual yang berkepanjangan hingga usia yang relatif lanjut.

Langkah kedua adalah memilih pasien yang tepat dengan mengidentifikasi tantangan diagnostik pada kelompok pasien tertentu. Penyakit langka umumnya memiliki presentasi klinis yang sulit dikenali dan didiagnosis. **Bab 3** mengungkap tantangan dalam diagnosis klinis penyakit Stargardt. Kesadaran akan kemungkinan tidak adanya kelainan retina pada

pasien muda memungkinkan diagnosis dini. Diagnosis ini dapat mencegah penderitaan, investigasi yang tidak perlu, dan terapi berbahaya serta mungkin terbukti penting pada inklusi awal dalam uji di masa mendatang. Inklusi dalam uji di masa mendatang juga memiliki tantangan pada pasien dewasa karena kelainan retina yang ditiru oleh penyakit yang berkaitan dengan usia. Degenerasi makula terkait usia dan Stargardt tahap lanjut dapat menunjukkan atrofi penyeimbang fovea yang progresif, tetapi keduanya berbeda dalam etiologi dan kecepatan perkembangan.

Langkah ketiga terdiri dari pilihan metode yang tepat untuk evaluasi hasil dengan mengembangkan teknik untuk mengukur perkembangan penyakit dengan akurasi tinggi. **Bab 4** menciptakan model perkembangan penyakit pada penyakit Stargardt. Konkordansi antar mata menurun seiring bertambahnya usia, yang memiliki konsekuensi penting dalam desain uji klinis. Efek pengobatan potensial paling tepat dinilai pada pasien muda. Selain itu, ukuran hasil gabungan dapat berpengaruh dalam evaluasi efikasi pengobatan dalam uji klinis untuk penyakit Stargardt dengan kohor kecil secara tepat waktu. Dalam evaluasi ini, tomografi koherensi optik dan pencitraan autofluoresensi fundus digunakan sebagai pengukuran yang menggambarkan perubahan makula struktural. Namun, kita harus ingat bahwa pasien dengan penyakit Stargardt umumnya berisiko tinggi mengalami stres foto-oksidatif. Namun demikian, perubahan makula struktural ini memberikan pengukuran yang sensitif terhadap perkembangan penyakit pada penyakit Stargardt. Pengukuran ini sangat berguna untuk evaluasi modalitas terapi baru dalam gangguan langka. Secara potensial, pengukuran ini dapat mengurangi biaya dan durasi uji klinis penting, sehingga diharapkan dapat mempermudah pengobatan yang efektif yang diidentifikasi semakin cepat bagi pasien dengan penyakit langka.

Terakhir, **Bab 5** menyajikan hasil yang disebutkan di atas dalam perspektif yang luas dan berorientasi ke depan. Produktivitas pengembangan obat menurun, sementara biaya untuk pengembangan obat semakin meningkat. Sintesis bukti harus berkembang, di mana ukuran hasil berperan penting. Tidak ada satu pun pengganti atau titik akhir klinis yang sempurna, karenanya dasar untuk persetujuan obat harus muncul dari pengukuran gabungan dalam rentang dari biomarker hingga hasil yang dilaporkan pasien. Pengukuran dan pelaporan universal serangkaian hasil inti dapat lebih mempercepat pengembangan dan persetujuan obat. Perubahan praktik sehari-hari kita pada akhirnya harus fokus untuk menjalin perawatan klinis dengan penelitian ilmiah; batas antara perawatan klinis, pendaftaran pasien, dan uji terapi harus dihilangkan.



Dankwoord

Een terugblik op een bijzondere reis van de afgelopen jaren; tijdens een promotietraject leer je je grenzen ontdekken, zowel op wetenschappelijk als op persoonlijk vlak. Het doet een beroep op je creativiteit om die grenzen te verleggen. Het vergt veel geduld en doorzettingsvermogen, maar gelukkig deel je dat met een groot en hardwerkend team. En samen onderzoek doen geeft je ook weer energie en voldoening. In drie jaar tijd heb ik veel mensen leren kennen en veel samengewerkt. Het is onmogelijk om iedereen te bedanken, maar een aantal mensen zou ik graag bij deze in het bijzonder willen bedanken.

Allereerst gaat mijn dank uit naar alle patiënten die aan het onderzoek hebben deelgenomen. Zonder hun medewerking was het onmogelijk om tot dit resultaat te zijn gekomen; en het zijn ook jullie voor wie dit resultaat uiteindelijk van belang zal zijn.

Prof. dr. Hoyng, beste Carel, jij stelt altijd dat belang van de patiënt voorop door de essentie van het onderzoek scherp op je netvlies te hebben. De praktische uitwerking bleef zo nu en dan nog in het midden, maar dat gaf mij wel de vrijheid om het uit te zoeken op een manier die bij mij paste. Bedankt voor het vertrouwen in mij om het onderzoek te kunnen volbrengen. En bedankt voor je humor en je laagdrempeligheid (en sorry dat ik die hoge drempel in de bocht over het hoofd had gezien).

Prof. dr. G.J. van der Wilt, beste Gert-Jan, de beste vragen waar wij als clinici niet direct aan denken, komen van jou! Ik heb veel geleerd door jou brede blik op zaken vanuit een unieke invalshoek.

Prof. dr. Klevering, beste Jeroen, bij jou kreeg ik alle zaken weer op een rij, zodat ik niet teveel af zou dwalen. Door jou kregen de projecten hun uiteindelijke vorm. Jij weet tenslotte altijd dondersgoed hoe je een boodschap moet overbrengen. Bedankt voor jouw kritische blik.

Lieve Nathalie, mijn Stargardtmaatje! Wat fijn om met jou te hebben samengewerkt. De manier waarop jij tegen dingen aankijkt in combinatie met een snufje chaos opent ideeën waar ik geen seconde aan zou hebben gedacht. Zo pakt het altijd weer goed uit en hebben we samen toch wat fraais neergezet. En ook de tripjes naar de Keys, Yellowstone, Londen, de bever en de eekhoorn...dat waren mooie avonturen! Waar gaat de volgende reis heen? Bedankt voor je openhartigheid en eerlijkheid. En altijd vrolijk, als je tenminste hebt gegeten... (zou dat een specifiek Indo-gen zijn?) Een kop chocolademelk of een saucijzenbroodje doet veel goed. Heel veel succes met de laatste loodjes!

Mijn lieve paranimfen, wat ben ik blij dat ik jullie naast mij heb staan. Lieve Mai, jij bent voor mij een luisterend oor: altijd oprecht geïnteresseerd hoe het gaat en waar ik in mijn hoofd allemaal mee bezig ben. En een steuntje in de rug op de momenten dat ik die wel kon gebruiken. Bedankt voor alle spelletjesavonden en je heerlijke sushi! Het is toch ook altijd gezellig met jou! En Sidney, was het eerst dat we zo enthousiast werden van de nieuwste hightech gadgets, een mooie gitaar of de laatste computerapparatuur, hebben we het nu over kinderwagens en babyboxen... Wat is er in al die tijd toch veel veranderd. Maar de eindeloze jam- en oefensessies herinner ik me als de dag van gisteren. Ik ben blij dat we na 15 jaar nog steeds regelmatig afspreken, ook al zal een game- of filmavond tot in de late uurtjes er waarschijnlijk niet meer in zitten.

Prof. dr. Keunen, beste Jan, het eerste jaar van mijn opleiding was niet makkelijk; eigenlijk waren er te veel ballen in de lucht te houden; promotie, opleiding, verhuizing, een kleine dondersteen erbij...ergens ook nog tijd voor sport en sociale contacten? Bedankt voor je begeleiding, zorgzaamheid en begrip hiervoor. High five!

Dr. Theelen, beste Thomas, bedankt voor alle laagdrempelige overleggen en brainstormmomenten om je uitgebreide kennis van imaging te kunnen benutten. Het heeft het onderzoek zeker tot een hoger niveau getild!

Beste Clarisa, Mark, Freerk en Bart, ook jullie bedankt voor de hulp en het delen van jullie kennis over alle imagingtechnieken.

Prof. dr. Cremers, beste Frans, al die genen vind ik nog steeds maar ingewikkeld. Bedankt voor je hulp over de essentiële genetische zaken in het onderzoek waar ik allemaal niet aan heb gedacht.

Drs. Groenewoud, beste Hans, wat een bron van statistische kennis en creativiteit ben jij! Je bent altijd enthousiast over van alles, en zelfs samen aan vele regels lange SAS-syntax is dan gewoon gezellig met jou. Foutmelding? Dat kan altijd opgelost worden!

Beste Clasien, het lijkt alweer zo lang geleden, maar bedankt voor de samenwerking in het RD5000-project en voor al het lekkers dat uit je tuin kwam!

Dear prof. dr. Holz, prof. dr. Fleckenstein, prof. dr. Schmitz-Valckenberg, Moritz, Matthias, and Matthias from the Universitäts-Augenklinik Bonn, thank you for the fruitful collaboration on foveal sparing. I am also glad we can agree that we should not always listen to Carel. Otherwise, we would have been the Foveal sparing Atrophy Research Team instead of the Study Team.

Also many thanks to our collaborators at Moorfields Eye Hospital; prof. dr. Webster, prof. dr. Moore, prof. dr. Michaelides, and Ana for our nice collaboration.

Beste Yara, Nicole, Freekje, Constantin, Myrte, Michel, Nathalie, Laura, Maartje, Roos, Eveline, Sanne, Vivian en Dyon, in de promovendikamer zaten we allemaal in hetzelfde schuitje; het is er hard werken tijdens een hele lange duurloop...en het is er vooral ook erg gezellig! Maar poeh he...wat vliegt er toch soms een hoop onzin door zo'n kamer. Gelukkig kan ik me daar goed van afsluiten, maar ja....dan krijg je ook niet altijd alles mee. Naast al dat onderzoek hebben we zeker ook heel wat afgereisd, spelletjesavonden gehad, gepubquized, film(marathon)s gekeken, taart gegeten, sushi gegeten, pizza gegeten, en nog meer gegeten. En het opnemen en inzingen van al die promotiefilmpjes leverden ook altijd hilarische momenten op. Bedankt voor al die mooie momenten! Niet bedankt trouwens voor alle schrikmomenten die jullie mij hebben bezorgd...

De etentjes en spellenavonden hebben we 'beneden' met een aantal van jullie mooi voortgezet in het 'AIOS-tijdperk' samen met Artin, Martijn, Mustapha, Elise, Linde en Robert. John, Dženita, Stefan, Jelina, Anita, Ramon en Ellen, jullie zijn inmiddels een tijdje AIOS af, maar ik wil jullie nog bedanken dat ik voor alle vragen als kersverse AIOS bij jullie terecht kon. En Nicole, ook jij bedankt dat je als mentormama mij wegwijs hebt gemaakt op de poli (ik weet alleen nog steeds niet alle lampschakelaars te vinden). Ramon, jou wil ik in het bijzonder bedanken voor je hulp en begeleiding tijdens mijn onderzoeksstage. Die archieven in de kelders (krochten?) van de afdeling waren wel saai hoor...en soms ook een beetje creepy. Jij zag echter een kansrijk eindresultaat voor ogen. Jouw enthousiasme heeft ook mij enthousiast gemaakt en misschien was ik anders wel nooit aan mijn promotietraject begonnen.

Maartje, Lianne en Ronald, dat DOPS-congres van een paar jaar terug...daar mogen we best trots op zijn! Wat een soepel en geslaagd congres was dat. Een geweldig, geolied team waren we!

Collega's van de verpleegpost, optometristen, administratie en het stafsecretariaat, bedankt voor gezelligheid en ondersteuning! Jack en Liesbeth in het bijzonder dat ik het maken van de ERG's en imaging van jullie heb mogen leren!

Lieve vrienden en vriendinnen, Sidney, Robin, Mai, Jimmy, Nynke, Aart, Sherien, Aletta, Renée, Samantha, Koen, Roy, Thijs, Nick, Melek, Fia...lekker badmintonnen, weekendjes weg, BBQ's, motorrijden, de spellenavonden, sushi maken, sushi eten (hoe vaak staat er nou al sushi in mijn dankwoord?!). Tja, het leven bestaat inderdaad uit meer dan alleen maar promoveren (en sushi). Bedankt dat jullie me daaraan hebben blijven herinneren. Nu ik dit kan afsluiten, wordt het hoog tijd om uit dat sociaal isolement te stappen.

Lieve Jonathan en Doshny, ook jullie staan klaar als ik hulp kan gebruiken. Bedankt daarvoor!

Ook wil ik mijn schoonfamilie bedanken, lieve Marianne, René, Leanne, Robin, Imre en opa Wim, bedankt voor al jullie betrokkenheid, gezelligheid, leuke uitjes en skivakanties. Ondanks dat ik inmiddels door jullie ook een beetje kan skiën, blijf ik het toch maar vreemd vinden dat jullie die ijskoude sneeuw maar al te graag verkiezen boven een vakantie met een warm zonnetje en een palmboom.

Kanggo kulawarga, matur suwun kanggo dukungan sampeyan kabeh. Wektu sedilik kanggo kumpul bebarengan iku wektu sing apik nemen lan bakal terus tak iling-iling. Sakjane aku kepingin njenengan ora adoh-adoh. Kanggo Mbah Kakung, matur suwun kanggo dungone sing kenceng. Njenengan mesti ono terus ing atiku. Kanggo Mbah Ibuk, rasane seneng banget kaya mulih nang omah nalika ndeleng kabungahan lan kebecikan ing mripat njenengan. Matur suwun wis bungah karo aku. Aku tresno njenengan.

Lieve mama, jij hebt altijd gezegd dat we zelf onze toekomst moeten opbouwen en daarvoor hard voor zullen moeten werken. Je krijgt het niet voor niets. Dankzij jou heb ik me kunnen ontwikkelen tot wie ik ben. Je staat altijd klaar voor mij, en altijd is er een warm welkom thuis (met lekker eten)! Hoe drukker het werd, des te minder dat ik je eigenlijk zag en vergeet ik weleens te zeggen hoe blij en dankbaar ik ben dat ik de allerliefste mama van de wereld heb!

Lieve Anouk, jij kan me zo goed weghalen van alle drukte om samen te ontspannen en te genieten van alle mooie kleine dingen. Lekker uitwaaien op de motor, op het strand, of simpelweg hier om de hoek. Die momenten samen waarbij we de rest van de wereld eventjes kunnen vergeten, zijn misschien wel de belangrijkste in het leven. Bedankt voor al je steun en liefde! De laatste maandjes, en ik denk wel het hele afgelopen jaar, waren erg zwaar: verhuizen, promoveren, de opleiding, tussendoor competitie spelen...en we hadden ook nog eens bedacht dat we een gezinnetje zouden willen stichten. Samen zijn we erdoorheen geslagen. Zonder jou was dit nooit gelukt, ik hou van je!

Lieve Yenthe, elke ochtend opstaan met een grote glimlach op je gezicht: hoe kan een dag voor een trotse vader nou beter beginnen? Je bent het beste wat mij is overkomen. We kunnen altijd rekenen op elkaar, wij met z'n drietjes!

Curriculum vitae

Stanley Lambertus was born on November 18th, 1987 in Gendringen, the Netherlands. He completed secondary school (VWO-certificate, Natuur, Techniek en Gezondheid) at the Almende College, Isala in Silvolde. He started his medical study in 2006 at the Radboud University in Nijmegen, and successfully completed this in 2012. His interest in research and ophthalmology developed in his final year, in which he took part in clinical ophthalmologic research on Stargardt disease at the Radboud university medical center. After his medical studies, he continued research in a PhD project on Stargardt disease, which resulted in this thesis. In March 2017, he started a residency in ophthalmology in the same institute.



Publications

Papers in international journals

Development of refractive errors —what can we learn from inherited retinal dystrophies?

Michelle Hendriks, Virginie J.M. Verhoeven, Gabriëlle H.S. Buitendijk, Jan Roelof Polling, Magda A. Meester-Smoor, Albert Hofman, [RD5000 Consortium](#), Maarten Kamermans, L. Ingeborgh van den Born, Caroline C.W. Klaver
Am J Ophthalmol. 2017 Oct;182:81-89.

Highly sensitive measurements of disease progression in rare disorders: developing and validating a multimodal model of retinal degeneration in Stargardt disease

[Stanley Lambertus](#), Nathalie M. Bax, Ana Fakin, Joannes M.M. Groenewoud, B. Jeroen Klevering, Anthony T. Moore, Michel Michaelides, Andrew R. Webster, Gert Jan van der Wilt, and Carel B. Hoyng
PLoS One. 2017 Mar 29;12(3):e0174020.

Photo-oxidative stress during fundus autofluorescence imaging

Michel M. Teussink, [Stanley Lambertus](#), Frits de Mul, Carel B. Hoyng, B. Jeroen Klevering, and Thomas Theelen
PLoS One. 2017 Feb 24;12(2):e0172635.

Differential disease progression in atrophic age-related macular degeneration and late-onset Stargardt disease

Moritz Lindner⁻, [Stanley Lambertus](#)⁻, Matthias M. Mauschitz, Nathalie M. Bax, Eveline Kersten, Anna Lüning, Jennifer Nadal, Steffen Schmitz-Valckenberg, Matthias Schmid, Frank G. Holz, Carel B. Hoyng, and Monika Fleckenstein for the Foveal sparing Atrophy Study Team (FAST)

Invest Ophthalmol Vis Sci. 2017 Feb 1;58(2):1001-1007.

Asymmetric inter-eye progression in Stargardt disease

[Stanley Lambertus](#), Nathalie M. Bax, Joannes M.M. Groenewoud, Frans P.M. Cremers, Gert Jan van der Wilt, B. Jeroen Klevering, Thomas Theelen, and Carel B. Hoyng

Invest Ophthalmol Vis Sci. 2016 Dec 1;57(15):6824-6830.

Progression of late-onset Stargardt disease

[Stanley Lambertus](#)⁻, Moritz Lindner⁻, Nathalie M. Bax, Matthias M. Mauschitz, Jennifer Nadal, Matthias Schmid, Steffen Schmitz-Valckenberg, Anneke I. den Hollander, Bernhard H.F. Weber, Frank G. Holz, Gert Jan van der Wilt, Monika Fleckenstein[†], and Carel B. Hoyng[†] for the Foveal sparing Atrophy Study Team (FAST)

Invest Ophthalmol Vis Sci. 2016 Oct 1;57(13):5186-5191

Early-onset Stargardt disease: phenotypic and genotypic characteristics

[Stanley Lambertus](#), Ramon A.C. van Huet, Nathalie M. Bax, Lies H. Hoefsloot, Frans P.M. Cremers, Camiel J.F. Boon, B. Jeroen Klevering and Carel B. Hoyng

Ophthalmology. 2015 Feb;122(2):335-44

The RD5000 Database: facilitating clinical, genetic, and therapeutic studies on inherited retinal diseases

Ramon A.C. van Huet, Clasien J. Oomen, Astrid S. Plomp, Maria M. van Genderen, B. Jeroen Klevering, Reinier O. Schlingemann, Caroline C.W. Klaver, L. Ingeborgh van den Born, Frans P.M. Cremers, and the [RD5000 Study Group](#)

Invest Ophthalmol Vis Sci. 2014 Nov 17;55(11):7355-60

Disruption of the basal body protein POC1B results in autosomal-recessive cone-rod dystrophy

Susanne Roosing⁻, Ideke J.C. Lamers⁻, Erik de Vrieze⁻, L. Ingeborgh van den Born⁻, [Stanley Lambertus](#), Heleen H. Arts, POC1B Study Group, Theo A. Peters, Carel B. Hoyng, Hannie Kremer, Lisette Hetterschijt, Stef J.F. Letteboer, Erwin van Wijk[†], Ronald Roepman[†], Anneke I. den Hollander[†], and Frans P.M. Cremers[†]

Am J Hum Genet. 2014 Aug 7;95(2):131-42

Members of the RD5000 Consortium/Study Group:

Nathalie M. Bax, Carel B. Hoyng, [Stanley Lambertus](#), Wendy A. van Zelst-Stams, Arthur A. B. Bergen, José Schuil, Mary J. van Schooneveld, Laurence Pierrache, Magda A. Meester-Smoor, Camiel J. F. Boon, Jan Willem R. Pott, Redmer van Leeuwen, Hester Y. Kroes, Yvonne de Jong-Hesse, and F. Nienke Boonstra.

⁻ joint first authors, [†] contributed equally.

Book chapters

Stargardt Disease

Carel B. Hoyng, [Stanley Lambertus](#), and Nathalie M. Bax

In: Querques G, Souied HE, editors. *Macular Dystrophies*. Cham: Springer International Publishing; 2016. p. 25-30.

Abstracts in conferences

Natural progression of Stargardt disease; the young go fast, the old take it easy

[Stanley Lambertus](#), Nathalie M. Bax, Dyon Valkenburg, Joannes M.M. Groenewoud, Gert Jan van der Wilt, B. Jeroen Klevering and Carel B. Hoyng
Nederlands Oogheelkundig Congres 2017

Foveal sparing in inherited retinal disease

Nathalie.M. Bax, Dyon Valkenburg, [Stanley Lambertus](#), B. Jeroen Klevering, Camiel J.F. Boon, Frank G. Holz, Frans P.M. Cremers, Monika Fleckenstein, Moritz Lindner, and Carel B. Hoyng, for the Foveal sparing Atrophy Study Team (FAST)
Nederlands Oogheelkundig Congres 2017

Insensitive short-term clinical trial endpoint in Stargardt disease: progression of best-corrected visual acuity

Sanne K. Verbakel, [Stanley Lambertus](#), Nathalie M. Bax, Dyon Valkenburg, Ramon A.C. van Huet, Joannes M.M. Groenewoud, Carel B. Hoyng
Association for Research in Vision and Ophthalmology Annual Meeting 2017

Differential progression of Stargardt disease between young infancy and late adulthood.

Dyon Valkenburg, [Stanley Lambertus](#), Nathalie M. Bax, Joannes M.M. Groenewoud, Gert Jan van der Wilt, B. Jeroen Klevering, Carel B. Hoyng
Association for Research in Vision and Ophthalmology, Annual Meeting 2017

Complex interaction and Hardy-Weinberg disequilibrium of ABCA4 disease-causing alleles provides insights into the pathogenesis of retinopathy

Ana Fakin, Valentina Cipriani, [Stanley Lambertus](#), Nathalie M. Bax, Anthony G. Robson, Kaoru Fujinami, John Chiang, Anthony T. Moore, Michel Michaelides, Graham E. Holder, Carel B. Hoyng, and Andrew R. Webster
Association for Research in Vision and Ophthalmology Annual Meeting 2017

Progression of late-onset Stargardt disease

[Stanley Lambertus](#), Moritz Lindner, Nathalie M. Bax, Matthias M. Mauschitz, Matthias Schmid, Steffen Schmitz-Valckenberg, Bernhard H.F. Weber, Frank G. Holz, Gert Jan van der Wilt, Monika Fleckenstein, and Carel B. Hoyng
Association for Research in Vision and Ophthalmology Annual Meeting 2016
6th International DOG-Symposium on AMD 2015
Dutch Ophthalmology PhD Students' Congress 2016

Clinical and genetic characteristics of intermediate-onset Stargardt disease

Nathalie M. Bax, [Stanley Lambertus](#), Cecile J.A. van der Poort, B. Jeroen Klevering, Frans P. Cremers, and Carel B. Hoyng
Association for Research in Vision and Ophthalmology Annual Meeting 2016

Comparison of geographic-atrophy progression in late-onset Stargardt disease and AMD

Moritz Lindner, [Stanley Lambertus](#), Nathalie M. Bax, Matthias M. Mauschitz, Eveline Kersten, Matthias Schmid, Steffen Schmitz-Valckenberg, Carel B. Hoyng, Frank G. Holz, and Monika Fleckenstein
6th International DOG-Symposium on AMD 2015

Asymmetric inter-eye progression in Stargardt disease

[Stanley Lambertus](#), Nathalie M. Bax, Gert Jan van der Wilt, and Carel B. Hoyng
Association for Research in Vision and Ophthalmology Annual Meeting 2015

The burden of disease in Stargardt patients

Nathalie M. Bax, [Stanley Lambertus](#), Lena Ye, Ellen J.M. van den Wittenboer, B. Jeroen Klevering, Chris M. Verhaak, and Carel B. Hoyng
Association for Research in Vision and Ophthalmology Annual Meeting 2015
Dutch Ophthalmology PhD Students' Congress 2015

Automatic quantification of geographic atrophy in autofluorescence images of Stargardt patients

Clara I. Sanchez, [Stanley Lambertus](#), Bart Bloemen, Nathalie M. Bax, Freerk G. Venhuizen, Mark J.J.P. van Grinsven, Bram van Ginneken, Thomas Theelen, and Carel B. Hoyng
Association for Research in Vision and Ophthalmology Annual Meeting 2015

The natural progression of early-onset Stargardt disease

[Stanley Lambertus](#), Ramon A.C. Huet, Nathalie M. Bax, Ellen J.M. van den Wittenboer, Frans P.M. Cremers, Camiel J.F. Boon, B. Jeroen Klevering, and Carel B. Hoyng
Association for Research in Vision and Ophthalmology Annual Meeting 2014

Analysis of ABCA4-related retinal dystrophies without fundus abnormalities

Nathalie M. Bax, [Stanley Lambertus](#), Ramon A.C. van Huet, Frans P.M. Cremers, and Carel B. Hoyng
Association for Research in Vision and Ophthalmology Annual Meeting 2014
Dutch Ophthalmology PhD Students' Congress 2014

Portfolio

S. Lambertus <i>Department of Ophthalmology</i> <i>Radboud Institute for Health Sciences</i>		PhD period: 1 January 2014 – 31 December 2016	
		<i>Promotors:</i> <i>Prof. dr. C.B. Hoyng</i> <i>Prof. dr. G.J. van der Wilt</i> <i>Prof. dr. B.J. Klevering</i>	
		Year(s)	ECTS
TRAINING ACTIVITIES			
<i>Courses & workshops</i>			
RIHS introduction course for PhD candidates	2014	0.50	
Basic course on regulations and organization for clinical investigators (BROK)	2014	1.50	
NIHES EWP Prognostic research and advanced analysis of prognosis studies	2014	1.80	
SPSS Course	2014	0.20	
ZonMW Workshop: Introduction to systematic reviews of animal studies	2014	0.20	
How to prepare your poster presentation	2014	0.20	
Radboud Institute for Health Sciences - Introductory course	2015	0.50	
Scientific integrity	2015	0.50	
Implementing systematic reviews of animal studies. The next steps	2015	0.20	
Academic writing	2015	3.00	
How to write a medical scientific paper	2015	0.20	
How to write a medical scientific abstract	2016	0.20	
Perfecting your academic writing skills	2016	1.50	
Presentation skills	2016	1.50	
<i>Seminars & lectures</i>			
Radboud Research Round Sensory Disorders (n = 5) [#]	2014-2016	0.75	
Ophthalmology referring evenings (n = 5)	2014-2016	0.50	
PhD defences (n = 6)	2014-2016	0.60	
Orations (n = 2)	2015-2016	0.20	
NOG electro-ophthalmology meetings (n = 2)	2015-2016	0.20	
Selective publication and the replicability crisis	2015	0.10	
Calculating power & sample size for clinical trials	2016	0.10	
An editor's perspective on scientific publishing	2016	0.10	
<i>Symposia & congresses</i>			
Novel therapies for inherited retinal dystrophies	2014	0.25	
Macula Symposium Rotterdam	2014	0.25	
Nederlands Oogheelkundig Congres	2014	0.25	
International DOG-Symposium on AMD*	2015	1.00	
JMD Symposium	2015	0.25	
Publieksavond Therapie in Zicht	2015	0.10	
Donders Perception Day*	2016	0.50	
OOG/ZOG (n = 3)	2014-2016	0.30	
Association for Research in Vision and Ophthalmology Annual Meeting (n = 3)**	2014-2016	4.50	
Dutch Ophthalmology PhD Students (DOPS) congress (n = 3)*	2014-2016	1.50	
<i>Other</i>			
RD5000 database development/meetings	2014-2015	0.50	
Taskforce genetic therapy meetings	2014	0.25	
Open Dag Radboudumc	2015	0.20	
American Academy of Ophthalmology Annual Meeting	2015	1.00	
Ocular gene therapy alignment meeting*			
TEACHING ACTIVITIES			
<i>Lecturing</i>			
Wetenschapsknooppunt RU	2014-2015	0.60	
Adobe InDesign and Illustrator workshops (n = 3)	2016	0.60	
<i>Supervision of internships/other</i>			
50+ Beurs	2015	0.20	
Dutch Ophthalmology PhD Students' Congress 2015 organization	2015	2.00	
Scientific publication reviews	2015-2016	0.20	
Internship supervision	2015-2016	1.00	
TOTAL			30.0 ECTS

[#] Oral presentation; * Poster presentation.

